Understanding host pathogen interactions in mycobacteria using CRISPR

By

Bala Tripura Sundari Annapurna Madduri

A thesis submitted to the University of Birmingham

for the degree of

DOCTOR OF PHILOSOPHY

Institute of Microbiology and Infection

School of Biosciences

College of Life and Environmental Sciences

University of Birmingham

ABSTRACT

Tuberculosis (TB) is one of the leading causes of death from a single infectious agent (*Mycobacterium tuberculosis*), second only to Coronavirus disease 2019 (COVID-19). The emergence of drug resistant strains, the variable efficacy of the BCG vaccination worldwide and the vulnerability of immunocompromised individuals infected with Human immunodeficiency virus suffering from acquired immune deficiency syndrome (HIV/AIDS) has prompted the scientific community to develop new strategies towards the development of novel anti-tubercular drugs, vaccine candidates and treatment strategies. The genus *Mycobacterium* has an elaborate and highly impermeable cell envelope, with additional molecular decorations contributing to its virulence and pathogenesis. Presence of this highly evolved cell envelope adds additional complexities in its treatment strategies, with the ongoing global pandemic exacerbating the situation, with tuberculosis claiming 1.5 million lives in 2020.

An understanding of mycobacterial cell wall assembly and host pathogen interactions are key aspects to tackle this disease. This thesis addresses these aspects in two separate projects with an overall aim to advance research on TB; and aid in the development of novel anti-tubercular therapeutics. Firstly, an essential enzyme involved in mycobacterial cell wall assembly has been characterised for its role in growth, biofilm formation and pathogenesis of *M. bovis* BCG - the vaccine strain of TB. Secondly, a host immune response regulator protein which was reported to encourage intracellular mycobacterial growth and proliferation has been studied to contributing to research on the development of host directed therapies to combat tuberculosis.

This thesis is dedicated to my family.

ACKNOWLEDGEMENTS

I would like to take the opportunity to thank everyone who made this thesis and the work behind it possible. Firstly, I am very grateful to Dr Luke Alderwick who gave me this opportunity to pursue doctoral studies at University of Birmingham. His constant support, motivation and guidance were the pillars behind my research work. I am very thankful to Prof Gurdyal Besra for his continuous guidance, especially in the final stages of thesis submission. I am grateful to Dr Apoorva Bhatt and Dr Patrick Moynihan for their valuable insights and suggestions to make this research better, and their guidance and support in furthering my scientific career. I would also like to thank the Darwin Trust of Edinburgh for funding this PhD and for making my stay in the UK very comfortable and affordable particularly during the global pandemic.

I would like to acknowledge the many people who contributed to this work. A very big thank you to Dr Stephen Taylor and Lauren Allen at Public Health England for processing my samples during a busy period while handling the COVID19 pandemic. Special thanks to Dr Farhat Khanim for training me in cell culture and helping me with CRISPR/Cas9 and Dr Alessandro Di Maio for his guidance in confocal microscopy. Also, thanks to Dr Pete Lund and Dr C M Santosh Kumar who provided the plasmids for CRISPR interference. Particular thanks have to go to Santosh and his wife Kalyani who became my very good friends and supported me during a very difficult time in my life.

Special thanks to everyone in Alderwick, Besra, Bhatt and Moynihan labs for your support and advice over the past four years. Especially, Albel, Nat, Rebecca, Ian and Parisa who helped me with science questions throughout my postgraduate research. A very big thank you to all my friends and fellow PhD students with whom I've shared the ups and downs of this journey, especially – Anja, Alice L, Alice M, Helen, Stephen, Chris, Nabiela, Perla, Charlotte and Alex who heard me rant and cry over results. Special thanks to Karn and Aishwarya who were my personal support bubble during my doctoral studies, Angie for being my rock during the global pandemic and national lockdown and for being a source of comfort and love when it was most needed. I would also like to thank all my friends over the years, for always reminding me why I started this journey.

Finally, I would like to thank my sister for her continuous admiration, respect and unwavering belief in me which acts as a driving force for me to live up to. Ultimately, I would like to thank my parents for their unlimited patience, love and support without which I could not have come this far.

TABLE OF CONTENTS

LIST OF FIGURES

LIST OF TABLES

LIST OF ABBREVIATIONS

µ: micro

1-D: 1 Dimensional

2-D: Two dimensional

Ac_2PIM_2: Diacyl phosphatidyl-myo-inositol dimannoside

Ac_2PIM_6: Diacyl phosphatidyl-myo-inositol hexamannoside

AES: Allelic exchange substrate

Aft: Arabinofuranosyltransferase

AftC: Arabinofuranosyltransferase

AG: Arabinogalactan

APC: Antigen presenting cells

Araf: D-arabinofuranosyl

ATc: Anahydro Tetracyclin

BCG: Bacillus Calmette–Guérin

bp: base pairs

Cas: CRISPR associated

Cas9n: Cas9 nickase mutant

CCL: C-C Motif Chemokine Ligand

CD: Cluster of differentiation

CESTET: Conditional expression specialised transduction essentiality test

CFU: Colony forming unit

CIS: cytokine inducible SH2 domain containing protein

CO_2: Carbon dioxide

COVID19: Corona virus disease

CR: Complement receptor

CRISPR/Cas: Clustered regularly interspaced short palindromic repeats/CRISPR-associated

CRISPRi: CRISPR interference

crRNA: CRISPR RNA

DAT: Diacyl Trehalose

DC: Dendritic cells

dCas9: catalytically inactive dead Cas9

DC-SIGN: Dendritic cell specific intercellular adhesion molecule (ICAM)-3 grabbing nonintegrin

DNA: Deoxyribonucleic acid

DSB: Double strand breaks

EPS: Extracellular polymeric substances

ECM: Extracellular Matrix

FAME: Fatty acid methyl esters

Galf: D-galactofuranosyl

GM-CSF: Granulocyte-macrophage colony stimulating factor

GMM: Glucose monomycolate

HDR: Homology Directed Repair

HDT: Host directed therapy

AIDS: Acquired immunodeficiency syndrome

HIV: Human Immunodeficiency Virus

IFN: Interferon

IL: Interleukin

JAK: Janus kinase

KIR: Kinase inhibitory region

LAM: Lipoarabinomannnan

LM: Lipoarabinomannam

MA: Mycolic acids

mAGP: mycolyl-arabinogalactan-peptidoglycan

MAME: Mycolic acid methyl esters

ManLAM: Mannose capped LAM

Manp: D-mannopyranosyl

MDR-TB: Multidrug-resistant TB

MIC: Minimum inhibitory concentration

MOI: Multiplicity of infection

MR: Mannose receptor

MTBC: Mycobacterium tuberculosis comples

MurNGlyc: N-gluconylmuramic acid

NHEJ: Non Homologoes End Joining

NK: Natural killer

OADC: Oleic Albumin Dextrose Catalase

OD: Optical density

ORF: Open reading frame

PAM: Protospacer adjacent motif

PAMP: Pathogen associated molecular pattern

PBS: Phosphate buffer saline

PCR: Polymerase chain reaction

PG: Peptidoglycan

PGE_2: prostaglandin E2

PI: Phosphatidylinositol

PIM: Phosphatidylinositol mannoside

PRR: Pattern recognition receptor

RNA: Ribonucleic acid

rRNA: ribosomal RNA

RT: Reverse transcription

sgRNA: single guide RNA

SH2: SRC homology 2

shRNA: small hairpin RNA

SL: Sulpholipid

SOCS: Suppressor of cytokine signalling

SR: Scavenger receptor

STAT: Signal transducer and activator of transcription

TB: Tuberculosis

TBS: Tris buffer saline

TDM: Trehalose Dimycolate

TetR: Tetracyclin inducible regulated promoter

TGF: Transforming growth factor

T_H: T-Helper cells

TLC: Thin Layer Chromatography

TLR: Toll like receptor

TNF: Tumor necrosis factor

tracrRNA: transactivation crRNA

WGS: Whole genome sequencing

WHO: World Health Organisation

Chapter 1 : General Introduction

1.1 Tuberculosis

1.1.1 History

Tuberculosis (TB) is an ancient disease which has evolved with humans for millions of years. Archaeological evidence has shown reports of infection and deformities caused by TB in Egyptian mummies dating back to 2400 BC (Zink *et al.*, 2001). The first written documents of this disease originate from India and China, dating back to 3300 and 2300 years ago, respectively, with symptoms including fever, sweating, coughing and blood stained sputum (Barberis *et al.*, 2017). The period from the 17th to mid-19th century TB was an epidemic in Europe with high mortality rates. During this time, it had various names including – consumption, phthisis and white plague. It was during this time when the first sanatoriums were introduced to isolate and treat patients with TB (reviewed in Barberis *et al.*, 2017).

1.1.2 Epidemiology of the disease

In 2019 (before COVID19), 10 million people were infected with TB and 1.4 million deaths were reported by the World Health Organisation (WHO). However, during the COVID19 pandemic these numbers have significantly increased (WHO, 2021), with 1.5 million deaths reported (WHO, 2021), and in fact this number may actually be higher due to under reported cases (WHO, 2020). There has also been a major drop in TB diagnosis and treatment which fell from 7.1 million reported new cases in 2019 to 5.8 million in 2020 (WHO, 2021). This is far short of the 10 million new TB cases in 2020, which is estimated to have much worse implications in 2022 (WHO, 2021).

TB is a poverty related disease with a higher prevalence observed in malnourished individuals living in overcrowded and unhygienic settings, mostly in underdeveloped and developing countries. Eight of these countries account for two-thirds of global TB cases, with a minimum of 100 000 cases each (Figure 1.1) as compared to developed nations which have less than 10 TB incidences per 100 000 population as shown in (Figure 1.2; WHO, 2020).

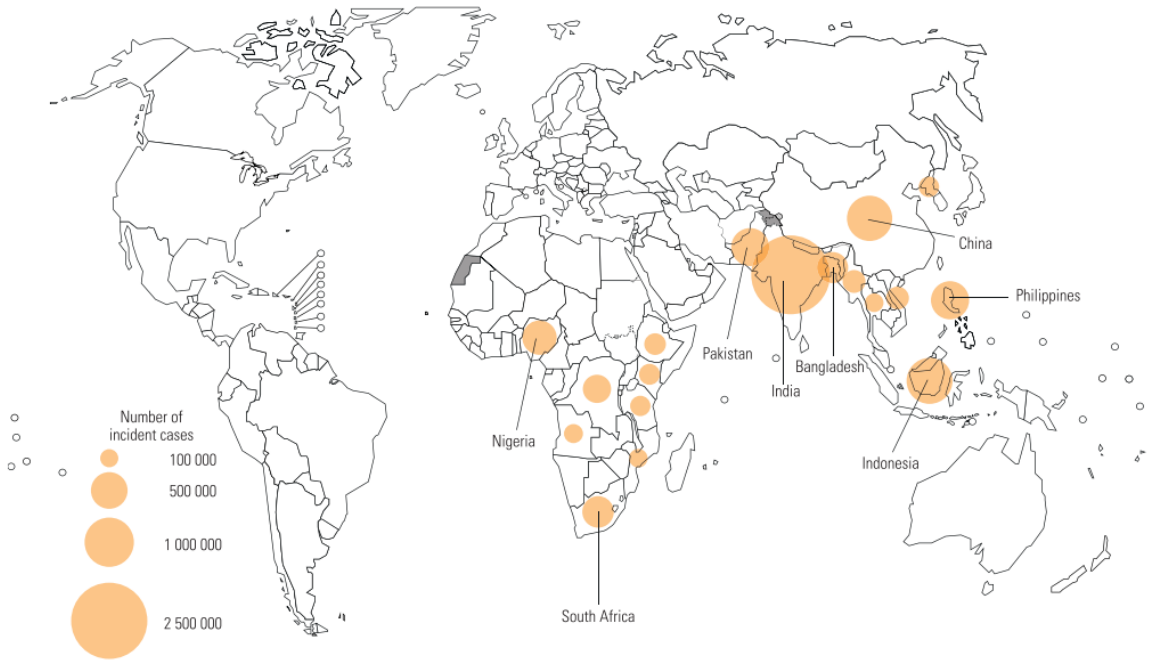

Figure 1.1: ***Countries with at least 100 000 TB cases in 2019*** *(used with permission from (WHO, 2020)).*

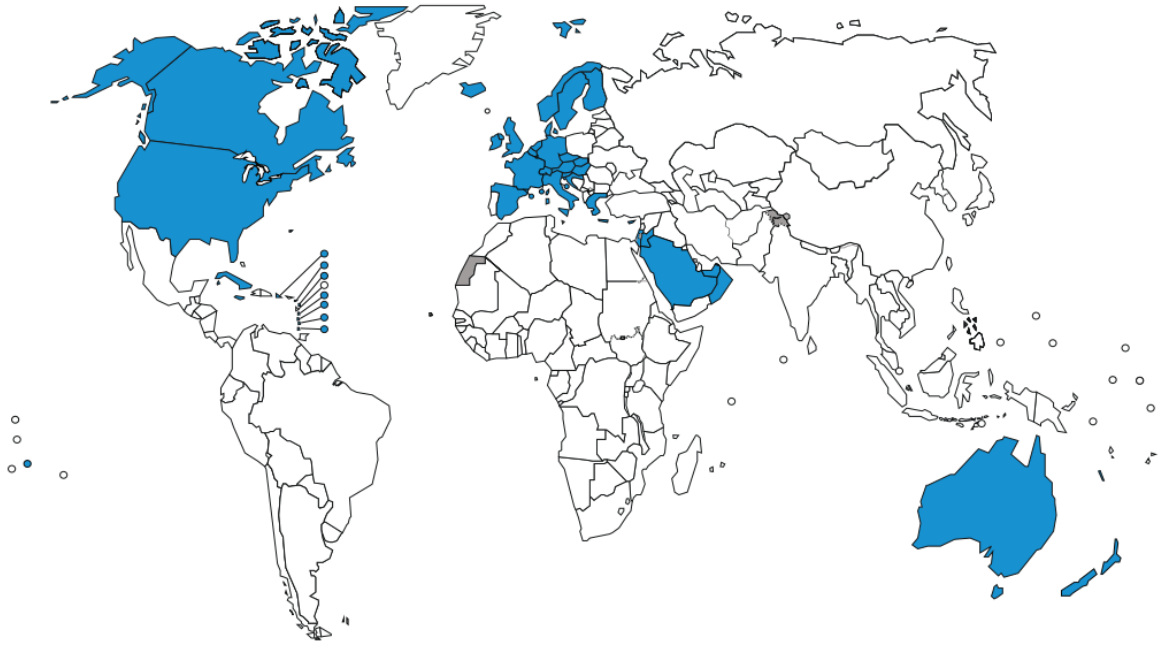

*Figure 1.2****: Countries with 10 TB cases per 100 000 population in 2019*** *(used with permission from (WHO, 2020)).*

1.1.3 Aetiological agent of Tuberculosis - MTB Complex

Mycobacterium tuberculosis is the causative agent for TB. It was first isolated and identified in 1882 by Robert Koch (Barberis *et al.*, 2017) as an aerobic, non-spore forming, non-motile bacilli, which belongs to the *Mycobacterium tuberculosis* complex (MTBC) of the family *Mycobacteriaceae* and the order *Actinomycetes* of the phylum *Actinobacteria* (Sneath, 2007; Vincent *et al.*, 2018). These slightly curved, rod-shaped bacilli were initially given the generic name *Mycobacterium* as they grew in mold-like fashion in liquid culture. They belong to a special group of Gram positive bacteria with a characteristic thick waxy coat on its cell surface, making them neutral to Gram staining. Acid fast staining is the traditional approach to detect mycobacteria which is named after its resistance to decolourisation by acids. In this approach a bacterial smear is first stained with carbol fuchsin which stains mycobacteria bright red. This stain is retained upon an acid alcohol wash preventing the counter stain using methylene blue (Vilchèze and Kremer, 2017).

M. tuberculosis complex (MTBC) including *Mycobacterium tuberculosis, Mycobacterium bovis, Mycobacterium africanum, Mycobacterium microti, Mycobacterium canettii, and Mycobacterium caprae*, among others, cause chronic pulmonary and non-pulmonary diseases in different species. Although, members of the group differ in their phenotype, pathogenicity and host tropism caused by evolutionary events resulting in the present speciation of *Mycobacterium* (Brosch et al., 2002; Wirth *et al.*, 2008), they contain a remarkable genetic homogeneity with 99.9% nucleotide sequence similarity and identical 16s rRNA sequences (Böddinghaus et al., 1990; Sreevatsan et al., 1997 Sneath, 2007). Members of the MTBC contain a high genomic proportion of guanine and cytosine, with no more than 2500 single nucleotide polymorphisms between two members of the complex. This along with whole genome comparative analyses suggests that members of MTBC evolved from a common ancestor (Sreevatsan *et al.*, 1997), with evidence suggesting *M. Canetti* could represent the most ancestral lineage (Fabre *et al.*, 2004). Infection with *M. tuberculosis* manifests in the disease TB, which is globally, one of the top 10 causes of death from a single infectious agent (WHO, 2021).

1.1.4 Pulmonary and Extra-pulmonary disease

M. tuberculosis is a major health problem causing pulmonary and extra-pulmonary infections. Pulmonary tuberculosis is localised in the lungs and has non-specific symptoms including a productive cough with or without haemoptysis, mucopurulent or purulent sputum, malaise, fever, breathlessness, loss of appetite and weight loss (Campbell and Bah-Sow, 2006). In advanced stages severe chest pain and sputum containing blood are major symptoms (CDC 2016).

M. tuberculosis disseminated from the lungs can cause extra-pulmonary infection commonly in lymph nodes, pleura, bones, and joints, along with infection in the nervous system, meninges, gastrointestinal, genitourinary and liver (Golden and Vikram, 2005). Whilst chest X-rays are a direct and efficient diagnostic tool to detect pulmonary TB, diagnosis of extra-pulmonary TB is elusive. It is difficult to identify using bacterial culture and acid fast staining techniques. To overcome this a range of novel diagnostic techniques using adenosine deaminase levels and polymerase chain reactions have proven to be useful (Golden and Vikram, 2005).

1.1.5 BCG Vaccine

Attempts to control the disease started more than a century ago with the introduction of the Bacillus Calmette-Guérin (BCG) vaccine. This is an attenuated strain of *Mycobacterium bovis*, developed as a vaccine candidate in 1921 by Albert Calmette and Camille Guérin (Copin *et al.*, 2014). To date, it is the only available vaccine against TB; although protective in children, it has variable efficacy against pulmonary TB, especially in adults (Rodrigues, Diwan and Wheeler, 1993; Colditz *et al.*, 1995; Trunz, Fine and Dye, 2006). Vaccination boosts T cell immunity which is effective against disseminated TB infection, however it is not so effective against pulmonary TB (Colditz *et al.*, 1995). Multiple passages over the years have induced mutations contributing to genetic variability among different strains of BCG (Behr and Small, 1999), resulting in differences in immunogenicity and thus the overall efficacy of different strains of BCG (Lagranderie *et al.*, 2000). Recent advances have shown that differences in culturing conditions and exposure to non-tuberculosis mycobacteria interferes with BCG efficacy

(Venkataswamy *et al.*, 2012). Therefore alternative anti-TB vaccines with better efficacy are currently being explored with sixteen novel TB vaccines in different phases of clinical trials (Davenne and McShane, 2016; Schito et al., 2015).

1.1.6 Diagnosis and Treatment

Once *M. tuberculosis* is inhaled, it is either eliminated by the host defence cells, or contained by alveolar macrophages manifesting in a latent TB infection, or in about 5% of cases host immune cells become overpowered by the bacteria resulting in an acute pulmonary infection. In such cases, TB can be diagnosed either by the traditional smear test examination of sputum for acid-fast bacilli or by histopathological examination for granulomatous formation and by culture. Novel rapid diagnostic tools including molecular techniques such as polymerase chain reaction, DNA probes, and IFN-γ tests provide quick, sensitive and specific tests not only for pulmonary infections, but also for certain forms of extra-pulmonary TB (Golden and Vikram, 2005; Campbell and Bah-Sow, 2006).

Once diagnosed to have chronic pulmonary TB, patients are administered chemotherapy through a combination of first line drugs, isoniazid, rifampicin, pyrazinamide, and ethambutol for two months, after which is isoniazid and rifampicin and continued for another four months (Golden and Vikram, 2005).

1.1.7 Emergence of drug resistant strains and Coinfection with HIV/AIDS

Inadequate or inefficient administration of anti-TB drugs, or interruption of chemotherapy due to side effects and non-adherence of patients, leads to the emergence of drug resistant strains of *M. tuberculosis* (Cole, 1994). Strains of *M. tuberculosis* resistant to at least one of the first line anti-TB drugs are termed drug-resistant TB (CDC 2016); drug-resistant TB resistant to isoniazid and rifampicin, are termed as multi-drug resistant TB strains (CDC, 2016). MDR-TB is treated with a combination of first line drugs and second line drugs, including kanamycin, moxifloxacin, prothionamide, clofazimine, for 4-6 months, followed by two second line drugs with any of the first line drugs for another 5 months. However, with

only a 54% successful treatment rate (WHO, 2016; WHO, 2018). Extensively drug-resistant TB (XDR-TB) is unresponsive to isoniazid and rifampicin, along with fluoroquinolones and any of the second-line anti-TB injectable drugs (amikacin, kanamycin, capreomycin) (CDC, 2016; CDC 2012). This leaves very few treatment options for patients with XDR- TB with successful treatment rates as low as 30% (WHO, 2018). The emergence of totally drug resistant strains of TB (TDR-TB) within the last decade, have made the identification of novel drugs a key priority (WHO 2018).

In 2019, approximately 3.3% of new TB cases and 18% of previously treated cases were reported to be MDR-TB. The highest proportion (more than 50%) of MDR-TB cases were reported in the Soviet Union (Figure 1.3).

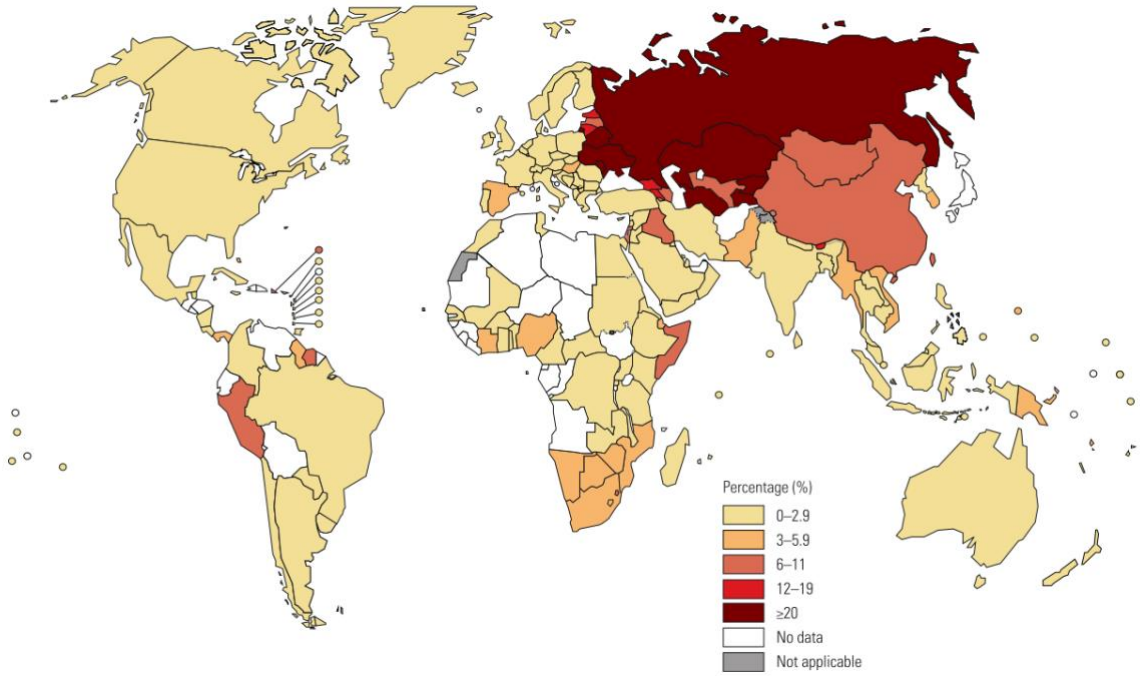

*Figure 1.3**: Global trend of emergence of MDR-TB** (used with permission from (WHO, 2020)).*

Co-infection of *M. tuberculosis* with HIV has exacerbated the situation with TB related deaths in AIDS patients. In 2019, amongst all the TB cases reported, 8.6% were reported in HIV positive patients, with an estimated 251 000 deaths (approximated 20% of total deaths) in patients co-infected with *M. tuberculosis* and HIV (Figure 1.4; WHO, 2020). The World Health Organisation has developed the 'End

TB strategy', however, the 'COVID19 pandemic has reversed these gains and set back the fight against TB by several years' (WHO, 2021).

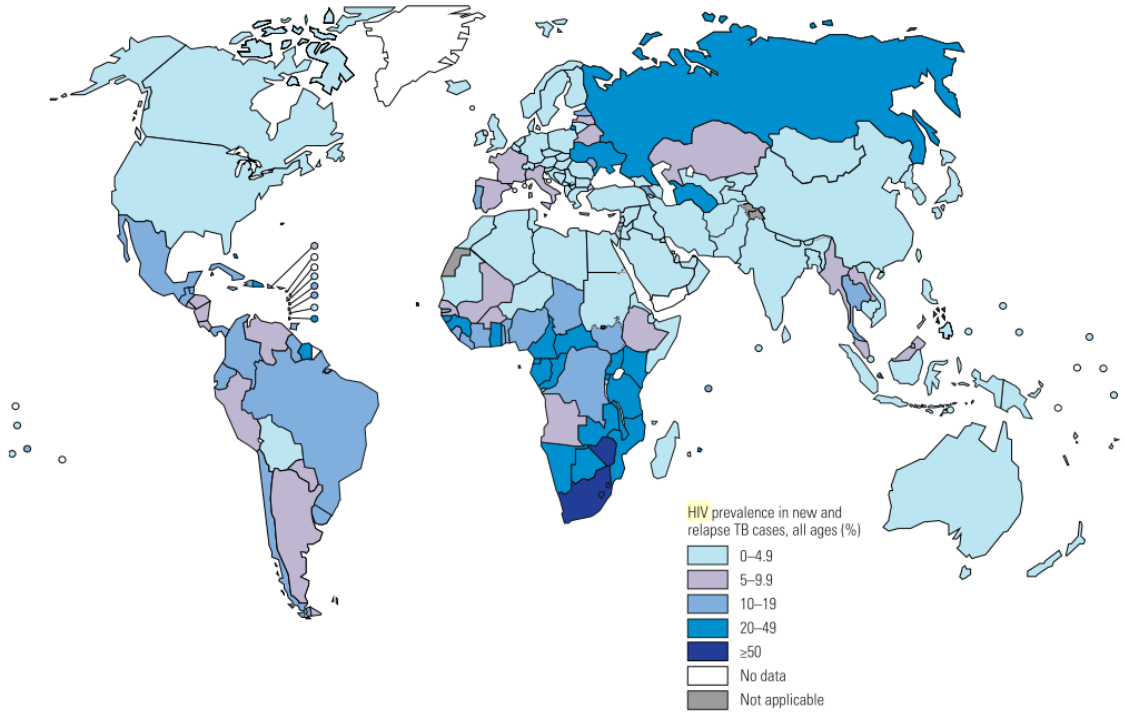

Figure 1.4: ***Percentage of HIV prevalence in new and relapse TB incidences in 2019*** *(used with permission from (WHO, 2020)).*

1.2 Mycobacterial cell envelope

1.2.1 mAGP complex

M. tuberculosis has an elaborate, complex cell envelope, which differs significantly from Gram negative and Gram positive bacteria. This multi-layered structure provides protection against antibiotics as well as against host immune responses (Jankute *et al.*, 2015a). In *M. tuberculosis*, the cytoplasmic membrane is encompassed by an inner layer of peptidoglycan (PG) which is connected by a layer of arabinogalactan (AG) to an outer membrane called the "mycomembrane" (Figure 1.5; Jankute *et al.*, 2015; Alderwick et al., 2015). The inner layer of the mycomembrane includes long chain fatty acids, called mycolic acids

(Bhowruth, *et al.*, 2008; Daffe, 2014). The outer layer of the mycomembrane is highly heterogeneous and species specific, mainly composed of lipids, lipoglycans and proteins essential for virulence and immunomodulation (Marrakchi, Laneelle and Daffe, 2014). The presence of this additional lipid rich layer provides protection against hydrophilic drugs, with a marked increase in hydrophobicity enabling aerosol formation and transmission (Bhowruth, *et al.*, 2008; Daffe, 2014; Jankute *et al.*, 2015; Alderwick et al., 2015).

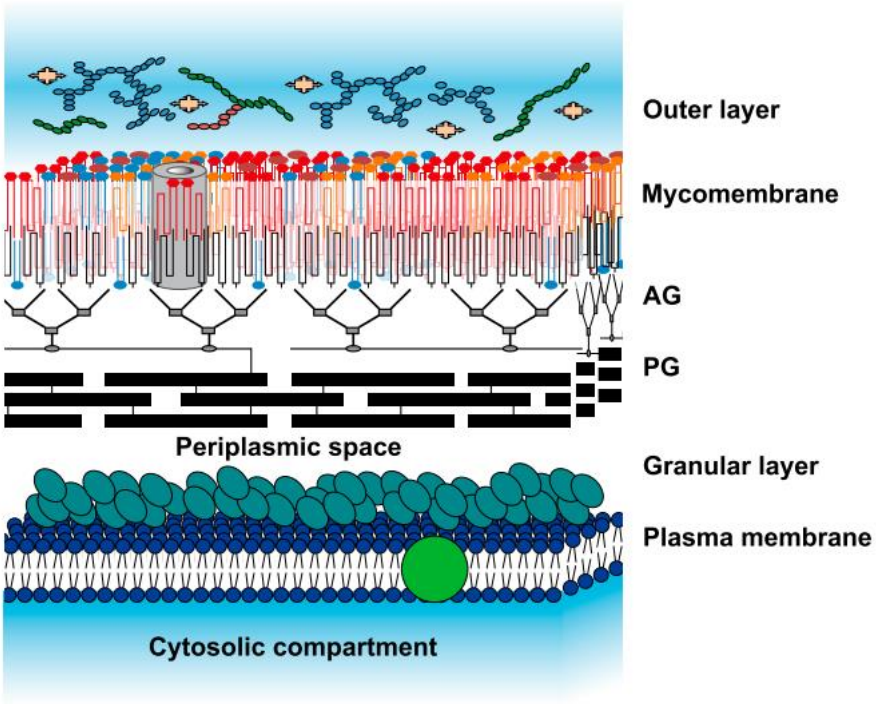

Figure 1.5: ***Overview of the mycobacterial cell envelope****. Plasma membrane is encapsulated by a granular layer. This is followed an extensively cross-linked layer of PG, which anchors a highly branched AG supporting the mycomembrane. The inner leaflet of the mycomembrane is composed of parallelly arranged long chain fatty acids called mycolic acids (in black). Image adapted with permission from (Marrakchi, Laneelle and Daffe, 2014).*

As depicted in Figure 1.5, the major components of the *M. tuberculosis* cell envelope are as follows: 1. an extensively cross-linked peptidoglycan layer; 2. a highly branched arabinogalactan structure; 3. long chain mycolic acids. Together these three biopolymers make up the mycolyl-arabinogalactan-peptidoglycan (mAGP) complex, which provides a protective barrier against anti-TB drugs and host toxic milieu, especially when the bacilli enter the non-replicative stage (Bhowruth *et al.*, 2008; Jankute *et al.*, 2015).

1.2.2 Peptidoglycan

The peptidoglycan (PG) layer is situated immediately outside the plasma membrane, providing a basal structure with rigidity, protecting the cell from osmotic pressure and maintaining its cellular integrity and shape (Schleifer and Kandler, 1972). Approximately. all eubacteria produce a PG layer with alternating repeating units of N-acetylglucosamine and N-acetylmuramic acid residues linked via β (1→4) linkages (Brennan and Nikaido, 1995). However, mycobacterial PG has a modification at the muramic acid residues, which are oxidised to N-glcoylmuramic acid residues (MurNGlyc) (Mahapatra *et al.*, 2005; Raymond *et al.*, 2005). This modification provides potential sites for hydrogen bonding, which is postulated to enhance the overall strength of PG, reducing its susceptibility to lysozyme (Brennan and Nikaido, 1995; Raymond *et al.*, 2005; Jankute *et al.*, 2015b). Linear strands of PG are cross-linked by tetrameric side chain peptides into a layered, mesh-like and honeycomb type structure (Schleifer and Kandler, 1972). These cross-links are significantly higher in *Mycobacterium* species at 70% - 80% as compared to only 50% in *E. coli* with (Lavollay *et al.*, 2008). Another significant difference between mycobacterial PG and the other eubacterial PG's is that it provides a site for attachment of the highly branched arabinogalactan (AG). Approximately, 10% - 12% of the muramyl units are connected at their 6 position to the disaccharide linker unit, α-L-rhamnopyranose-(1→3)-α-D-GlcNAc-(1→P) via a phosphodiester bond (McNeil, Daffe and Brennan, 1990).

1.2.3 Arabinogalactan

Arabinogalactan (AG) is a heteropolysaccharide consisting of arabinose and galactose in the furanoid ring form - D-arabinofuranosyl (Ara*f*) and D-galactofuranosyl (Gal*f*), respectively (McNeil *et al.*, 1987). As summarised in Figure 1.6 the highly branched AG is attached to the PG layer through its galactan domain *via* the linker unit to the C-6 position of MurNGlyc residues (McNeil, Daffe and Brennan, 1990). The galactan component of AG is a linear chain of 30 Gal*f* residues with alternating β (1→5) and β (1→6) linkages. This entire unit is attached to the rhamnosyl residue of the linker unit (Daffe, Brennan and McNeil, 1990). The C-5 position of 8^{th}, 10^{th} and 12^{th} Gal*f* residues on the galactan chain with β (1→6) linkages provide a site of attachment for the highly branched arabinan chain, each containing

around 23 Ara*f* residues (Besra *et al.*, 1995; Alderwick *et al.*, 2005; Lee *et al.*, 2006; Bhamidi *et al.*, 2008). The arabinan domain contains α (1→5) linked D-Ara*f* residues with branching introduced by 3, 5-α-D-Ara*f* residues (Daffe, Brennan and McNeil, 1990). Each AG chain is substituted with either galactosamine (D-GalN) or succinyl substituents at the C-2 position of some of the inner 3, 5-α-D-Ara*f* residues (Draper *et al.*, 1997; Lee *et al.*, 2006; Bhamidi *et al.*, 2008; Peng *et al.*, 2012). One D-GalN residue per AG was identified exclusively in slow growing bacteria and up to three succinyl esters were identified in both slow- and fast-growing bacteria, with no overlapping among substituents (Draper *et al.*, 1997; Lee *et al.*, 2006; Bhamidi *et al.*, 2008; Peng *et al.*, 2012). The non-reducing ends of the arabinan chain terminates with a distinctive hexa-arabinoside, [β-D-Ara*f*-(1→2)-α-D-Ara*f*]$_2$-3,5-α-D-Ara*f*-(1→5)-α-D-Ara*f*; of which two-thirds are esterified with mycolic acids at the C-5 position of the terminal β-D-Ara*f* and the penultimate 2-α-D-Ara*f* residues (McNeil, Daffe and Brennan, 1991).

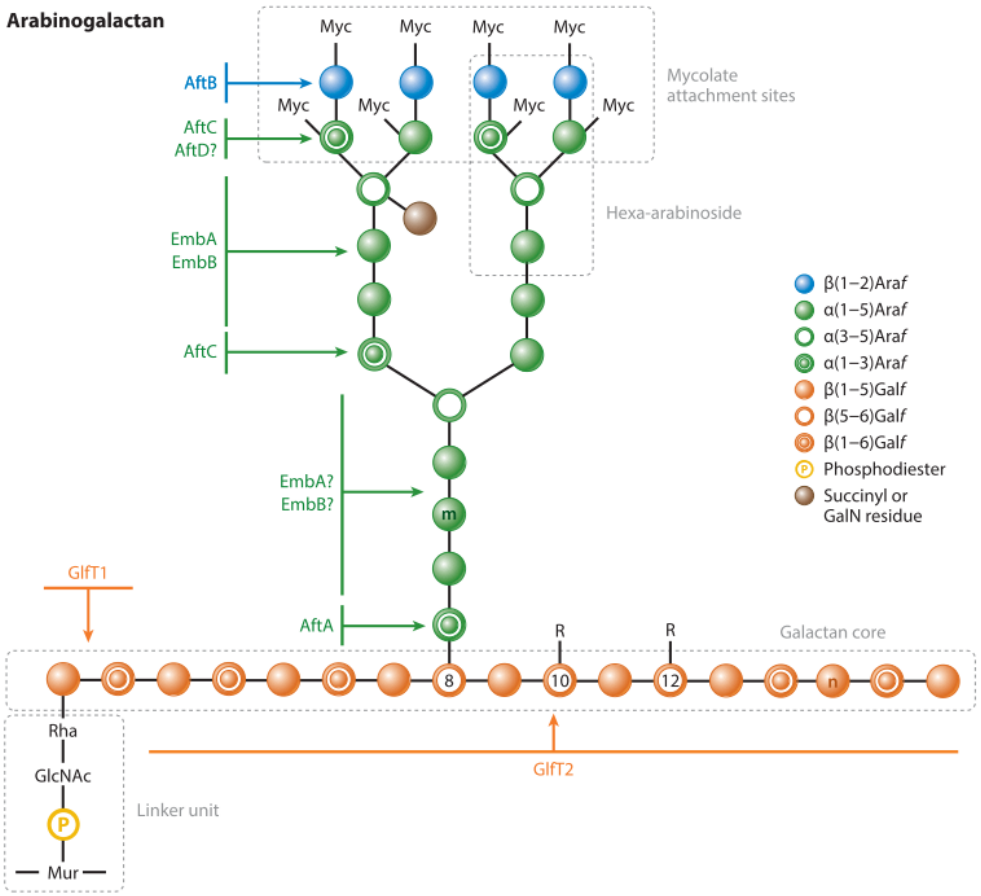

Figure 1.6: ***Structure of the mycobacterial arabinogalactan and roles of key enzymes that are responsible for its biosynthesis****. Image used with permission from (Jankute et al., 2015b)*

1.2.4 Mycolic acids

Mycolic acids (MA) are long chain ($C_{70–90}$) α-alkyl-β-hydroxy fatty acids (Figure 1.7), which form the inner leaflet of the outer mycomembrane (Liu *et al.*, 1996; Daffe, 2014). Mycolic acids confer numerous physiological properties to mycobacteria, including characteristic serpentine like growth and cord formation. They are crucial in biofilm formation and the induction of foamy macrophages in TB granulomas (Arias, Cardona and Prats, 2020). Numerous analytical techniques including thin layer chromatography (TLC) liquid chromatography, mass spectrometry, gas chromatography and nuclear magnetic resonance spectroscopy have enabled elucidation of mycolic acid structure and assembly in the insoluble cell wall skeleton. There are three major types of MAs present in *M. tuberculosis*: α-, methoxy-, and keto- MA. Hydroxy-MA are one of the less abundant forms in *M. tuberculosis* (Watanabe *et al.*, 2001, 2002). They are folded or extended in terms of their physical confirmation providing inherent thickness to the mycomembrane, thus conferring a physical barrier for hydrophilic drugs as well as to the anti-bacterial milieu within macrophages (Jankute *et al.*, 2015b). They are also the primary target to the first- anti-TB drug isoniazid (INH) (Winder and Collins, 1970; Takayama, Wang and David, 1972).

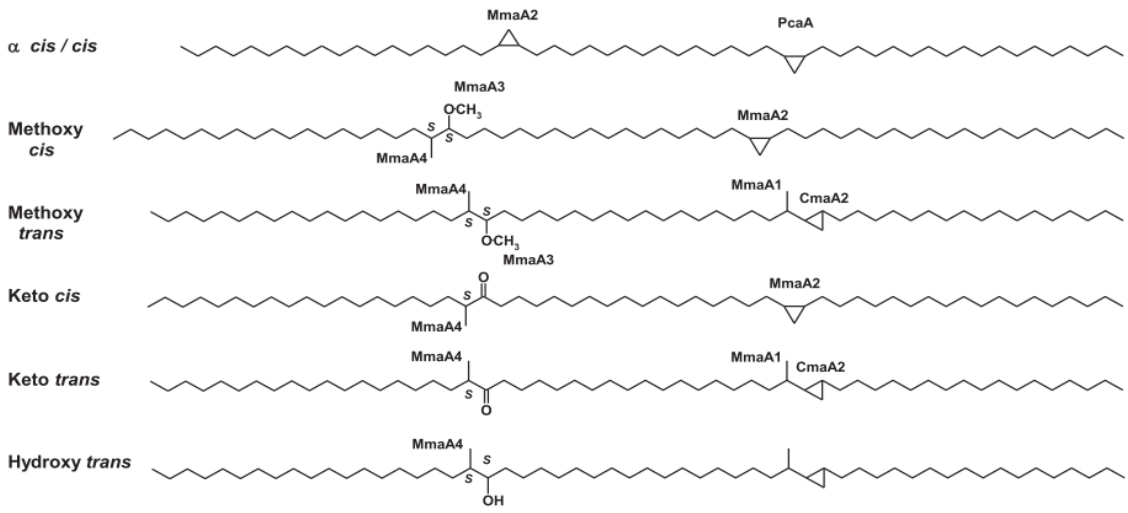

Figure 1.7: ***Structures of mycolic acids in M. tuberculosis along with enzymes involved in cyclopropanation resulting in sterically distinct mero-chains.*** *α-, methoxy, and keto mero chains are either cis or trans (with an adjacent methyl branch). The stereochemistry of the asymmetric carbon atoms in the mero chain is noted (S or R), i.e., carbon bearing methyl, methoxyl, or hydroxyl groups. Image adapted with permission from (Marrakchi, Laneelle and Daffe, 2014).*

1.2.5 LM and LAM

A number of non-covalently linked solvent extractable lipids and lipoglycans intercalate within the cell mAGP wall core and are crucial in pathogenesis (Jankut*e et al*., 2015b; Alderwick et al., 2015). Of these, lipoarabinomannam [LM] and lipoarabinomannnan [LAM] are essential for immune evasion strategies along with the glycerophospholipids - phosphatidylinositol [PI] and the mannosylated forms of PI collectively termed PIMs (Figure 1.8; Nigou *et al.*, 2002; Maeda *et al.*, 2003; Mishra *et al.*, 2011).

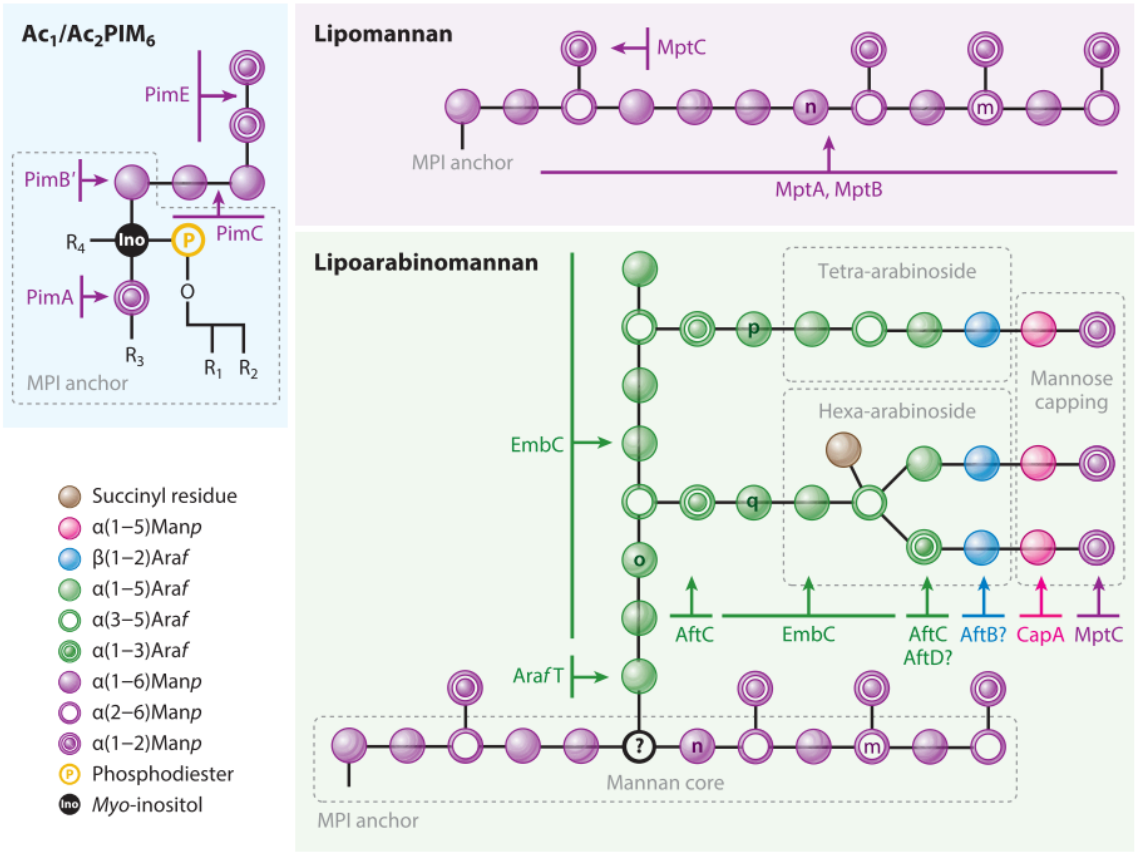

Figure 1.8: ***Structures of phosphatidyl myo-inositol mannoside (PIM), lipomannan (LM) and lipoarabinomannan (LAM), along with the crucial enzymes involved in their biosynthesis****. Image used with permission from (Jankute et al., 2015b)*

LM and LAM are glycosylated end products of PIMs. They are all built on a common mannosyl phosphate inositol anchor, which is a glycero-phosphatidyl-*myo*-inositol. This unit is further glycosylated with two D-mannopyranosyl (Man*p*) residues (Ballou, Vilkas and Lederer, 1963; Ballou and Lee, 1964; Severn *et al.*, 1998; Nigou *et al.*, 2004). These PIMs are then precursors in LAM

biosynthesis, and are composed of a phosphatidyl-myo-inositol (PI) unit, mannosylated with up to six Man*p* residues and acylated at up to four hydroxyl sites (Figure 1.8; (Khoo *et al.*, 1995)). LM and LAM, both possess a PI anchor and a mannan core as shown in Figure 1.8 (Jankute *et al.*, 2015b). The mannan core contains approximately 21 – 34 α (1→6)-linked-Man*p* residues intermittently decorated with 5 – 10 single α(1→2)-Man*p* residues (Chatterjee, Hunter, *et al.*, 1991; Kaur *et al.*, 2008). In terms of LAM, the mannan core is further glycosylated with approximately 55–72 Ara*f* residues. Enzymes similar to those involved in AG biosynthesis are involved in LAM assembly. Henceforth, similar to AG, the arabinan backbone in LAM is made of α (1→5)-linked Ara*f* with residues with branching introduced by 3, 5-α-D-Ara*f* residues, and some of these substituted with succinyl groups (Kaur *et al.*, 2008; Birch *et al.*, 2010). The non-reducing end also terminates in a characteristic fashion, either in a branched hexa-arabinoside {[β-D-Ara*f*-(1→2)-α-D-Ara*f*]$_2$-3,5-α-D-Ara*f*-(1→5)-α-D-Ara*f*]} or with a linear tetra arabinoside [β-D-Ara*f*-(1→2)-α-D-Ara*f*-(1→5)-α-D-Ara*f*-(1→5)-α-D-Ara*f*] (Chatterjee, Bozic, *et al.*, 1991; Chatterjee *et al.*, 1993; McNeil *et al.*, 1994). However, unlike AG, these termini are further decorated with capping moieties. These capping moieties are species-specific. Fast growing mycobacteria, such as *M. smegmatis* contain phosphoinositide caps, termed as PILAM; and slow growing mycobacteria, such as *M. tuberculosis* and *M. leprae* contain mannose capped and termed ManLAM (Chatterjee *et al.*, 1992; Khoo *et al.*, 1995; Nigou, Gilleron and Puzo, 2003). *M. chelonae* has been reported to have no such capping motifs and is termed AraLAM (Gueardel *et al.*, 2002). *M. tuberculosis* ManLAM is said to poses crucial immunomodulatory properties enabling its survival within macrophages (Hamasur, Kallenius and Svenson, 1999; Vignal *et al.*, 2003; Appelmelk *et al.*, 2008; Fukuda *et al.*, 2013).

1.2.6 Arabinofuranosyltransferases

Numerous, yet to be identified glycosyl transferases are responsible for the biosynthesis of the mycobacterial cell wall complex. Arabinofuranosyltransferases (Afts) are among the GT-C superfamily which utilise decaprenyl-monophosphoryl-D-arabinose (DPA) as a sugar donor in assembling the arabinan chains of AG and LAM (Mikusova *et al.*, 2005). So far, seven different Afts have been

identified, which include the Emb proteins - the molecular targets of ethambutol (EMB) (Jankute *et al*., 2015b; Alderwick et al., 2015).

In AG biosynthesis, AftA is responsible for priming the galactan core with the first arabinan residue. Deletion studies in *C. glutamicum* led to the identification that the 8th, 10th, and 12th Gal*f* residues in the galactan domain are primed with singular Ara*f* residues by AftA (Alderwick *et al.*, 2006). Elongation of the arabinan chain is catalysed by EmbA and EmbB through the addition of 30 Ara*f* residues via α (1→5) linkages (Alderwick *et al.*, 2005).

However, in LAM, an unidentified Aft (shown as Ara*f* T in Figure 1.8) is responsible for priming the mannan core (Mishra *et al.*, 2011; Jankute, Grover, *et al.*, 2014) and its elongation is mediated by EmbC through the addition of 12-16 Ara*f* residues, in contrast to EmbAB in AG (Alderwick *et al.*, 2011). Deletion mutants in *M. smegmatis* had altered non-reducing termini, which are the location of MAs in AG and capping motifs in LAM, making the deletion mutants susceptible to anti-TB drugs (Shi *et al.*, 2006; Alderwick *et al.*, 2011). AftC (Rv2673) is crucial for the internal branching of the arabinan chain forming an α(1→3) linkage in both AG and LAM (Birch *et al.*, 2008, 2010). Deletion studies in *M. smegmatis* emphasised AftC's essentiality with complete absence of 3,5-Ara*f* branching residues, rendering the bacilli susceptible to hydrophobic antibiotics rifampicin and chloramphenicol along with EMB (Birch *et al.*, 2008). AftD is proposed to be responsible for the introduction of a second α (1→3) linkage in both AG and LAM (Skovierov *et al.*, 2009). AftB is responsible for the addition of the terminal β (1→2) linkage in AG (Seidel *et al.*, 2007; Jankute, *et al.*, 2014; Jankute *et al.*, 2017), although a similar activity is proposed in LAM.

1.3 Pathogenesis

1.3.1 Life cycle of bacteria within host

Mycobacteria enter the lungs of the host through inhalation. Inhaled bacilli first encounter alveolar resident macrophages, whose intrinsic antimicrobial capacity coupled with mycobacterial virulence determine effective bacterial killing at this stage (Bose Dasgupta and Pieters, 2014). Once mycobacteria overcome this initial destruction, they multiply and disrupt the macrophages. This results in a chemokine mediated attraction of monocytes and other inflammatory cells to the site of infection (Nunes-Alves *et al.*, 2014). These monocytes differentiate into macrophages and ingest mycobacteria without killing them. In this stage they multiply logarithmically with hardly any tissue damage. Two to three weeks post-infection, T cell mediated adaptive immunity develops, resulting in the accumulation of antigen-specific T lymphocytes (BoseDasgupta and Pieters, 2014; Nunes-Alves *et al.*, 2014). These then proliferate within the early lesions or tubercles, releasing pro-inflammatory cytokines including interferon gamma (IFN-γ), resulting in macrophage activation aimed at mycobacterial killing (BoseDasgupta and Pieters, 2014). Consequently, logarithmic bacillary growth stops, and extracellular mycobacterial growth is inhibited and restricted to central solid necrosis in these primary lesions, now termed granulomas. This is followed by one of the following scenarios (Figure 1.9): (a) complete bacterial clearance by the host immune response, (b) survival and proliferation of *M. tuberculosis* within immune cells leading to active disease, (c) immune evasion and latent survival of bacteria with a possibility of reactivation (one-third of the world populations is latently infected with *M. tuberculosis*), (d) hematogenous dissemination resulting in extra-pulmonary TB, which can happen months or years after primary infection upon immune suppression (Crevel, Ottenhoff and Meer, 2002; Kleinnijenhuis *et al.*, 2011; BoseDasgupta and Pieters, 2014; Peddireddy, Doddam and Ahmed, 2017).

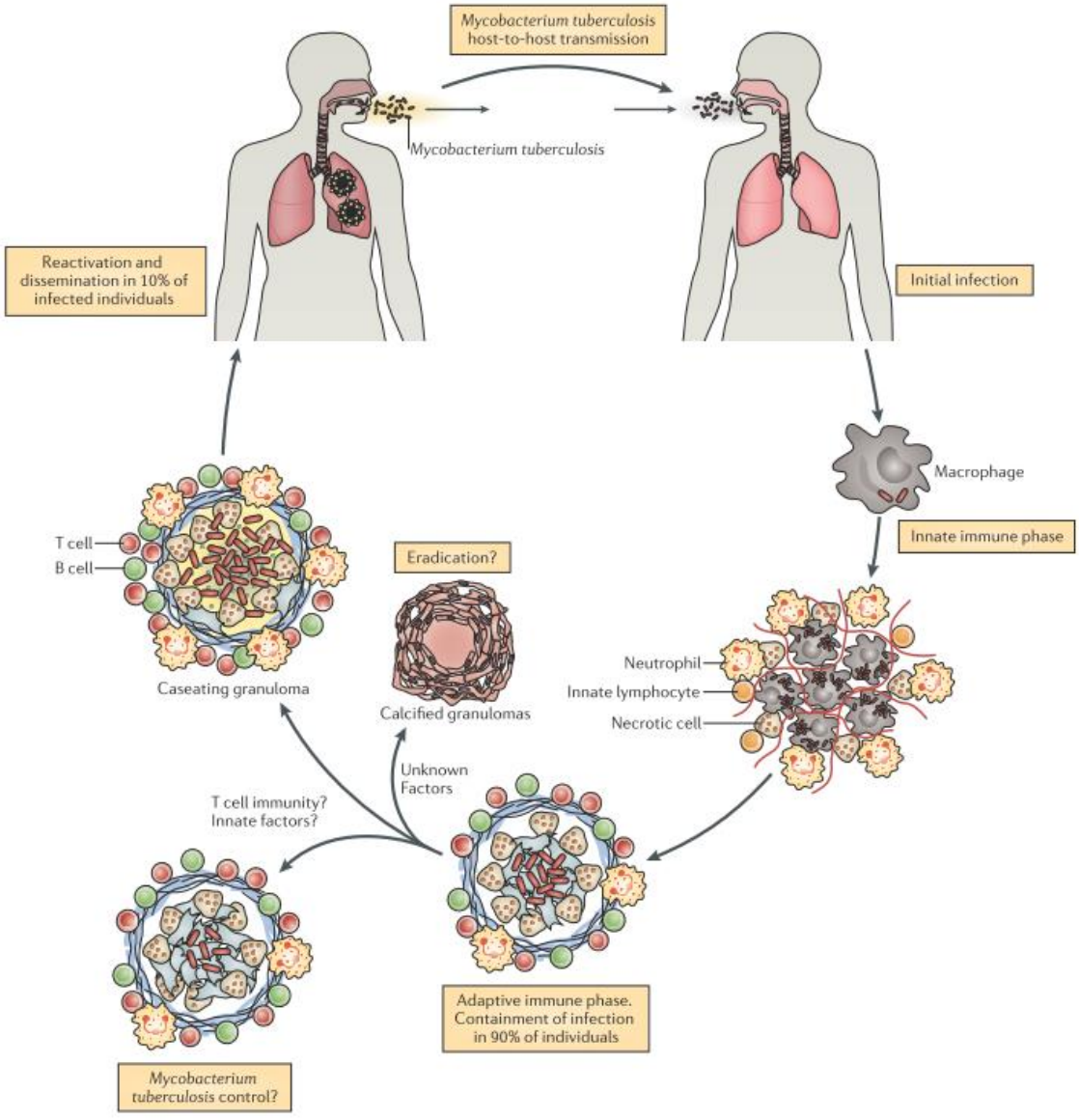

Figure 1.9: ***TB pathogenesis.*** *Inhaled aerosolised mycobacteria infects distal alveolar macrophages. This initiates an innate immune response resulting in the recruitment of inflammatory cells to infection site to limit bacterial growth and dissemination. Antigen presentation to T and B cells in draining lymph nodes leads to T cell priming and expansion of antigen specific lymphocytes initiating adaptive immune response. Recruitment of lymphocytes and activated phagocytes to the site of infection initiates the formation of granulomas which can contain M. tuberculosis. Most infected individuals (about 90%) remain in this latent state of infection, with no clinical symptoms. 5-10% of infected individuals develop active disease where mycobacteria disseminate from the granulomas leading to formation of multiple tubercles. When individuals with active tuberculosis cough, they generate aerosolised mycobacteria that can transmit the infection. Image used with permission from* (Nunes-Alves *et al.*, 2014)

1.3.2 *M. tuberculosis* infection – First line of defence

The tubercle bacillus usually spreads from infected patients via aerosol droplets with a droplet size varying from 0.65 μm to 7.0 μm with an infection dosage of 3 -4 bacilli, which when inhaled causes *M. tuberculosis* infection (Fennelly and Jones-López, 2015). While the larger droplets are trapped in the upper airway leading to tuberculosis of the oropharynx or cervical lymph nodes, smaller droplets reach the lower respiratory tract (Fennelly and Jones-López, 2015), where they are first encountered by the airway epithelial cells (Harriff *et al.*, 2014). These are "non-professional" immune cells which perceive *M. tuberculosis* through their pattern recognition receptors (PRR) stimulating the production of interferon gamma (IFN-γ) and tumor necrosis factor alpha (TNF-α) (Harriff *et al*., 2014). This signals the recruitment of alveolar macrophages which are the first line of defence against *M. tuberculosis*.

These phagocytes recognise the foreign entity through expression of various cell surface receptors through which they bind and internalise *M. tuberculosis*. Once it is internalised, they mount an innate immune response, including the production of pro-inflammatory cytokines (reviewed in (Guirado, Schlesinger and Kaplan, 2013). They also encounter reactive oxygen species, nitric oxide and toxic metals, such as copper and zinc, which are aimed at pathogen clearance, reviewed in (Guirado, Schlesinger and Kaplan, 2013)). Other cells, such as neutrophils, dendritic cells (DC), and natural killer (NK) cells are also attracted to the site of infection to aide alveolar macrophages. *M. tuberculosis* infected NK cells are crucial for their cytotoxic ability, producing anti-bacterial mediators, including granulysin, which mediates lysis of infected cells (Esin and Batoni, 2015). Dendritic cells internalise *M. tuberculosis* and primarily act as antigen presenting cells (APCs) through the major histocompatibility complex class II to T lymphocytes at lymph nodes (Khan *et al.*, 2016). This induces an adaptive immune response and initiates the migration of T and B lymphocytes to the site of infection (Khan *et al.*, 2016). Along with phagocytes, *M. tuberculosis* is internalised by non-phagocytic alveolar endothelial cells as well, including M cells, type I and type II epithelial cells; where infection is initiated and if uncontrolled can spread to various extra-pulmonary sites, with lymphatics and lymph nodes being the main site of extra pulmonary TB before adaptive immunity kicks in (Peddireddy, Doddam and Ahmed, 2017; Bussi

and Gutierrez, 2019). As a slow growing microbe, with a generation time of 20 hours, *M. tuberculosis* has evolved elaborate strategies to evade the immune antimicrobial response resulting in a long-term co-habitation within host cells. This complex and elaborate interplay between innate and adaptive immune responses decides the fate of mycobacterial clearance (Figure 1.10).

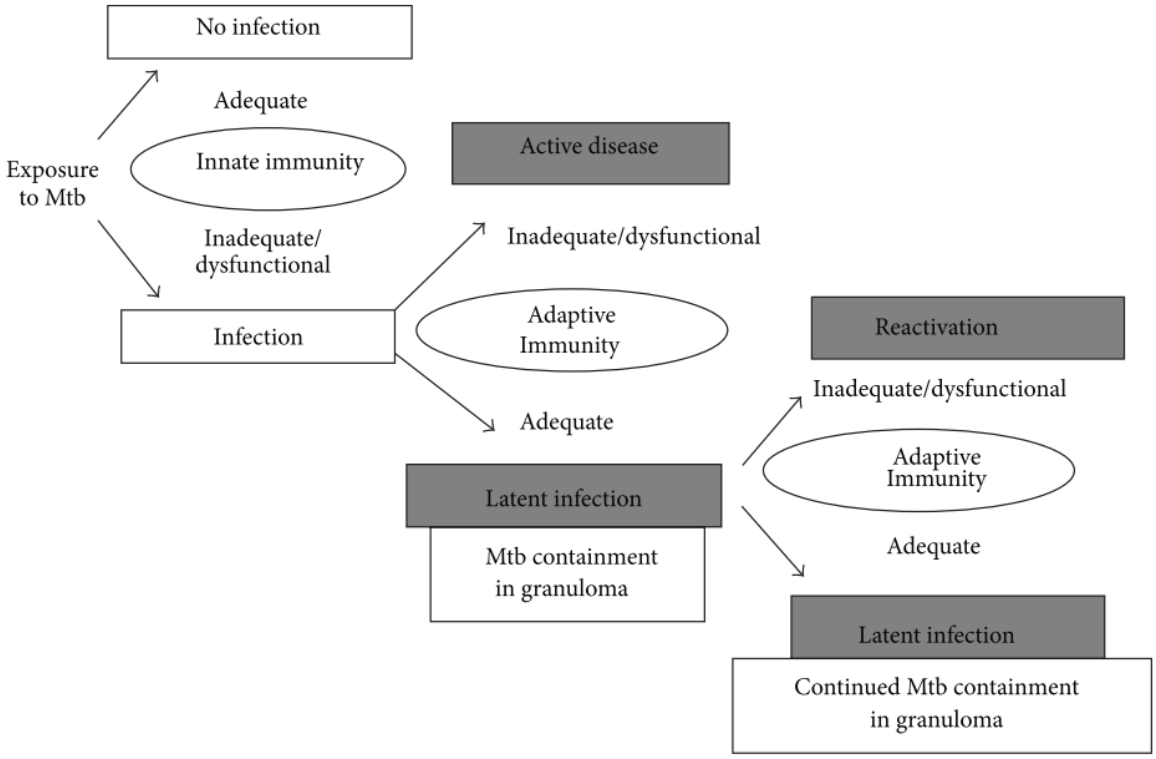

Figure 1.10: ***Role of Innate and Adaptive immunity in Pathogenesis of M. tuberculosis.*** *In majority of people adequate innate immunity prevents mycobacterial infection. In case of inadequate innate immunity, adequate adaptive immunity restricts mycobacteria in granuloma resulting in latent mycobacterial infection. Inadequate adaptive immunity causes active TB and reactivation of latent TB. Image used with permission from* (Hossain and Norazmi, 2013)

1.3.3 Immune recognition of *M. tuberculosis* during phagocytosis

The mycobacterial cell wall displays various ligands – called pathogen associated molecular patterns (PAMPs), which are recognised by a large repertoire of pattern recognition receptors (PRRs) on the surface of phagocytes (Bose Dasgupta and Pieters, 2014). This recognition triggers the production of various pro-inflammatory cytokines aimed at mycobacterial clearance (Hossain and Norazmi, 2013). Cellular receptors involved in the endocytosis of *M. tuberculosis* include Toll-like receptors (TLRs), complement receptors (CRs), mannose receptor s(MRs), scavenger receptors (SRs), C-type lectins, such

as dendritic cell specific intercellular adhesion molecule (ICAM)-3 grabbing nonintegrin (DC-SIGN), Fc receptor and CD-14 receptor (Figure 1.11; Pieters, 2008; Schäfer *et al.*, 2009). Of these, the TLRs are the major contributors of *M. tuberculosis*-induced macrophage activation and cytokine production in phagocytes (Saraav, Singh and Sharma, 2014).

TLRs are expressed abundantly on the cell membrane of macrophages, dendritic cells and APCs, recognise a variety of mycobacterial components and facilitate the induction of adaptive immune response (Visintin *et al.*, 2001). These transmembrane proteins interact with PAMPs through their leucine rich motifs in the extracellular domain (Visintin *et al.*, 2001). This interaction, aided by the adapter molecule – myeloid differentiation factor 88 (MyD88) triggers numerous signalling pathways, which are initiated by the recruitment of interleukin-1 (IL-1) receptor associated kinase (IRAK), TNF receptor associated factor (TRAF) 6, transforming growth factor (TGF)-β-activated protein kinase (TAK) 1 and mitogen-activated protein kinases (MAPKs) at their cytoplasmic domain (Visintin *et al.*, 2001; Goldberg, Saini and Porcelli, 2013; Hossain and Norazmi, 2013). Subsequently, transcription factors including, activator protein 1 (AP-1) and nuclear factor κB (NFκB; (Kawai and Akira, 2006)) are activated and translocated into the nucleus, which then initiate an innate immune response, mainly through production of pro-inflammatory cytokines, TNF-a, IL-1, IL-12 along with nitric oxide (Medzhitov and Janeway, 1998; Takeda and Akira, 2005; Akira, Uematsu and Takeuchi, 2006). In addition, to the MyD88-dependent pathway, TLR4 is involved in the MyD88-independent pathway, aided by Toll/IL-1R (TIR) domain- containing adapter, which is essential for autophagy and phagosome – lysosome fusion, the crucial anti-mycobacterial defence strategy (Hossain and Norazmi, 2013).

Amongst, the 12 mammalian TLRs, TLR2 in association with TLR1 and TLR6 is involved in the recognition of mycobacterial lipoproteins and glycolipids - LM, LAM and PIMs (Means *et al.*, 1999; Jones *et al.*, 2001; Thoma-uszynski *et al.*, 2001; Saraav, Singh and Sharma, 2014). A Few other lipoproteins and mycobacterial DNA are recognised by TLR4 and TLR9, respectively (BoseDasgupta and Pieters, 2014; Saraav, Singh and Sharma, 2014).

Once recognised and internalised, mycobacteria are stored in endocytic compartments – where they are deprived of nutrients (Saraav, Singh and Sharma, 2014). These endosomes then mature to phagosomes which subsequently fuse with lysosomal compartments where mycobacteria is degraded (Hossain and Norazmi, 2013). Interestingly, diverse ligands on mycobacteria can engage different receptors simultaneously and the receptor involved in phagocytosis can affect the downstream signalling and phagosomal fate irrespective of other phagosomes within the same cell (Bussi and Gutierrez, 2019).

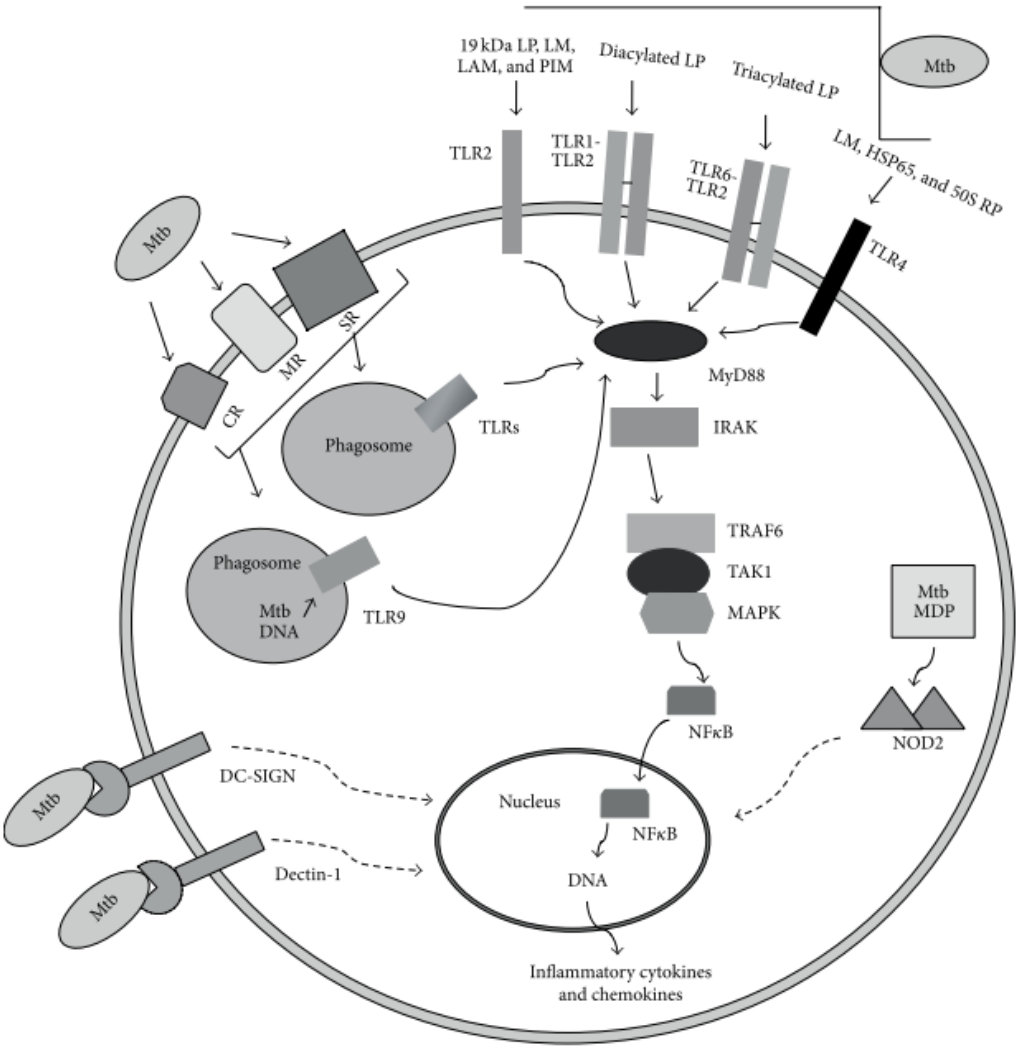

Figure 1.11: ***Immune recognition of M. tuberculosis during phagocytosis****. PRRs on phagocytes recognise PAMPs on mycobacteria. TLR2 recognises 19 kDa LP, LM, LAM. TLR1-TLR2 and TLR6-TLR2 heterodimers bind to diacylated and triacylated LP, respectively. TLR4 binds to LM, heat shock protein 65 (HSP65), and 50S ribosomal protein (50S RP). TLR9 recognises mycobacterial DNA. CR phagocytose opsonised M. tuberculosis and MR and SR phagocytose non-opsonised M. tuberculosis. TLR signalling is carried by MyD88-dependent signalling cascade resulting in NF-kB mediated production of inflammatory molecules. TLRs are expressed on phagocytic cell surface and in phagosomes. Image used with permission from (Hossain and Norazmi, 2013).*

1.3.4 Pro-inflammatory cytokines

Cytokines are small soluble proteins, produced by all nucleated cells, which can influence the activity of other cells to maintain the body's homeostasis (Domingo-Gonzalez *et al.*, 2016). Mycobacterial recognition triggers cytokines which aide in increasing their levels through a series of complex regulation and cross-regulation processes. Pro-inflammatory cytokines, as the name suggests, are responsible for inflammatory response aimed at bacterial clearance. Some of the crucial pro-inflammatory cytokines involved in *M. tuberculosis* infection are TNF-α, IFN-γ, IL-1, IL-12, IL-18, IL-6, IL-17 and IL-23 (Table 1.1; Domingo-Gonzalez *et al.*, 2016).

TNF-α is a crucial pro-inflammatory cytokine with immunomodulatory properties, essential for macrophage activation upon mycobacterial stimulation (Orme and Cooper, 1999). Although, initially produced by monocytes, macrophages and dendritic cells (Henderson, Watkins and Flynn, 1997), TNF-α produced by CD4 and CD8 T cells is important in limiting the bacterial burden through granuloma formation (Kindler and Grau, 1989; Lin *et al.*, 2007). TNF-α deficient mice have succumbed to mycobacterial infection within 2-3 weeks, with increased bacterial burden and dissemination to the central nervous system (Tsenova *et al.*, 1999) and defective granuloma formation (Flynn *et al.*, 1995). TNF-α is crucial in the expression of chemokines, whose receptors are expressed on both innate (macrophages and neutrophils) and adaptive (T and B cells) immune cells, aiding their recruitment to the site of infection, thus enabling granuloma formation and bridging the innate and adaptive immune systems (Farber, 1997; Cole *et al.*, 1998; Griffith, Sokol and Luster, 2014).

IFN-γ is another key regulator of protective immunity against *M. tuberculosis* infection. It is responsible for macrophage activation and intracellular control of the pathogen through phagosome – lysosome fusion, nutrient lockout, production of reactive oxygen and nitrogen species and rapid acidification of the phagosome (Mosmann *et al.*, 1986; Nagabhushanam *et al.*, 2003; Kalupahana *et al.*, 2005; Kawai and Akira, 2006; Hossain and Norazmi, 2013; Nunes-Alves *et al.*, 2014; Zhu *et al.*, 2018). Abnormalities in IFN-γ production in humans is associated with increased susceptibility to mycobacterial disease and Mendelian susceptibility to mycobacterial disease (Filipe-Santos, Bustamante, Chapgier, *et al.*, 2006;

Zhang *et al.*, 2008). Similarly, HIV infected patients with defects in T lymphocytes and insufficient IFN-γ levels readily develop TB. Knock out studies in mice have also shown that disruption of IFN-γ or its receptors results in disseminated *M. tuberculosis* infection in both low aerosol dose and intravenous infection with poor macrophage activation and exacerbated granulocytic inflammation (Cooper *et al.*, 1993; Dalton *et al.*, 1993; Flynn *et al.*, 1993).

IFN-γ production is tightly regulated by IL-12 (Feng *et al.*, 2005) and IL-18 (Schneider *et al.*, 2010), mice with defects in either of these showed increased mycobacterial dissemination and reduced survival. IL-1 is another crucial pro-inflammatory cytokine as mice lacking it were susceptible to chronic mycobacterial infection (Mayer-Barber *et al.*, 2011). IL-23 is another essential cytokine which belongs to IL-12 family, and drives the double expression of IL-17 and IFN-γ (Hirota *et al.*, 2011). IL-17 is essential for neutrophil and lymphocyte accumulation at the granulomatous region (Umemura *et al.*, 2007), downregulation of anti-inflammatory IL-10 cytokine (Gopal *et al.*, 2012) and IL-12 mediated induction of IFN-γ, which is especially important in virulent strains of *M. tuberculosis* (Umemura *et al.*, 2007; Gopal *et al.*, 2012). IL-23 knock-out mice display insufficient B cell generation and differentiation in response to the complete absence of IL-17 (Khader *et al.*, 2011). This is also accompanied by lymphocyte accumulation around blood vessels rather than within the granulomatous region (Khader *et al.*, 2011). IL-22 is another Il-23 dependent cytokine involved in intracellular growth control of *M. tuberculosis* in human monocyte derived macrophages by promoting phagolysosomal fusion (Dhiman *et al.*, 2014). IL-6 is another crucial pro-inflammatory cytokine in the absence of which mice have an increased susceptibility to *M. tuberculosis* infection (Appelberg *et al.*, 1994; Ladel *et al.*, 1997). The above highlights the complex interplay between different cytokines upon mycobacterial stimulation to limit bacterial dissemination (summarised in Table 1.1).

Table 1.1: ***Crucial pro-inflammatory cytokines produced during M. tuberculosis infection*** *(Domingo-Gonzalez et al., 2016)*

Cytokine	**Secreted by**	**Function**	**Reference**
TNF-α	Macrophages, lymphocytes, mast cells, endothelial cells and fibroblasts	Mycobacterial clearance; macrophage activation; chemokine mediated attraction of innate and adaptive cells; granuloma formation	(Kindler and Grau, 1989; Flynn *et al.*, 1995; Wajant, Pfizenmaier and Scheurich, 2003)
IFN-γ	Phagocytes, antigen-specific T cells, α/β T cells, $CD4^+$ and $CD8^+$ T cells,	Phagocytes activation; chemokine mediated T cell migration; granuloma formation; and mycobacterial clearance	(Mogues *et al.*, 2001; Serbina, Lazarevic and Flynn, 2001; Green, DiFazio and Flynn, 2013)
IL-6	Lymphoid and non-lymphoid cells in response to IL-1, TNF-α and IFN-γ	Pleiotropic cytokine involved in differentiation; proliferation and apoptosis in potentiating immunity during *M. tuberculosis* infection	(Sanceau *et al.*, 1989; Van Snick, 1990; Appelberg *et al.*, 1994; Ladel *et al.*, 1997)
IL-1α and β	All nucleated cells including endothelial cells, monocytes, macrophages, neutrophils, and dendritic cells	Recruitment and coordination of pro-inflammatory response; prostaglandin E2 mediated inhibition of permissive macrophages at the site of infection to maintain bactericidal phagocytes to promote bacterial clearance	(Dinarello, 1991; Desvignes, Wolf and Ernst, 2012; Guo *et al.*, 2014)
IL-18	All nucleated cells including endothelial cells, monocytes, macrophages, neutrophils following stimulation by caspase-1, IL-4 or IFN-γ	Essential for optimal IFN-γ induction during TB; regulation of phagocyte accumulation mirroring IL-1	(Dinarello, 1991; Bohn *et al.*, 1998; Marshall *et al.*, 1999; Schneider, Bianca *et al.*, 2010)

Cytokine	Secreted by	Function	Reference
IL-12	Macrophages, dendritic cells, and B cells	Crucial for stable and prolonged IFN-γ production to limit long-term bacterial growth; facilitate dendritic cell migration to draining lymph nodes to prime naïve T cells as antigen specific T cells	(Ma and Trinchieri, 2001; O'Shea and Paul, 2002; Feng *et al.*, 2005; Khader *et al.*, 2011)
IL-23	Macrophages and dendritic cells	Stabilises the induction of TH17 cell subset (which produces IL-17 family of cytokines) along with transforming growth factor β (TGFβ) and IL-6; required for double expression of IL-17 and IFN-γ	(Weaver *et al.*, 2007; Hirota *et al.*, 2011; Domingo-Gonzalez *et al.*, 2016)
IL-17	Lung-resident γδ T cells, other lymphocytes and innate immune cells	Down regulation of anti-inflammatory IL-10 production, thereby promoting IL-12 mediated IFN-γ production to enhance mycobacterial clearance	(Lockhart, Green and Flynn, 2006; Gopal *et al.*, 2012)
IL-22	$CD4^+$ T cells, γδ T cells, NK cells and innate lymphoid cells	Regeneration and survival of the intestinal, airway and external epithelium; stimulates the secretion of antimicrobial peptides including lipocalin and β-defensins; promotes macrophage activation and phagolysosomal fusion	(Dhiman *et al.*, 2009, 2014; McAleer and Kolls, 2014)

1.3.5 Anti-inflammatory cytokines

Pro-inflammatory responses are antagonised by a set of anti-inflammatory responses (Table 1.2), which act by either inhibiting their production or undermining their responses (Domingo-Gonzalez *et al*., 2016). Three anti-inflammatory cytokines, IL-4, IL-10 and transforming growth factor β (TGF-β), are of special importance with respect to TB and each of these are stimulated by one or more mycobacterial antigens (Domingo-Gonzalez *et al*., 2016).

Mycobacterial LAM induces IL-10 in macrophages and DCs (Dah*l et al*., 1996). IL-10 antagonises the pro-inflammatory responses of IFN-γ hindering phagosome maturation and macrophage activation. It also downregulates the production of crucial inflammatory cytokines - IFN-γ, TNF-α, and IL-12 in macrophages (Oswald *et al.*, 1992; O'Leary, O'Sullivan and Keane, 2011). In DCs it interferes with antigen presentation and T cell priming (Copin *et al.*, 2014). High levels of IL-10 were also observed in patients with pulmonary TB with an increased bacterial burden (Eum *et al.*, 2008; Kumar *et al.*, 2015). Some reports using knockout-mice have shown the role of IL-10 with increased bacterial burden (Redford, Murray and O'Garra, 2011), this hasn't been confirmed; however, the correlation between virulent strains and IL-10 induction has been confirmed (Erb *et al.*, 1998).

TGF-β is another regulatory anti-inflammatory cytokine, with a negative role in context of *M. tuberculosis* infection (Hirsch *et al.*, 1994). It is produced by macrophages and dendritic cells, upon stimulation with mycobacterial antigens, especially LAM (Dahl *et al.*, 1996). TGF-β inhibits T-cell mediated immunity, affecting their proliferation and anti-bacterial activity (Hirsch *et al.*, 1997). It also induces IL-10 and synergises with it in the suppression of IFN-γ production and macrophage activation (Othieno *et al.*, 1999), thereby promoting intracellular survival of *M. tuberculosis* (Hirsch *et al.*, 1994). Increased levels of TGF-β in blood monocytes has been observed in TB patients (Toossi *et al.*, 1995).

IL-4 is a pleiotropic cytokine having variable association with disease profile. It promotes intracellular mycobacterial survival in conjugation with TGF-β and IL-10 (Lucey, Clerici and Shearer, 1996). Although, it is associated with disease progression and reactivation of latent infection (Howard and

Zwilling, 1999), knock out studies showed normal levels of infection rather than decreased susceptibility to mycobacterial infection in mice (Erb *et al.*, 1998), with a further study showing increased granuloma and mycobacterial outgrowth (Sugawara *et al.*, 2000). This was accompanied with excessive pro-inflammatory cytokine levels and tissue damage (Sugawara *et al.*, 2000). Hence, the definitive role of IL-4 is yet to be confirmed with respect to TB pathogenesis.

IL-5 and IL-13 are other regulatory cytokines which promote intracellular mycobacterial growth, while resolving tissue inflammation by suppressing inflammatory cytokines (Lucey, Clerici and Shearer, 1996). Although, limited information is available on the role of IL-5 during *M. tuberculosis* infection, disrupted $CD4^+$ T cell levels were observed in non-human primates upon coinfection with the Simian Immunodeficiency Virus (SIV; (Mosman*n et al.*, 1986; Killar *et al.*, 1987; Diedrich, Mattila and Flynn, 2013)). IL-13 on the other hand is another potent inhibitor of pro-inflammatory cytokines, preventing autophagy and IFN-γ mediated *M. tuberculosis* killing (Ying *et al.*, 1997; Gessner, Mohrs and Mohrs, 2005; Harris *et al.*, 2007).

Although, pro-inflammatory cytokines are essential in pathogen removal, unrestrained inflammatory responses can result in tissue damage as seen in IL-4 knock-out mice (Sugawara *et al.*, 2000). Also, pre-disposed anti-inflammatory responses can interfere with inflammatory responses favouring intercellular bacterial survival (Howard and Zwilling, 1999). Hence a balance of pro-inflammatory and anti-inflammatory responses is essential to limit bacterial outgrowth.

Table 1.2: ***Crucial anti-inflammatory cytokines produced during M. tuberculosis infection*** *(Domingo-Gonzalez et al., 2016)*

Cytokine	**Secreted by**	**Function**	**Reference**
IL-10	T_{REG} and T_H2, macrophages, some dendritic cell subsets, myeloid derived suppressor cells, B cells and neutrophils	In macrophages - inhibits IFN-γ mediated macrophage activation; block phagosome maturation and promotes mycobacterial growth and survival within phagosomes. In DCs - inhibits antigen presentation; IL-12 production and DC trafficking to lymph nodes for T cell priming	(Vieira *et al.*, 1991; Oswald *et al.*, 1992; O'Leary, O'Sullivan and Keane, 2011; Redford, Murray and O'Garra, 2011)
TGFβ	All leukocytes - lymphocytes, macrophages, monocytes, dendritic cells	Inhibits both T cell responses and anti-bacterial activity; Induces IL-10 and synergises in suppression of IFN-γ production; promotes intracellular mycobacterial survival	(Massague, 1990; Hirsch *et al.*, 1997; Letterio and Roberts, 1998; Othieno *et al.*, 1999)
IL-4	T_H2 T cells	Promotes intracellular mycobacterial survival	(Mosmann *et al.*, 1986; Mazzarella *et al.*, 2003; Bezuidenhout *et al.*, 2009; Killar *et al.*, 2021)
IL-5	T_H2 T cells	Disrupts $CD4^+$ T cell levels during coinfection with HIV	(Mosmann *et al.*, 1986; Killar *et al.*, 1987; Diedrich, Mattila and Flynn, 2013)

Cytokine	Secreted by	Function	Reference
IL-13	T_H2 T cells, invariant NK T cells (iNKT), granulocytes (e.g. basophils, eosinophils, and mast cell), murine group 2 innate lymphoid cells (ILC2s)	Inhibits pro-inflammatory cytokine production; inhibits autophagy and IFN-γ induced autophagy-mediated killing of *M. tuberculosis*	(Ying *et al.*, 1997; Gessner, Mohrs and Mohrs, 2005; Harris *et al.*, 2007)

1.3.6 JAK/STAT signalling and SOCS proteins

The Janus kinase (JAK) signal transducer and activator of transcription (STAT) pathway is an evolutionarily conserved signalling pathway, whereby external factors including diverse cytokines, interferons, growth factors, hormones and related molecules control gene expression (Murray, 2007; O'Shea and Murray, 2008; O'Shea et al., 2015). It provides a direct communication from transmembrane receptors to the nucleus. All the major cytokines mediate their signalling through JAK/STAT molecules.

JAK/STAT signalling is regulated by a family of cytokine inducible intracellular proteins called suppressor of cytokine signalling (SOCS) molecules and cytokine-inducible SRC homology 2 (SH2)-domain-containing proteins (CIS). They are generally induced by cytokines and act in a negative feedback loop to regulate the quality and quantity of STAT signals from cytokine receptors to inhibit excessive cytokine signalling and maintain tissue homeostasis (Hanada and Yoshimura, 2002; Kubo, Hanada and Yoshimura, 2003; Yoshimura, Naka and Kubo, 2007; Yoshimura et al., 2012; Chikuma et al., 2017). There are 8 members in the CIS/SOCS family (CIS and SOCS1-SOCS7), each of which has a characteristic central SH2 domain and a 40 amino acid long SOCS box (after which they are named) in their carboxy terminal (Yoshimura *et al.*, 2012). Through SOCS box these proteins recruit elongin BC, cullin-5 and RING-box-2 (RBX2) resulting in the recruitment of of E2 ubiquitin transferase and subsequent unibuitination of associated proteins (Kamura *et al.*, 2004).

Mycobacteria induce premature upregulation of SOCS proteins, especially SOCS1 and SOCS3 resulting in inhibition of IFN-γ responses, thereby promoting intracellular mycobacterial survial (Carow *et al.*, 2011; Masood *et al.*, 2013). SOCS1 and SOCS3 have a unique kinase inhibitory region (KIR) which is hypothesised to be crucial for their action (Kubo, Hanada and Yoshimura, 2003). They affect the phosphorylation and activation of STAT1, thereby preventing the transcription of IFN-γ responsive genes (Lee *et al.*, 2017). $SOCS1^{-/-}$ improved mycobacterial clearence in IFN-γ dependent manner (Carow *et al.*, 2011).

1.3.7 Granuloma formation

Granuloma is a hallmark structure of TB, it is an "immune microenvironment" to control infection (Mira*nda et al*., 2012). In this, mycobacteria phagocytosed mature macrophages form a compact organised aggregate to restrict and eradicate *M. tuberculosis* (Ramakrishnan, 2012; Ehlers and Schaible, 2013).

The discovery of granulomatous structures predates that of the aetiological agent responsible for TB (Ramakrishnan, 2012). They were originally called "tubercles" and were thought to cause tuberculosis (Sylvius, 1679). Although, this notion was quickly dismissed and granulomas were thought to curtail pathogen proliferation and dissemination, there has always been an ambiguity on the role of granulomas in context of TB. Recent reports suggest that granulomas provide a replicative niche for mycobacteria, enabling it to modulate immune response to ensure its long-term survival (Miranda *et al.*, 2012; Ramakrishnan, 2012; Ehlers and Schaible, 2013).

Recent advances in live cell imaging and microscopy has shed light on the dynamic events in granuloma formation, especially using optically transparent zebrafish (*M. marinum* causes granulomatous infection - histologically similar to TB in fish and therefore provides the advantage of natural host-pathogen pair comparisons (Ramakrishnan, 2012)). They revealed the cellular arrangement, mechanism, and consequences of granuloma formation.

After aerosol inhalation, mycobacteria are phagocytosed by alveolar macrophages, these cells even in events when they fail to kill the bacteria produce chemoattractants to recruit neutrophils, monocyte-derived macrophages, NK cells and γδ-T cells (Feng *et al.*, 2006; Lockhart, Green and Flynn, 2006; Eum *et al.*, 2010). These cells work together to promote inflammation, tissue remodelling and macrophage maturation (Feng *et al.*, 2006; Lockhart, Green and Flynn, 2006; Eum *et al.*, 2010). Mature macrophages have increased cytoplasmic cell size, a larger number of organelles and ruffled cell membranes – all these changes render them more phagocytic and microbicidal (Dannenberg, 1968; Adams, 1974; Bouley *et al.*, 2001). They undergo further changes to form multinucleated giant cells (multiple cells fuse into one cell); (Helming and Gordon, 2008)), foamy cells (characterised by lipid

accumulation; (Peyron *et al.*, 2008)) and epithelioid cells (they have interlocked cell membranes that link adjacent cells in a zipper like fashion; (Adams, 1974)). Simultaneously, DCs activate T cells at regional lymph nodes which are then recruited by chemoattractants to the site of infection (Khan *et al.*, 2016). Activated T cells constitute 15 to 50% of the granulomatous structure, of which 60-70% are $CD4^+$, 15-30% are $CD8^+$ α/β and about 2% γ/δ T cells (Tsai *et al.*, 2006). NK T cells and B cells are also present in granulomas surrounding the central macrophages (Apostolou *et al.*, 1999; Maglione, Xu and Chan, 2007). With the recruitment of activated lymphocytes, the granuloma becomes fully organised with mycobacteria phagocytosed macrophages at the centre (Figure 1.12). Granuloma formation is much more dynamic with continuous cell death, cellular replenishment and vascular and tissue remodelling influenced by the host, pathogen and environmental factors (North and Jung, 2004).

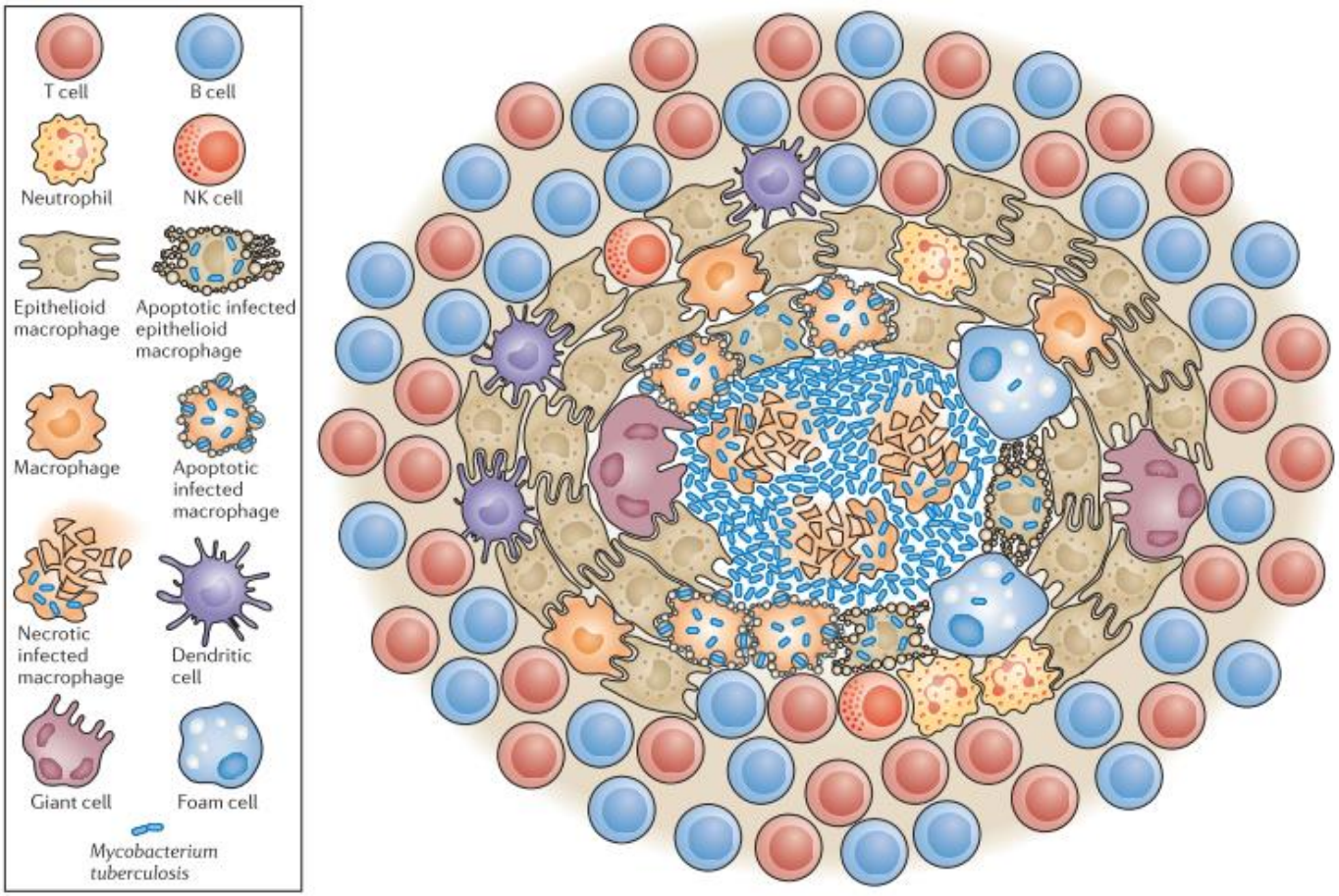

Figure 1.12: ***Cellular arrangement within tuberculous granuloma****. Compact, organised epithelioid granuloma is formed during M. tuberculosis infection. Epithelioid macrophages form a tightly interdigitate cell membrane linking with the adjacent cells that barricading the central necrotic region and mycobacteria phagocytosed macrophages (along with giant cells and foamy cells). Dendritic cells act as antigen presenting cells priming T and B lymphocytes. Neutrophils and NK cells are also present in granulomas. Image used with permission from (Ramakrishnan, 2012)*

1.3.8 Mycobacterial dissemination and transmission from granuloma

Apoptosis and necrosis are pre-dominant in cell death pathways observed in human TB granulomas (Figure 1.13). Traditionally apoptosis is thought to be detrimental to mycobacteria, in contrast to necrosis which favours bacterial growth (Behar *et al.*, 2011). However, both types of cell death can promote bacterial proliferation under certain circumstances, but inhibit them under other conditions (Ramakrishnan, 2012).

Macrophage necrosis results in the formation of a caseating granuloma (Shammari *et al.*, 2015). Caseating lesions in early granulomas are associated with increased bacterial numbers and are growth promoting. On the contrary, in mature granulomas a 'hard' caseum with sparse bacteria due to onset of adaptive immunity is observed (Davis and Ramakrishnan, 2009). Upon macrophage necrosis, mycobacteria are released into the extracellular environment where it can grow even more exuberantly than within macrophages (Ramakrishnan, 2012). Once mycobacteria are released into the extracellular milieu it can disseminate to other areas of the lung and can also cause extrapulmonary infections.

Contrary to necrosis, macrophages undergoing apoptosis result in cellular fragmentation and spherical remnants with bacteria enclosed in intact membranes of apoptotic macrophages (Davis and Ramakrishnan, 2009). This signals further migrating macrophage recruitment and subsequent phagocytosis, thereby providing a new niche for bacterial proliferation in the newly infected macrophage (Ramakrishnan, 2012). Therefore, in either case of mycobacterial dissemination and transmission is possible.

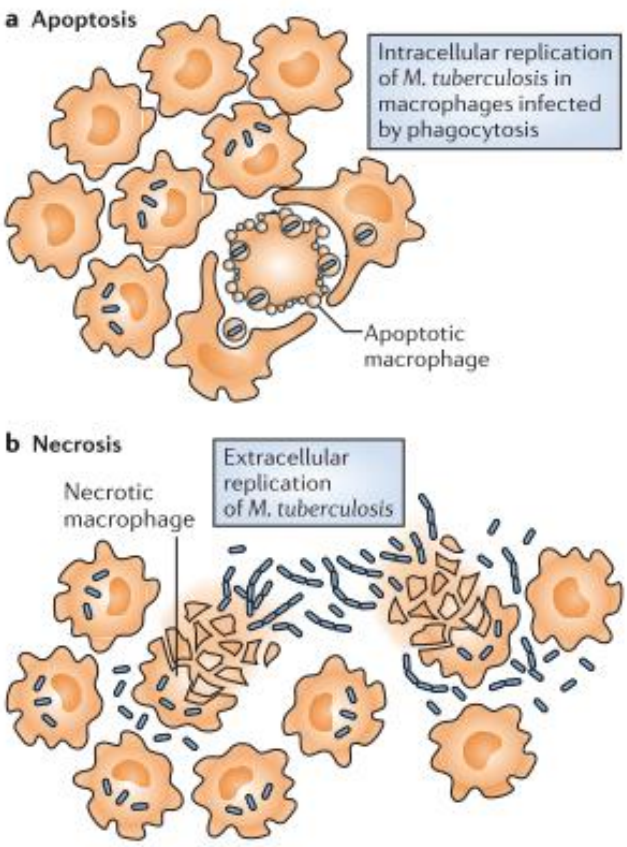

Figure 1.13: ***Both apoptotic and necrotic cell death pathways can promote bacterial growth****. a) Apoptotic remnants are phagocytosed by new migrating macrophages which provide new niches for mycobacterial growth and proliferation b) necrotic macrophages release mycobacteria into extracellular environment leading to uncontrolled and exuberant mycobacterial growth and proliferation. Image used with permission from (Ramakrishnan, 2012).*

1.4 Mycobacterial biofilms

Biofilms are multicellular adherent bacterial communities typically encapsulated by an extracellular matrix (ECM) that have a natural propensity to a sessile lifestyle (Hall-Stoodley and Stoodley, 2005; Richards and Ojha, 2014). These microbial communities are self-assembled through a genetically distinct developmental process as compared to their unattached, free living single cell planktonic counterparts (Stoodley *et al.*, 2002; Lopez, Vlamakis and Kolter, 2010). As a result of this, combined with their high cell density and cell-cell contacts they have a unique phenotype which supports antibiotic tolerance and immune evasion within the host (Stoodley *et al.*, 2002; Lopez, Vlamakis and Kolter, 2010; Richards and Ojha, 2014). Although, *in vitro* studies largely focus on planktonic bacterial cultures, 99% of naturally occurring bacteria grow in biofilms (Costerton, Geesey and Cheng, 1978; Davey and Toole, 2000).

Bacterial biofilms can be seen on various surfaces in human environments including household pipelines, shower heads, medical devices, human tissue, most common being dental plaques (Costerton, Stewart and Greenberg, 1999). Biofilms can colonise human host and implantable devices and are of tremendous clinical significance as 80% of human bacterial infections are associated with biofilm formation and recalcitrance to antibiotics (Römling and Balsalobre, 2012; Aparna and Yadav, 2008). Some typical examples include urinary tract infections caused by uropathogenic *Escherichia coli* (Anderson *et al.*, 2001), chronic wounds (James *et al*., 2007) and lung infections in cystic fibrosis patients infected with *Pseudomonas aeruginosa* (Singh *et al*., 2000), and osteomyelitis caused by *Staphylococcus aureus* (Brady *et al*., 2007).

Mycobacteria including *M. tuberculosis, M. smegmatis, M. bovis* BCG, *M. avium, M. chelonae* and *M. abscessus* are known to form spontaneous biofilms in nature and *in vitro* (reviewed in Chakraborty and Kumar, 2019; Vega-Dominguez *et al*., 2020; Dokic *et al*., 2021). Its ability to clump when grown in the absence of detergent facilitates instantaneous biofilm formation (Islam *et al*., 2012; Zambrano and Kolter, 2005). They generally form pellicles in the liquid air interface, but surface (hydrophobic solid

surfaces) attached biofilms were also reported for *M. chelonae*, *M. smegmatis* and, *M. abscessus* (Recht and Kolter, 2001; Rose *et al*., 2015). Mycobacterial biofilm formation involves a series of steps starting from initial reversible attachment of bacteria to the substratum, followed by cell aggregation and microcolony formation. This results in irreversible surface attachment which is followed by layering of aggregates with ECM and biofilm maturation. In the final stages, upon achieving its maximum thickness it disperses due to nutrient scarcity and overcrowding of cells only to reattach at a new site (Aparna and Yadav, 2008; Sauer, 2003; Chakraborty and Kumar, 2019).

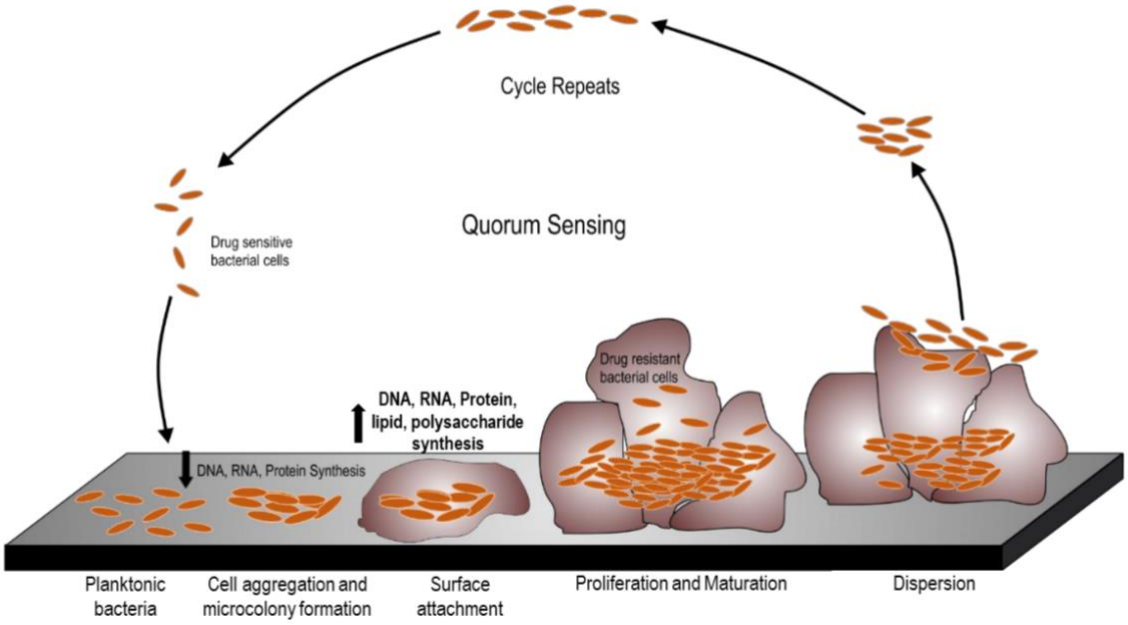

Figure 1.14: ***Biofilm formation and dispersion.*** *Planktonic bacteria aggregates to form microcolonies of mycobacteria, which attach to surface and release ECM. Within ECM, biofilms mature and proliferate before dispersing to another site for subsequent localisation and attachment. Image adapted from (Chakraborty and Kumar, 2019)*

1.4.1 Biofilm models

Mycobacterial pellicle is the extensively studied model for biofilm formation. Pellicles grown at the liquid-air interface in minimal media is a simple model which enables tracking of different developmental stages during biofilm maturation and facilitates the study of ECM components (Chakraborty and Kumar, 2019). Leukocyte lysate induced biofilm is another model for biofilm formation were surface attached microcolonies of drug resistant *M. tuberculosis* were observed in tissue

culture medium supplemented with leukocytes lysate (Ackart *et al.* 2014a). These microcolonies grown on the extracellular matrix derived from lysed human leukocytes were dispersed and rendered drug susceptible upon DNase I or Tween 80 treatment (Ackart *et al.* 2014a). This is an important model with a potential to mimic *in vivo* biofilm formation and has been used in the discovery of biofilm dispersing molecules which could improve the activity of first-line anti-TB drugs (Ackart *et al.* 2014b). Thiol reductive stress induced biofilm is a novel model wherein rapid biofilm formation is observed in response to reductive stress, forming both submerged biofilms adherent to substratum and at the liquid air interface adherent to the walls of the culture dish depending on culture conditions (Trivedi *et al.,* 2016). Using this model Kumar and others showed that cellulose is an important component of ECM (Trivedi *et al.,* 2016) which was then used as a biomarker to detect *in vivo* biofilm formation in *M. tuberculosis* infected mice, non-human primates and in lung tissue sections of TB patients (Chakraborty *et al*., 2021).

1.4.2 Extracellular matrix

ECM is the hallmark of biofilm formation. Characteristic differences between biofilms formed by the different mycobacterial species are observed in the composition of ECM, and the relative amounts of different extracellular polymeric substances (EPS). ECM serves as a nutrient source and EPS define the ultrastructure of mycobacterial biofilms and provide mechanistic stability and physicochemical barrier shielding the bacteria from antibiotic penetration and immune defence strategies (Tsuneda *et al.,* 2003; Chakraborty and Kumar, 2019). Water constitutes 97% of ECM (Potts, 1994), along with this four major EPS – lipid, polysaccharides, extracellular DNA and proteins are identified (Karygianni *et al*., 2020). Brief description on the role of each component is summarised below.

1.4.2.1 Lipids

Lipids in ECM are extremely important in mycobacterial biofilm formation and mutant strains with defects in lipid metabolism fail to form biofilms (Recht *et* al., 2000; Recht and Kolter, 2001; Wang *et al*., 2006; Ojha *et al*., 2008; Pang *et al*., 2012; Pacheco *et al*., 2013; Rose and Bermudez, 2014). Presence

of copious amounts of lipids in these biofilms suggest that they are held together by a waxy ECM (Zambrano and Kolter, 2005) which increases surface hydrophobicity facilitating cell-to-cell interaction (Chakraborty and Kumar, 2019).

Accumulation of free mycolic acids is a characteristic feature of mycobacterial biofilm formation and is observed in *M. tuberculosis, M. smegmatis, M. chelonae* and *M. abscessus* (Ojha *et al*., 2008, 2010; Sambandan *et al*., 2013; Totani *et al*., 2017; Vega-Dominguez *et al*., 2020; Dokic *et al*., 2021). Importantly, short chain free mycolic acids (C_{56}-C_{68}) are accumulated unlike the long chain mycolic acids (C_{70}-C_{90}) anchored to the cell envelope through covalent linkage to arabinogalactan. The chaperone molecule GroEL1 mediates this accumulation of free mycolic acids in *M. smegmatis* and mutants lacking it fail to form pellicle biofilms (Ojha *et al*., 2005). This accumulation is partially facilitated by the enzymatic hydrolysis of TDM and thus this glycolipid is also essential for biofilm formation in *M. smegmatis* (Ojha *et al*., 2010). However, contradicting evidence in *M. avium* has been reported where a reduction in TDM is observed without an accumulation in free mycolic acids during biofilm formation (Totani *et al*., 2017). Also, mycolic acid subtypes also effect biofilm formation as *M. tuberculosis* mutants defective of ketomycolic acids fail to biofilms (Sambandan *et al*., 2013).

Meromycolate diacylglycerols (MDAG) and glycopeptidolipids (GPL) are also crucial in biofilm formation. Acylated GPL is essential for surface attachment of bacilli but not vital in pellicle formation (Recht and Kolter, 2001; Yang *et al*., 2017). MDAGs are also essential for biofilm formation in *M. smegmatis* (Chen et al., 2006) and mycobacteria membrane protein large 11 (MmpL11) is involved in the transport of MDAG and mycolate wax ester is also essential for biofilm formation (Pacheco et al., 2013; Wright et al., 2017).

1.4.2.2 Polysaccharides

The mycobacterial genome has a scarcity in genes encoding exopolysaccharide production, because of this their biofilms were presumed to lack exopolysaccharides in their ECM (Whiteley et al., 2001). However, multiple studies using carbohydrate specific stains, confocal laser scanning microscopy and

biochemical analyses of ECMs have shown that polysaccharides form the bulk of the biofilm architecture (Lemassu *et al*., 1996b; Lemassu and Daffé, 1994; Trivedi et al., 2016).

Earlier studies identified α-glucan as the predominant polysaccharide in the ECM (Lemassu et al., 1996b; Lemassu and Daffé, 1994). However, a recent study identified cellulose with β(1→4) glycosidic linkage as the primary polysaccharide in *M. smegmatis* and *M. tuberculosis* pellicles. These pellicles were disrupted by cellulase and not by amylase, which specifically digests α(1→4) glycosidic bonds (Trivedi et al., 2016). In another study overexpression of cellulase in *M. smegmatis* prevents it from biofilm formation supporting the significance of cellulose in mycobacterial biofilm formation (Wyk *et al*., 2017).

M. smegmatis mutants with defects in peptidoglycan synthesis also failed to produce pellicles (Röse, Kaufmann and Daugelat, 2004; Kang *et al*., 2013). Deletion of *upk*, which encodes a phosphokinase in peptidoglycan synthesis resulted in weak adherence to substratum and missing ECMs resulting in defective biofilm formation despite having an intact cell wall in planktonic *M. smegmatis* bacilli (Röse, Kaufmann and Daugelat, 2004). Similarly, a *glmM* gene knockdown, a phosphoglucosamine mutase in peptidoglycan synthesis affected biofilm formation in *M. smegmatis*. Reduced GlmM expression affected cell wall integrity with reduced mycolic acids covalently attached to AG resulting in defective biofilm formation (Kang *et al*., 2013). These studies suggest that bacilli with compromised cell wall integrity can have defective biofilm formation.

1.4.2.3 Proteins

There is limited information on the role of proteins in mycobacterial biofilm formation. However, their role in aggregation and adhesion has been shown in *M. tuberculosis* thiol reductive stress induced biofilms using proteinase K, which dispersed the biofilm and prevented biofilm formation (Trivedi et

al., 2016; Chakraborty and Kumar, 2019). There are many more proteins involved in formation and maintainance of mycobacterial biofilms which need to be identified.

1.4.2.4 Extracellular DNA

Extracellular DNA is an essential component of mycobacterial biofilms which confers drug tolerance and provides an attachment scaffold to microcolonies during various stages of biofilm formation (Tetz, Artemenko and Tetz, 2009; Cavaliere *et al*., 2014; Rose *et al*., 2015; Ibáñez de Aldecoa, Zafra and González-Pastor, 2017; Pakkulnan *et al*., 2019). The role of eDNA in maintaining strutctural integrity of biofilms was also observed in thiol-induced biofilms (Trivedi et al., 2016) and reduced drug tolerance of microcolonies was observed in leukocyte lysate induced biofilms upon DNase treatment (Ackart *et al.* 2014a). eDNA was detected in pellicles formed by *M. tuberculosis, M. avium, M. abscessus, M. fortuitum* and *M. chelonae* (Whitchurch *et al*., 2002; Rose *et al*., 2015; Rose and Bermudez, 2016; Toyofuku *et al*., 2016; Trivedi *et al*., 2016; Aung *et al*., 2017; Vega-Dominguez *et al*., 2020; Dokic *et al*., 2021).

1.4.3 Biofilm formation by extracellular *M. tuberculosis* in necrotizing lesions

Mycobacteria within the granulomatous region (Figure 1.12) can enter an extracellular region through necrosis or lesion cavitation as explained earlier (Figure 1.13). Once *M. tuberculosis* enters these necrotizing lesions and adapts to its extracellular lifestyle, it can quickly switch from planktonic to biofilm growth conditions (Basaraba and Ojha, 2017).

Necrotic lesions have relatively normal oxygen levels as they are connected with airways which promotes bacterial proliferation leading to further inflammation and necrosis (Grosset, 2003; Hoff *et al*., 2011; Lenaerts, Barry and Dartois, 2015). It also provides a physical separation from circulating immune cells providing resistance to phagocytosis. As it has little or no blood supply it limits the penetration and accumulation of antibiotics (Prideaux *et al*., 2015). These factors provide favourable conditions for biofilm formation and long-term cohabitation of mycobacteria within necrotic lesions

(Basaraba and Ojha, 2017). Even if mycobacteria are sequestered into microenvironments in hypoxic conditions, it can survive and persist in a non-replicative latent phase for a long period of time (Via *et al*., 2008, 2012; Datta *et al*., 2016).

Animal studies have shown necrosis associated extracellular clusters of bacilli (NEC) *in vivo* (Orme, 2014; Wong and Jacobs, 2016). NECs contribute to antibiotic drug tolerance especially in animal models that develop necrotic granulomas (Lanoix, Lenaerts and Nuermberger, 2015; Lenaerts, Barry and Dartois, 2015). This was confirmed in a guinea pig model which develops well organised granulomas similar to those in humans. They displayed antibiotic persistent bacilli along the acellular rim of the necrotising lesion (Lenaerts et al., 2007; Hoff et al., 2011). In these animal models diffused rhodamine staining patterns around the acellular rims of necrotising lesions was observed. The authors speculated that the diffused material could likely be either *M. tuberculosis* derived mycolic acids, actively secreted by viable bacilli or accumulated after bacterial death and degradation (Lenaerts et al., 2007; Hoff et al., 2011; Basaraba and Ojha, 2017). Presence of antibiotic tolerant persisters and co-localisation of mycolic acids along the acellular rim of necrotising lesions suggests biofilm growth of mycobacteria in such host niches (Basaraba and Ojha, 2017). As a consequence of extracellular of biofilm formation, mycobacteria can persist and co-localise in distal airways for long time.

Supporting this idea of *in vivo* biofilm formation, a recent study detected mycobacterial cells encapsulated in a cellulose matrix with a biofilm like phenotype in *M. tuberculosis* infected mice and rhesus macaques. With this observation, they've used cellulose as a biomarker to show biofilm like phenotype in human lung samples infected with *M. tuberculosis* (Chakraborty *et al*., 2021). Cellulase overexpressing strain of *M. tuberculosis* were highly attenuated in mice model and failed to establish infection two weeks post infection. Also, the cellulase overexpression strain has progressive reduction in CFU after four weeks of infection. This study suggests that *M. tuberculosis* forms biofilms *in vivo* to establish infection and to evade innate and adaptive immune responses (Chakraborty *et al*., 2021).

1.5 Thesis aims

It is well established that *M. tuberculosis* is a successful pathogen which is estimated to cause latent infection in one-third of the world's population, with a high morbidity and mortality rate in immunocompromised people especially with HIV/AIDS (WHO, 2020, 2021). The only available vaccine for TB is BCG which was first discovered more than 100 years ago and has variable efficacy in adults (Kaufmann, 2013; Nunes-Alves *et al.*, 2014; Davenne and McShane, 2016; Zhu *et al.*, 2018). The emergence of MDR strains of TB (WHO, 2021) is also an alarming cause for the development of novel therapeutics and vaccine candidates to combat TB.

Currently administered chemotherapy lasts for at least 6 months with a high drug toxicity and side effects, resulting in patient non-compliance. Host directed therapies (HDT) is a new promising ancillary therapeutic to antibiotic chemotherapy, where the host immune response is modulated to achieve better control of TB. This is a promising treatment strategy to combat MDR and XDR strains as well as co-infection with HIV/AIDS, all while reducing treatment duration (Kolloli and Subbian, 2017). Understanding host pathogen interactions of *M. tuberculosis* is imperative for the development of novel therapeutics (chemotherapeutic and HDTs) and vaccine candidates. This thesis has two main projects which contribute to understanding mycobacterial cell wall biology and host pathogen interactions with an overarching aim to contribute towards vaccine and HDT studies. The biosafety level 2 pathogen- *M. bovis* BCG was used in these projects because of its genetic and phenotypic similarity to the slow growing *M. tuberculosis*. Also, as it is the vaccine strain, it is ideal for the project involved in the studying the immunogenicity of cell wall mutants. The specific aims of each project are as described.

1.5.1 Project 1 (Chapters 2 and 3)

To study immunogenicity of mycobacterial cell wall mutants, enzymes involved in mycobacterial cell wall assembly were explored. AftC was shown to be a crucial enzyme involved in the biosynthesis of the arabinan domain of AG and LAM. Earlier studies in *M. smegmatis* revealed its non-essentiality along with significant growth defect in liquid medium (Birch *et al.*, 2008) and truncation of AG (Birch *et al.*,

2008) and LAM (Birch *et al.*, 2010). Functional characterisation revealed the role of *aftC* in the introduction of the first branching *Araf* residue in the backbone of both AG and LAM through an α(1→3) linkage (Birch *et al.*, 2008, 2010). Similar attempts to generate *aftC* deletion mutants in *M. tuberculosis* were unsuccessful (Sassetti *et al.*, 2003) emphasising the essentiality of the gene and the species' intolerance to cell-wall changes making it the ideal drug target or plausible immunogenic. This project aims to analyse the immunogenicity of AftC depletion strain of *M. bovis* BCG to analyse its efficacy as a potential immunogenic candidate.

Composition and integrity of cell wall assembly affects biofilm formation. For example, MDAG mutants fail to form pellicles (Chen et al., 2006; Pacheco et al., 2013; Wright et al., 2017), similarly GPL mutants had delayed biofilm formation (Recht and Kolter, 2001; Yang *et al*., 2017). *M. smegmatis* and *M. tuberculosis* mutants with defective mycolic acid profiles could not initiate biofilm formation (Ojha *et al*., 2008, 2010; Sambandan *et al*., 2013). Earlier *aftC* deletion studies in *M. smegmatis* revealed aberrant mycolic acid profiles (Birch *et al.*, 2008). However, they did not quantify the consequences of this on biofilm formation. Also, a *glmM* knockdown and *upk* deletion in *M. smegmatis* affected its biofilm formation. These mutants with defects in PG synthesis failed to form biofilm possibly due to reduced covalently attached mycolic acids or overall change in the cell wall composition affecting cell wall integrity. Therefore, it will be interesting to study the effect of AftC depletion on biofilm formation as it is known to effect mycobacterial cell wall integrity (Birch *et al.*, 2008).

Aim: Develop and analyse the infectivity an immunogenicity of AftC depleted *M. bovis* BCG in *in vitro* assays using macrophage cell line.

- Generate AftC depleted *M. bovis* BCG strain
- Establish the phenotypic and functional consequences of AftC depletion on *M. bovis* BCG planktonic cultures
- Understand the effect of AftC depletion on biofilm formation of *M. bovis* BCG
- Characterise the effect of AftC depletion on infectivity of *M. bovis* BCG in macrophage cell line

1.5.2 Project 2 (Chapter 4)

Multiple host immune factors were reported to encourage intracellular mycobacterial growth and proliferation. SOCS1 is one such protein involved in the downregulation of IFN-γ and other pro-inflammatory cytokines during *M. tuberculosis* infection. SOCS1 mimetics and antagonists are currently under investigation to be used as HDTs in viral infections and cancer. In this project we tried to fill the knowledge gap in the role of SOCS1 during mycobacterial infection which can aid in the development of SOCS1 antagonists in HDTs against TB.

Aim: Identify the role of SOCS1 in suppression of JAK/STAT signalling

- Generate SOCS1$^{-/-}$ cell line to establish its role during mycobacterial infection
- Identify the crucial domain or residues in SOCS1 for its function during mycobacterial infection

Chapter 2 : Homologous recombination mediated *aftC* (*Mb2692*) deletion in *M. bovis* BCG

2.1 Introduction

M. tuberculosis is a complex slow growing pathogen with approximately 4000 genes (Choudhary, Lunge and Agarwal, 2016; Chhotaray *et al.*, 2018). With the advent of whole genome sequencing (WGS) the entire 4.4 million base pair long mycobacterial genome was sequenced two decades ago, and yet, about one quarter of the genome remains uncharacterised (Choudhary, Lunge and Agarwal, 2016; Chhotaray *et al.*, 2018). Particularly, 5% of the uncharacterised gene pool is predicted to be essential and essential genes are ideal drug targets (Choudhary, Lunge and Agarwal, 2016).

Amongst, the multiple mycobacterial genome editing technologies which are based on: 1) homologous recombination, 2) controlled proteolysis, and 3) transcriptional repression strategies; the gene replacement strategy based on homologous recombination has been the conventional method to identify the function of a targeted gene. The gene replacement repertoire includes allelic exchange and regulatory expression systems (Choudhary, Lunge and Agarwal, 2016).

Homologous recombination based genetic manipulation strategies are based on switching the targeted gene with *in vitro* engineered homologous sequence as depicted in Figure 2.1. Allelic exchange based homologous recombination involves replacement of the targeted gene with an antibiotic resistance cassette resulting in gene inactivation (Chhotaray *et al.*, 2018). It works best in fast growing mycobacteria, such as *Mycobacterium smegmatis.* However, in slow growing mycobacteria, such as *Mycobacterium bovis* BCG, 80% of the transformants exhibited integration of exogenous DNA without replacement of the targeted gene (Choudhary, Lunge and Agarwal, 2016). To overcome this difficulty, Bardarov *et al.* developed specialised transduction where a conditionally replicating shuttle phasmid carrying the allelic exchange substrate is used to generate specialised transducing mycobacteriophages (Bardarov *et al.*, 2002). This method has made allelic exchanges possible in slow growing mycobacterial species and provides two major advantages: 1) it ensures high frequency delivery of recombination substrate to the recipient cells, and 2) ensures legitimate recombination, in the absence of which phage DNA becomes toxic to the bacterium (Bardarov *et al.*, 2002; Choudhary, Lunge and Agarwal, 2016).

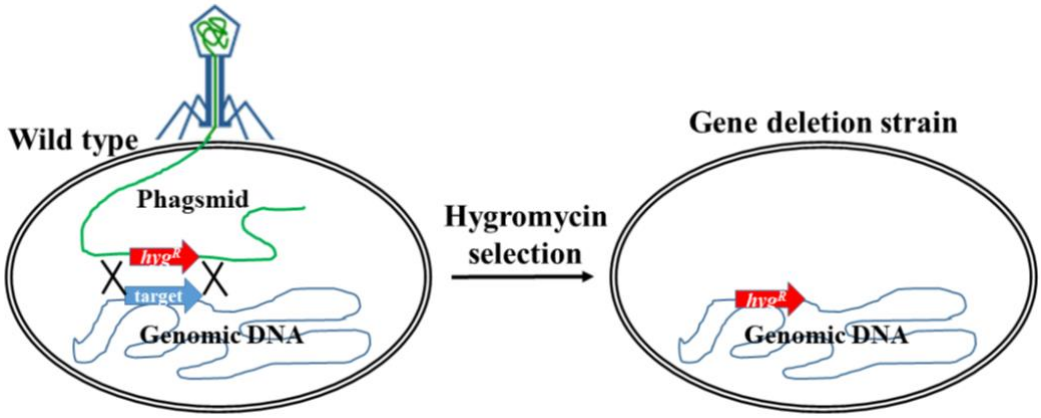

Figure 2.1: ***Schematic representation of allelic exchange strategy employed to generate mycobacterial gene deletion strain***.

The allelic exchange substrate (AES) for homologous recombination is constructed by cloning a 1kb long DNA sequence flanking the gene of interest on either side of a hygromycin resistance gene for selection and *sacB* gene for counter-selection into a λ cosmid vector. This AES is packaged into a conditionally replicating temperature sensitive shuttle phasmid – phAE159 to generate a specialised transducing mycobacteriophage (Figure 2.1). This phasmid replicates at a permissible temperature of 30°C but fails to replicate at a non-permissible temperature of 37°C. Incubation of the high titre phage lysate with mycobacteria at the non-permissive 37°C ensures efficient transduction of AES into mycobacteria enabling homologous recombination to generate targeted gene disruption (Figure 2.1). Transductant colonies are isolated on hygromycin selective media and isogenic strains differing at the defined locus are compared for functional analysis (Bardarov *et al.*, 2002; Jain *et al.*, 2014).

In cases of essential genes which are critical for the *in vitro* growth of mycobacteria, conditional gene expression technology is used. In this case, a second copy of gene is introduced by a single copy integrating plasmid under a tightly regulated promoter, for example the tetracycline inducible promoter Tet^R. This generated merodiploid strain which is used for transduction to enable homologous recombination and targeted gene replacement with the hygromycin resistance cassette in the presence of the second copy induced by the promoter (Figure 2.2). This tetracycline induced conditional depletion of the essential genes is effective in both slow and fast growing mycobacteria (Choudhary, Lunge and Agarwal, 2016; Chhotaray *et al.*, 2018).

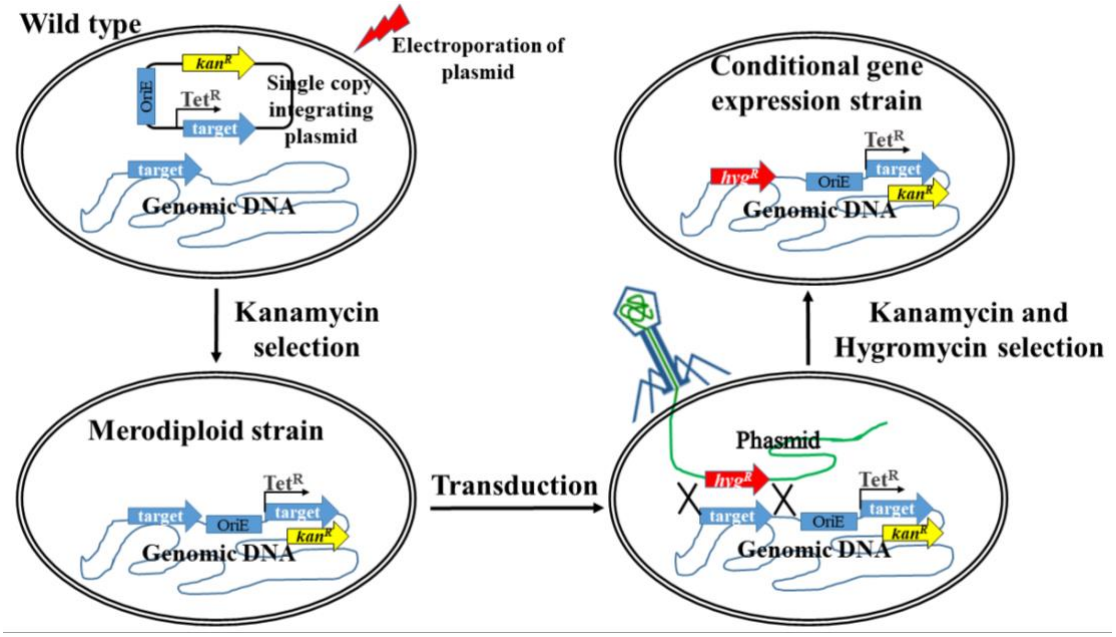

Figure 2.2: ***Schematic explaining conditional gene depletion strategy used to study essential genes in mycobacteria***.

Previous studies from our laboratory have established the non-essentiality of *aftC (MSMEG2785)* in *M. smegmatis* using AES mediated homologous recombination and gene deletion. This gene deletion has produced a growth defect in liquid medium (Birch *et al.*, 2008) with truncation in AG (Birch *et al.*, 2008) and LAM (Birch *et al.*, 2010) of *M. smegmatis*. They also identified the function of *aftC* as the first branching *Araf* residue in the backbone of both AG and LAM through an α(1→3) linkage (Birch *et al.*, 2008, 2010). Despite the availability of an *M. smegmatis aftC* knockout strain, we are unable to use this strain due to its poor infectivity in THP1 cell line. In addition, due to the structural differences between LAM in *M. smegmatis* and *M. bovis* BCG, and to study the effect of *aftC* depletion on infectivity of pathogenic mycobacterial species, we sought to generate an *aftC (Mb2692)* null mutant strain of *M. bovis* BCG using specialised transduction to study the consequences of deletion on growth, viability and virulence of the recombinant strain.

2.2 Results

2.2.1 Attempts to generate *M. bovis* BCG*ΔMb2692* null knockout strain were unsuccessful

Previous reports in *M. smegmatis* have shown that *aftC* is a non-essential gene (Birch *et al.*, 2008) through homologous recombination using an allelic exchange substrate to generate a null mutant stain. We employed the same methodology to attempt to generate an *aftC (Mb2692)* null mutant strain in *M. bovis* BCG (Figure 2.3).

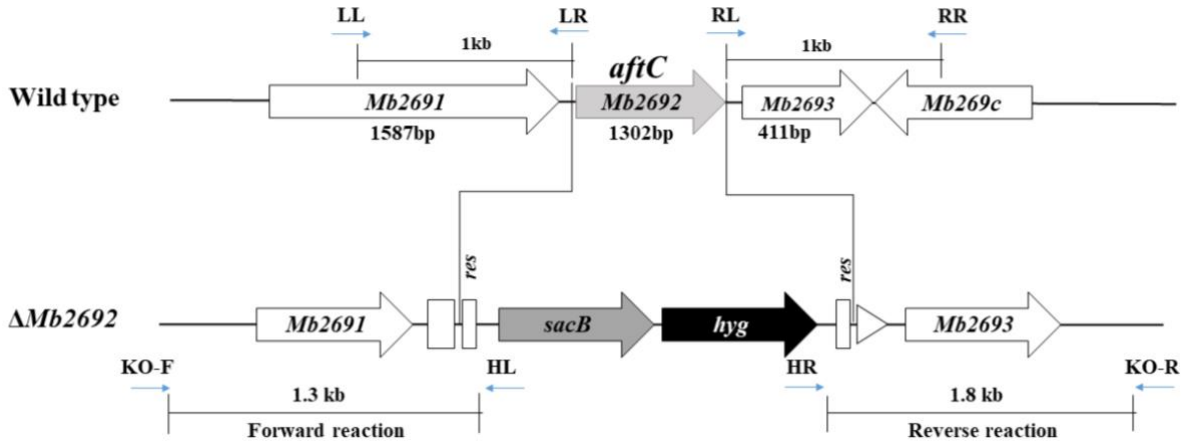

Figure 2.3: ***Construction of M. bovis BCG Mb2692 deletion mutant****. A schematic representation showing gene replacement of Mb2692 with hyg^R-sacB cassette. sacB - sucrose counter-selectable gene from Bacillus subtilis; hyg - hygromycin resistance gene; res - γδ-resolvase site.*

Approximately, 1kb flanking regions upstream and downstream of *Mb2692* were PCR amplified using LL, LR, RL and RR primers (Table 6.5) and cloned on either side of a hygromycin resistance cassette in a p0004s - λ cosmid. This recombinant plasmid containing AES was packaged into a mycobacteriophage to deliver the AES for homologous recombination to generate the *aftC* knockout strain. The temperature sensitive shuttle phasmid phAE159 was used for this approach which propagates only at 30°C and infects mycobacteria at 37°C without propagating in infected cells (Bardarov *et al.*, 2002; Jain *et al.*, 2014). Using this method developed by Bardarov *et al.* the allelic exchange substrate was delivered into *M. bovis* BCG to enable homologous recombination and an *aftC* knockout strain

(refer **6.1.10.**). Gene deletion was confirmed using PCR with primers located within the hyg-sacB cassette, and in the neighbouring genes, to generate PCR products of approximately between 1.3 kb and 1.8 kb in the case of a successful gene deletion (Figure 2.3).

PCR amplified left and right flank sequences with a Van91I restriction site inserted at their 5' ends were quadruple ligated with the hygromycin resistance cassette and λ cosmid containing oriE from Van91I digested p0004s plasmid to construct AES. Cloned AES was re-digested by Van91I to confirm the recombinant plasmid. A total of 5 bands - 3.68kb (λ cosmid containing oriE), 1.68kb (hyg – sacB cassette), 1kb (from left homologous region), 400bp and 600bp (from right homologous region) were observed due to the presence of an internal Van91i restriction site in the right flanking sequence resulting in 400 and 600bp segments. The right homology sequence was re-ligated without changing its orientation as confirmed by sequencing (Figure 2.4A). This AES was cloned into phAE159 between two PacI sites within the non-essential region in phAE159 phasmid and packaged into mycobacteriophage particles. Recombinant phasmid - phΔMb2692 was confirmed by PacI digestion and visualised by agarose gel electrophoresis by two bands, one corresponding to pΔMb2692 (7.3kb) and the other large band (~40kb) corresponding to packaging material confirming phasmid construction (Figure 2.4B). As phAE159 is a temperature sensitive phasmid, it only propagates at 30°C and infects at its growth non-permissive temperature of 37°C (Bardarov *et al.*, 2002; Jain *et al.*, 2014). Mycobacteriophage generated through electroporation of phΔMb2692 into *M. smegmatis* were amplified at 30°C to obtain high titre phage lysate (Figure 2.4C).

Specialised transduction was performed by incubating 10^{10} PFU per ml with *M. bovis* BCG at 37°C (non-permissive temperature for phage replication) for 4 hours to allow phage infection and transduction of the allelic exchange substrate. Transductants were selected on hygromycin plates. However, no transductant colonies were observed in: (i) *M. bovis* BCG infected with high titre phage lysate, (ii) *M. bovis* BCG infected with MP buffer as a negative control (Figure 2.4D). This process was repeated three times and still no *aftC (Mb2692)* null mutants were obtained in *M. bovis* BCG, this raised the possibility that *aftC* may be an essential gene in *M. bovis* BCG.

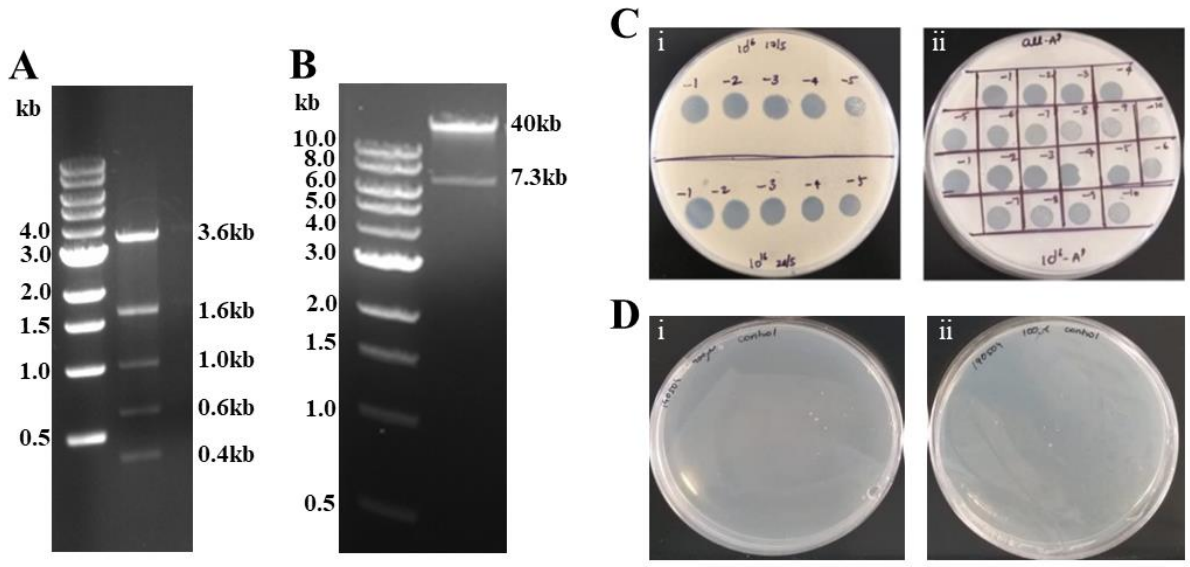

Figure 2.4: ***Attempts to generate an M. bovis BCG ΔMb2692 null knockout strain.*** *(A) Confirmation of AES by Van91i digestion (B) Confirmation of phΔMb2692 by PacI digestion. (C) High titre phage lysate generation. (D) Specialised transduction of M. bovis BCG with 10^{10} PFU per ml of phΔMb2692 mycobacteriophage.*

2.2.2 *aftC* is an essential gene in *M. bovis* BCG

To confirm if *aftC* is an essential gene in *M. bovis* BCG conditional expression – specialised transduction essentiality test (CESTET) was performed (refer **6.1.10.7**). Figure 2.5 is a schematic outlining the methodology – a merodiploid strain with a second copy of *aftC* was introduced into *M. bovis* BCG under the control of a Tet^R promoter. This strain is then infected with a high titre phage to enable homologous recombination and replacement of the chromosomal *aftC (Mb2692)* copy with a hygromycin resistance cassette in the presence of ATc, which is inducing AftC expression from a single integrative copy of pTIC6a-Mb2692 plasmid harbouring a tetracycline-inducible promoter (Jankute *et al.*, 2017).

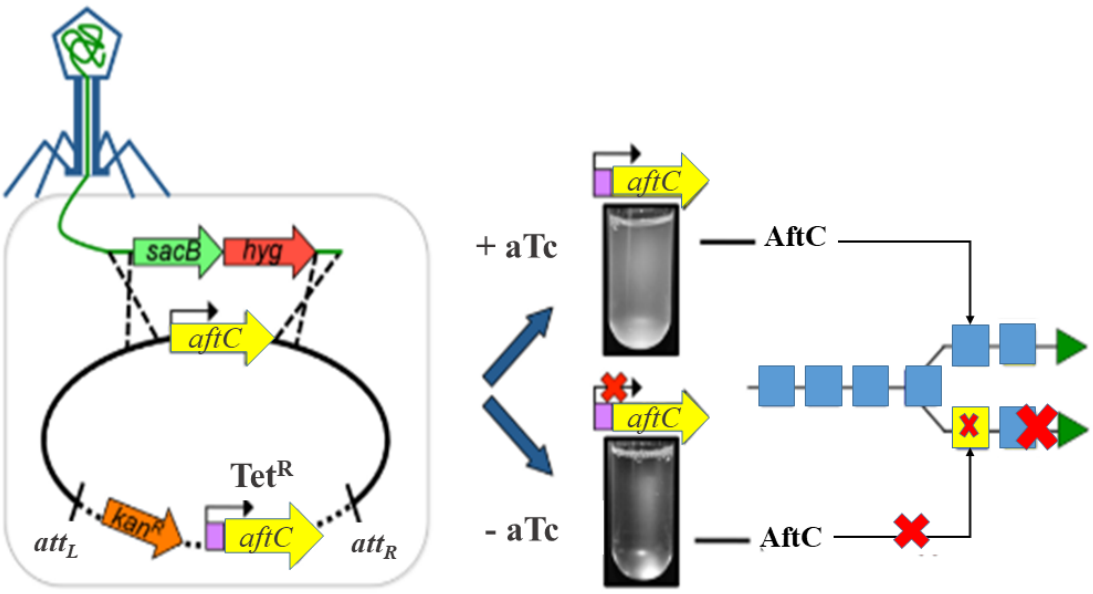

Figure 2.5: ***Conditional expression-specialised transduction essentiality test.*** *(image adapted from* (Jankute *et al.*, 2017)*)*

The rescue plasmid carrying a second copy of *aftC* was cloned into pTIC6 (single copy integrative plasmid with a kanamycin resistance cassette and tetracycline inducible promoter) to generate pTIC6-Mb2692. The sequence fidelity was confirmed, and the plasmid introduced into *M. bovis* BCG through electroporation (refer **6.1.10.6**). Genomic DNA was extracted from the *M. bovis* BCG::pTIC6-Mb2692 merodiploid strain and colony PCR was performed using the primers pTIC6-F and Mb2692_Comp_R (Table 6.5). A prominent band corresponding to a 1.3kb *Mb2692* fragment confirmed the integration of pTIC6-Mb2692 in *M. bovis* BCG::pTIC6-Mb2692 (Figure 2.6A).

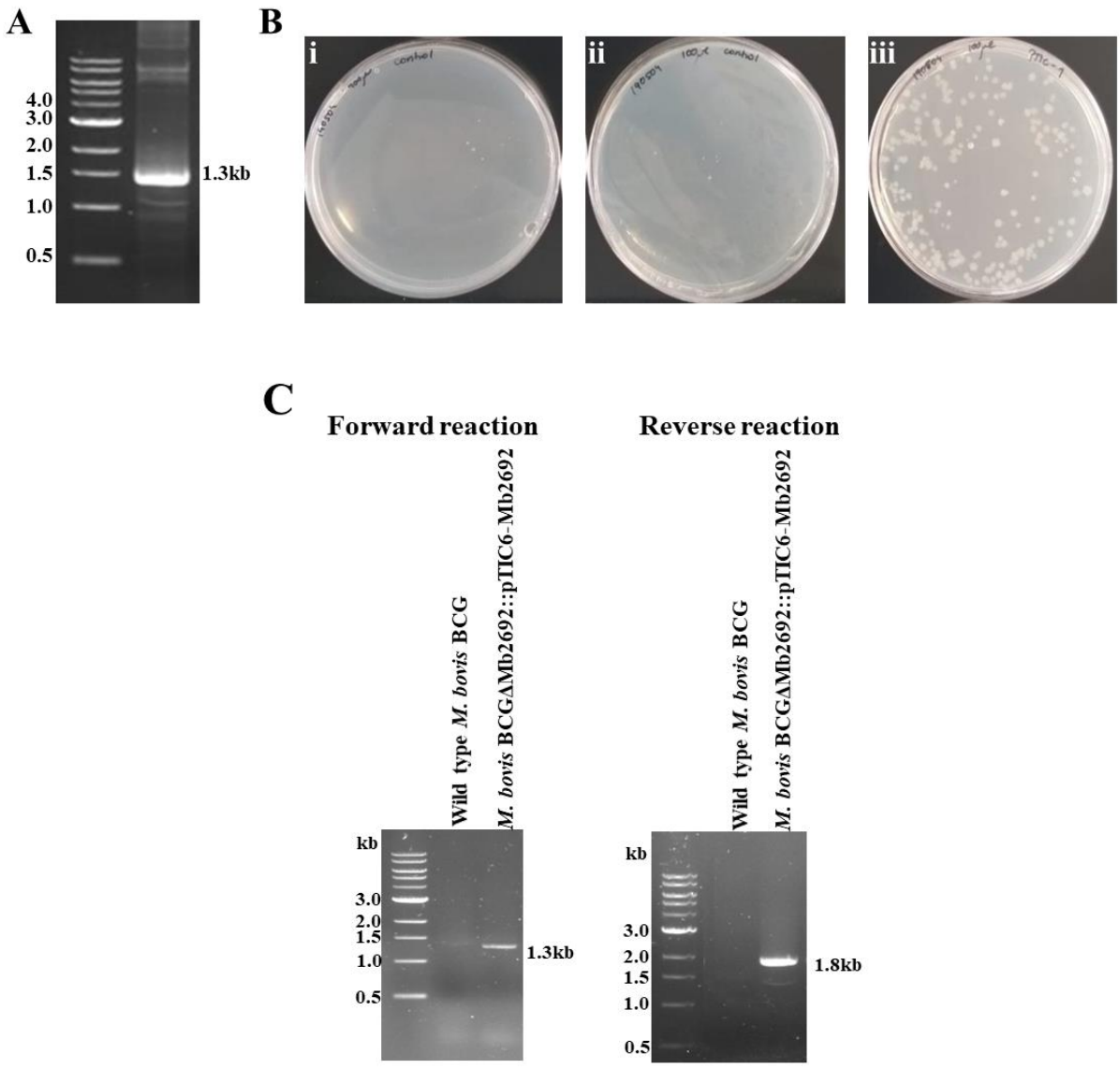

Figure 2.6: ***Construction of aftC (Mb2692) deletion mutants in M. bovis BCG.*** *(A) Confirmation of merodiploid strain generation (integration of pTIC6-Mb2692 plasmid into wild type M. bovis BCG) by colony PCR. (B) Merodiploid strain M. bovis BCG::pTIC6-Mb2692 infected with high titre phage lysate and screening mutant colonies (C) M. bovis BCGΔMb2692:: pTIC6-Mb2692 was verified for aftC deletion using two PCR reactions with (i) Forward reaction to obtain a 1.3 kb band (ii) Reverse reaction to obtain a 1.8 kb band to confirm the chromosomal deletion of aftC.*

The merodiploid strain *M. bovis* BCG::*pTIC6-Mb2692* containing a single copy of the integrating plasmid pTIC6-Mb2692 was infected with phΔMb2692 high titre phage lysate for 4 hours at 37°C. Transductants were selected on kanamycin and hygromycin plates, with colonies appearing only in the merodiploid strain *M. bovis* BCG::pTIC6-Mb2692 infected with a high titre phage lysate (Figure 2.6B-

iii) as compared to *M. bovis* BCG infected with high titre phage lysate (Figure 2.6B-ii) or *M. bovis* BCG incubated with MP buffer (Figure 2.6B-i).

The chromosomal deletion of *aftC* was achieved only in the presence of a rescue plasmid carrying a second copy of *aftC*, confirming that *aftC* is essential for the viability of *M. bovis* BCG (Figure 2.6B). The replacement of the native chromosomal copy of *aftC* by a hygromycin resistance cassette in the transductant was confirmed by PCR reaction (Figure 2.6C). Two independent PCR reactions were performed to confirm the deletion and substitution of *Mb2692*. Genomic DNA was extracted and used in the forward reaction with the primers Mb2692_KO_F and HL (Table 6.5). As expected *M. bovis* BCG did not show a band, whereas *M. bovis* BCGΔ*Mb2692::pTIC6-Mb2692* showed a band corresponding to 1.3kb confirming the presence of a hygromycin resistance cassette in place of chromosomal *aftC*. The reverse reaction using Mb2692_KO_R and HR similarly showed a 1.8kb band from *M. bovis* BCGΔ*Mb2692::pTIC6-Mb2692*, which was absent in *M. bovis* BCG (Figure 2.6C). *M. bovis* BCGΔ*Mb2692::pTIC6-Mb2692* was also confirmed for deletion – substitution of chromosomal *aftC* with a hygromycin resistance cassette by WGS (refer **6.1.10.8**).

These results are in contrast to the previously published studies in *M. smegmatis* (Birch *et al.*, 2008, 2010). *AftC* is confirmed to be a non-essential gene in *M. smegmatis*, however repeated unsuccessful attempts to generate a null knockout strain in *M. bovis* BCG coupled with *aftC* disruption only in the presence of a rescue plasmid, suggests the essentiality of *aftC* in *M. bovis* BCG.

2.2.3 *M. bovis* BCGΔ*Mb2692::pTIC6-Mb2692* has uncontrolled expression of AftC

Previous studies demonstrated that conditional depletion of essential genes using CESTET results in growth defects and cell lysis in mycobacterial cells (Bhatt *et al.*, 2005; Brown *et al.*, 2007; Rana *et al.*, 2012). To examine for such a possible phenotype, *M. bovis* BCGΔ*Mb2692*::*pTIC6-Mb2692* was monitored on agar plates and liquid medium. The AftC conditional depletion strain were streaked onto agar plates supplemented with or without Tc. *M. bovis* BCGΔ*Mb2692::pTIC6-Mb2692* grew in the presence of ATc in all antibiotic conditions as shown in Table 2.1. However, it also grew in the absence

of ATc in all the antibiotic combinations Table 2.1. This observation is contradictory to the previous observations (Birch *et al.*, 2008), where *aftC* deletion resulted in growth defects. Similar observations were made in liquid culture. The growth of *M. bovis* BCGΔ*Mb2692::pTIC6-Mb2692* was also monitored in liquid medium with and without ATc (100 ng/ml) over a period of 10 days. No significant difference was observed in OD_{600} measurement upon AftC depletion (Figure 2.7). This is contradictory to AftC depletion in *M. smegmatis* where *M. smegmatis*Δ*aftC* strain showed significant growth defect in liquid medium (Birch *et al.*, 2008).

Table 2.1: ***Antibiotic selection matrix for the attempted deletion of M. bovis BCGΔMb2692::pTIC6-Mb2692.*** *AftC conditional depletion strains were streaked on agar plates with or without ATc in different antibiotic combinations. M. bovis BCGΔMb2692::pTIC6-Mb2692 has grown in the presence of ATc in all antibiotic conditions. However, it has also grown in the absence of ATc in all the antibiotic combinations (Y- represents growth; N- represents no growth).*

Strain	**Kan /Hyg**	**Kan /Hyg +ATc**	**Hyg**	**Hyg +ATc**	**Kan**	**Kan +ATc**	**No Ab**	**No Ab + ATc**
M. bovis BCGΔMb2692::pTIC6-Mb2692	Y	Y	Y	Y	Y	Y	Y	Y
M. bovis BCG::pTIC6-Mb2692	Y	Y	N	N	Y	Y	Y	Y
M. bovis BCG	N	N	N	N	N	N	Y	Y

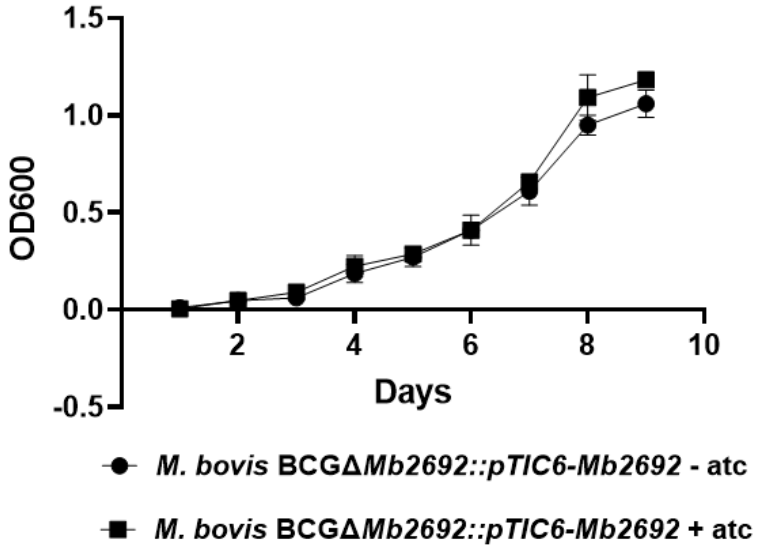

Figure 2.7: ***Growth profile of M. bovis BCGΔMb2692::pTIC6-Mb2692.*** *The growth of M. bovis BCGΔMb2692::pTIC6-Mb2692 in liquid medium with and without ATc was monitored over a period of 10 days. No significant difference has been observed in OD_{600} measurement upon AftC depletion.*

To address this discrepancy, *M. bovis* BCGΔ*Mb2692*::*pTIC6-Mb2692* was sent for WGS (outsourced to Microbes NG) along with *M. bovis* BCG and the *M. bovis* BCG::pTIC6-Mb2692 merodiploid strain. WGS results indicated mutations in the *rspA* promoter containing two *tetO* operators, thereby resulting in leaky expression of *Mb2692* (Figure 2.8). Point mutations in *tetO* imply insufficient and loose binding of Tet repressor (TetR) which should otherwise be tightly bound to prevent the transcription of *aftC.* Only in the presence of ATc (which would bind to TetR and induce conformational changes in it resulting in its dissociation from *tetO*) transcription of TetR regulated genes should be achieved (Ehrt *et al*., 2005). However, in our case point mutations in the *rspA* promoter containing *tetO* operators led to uncontrolled expression of AftC irrespective of ATc addition. Strong selection at synonymous sites in mutants grown in the presence of ATc can be a crucial reason for the emergence of these point mutations (Ehrt *et al*., 2005; Sharma *et al*., 2019). In any case, uncontrolled expression of AftC in *M. bovis* BCGΔ*Mb2692::pTIC6-Mb2692* prevented us from studying the functional consequences of *aftC* depletion on *M. bovis* BCG cell wall assembly and infectivity. For this reason, we looked at alternative *aftC* depletion strategies in *M. bovis* BCG.

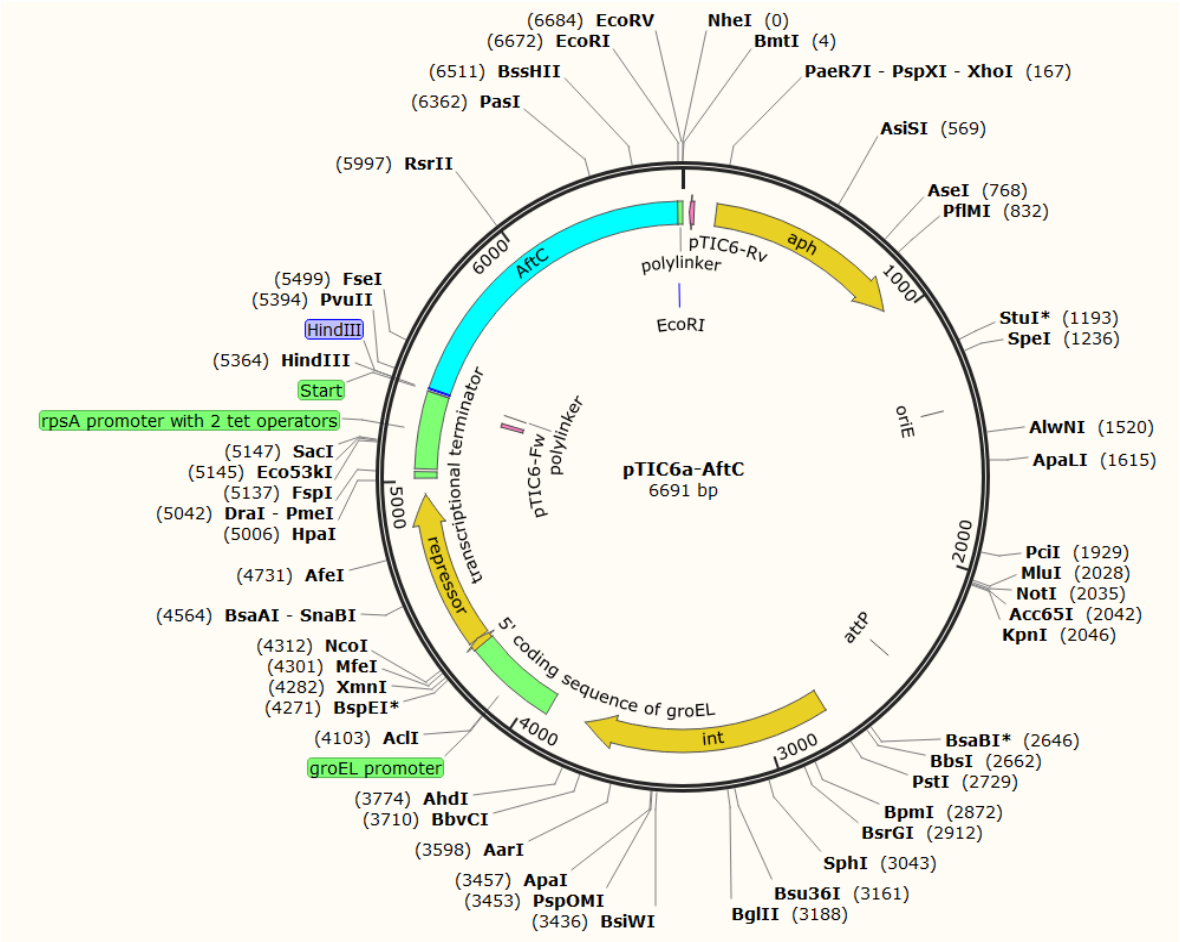

Figure 2.8: ***Vector map of pTIC6a-Mb2692 used in the generation of M. bovis BCG::pTIC6-Mb2692 merodiploid strain***

2.3 Discussion

The earlier *aftC* depletion studies performed in *M. smegmatis* revealed its non-essentiality in the non-pathogenic fast-growing *M. smegmatis* strain. Birch *et al.* identified this novel glycosyltransferase involved in AG biosynthesis through *in vitro* and *in vivo* analysis using *MSMEG2785 (aftC* in *M. smegmatis), Rv2673 (aftC* in *M. tuberculosis)* and *NCgl1822 (aftC* in *C. glutamicum)* (Birch *et al.*, 2008). This novel arabinofuranosyltransferase (AftC) is responsible for priming the α(1→5) arabinan backbone with an α(1→3) linked Ara*f* sugar which is then extended by other arabinofuranosyltransferase enzymes through α(1→5) linkages (Birch *et al.*, 2008). More precisely, AftC catalyses the addition of an α(1→3) Ara*f* residue resulting in a 3,5-Ara*f* branching residue in both AG (Birch *et al.*, 2008) and LAM (Birch *et al.*, 2010).

To understand the significance of *aftC* depletion on infectivity of mycobacteria, we decided to generate an *aftC (Mb2692)* knockout in *M. bovis* BCG which has mannose capped LAM, similar to *M. tuberculosis* in contrast to *M. smegmatis*, which has PI capped LAM molecules in its outer cell envelope. For this, homologous recombination-based gene replacement strategy was used to generate a *M. bovis* BCG null knockout strain (Figure 2.1 and Figure 2.3). Multiple unsuccessful attempts prompted us to verify the essentiality of *Mb2692.* Conditional expression - specialised transduction essentiality test (CESTET) was used to generate an *aftC* deletion mutant in *M. bovis* BCG in the presence of a second copy of *Mb2692* regulated by a Tet^R promoter to confirm the essentiality of the gene (Figure 2.2 and Figure 2.5). Deletion of the chromosomal *aftC* in *M. bovis* BCG was achieved only in the presence of *aftC* expressed from the second copy in the presence of anhydrotetracycline (ATc) (Figure 2.6). This data confirms the essentiality of *Mb2692* for the viability of *M. bovis* BCG. These results are in contrast to the previously published studies in *M. smegmatis*, where *MSMEG2785* is proven to be non-essential (Birch *et al.*, 2008, 2010).

M. bovis is a pathogenic slow-growing mycobacteria where *aftC* plays a crucial role in its viability and virulence. *AftC* depletion results in generation of a truncated unbranched AG and LAM (Birch *et al.*,

2008, 2010), which are crucial in maintaining cell wall integrity and protecting the bacilli from external stresses, such as antibiotics and toxic bactericidal milieu within phagocytes, therefore they are crucial for pathophysiology (*Jankute et al*., 2015b). This is the possible explanation for *aftC* being an essential gene in pathogenic mycobacterial species. Consistent with this, earlier attempts to generate *aftC* deficient strains of *M. tuberculosis* were unsuccessful (Sassetti, Boyd and Rubin, 2003). Truncation of AG reduces the non-reducing terminal of the arabinan unit which serves as the site for mycolic acid attachment (Birch *et al.*, 2008; Jankute *et al.*, 2015b). Reduction in arabinan branching (as in case of *aftC* depletion) has a direct impact on the outer membrane of the mycobacterial cell envelope thereby affecting its cell wall integrity (Birch *et al.*, 2008). This can also be seen in the *aftC* depletion strain of *M. smegmatis* which has reduced acid-fastness, viability, and antibiotic tolerance (rifampicin, chloramphenicol, and ethambutol) (Birch *et al.*, 2008). LAM is also a crucial immunomodulator essential for pathogenicity of mycobacteria and *aftC* depletion affected the cytokine stimulatory profile of *M. smegmatis aftC* depleted strain (Birch *et al.*, 2010). As *M. smegmatis* is a non-pathogenic fast-growing bacterium, *aftC* is dispensable for its growth and viability; but in case of pathogenic mycobacteria such as *M. bovis*, *aftC* is an indispensable gene for its growth, viability and virulence. For this reason, *aftC* is an essential gene in *M. bovis* BCG.

We have generated and confirmed chromosomal deletion of *aftC* in *M. bovis* BCG but were unable to see the anticipated growth defects upon *aftC* depletion (Figure 2.7 and Table 2.1). This observation is contrast to the previous observations where *aftC* depletion resulted in growth defects in *M. smegmatis* (Birch *et al.*, 2008). Growth of *M. bovis* BCGΔ*Mb2692::pTIC6-Mb2692* in the absence of ATc in all the antibiotic combinations suggested leaky expression of AftC from pTIC6 plasmid which was supported by WGS. Point mutations in the *rspA* promoter containing two *tetO* operators led to insufficient - loose binding of TetR resulting in uncontrolled expression of AftC even in the absence of the inducer – Atc (Figure 2.8). Strong selection at synonymous sites in mutants grown in the presence of ATc can be a crucial reason for the emergence of these point mutations (Ehrt *et al*., 2005; Sharma *et al*., 2019). In any case, uncontrolled expression of AftC in *M. bovis* BCGΔ*Mb2692::pTIC6-Mb2692* prevented us from studying the functional consequences of *aftC* depletion on *M. bovis* BCG cell wall

assembly and infectivity. For this reason, we looked at alternative *aftC* depletion strategies in *M. bovis* BCG.

Summary:

In this chapter we found that *aftC* is an essential gene. However, we could not use the *aftC* deletion strain generated using the merodiploid strain due to uncontrolled leaky expression of AftC from the pTIC plasmid.

Chapter 3 : CRISPR interference mediated transcriptional repression of *aftC* (*Mb2692*) in *M. bovis* BCG

3.1 Introduction

CRISPR/Cas (clustered regularly interspaced short palindromic repeats/CRISPR-associated) is a bacterial adaptive immune system developed against invading bacteriophages and plasmids (Ran *et al.*, 2013; Hryhorowicz *et al.*, 2017). This prokaryotic system is developed as a molecular biology tool to enable endogenous gene manipulation in various species and cell types (Ran *et al.*, 2013). This simple, robust and rapid tool revolutionised basic research, biotechnology and medicine. CRISPRs were first discovered in *E. coli* in 1987 when repetitive sequences with unknown function (Ishino *et al.*, 1987). With the advent of WGS CRISPR loci are reported to be present in 40% of bacteria and 90% of archaea (Hryhorowicz *et al.*, 2017). This highly adaptable and heritable microbial immune system incorporates short sequences from foreign nucleic acid (called protospacers) into their CRISPR loci, which are then transcribed into small RNAs that guide endogenous nucleases (CRISPR associated genes) towards the destruction of invading nucleic acids (Figure 3.1A) (Hryhorowicz *et al.*, 2017). There are three types of CRISPR/Cas systems based on sequence and structure of Cas proteins (Hryhorowicz *et al.*, 2017). The type II CRISPR/Cas is the simplest, which uses a single multifunctional Cas9 endonuclease (Gasiunas *et al.*, 2012; Jinek *et al.*, 2012). *In vitro* application of the type II CRISPR/Cas9 system from *Streptococcus thermophilus* and *Streptococcus pyogenes* for targeted gene deletion were first reported in 2012 (Gasiunas *et al.*, 2012; Jinek *et al.*, 2012). From then, it has been widely developed, accepted, and used as a versatile platform for genetic engineering in bacteria.

The CRISPR/Cas9 system relies heavily on the efficient hybridisation of single guided RNA (sgRNA) to a targeted genome sequence, as it is this hybridisation event that directs the Cas9 nuclease to the gene of interest for its excision and inactivation. sgRNA is a fusion of CRISPR RNA (crRNA) and transactivation crRNA (tracrRNA) (Garneau *et al.*, 2010; Gasiunas *et al.*, 2012). crRNA contains a 20-nucleotide guided sequence complementary to the gene of interest. tracrRNA contributes to crRNA maturation and formation of the Cas9 complex (Garneau *et al.*, 2010; Gasiunas *et al.*, 2012). Watson-Crick base pairing of crRNA to the target DNA is also governed by the presence of a protospacer adjacent motif (PAM), which are evolutionarily conserved sequences and present in viral genomes

enabling bacterial viral genome distinction from self (Jinek *et al.*, 2012). As the endonuclease cleaves the target DNA by introducing double strand breaks (DSB) 3 bp upstream of PAM, target DNA must immediately precede a PAM (5'-NGG-3' in *S. pyogenes* CRISPR/Cas9 system is used in this chapter) (Jinek *et al.*, 2012). In this way, Cas9 can be re-directed towards almost any gene of interest preceding a PAM sequence by designing the 20 nucleotide guided sequence within the sgRNA (Figure 3.1B; (Ran *et al.*, 2013)).

DSBs introduced by Cas9 are repaired in one of the two DNA damage repair pathways - non homologous end joining (NHEJ) or homology directed repair (HDR) (Figure 3.1C; (Jinek *et al.*, 2012; Ran *et al.*, 2013)). In the absence of a repair template, DSBs are rapidly ligated by NHEJ which is an error prone repair strategy (Perez *et al.*, 2012). Random insertion/deletion mutations inserted at the site of the junction can create frameshift mutations or a premature stop codon in the coding region of the targeted gene, resulting in its inactivation (Perez *et al.*, 2012). This is a widely used method to obtain gene knockouts (Ran *et al.*, 2013). HDR on the other hand is a high fidelity DNA repair strategy which occurs in the presence of an exogenously introduced repair template (provided in the form of a plasmid or single stranded DNA oligonucleotide) to obtain precise modifications in the targeted gene locus (Chen *et al.*, 2013). Using this method precise edits can be achieved in the genome including insertion of single nucleotide mutations for probing causal genetic variations (Figure 3.1C; (Chen *et al.*, 2013; Ran *et al.*, 2013)). Modified eukaryotic cell lines and transgenic mice generated using this DNA editing technology advanced the knowledge of intractable disease causing genes (Ran *et al.*, 2013).

CRISPR/Cas9 technology holds an enormous potential of functionalising Cas9 for diverse applications (Ran *et al.*, 2013). This is mediated by the presence of two nuclease domains – HNH and RuvC in Cas9 which carry out strand specific cleavage at DNA complementary strand and the non-complementary strands, respectively (Gasiunas *et al.*, 2012; Jinek *et al.*, 2012). Specific mutations in either or both the nucleases can alter Cas9 activity. Single point mutation in RuvC from aspartate-to-alanine (D10A) renders RuvC nuclease catalytically inactive reducing Cas9 nuclease to Cas9 nickase mutant (Cas9n); (Gasiunas *et al.*, 2012; Jinek *et al.*, 2012)). Cas9n nicks DNA complementary strand rather than cleave

the targeted DNA, yielding single stranded breaks which can be repaired through preferential HDR decreasing unwanted mutations at target gene locus (Gasiunas *et al.*, 2012; Jinek *et al.*, 2012).

3.1.1 CRISPR interference

CRISPR interference (CRISPRi) is a recent modification of CRISPR/Cas9 with point mutations in both HNH (H840A) and RuvC (D10A) nuclease domains of Cas9 rendering it to be catalytically inactive (dCas9), thereby enabling transcriptional repression of a targeted gene (Choudhary, Lunge and Agarwal, 2016). Targeted gene regulation using CRISPRi was first developed and used in *E. coli* with up to 1,000-fold gene repression and no detectable off-target effects (Qi *et al.*, 2013). In this system the dcas9 – sgRNA complex induces transcriptional repression either by blocking RNA polymerase from binding to the target gene promoter or by causing a steric block to transcriptional elongation (Rock *et al.*, 2017). Among the two transcriptional repression strategies, sgRNA targets both template and non-template strands and can be used to block the targeted gene promoter, whereas sgRNA is specific to a non-template strand and is more effective, producing up to a 300-fold repression (Bikard *et al.*, 2013; Qi *et al.*, 2013). In this way, this reversible gene inactivation strategy can be extended to simultaneous multiple gene repressions in both bacterial and mammalian cell types (Qi *et al.*, 2013).

Mycobacteria has a type III CRISPR/Cas system present as a single locus comprising of 9 genes from Rv2816c to Rv2824c - homologous to Cas2, Cas1, Csm6, Csm5, Csm4, Csm3, Csm2, Cas10 and Cas6 proteins, respectively. Earlier attempts to implement CRISPRi in mycobacteria were less impressive with only a 4 fold knockdown of gene expression (Rock *et al.*, 2017) as opposed to a 300-fold observed in *E. coli* and *B. subtilis* (Bikard *et al.*, 2013; Qi *et al.*, 2013). To overcome this, three independent groups tried to optimise CRISPRi in mycobacteria (Choudhary *et al.*, 2015; Singh *et al.*, 2016; Rock *et al.*, 2017).

|The first used a type II CRISPR/Cas system which is absent in mycobacteria (Choudhary *et al.*, 2015). They introduced codon optimised *dCas9* from *S. pyogenes* into *M. smegmatis, M. bovis* BCG and *M. tuberculosis* under a Tet^R promoter using an integrating plasmid. Once they established the stable

expression of dCas9 and the absence of dCas9 induced toxicity in mycobacteria, they studied 13 essential genes across a broad range of expression levels in evaluating the silencing efficiency of CRISPRi in mycobacteria. They have demonstrated the technique to be useful in identifying essential genes in mycobacteria, as well as the efficiency of the CRISPRi system in silencing multiple genes simultaneously (Choudhary *et al.*, 2015).

Following this study, a separate study used two different plasmids for expressing dCas9 and sgRNA, both from an inducible Tet^R regulated promoters that can be titrated to achieve a range of inhibition of target gene expression (Singh *et al.*, 2016). In this study both plasmids were transformed simultaneously into *M. tuberculosis*, thereby reducing the generation time in slow-growing mycobacterial species. They also demonstrated the potent and sustained targeted gene knockdown using several essential *M. tuberculosis* genes, and particularly the ability to modulate the extent of transcriptional repression (Singh *et al.*, 2016).

The third study, examined eleven orthologues of *S. pyogenes* - dCas9 (belonging to Type IIA and Type IIC subfamilies of CRISPR/Cas) using a single plasmid platform that expressed the dCas9 allele under an ATc -inducible promoter and the cognate sgRNA under the control of a strong, constitutive promoter (Roc*k et al*., 2017). The study measured gene silencing using a luciferase-based reporter assay. Using this system, they identified *S. thermophilus* - dCas9 to produce the most robust and consistent gene silencing and studied mycobacterial folate biosynthesis pathway. They demonstrated the utility of CRISPRi in functional genomics, genetic interaction mapping and drug-target profiling in slow growing *M. tuberculosis* (Roc*k et al*., 2017).

The earlier chapter established the essentiality of *aftC (Mb2692)* in *M. bovis* BCG and the inability to perform functional genomics. In this chapter we aim to overcome this inability using a CRISPRi mediated transcriptional repression system using an established protocol (Singh *et al.*, 2016). The objectives of this chapter are:

1. To generate an *aftC* repressed strain of *M. bovis* BCG and characterise the phenotypic and functional consequences of *aftC* knockdown in planktonic cultures of *M. bovis* BCG

a. Characterise the effect of *aftC* repression on growth and viability of *M. bovis* BCG
b. Understand the phenotypic consequences of *aftC* repression in *M. bovis* BCG
c. Study the biochemical consequences of *aftC* repression on cell envelope of *M. bovis* BCG

2. Optimise CRISPRi in mycobacterial biofilm cultures to study the implications of *aftC* repression in *M. bovis* BCG biofilms
    a. Optimise CRISPRi in *M. bovis* BCG biofilms
    b. Study the effect of *aftC* repression on biofilm formation of *M. bovis* BCG
    c. Characterise the biochemical consequences of *aftC* repression on extracellular matrix, lipid and lipoglycan profiles of *M. bovis* BCG biofilms
3. Characterise the effects of *aftC* repression on pathogenesis of *M. bovis* BCG
    a. Study the infectivity of *aftC* repressed *M. bovis* BCG in THP1 cell line
    b. Study the immunogenicity of *aftC* repressed *M. bovis* BCG in terms of early and late cytokine profiles of infected THP1 cells

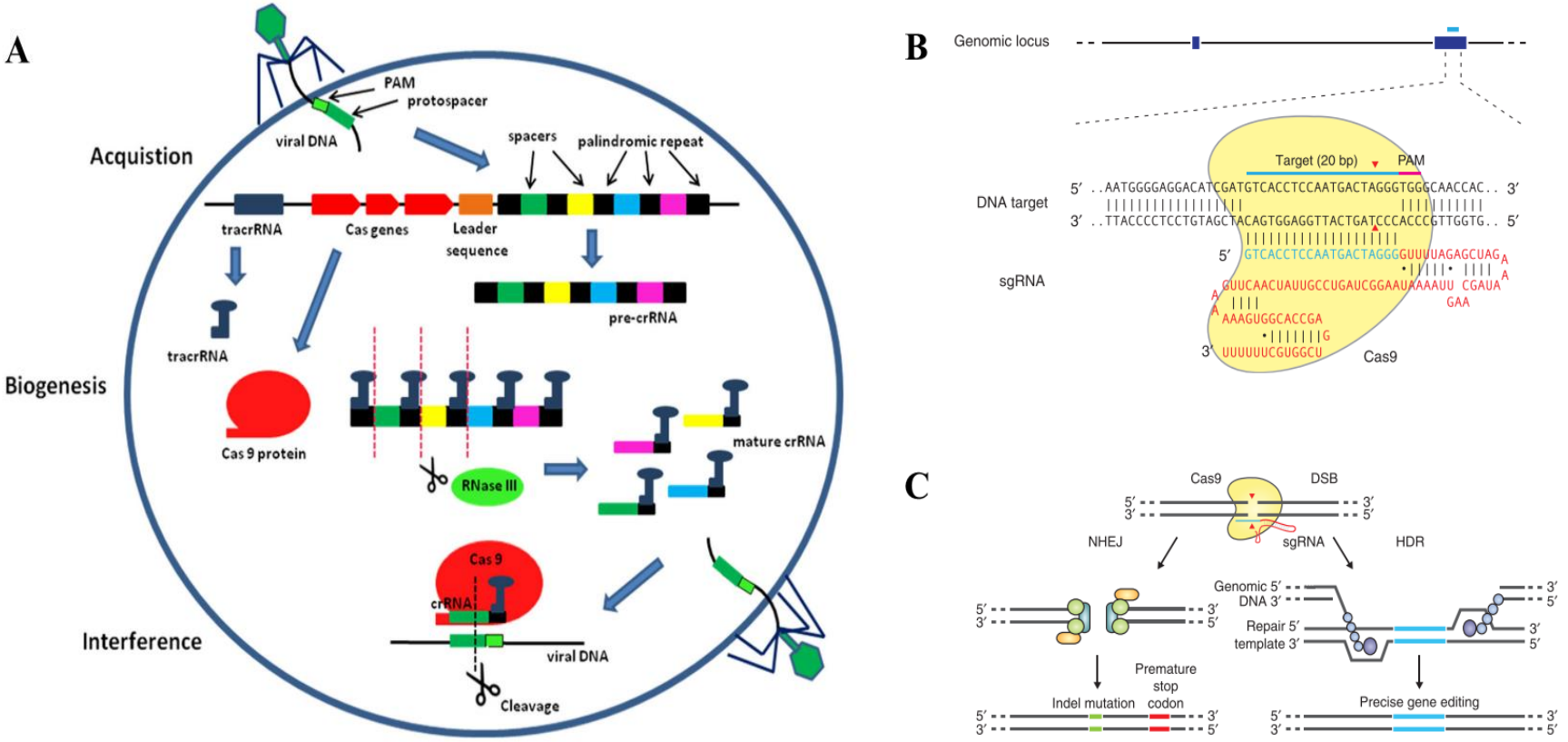

Figure 3.1: ***Overview of CRISPR/Cas system.*** *(A) Three stages of type II CRISPR/Cas system: In the first acquisition stage invading nucleic acid is processed by Cas nuclease into small DNA protospacer fragments which are incorporated into CRISPR locus; in the second biogenesis stage CRISPR locus is transcribed into long precursor crRNA to which tracrRNA hybridises. This complex is cleaved by RNAseIII to produced mature crRNA-tracrRNA complex; in the final interference stage crRNA-tracrRNA complex guides Cas9 nuclease to the complementary foreign nucleic acids resulting in their degradation (B) RNA guided Cas9 cleavage of target DNA: sgRNA consisting of crRNA (blue – hybridises with target DNA) and tracrRNA (red – crucial for the association of sgRNA with Cas9) direct Cas9 to generate DSB 3 bp upstream of PAM (red triangles) (C) DSB repair: DSBs (yellow) can be repaired by error prone NHEJ or high fidelity HDR (images adapted from (Ran et al., 2013; Hryhorowicz et al., 2017)*

3.2 Results

3.2.1 Effect of *aftC* repression on planktonic cultures of *M. bovis* BCG

3.2.1.1 Generation of *aftC (Mb2692)* depletion mutants of *M. bovis* BCG using CRISPR interference

We used CRISPR interference to generate *aftC* depleted strains of *M. bovis* BCG. For this we used two plasmids: 1) pRH2502- expressing catalytically inactive - dead Cas9 (dCas9) under an inducible Tet^R regulated promoter, and 2) pRH2521- expressing a single guide RNA (sgRNA) targeting *aftC* controlled by the same Tet^R regulated promoter. The transcriptional repression using these two plasmids have been optimised and verified in *M. smegmatis, M. bovis* BCG and *M. tuberculosis* in a separate study (Singh *et al.*, 2016).

Three sgRNA's targeting *Mb2692* at ORF positions +112 (sgRNA1), +144 (sgRNA2), and +337 (sgRNA3) were designed (Figure 3.2) with the least off target effects to obtain transcriptional repression of *aftC* (section **6.2**). These sgRNAs were cloned into the pRH2521 plasmid according to an optimised protocol (Ran *et al.*, 2013). The pRH2521 clones containing sgRNA were transformed into *M. bovis* BCG along with pRH2502 plasmid to obtain mutant strains (section **6.2.1**). Empty pRH2521 (without sgRNA) and pRH2502 plasmids were transformed into *M. bovis* BCG, which was used as the control strain in all the subsequent assays. Eventually four mutant strains were generated: 1) BCG-VC (pRH2502 and empty pRH2521), 2) BCG-sgRNA1 (pRH2502 and sgRNA1 cloned pRH2521), 3) BCG-sgRNA2 (pRH2502 and sgRNA2 cloned pRH2521), and 4) BCG-sgRNA3 (pRH2502 and sgRNA3 cloned pRH2521).

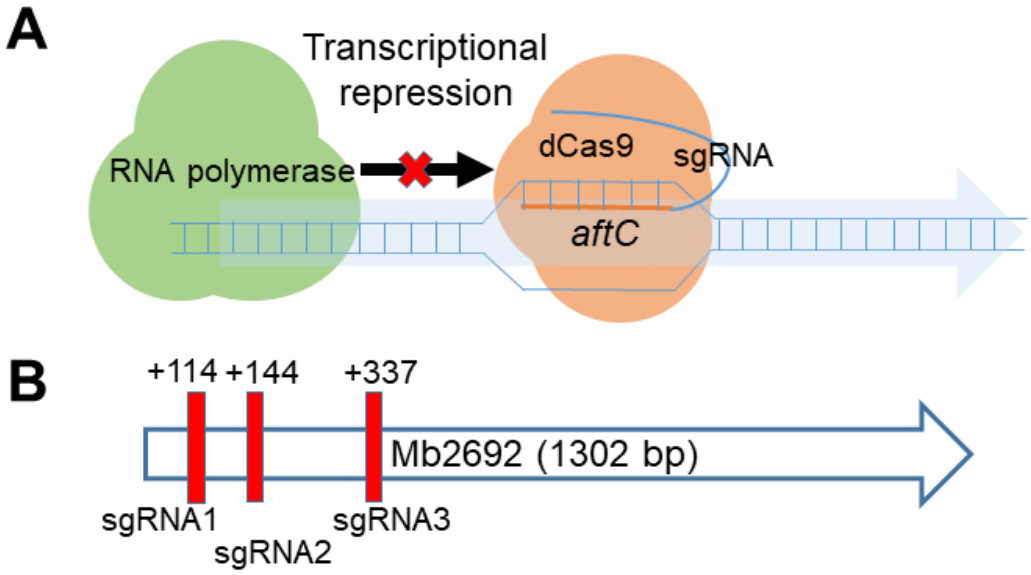

C

Primer	Sequence (5' – 3')
sgRNA1 – F	GGGA TAT AGA TGT CCC ATC CGC GC
sgRNA1 – R	AAAC GC GCG GAT GGG ACA TCT ATA
sgRNA2 – F	GGGA CGG GGG GAT ACA GGT AGT GC
sgRNA2 – R	AAAC GC ACT ACC TGT ATC CCC CCG
sgRNA3 – F	GGGA GGG TGC CAC CGG GGG GAT AC
sgRNA3 – R	AAAC GT ATC CCC CCG GTG GCA CCC

Figure 3.2: ***Generation of aftC repressed M. bovis BCG using CRISPRi****. (A) Schematic of CRISPR interference technique used to generate transcriptionally repressed M. bovis BCG. (B) The position of single guide RNAs used in CRISPRi. (C) Three pairs of oligonucleotides were used for transcriptional repression of aftC in M. bovis BCG their sequences are as shown*

Previous studies have performed ATc titration assays to determine its optimum working concentration that induce maximum transcriptional repression of targeted genes (Singh *et al.*, 2016). In this study, a dose response between ATc concentration in the culture and the extent of mRNA depletion identified a concentration of 200 ng/ml of ATc to produce the maximum induction of *dCas9* and sgRNA, which sustained transcriptional repression of targeted genes when supplemented once every 48 hours (Singh *et al.*, 2016). ATc concentrations of 25, 50, 100, 150, 200 ng/ml were tested and using RNA extraction, reverse transcription and PCR reaction (**6.2.3**), the optimum ATc concentration to achieve the maximum transcriptional repression of *aftC* in *M. bovis* BCG was found to be 200 ng/ml. Reaction primers were

designed to amplify 300 bp of *aftC* to confirm the presence or absence of *aftC* transcripts in total RNA extracted. Total RNA extracted was subjected to rigorous DNAse treatment and the absence of contaminating DNA was confirmed using the same primers in a PCR reaction. Subsequent cDNA synthesis using the same *aftC* specific reverse primer and PCR reaction confirmed the absence of *aftC* transcripts at ATc concentration of 200 ng/ml (Figure 3.3). As a result, a concentration of 200 ng/ml of ATc was used to induce *aftC* repression, which was replenished every 48 hours for the entire duration of culturing.

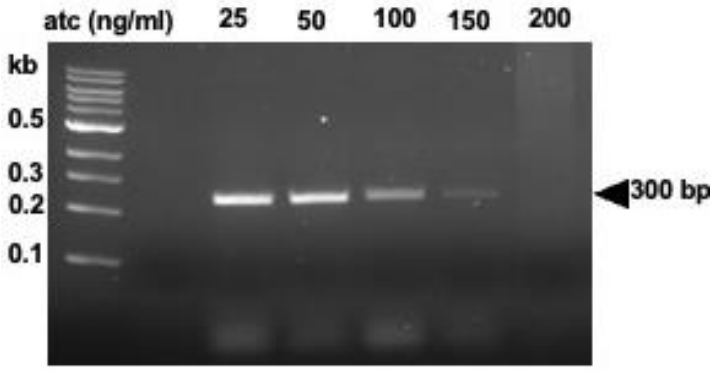

Figure 3.3: ***ATc titration in aftC knockdown M. bovis BCG****: AftC transcripts were analysed from cultures grown in 25, 50, 100, 150 and 200 ng/ml ATc and 200 ng/ml*

Three colonies (representing three biological replicates) of each strain were picked to analyse growth kinetics. An OD_{600} was used to measure the growth of each strain and the experiment repeated three times using three biological replicates for each strain. Strains were then inoculated from a plate and grown in 7H9-OADC-tween medium for 1 day after which the culture was split into two equal volumes and one half was supplemented with ATc to a final concentration of 200 ng/ml (to induce *dCas9* and sgRNA for transcriptional repression of *Mb2692*). The growth rate was monitored using OD_{600}, which was measured every day over 8 days (**6.2.2**).

BCG-VC was used as the control strain which only expressed dCas9 without an sgRNA directing it to the site of transcriptional repression. The growth rate of BCG-VC was compared to wild type *M. bovis* BCG which was grown in the same media and under the same conditions as BCG-VC (Figure 3.4). BCG-VC showed growth rates similar to wild type *M. bovis* BCG. Also, ATc addition had no effect on

the growth of BCG-VC (Figure 3.4). Ectopic expression of dCas9 without sgRNA targeting *Mb2692* has no effect on growth of *M. bovis* BCG. This also confirms the absence of ATc induced cytotoxicity in mycobacterial cells. Therefore, BCG-VC is an ideal control for all the subsequent analyses and CRISPRi mediated transcriptional repression is sufficient to study the effect of transcriptional repression of *aftC (Mb2692)* in *M. bovis* BCG.

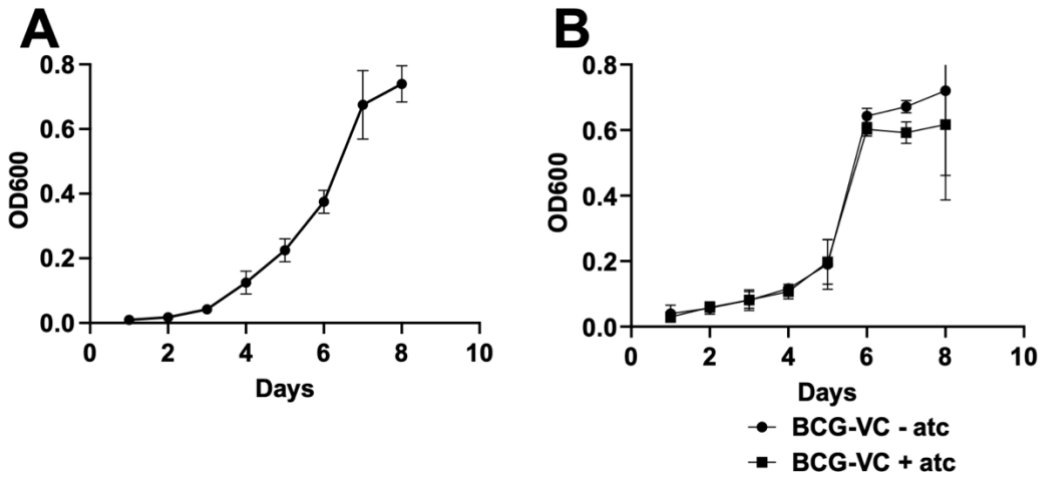

Figure 3.4: ***Comparison of growth kinetics between wild type M. bovis BCG and BCG-VC:*** *Absorbance at 600 nm was measured to estimate growth kinetics of wild type M. bovis BCG and BCG-VC over 8 days*

BCG-sgRNA1 expressing sgRNA1 targeting *Mb2692* at ORF +114 has abnormally increased growth rate with OD_{600} measuring 1.3 when grown in the absence of ATc and 1.2 when grow in the presence of ATc at the end of 8 days (Figure 3.5B). This is contrary to earlier studies performed in *M. smegmatis* where a growth defect (measured by optical density) was observed upon *aftC* depletion (Birch *et al.*, 2008). The possible explanation for this anomaly is inefficient binding of sgRNA1 to the target site resulting in inefficient transcriptional repression of *Mb2692* (Bikard *et al.*, 2013; Choudhary *et al.*, 2015; Singh *et al.*, 2016; Rock *et al.*, 2017). Similar inefficient guided RNA binding is seen in multiple earlier reports, suggesting the use of multiple sgRNA's to target each gene (Bikard *et al.*, 2013; Choudhary *et al.*, 2015; Singh *et al.*, 2016; Rock *et al.*, 2017).

BCG-sgRNA2 expressing sgRNA2 targeting *Mb2692* at ORF +144 has contrasting growth kinetics as compared to BCG-sgRNA1, where the strain has hampered growth even in the absence of ATc induced transcriptional repression of *aftC*. The OD_{600} measured 0.3 after 8 days when grown in the absence of ATc and 0.09 when grown in the presence of ATc (Figure 3.5C). This suggests that sgRNA2 expression and targeting *Mb2692* at ORF +144 is lethal for mycobacterial growth and viability.

Earlier studies have shown that sgRNA targeting the sense strand of the coding region are efficient in silencing gene expression, especially when less than 100 bp upstream of a transcription start site (Choudhary *et al.*, 2015). Although, targeting the 5' untranslated region of *Mb2692* for transcriptional repression would have produced better gene silencing (Choudhary *et al.*, 2015) it shares an operon with *Mb2691* and they have a common transcriptional start site. Therefore, we designed all the sgRNAs targeting the sense strand of the *Mb2692* coding region. Despite this, BCG-sgRNA1 and BCG-sgRNA2 show contrasting growth kinetics as measured by OD_{600}. The exact reason behind this discrepancy remains unknown. Due to inability to obtain the required biomass from BCG-sgRNA2, it was disregarded from all the subsequent analyses.

BCG-sgRNA3 expressing sgRNA3 targeting *Mb2692* at ORF +337 showed a growth defect upon ATc mediated transcriptional repression of *Mb2692*, which is consistent with earlier *aftC* knockout studies in *M. smegmatis* (Birch *et al.*, 2008). At day 8, BCG-sgRNA3 measured OD_{600} of 0.7 when grown in the absence of ATc and OD_{600} of 0.1 when grown in the presence of ATc (Figure 3.5D). As, optical density only measures the cloudiness of a culture as quantified by the light scattered by obstructing particles, it is not an accurate measurement of cell viability. It fails to distinguish between viable cells, dead cells and cell debris, and other components including lipids secreted by mycobacteria (Birch *et al.*, 2008). CFU assay would present an accurate measurement of viable cells and the population that is repressed within the culture. This is the limitation of this growth kinetic assay.

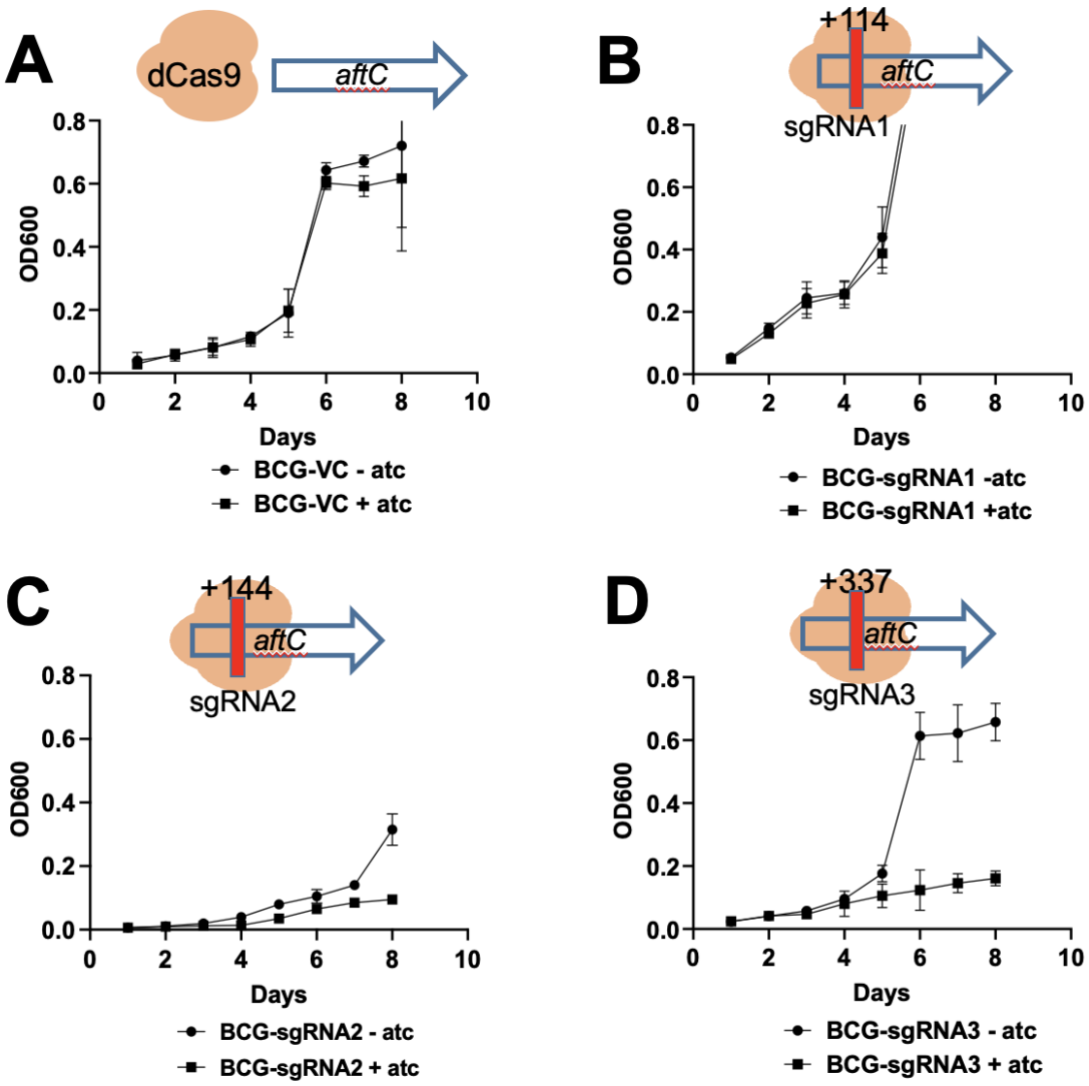

Figure 3.5: ***Growth kinetics of aftC knockdown M. bovis BCG.*** *(A) BCG-VC (B) BCG-sgRNA1 (C) BCG-sdgRNA2 (D) BCG-sgRNA3 were grown in the presence or absence of ATc. Absorbance at 600 nm was measured to estimate growth kinetics of each strain. Three biological replicates were used for each strain and the experiment was repeated three times to generate error bars*

As we were able to obtain required biomass by scaling up the volume of BCG-sgRNA3 when grown in the presence of ATc, it was used for confirmation of transcriptional repression of *aftC* by RNA extraction and RT-PCR. BCG-VC and BCG-sgRNA3 were grown in the presence and absence of 200 ng/ml ATc for 8 days, with ATc supplemented every 48 hours. *aftC* transcripts in knockdown cultures were analysed by RT-PCR, for which primers were designed 200 bp into *Mb2692* to amplify 300 bp of the transcript. Total RNA was extracted from BCG-sgRNA3 grown in the presence or absence of 200 ng/ml ATc along with control strain – BCG-VC grown in the exact conditions (**6.2.3**). Extracted total

RNA was subjected to rigorous DNAse treatment and the absence of contaminating DNA in the RNA used for reverse transcription was confirmed using the primers Mb2692-F and Mb2692-R (Table 6.9) in a PCR reaction (Figure 3.6). Subsequent cDNA synthesis using *aftC* specific reverse primer (designed for the PCR rection) and PCR reaction revealed complete absence of *aftC* transcripts in BCG-sgRNA3 when it was grown in the presence of ATc as compared to the same strain grown in the absence of Atc (Figure 3.7). This was standardised against the housekeeping gene- *sigA*, which was present consistently irrespective of ATc addition (Figure 3.7). BCG-VC contained *aftC* and *sigA* transcripts irrespective of ATc addition (Figure 3.7).

RT-PCR used here is a qualitative approach and fails to account for the quantitative transcriptional reduction seen during CRISPRi mediated *aftC* silencing. qRT-PCR is a better quantitative approach which would have established the effect and extent of ATc mediated transcriptional repression on the RNA levels of *aftC*. Nevertheless, qualitative RT-PCR used here shows that sgRNA3 enables transcriptional repression of *aftC*, resulting in growth defects seen in BCG-sgRNA3 (Figure 3.5D) and corroborates the efficacy of CRISPR interference in generating *aftC* repressed *M. bovis* BCG.

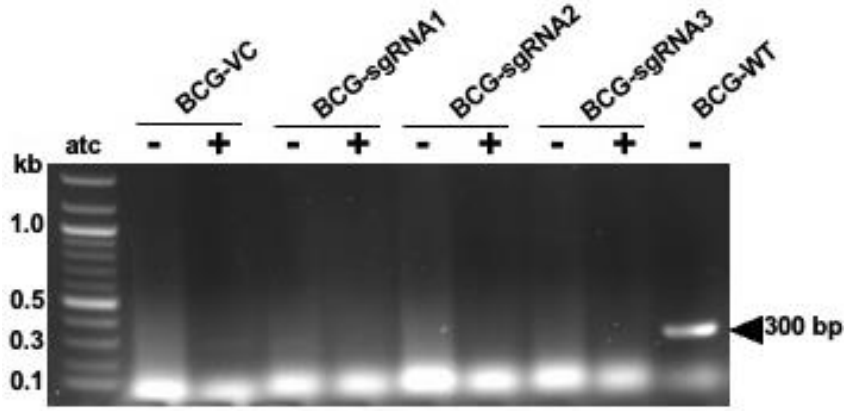

Figure 3.6: ***Absence of contaminating DNA in RNA extraction****: Prior to cDNA synthesis absence of contaminating DNA was confirmed using PCR reaction using the primers Mb2692-F and Mb2692-R (Table 6.9)*

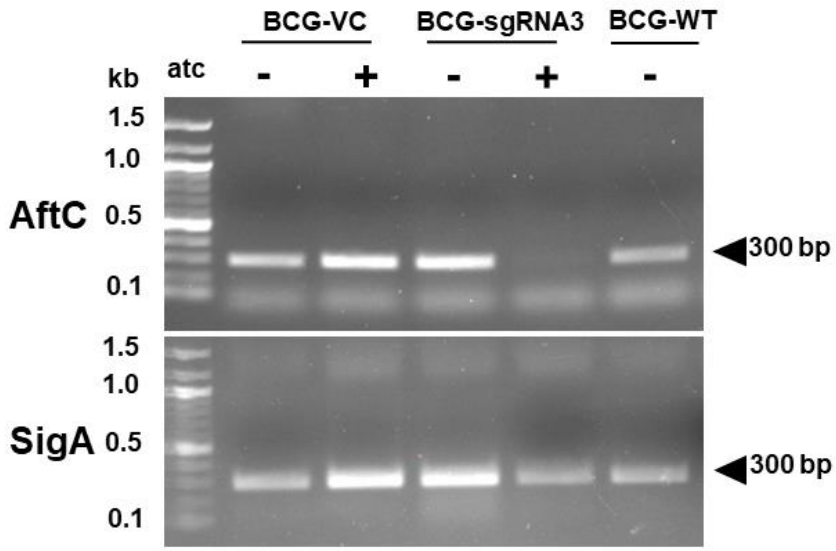

Figure 3.7: ***Confirmation of aftC knockdown in BCG-sgRNA3 using semi quantitative RT-PCR.*** *Total RNA extraction, reverse transcription and semi quantitative PCR using ethidium bromide-stained agarose gel electrophoresis were performed on BCG-VC and BCG-sgRNA3 grown in the presence and absence of ATc to confirm aftC knockdown induced by ATc in BCG-sgRNA3 when compared to BCG-VC and BCG-WT.*

3.2.1.2 Transcriptional repression of *aftC* affected the cell size and morphology of *M. bovis* BCG

In all the following assays BCG-sgRNA3 grown in the presence and absence of ATc along with BCG-VC were examined. There are three reasons for this; Firstly BCG-sgRNA1 is not in accordance with the established phenotype of the growth defect which was previously seen with an *aftC* depletion mutant (Figure 3.5; Birch *et al.*, 2008), secondly BCG-sgRNA2 has growth defects when grow in the absence of ATc preventing the generation of the required biomass for subsequent assays (Figure 3.5), and thirdly, *aftC* gene silencing was confirmed in the BCG-sgRNA3 strain upon ATc addition (Figure 3.7). For these reasons, we have only used BCG-sgRNA3 in all the subsequent assays.

As *aftC (Mb2692)* repressed *M. bovis* BCG growth similar to the *aftC* knockout *M. smegmatis* (Birch *et al.*, 2008), phenotypic and morphological consequences of this mutant were characterised. For this, bacteria were grown to log phase and immobilised on agarose and individual bacilli were visualised using confocal microscopy to analyse the effect of *aftC* repression on cell size and morphology of *M.*

bovis BCG (**6.2.4**). Microscopy was performed on three biological replicates of BCG-sgRNA3 along with three biological replicates of BCG-VC and the assay was repeated twice for statistical significance.

M. bovis BCG was visualised under a confocal microscope to standardise the conditions to view *aftC* repressed *M. bovis* BCG (Figure 3.8). Once these conditions were optimised, BCG-VC and BCG-sgRNA3 grown in the presence and absence of ATc and were grown to exponential log phase and visualised to examine the effect of transcriptional repression of *aftC* on cell size and morphology. BCG-VC when grown in the presence and absence of ATc looked morphologically similar to *M. bovis* BCG (Figure 3.9A). In contrast, BCG-sgRNA3 has aberrant cell size and morphology when compared to BCG-VC and *M. bovis* BCG (Figure 3.8 and Figure 3.9A). BCG-sgRNA3 when grown in the absence of ATc exhibited a heterogeneous population with much smaller and fluffier bacilli, possibly due to a defective cell wall, along with some normal sized bacilli (Figure 3.9A). This defective cell size observed in BCG-sgRNA3 grown in the absence of ATc is possibly due to leaky expression of sgRNA3 and dCas9. Earlier reports, described leaky expression from ATc promoters affecting mycobacterial growth in the absence of CRISPRi induction (Rock *et al.*, 2017). Although, this might be similar to earlier reports, there is no evidence to support this explanation during the RNA extraction and semi-quantitative PCR analyses (Figure 3.7). The aberrant cell morphology was amplified in BCG-sgRNA3 when it was grown in the presence of ATc, with a much higher number of shorter sized bacilli. This population had two major types of defective bacilli: 1) bacilli of normal length but with a discontinuous cell wall with fluffier appearance, 2) bacilli of significantly smaller cell length (Figure 3.9A). To enumerate this reduction of cell length, 100 different bacilli from each strain were measured using ImageJ-Fiji software and compared for statistically significant differences (Figure 3.9B). These results confirm a statistically significant reduction in cell length in BCG-sgRNA3 as compared to BCG-VC (Figure 3.9B). There is also a significant reduction in cell length of BCG-sgRNA3 grown in the absence of ATc as compared to BCG-VC, and this effect was amplified upon ATc addition (Figure 3.9B). This confirms the effect of transcriptional repression of *aftC* on morphology and cell size of *M. bovis* BCG.

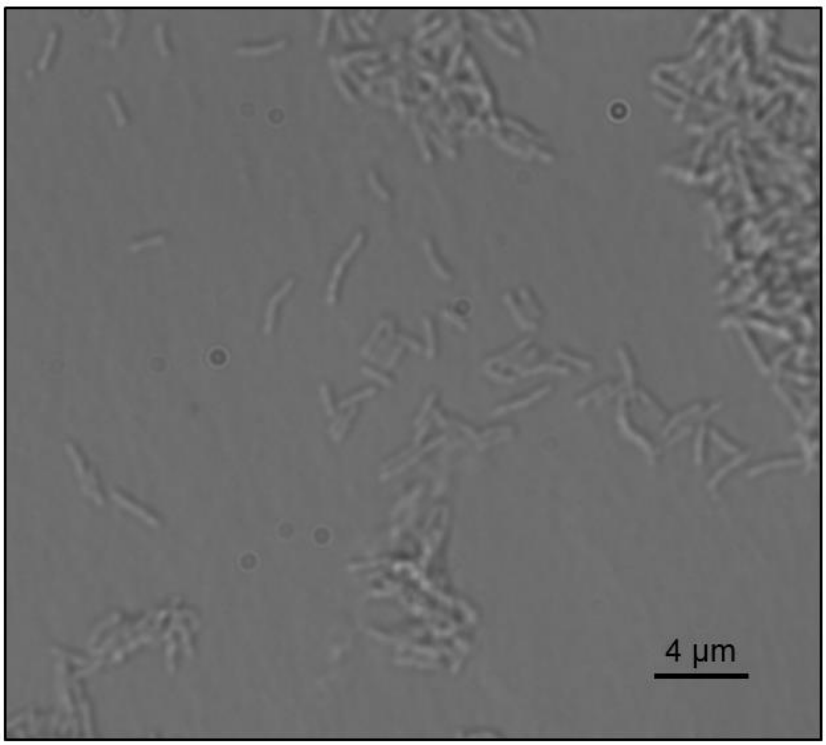

Figure 3.8: ***Standardising the visualising conditions of M. bovis BCG using confocal microscope.*** *Wild type M. bovis BCG grown to mid log phase were immobilised on an agar plate and visualised using a confocal microscope at 100x magnification*

A

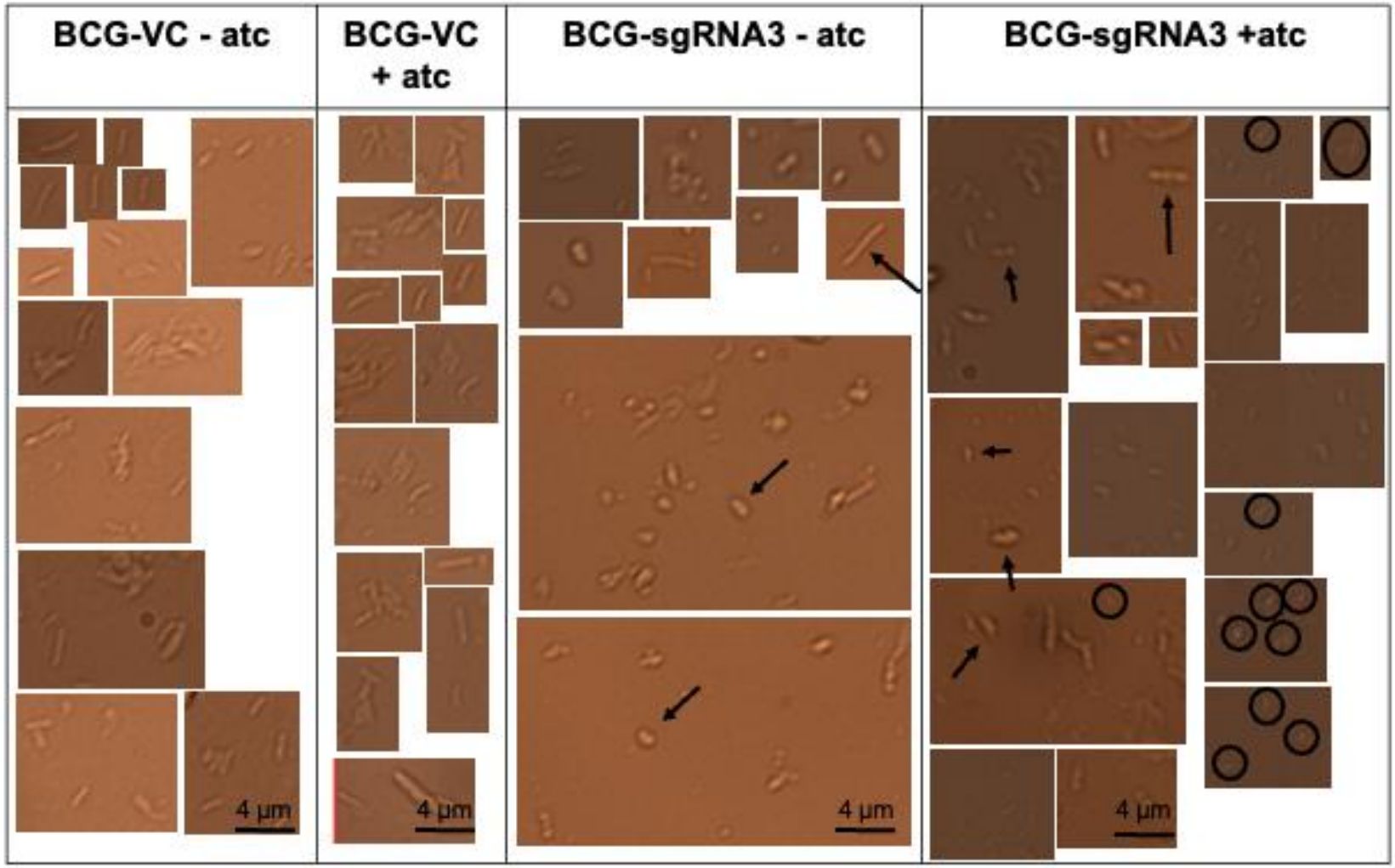
BCG-VC - atc
BCG-VC + atc
BCG-sgRNA3 - atc
BCG-sgRNA3 +atc
4 µm
4 µm
4 µm
4 µm

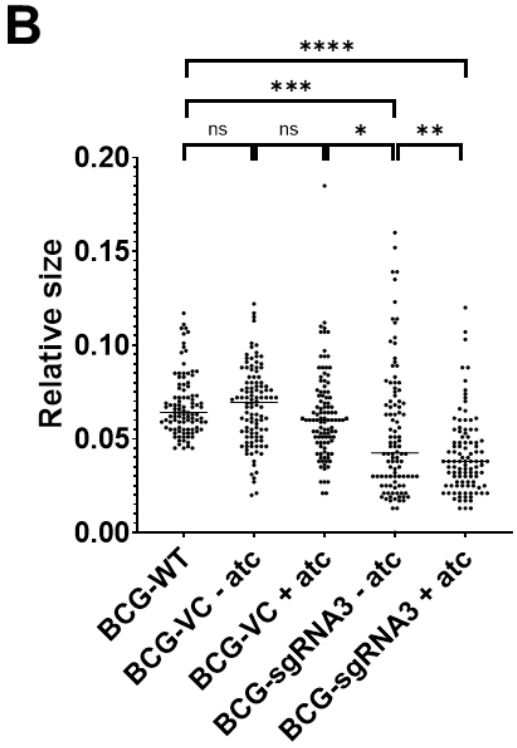

Figure 3.9: ***AftC repression affected the cell size of M. bovis BCG bacilli*** *(A) BCG-VC and BCG-sgRNA3 grown in the presence and absence of ATc were visualised using confocal microscopy. BCG-VC bacilli looked healthy and of normal length whereas BCG-sgRNA3 had defective bacilli. (B) Length of 100 different bacilli from each strain were measured using ImageJ-Fiji software and the results were plotted using GraphPad Prism 9.0.1. Statistical analysis was performed between individual groups using unpaired parametric t-test with Welch's correction (p<0.05 (*), p<0.01 (**), p<0.001 (***), p<0.0001 (****))*

3.2.1.3 Transcriptional repression of *aftC* resulted in generation of a truncated, unbranched LAM in the cell envelope of planktonic *M. bovis* BCG

To analyse the biochemical consequences of *aftC* repression on cell envelope biosynthesis and assembly of *M. bovis* BCG, we extracted the solvent-soluble polysaccharides and analysed these products using silver staining and Western blotting (Figure 3.10).

Three replicates of BCG-VC and BCG-sgRNA3 planktonic cultures were grown in the presence and absence of ATc and radiolabelled using [^{14}C]-acetate. The bacterial pellet was subjected twice to ethanol reflux to extract the cell envelope polysaccharides. The supernatant was treated with proteinase K followed by dialysis to obtain a polysaccharide fraction containing α-glucan, LM, LAM and PIMs

(**6.2.6**). This polysaccharide mixture obtained from radiolabelled cultures was used to analyse the biochemical consequences of *aftC* repression on *M. bovis* BCG.

Autoradiography suggests no change in carbohydrate profile of BCG-VC when grown in the presence or absence of ATc (Figure 3.10). Ectopic expression of dCas9 in BCG-VC grown in the presence of ATc had no visible effect on the cell envelope carbohydrate composition as indicated by autoradiography (**6.2.10**) and Western blotting (**6.2.8**; Figure 3.10). However, BCG-sgRNA3 has a change in its cell envelope carbohydrate composition. LAM appeared to be smaller in size in BCG-sgRNA3 grown in the presence of ATc, as compared in the absence of ATc (labelled as 'AftC-LAM'; Figure 3.10). Earlier knockout studies in *M. smegmatis* showed the role of *aftC* in branching AG and LAM by addition of the first Ara*f* residue through an α(1→3) linkage to an α(1→5) arabinan backbone (Birch *et al.*, 2008, 2010). Depletion of AftC resulted in the depletion of 3,5-Ara*f* branching residues in LAM and a significant reduction in t-Ara*f*, 2-Ara*f* and 5-Ara*f*-linkages in LAM, thereby resulting in the generation of an intermediary sized 'AftC-LAM' (Birch *et al.*, 2008). Those results support these findings in *M. bovis* BCG. Although, the total sugar analysis using alditol acetate derivatisation followed by gas chromatography would have quantified the reduction in LAM size to a greater extent, we were unable to perform this due to technical difficulties and Covid-19 constraints at the time.

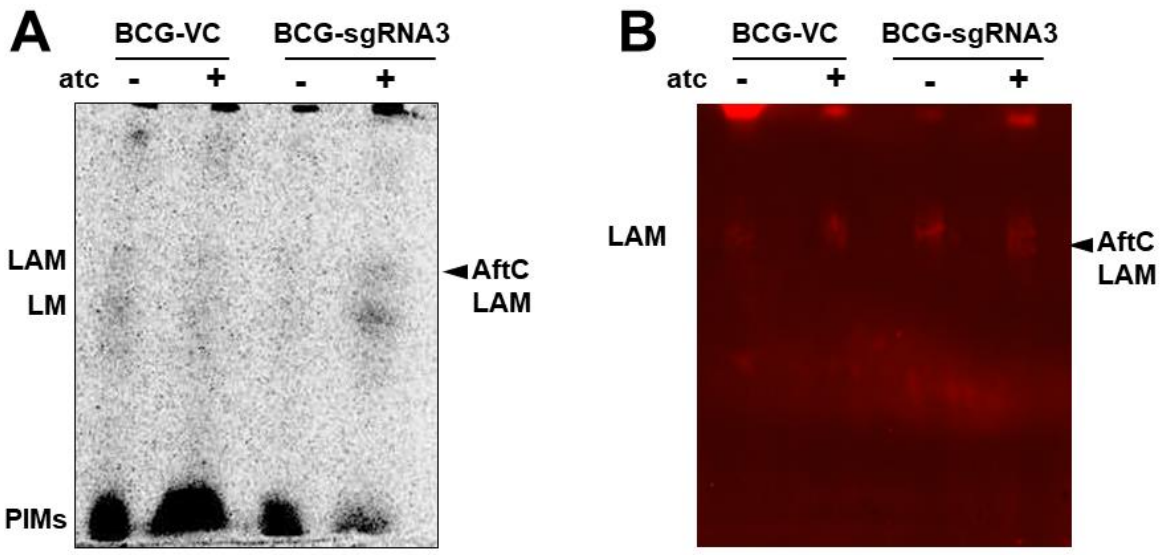

Figure 3.10: ***Cell wall carbohydrate analysis of aftC knockdown M. bovis BCG planktonic cultures*** *(A) Carbohydrates were separated on an Any kD SDS-PAGE gel and corresponding radioactivity was visualised using phosphor screen autoradiography. (B) Western blotting using cs-35 antibody*

3.2.1.4 Transcriptional repression of *aftC* has a minor effect on cell envelope lipid composition of planktonic cultures of *M. bovis* BCG

AftC is involved in 3,5-Ara*f* branching of AG and LAM thereby increasing the number of non-reducing terminal of arabinan domains in AG and LAM (Birch *et al.*, 2008, 2010). These non-reducing terminal act as sites for mycolic acid attachment (Jankute *et al.*, 2015). Transcriptional repression of *aftC* was shown to impact the cell envelope carbohydrate composition of *M. bovis* BCG (Figure 3.10), this could potentially reduce the mycolic acid attachment sites and alter the cell wall lipid composition in *aftC* knockdown *M. bovis* BCG. Alteration in cell wall lipid composition implies change in drug sensitivity as lipid rich waxy outer membrane protects the bacilli from hydrophilic drugs and host immune responses.

To study the changes in the lipid profile of this mutant strain, three biological replicates of BCG-VC and BCG-sgRNA3 were grown in the presence and absence of ATc using [^{14}C]-acetate and cell wall bound lipids were extracted. Pellets from the carbohydrate extraction were subjected to chloroform: methanol: water (10:10:3 v/v) extraction twice to obtain cell wall associated lipids. These were then cleaned through a biphasic wash using chloroform: methanol: water (3:47:48 v/v) (**6.2.9**) and analysed

by TLC (**6.2.11**). The same delipidated culture pellet was used for the extraction of cell wall bound mycolic acids using tetra-butyl-ammonium hydroxide hydrolysis followed by methylation to afford FAMEs and MAMEs (**6.2.9**). FAMEs and MAMEs were analysed by TLC from the *aftC* repressed *M. bovis* BCG strain (**6.2.11**). Densitometry was performed on individual lipid spots from three technical repeats using ImageJ – Fiji software followed by statistical analysis and the result plotting on Graphpad Prism 9.0.1.

Free fatty acids and free mycolic acids were analysed on a 2-D TLC in solvent system C (Table 6.12) as described in **6.2.11**. While free fatty acids remain consistent in BCG-VC grown in the presence and absence of ATc, there is a slight accumulation in BCG-sgRNA3 grown in the absence of ATc. However, this accumulation is absent in the BCG-sgRNA3 grown in the presence of ATc. Free mycolic acids remained consistent across the strains grown in the presence and absence of ATc as shown by TLC-autoradiography (Figure 3.11A).

DAT and GMM were analysed similarly by 2-D TLC in solvent system D (Table 6.12). TLC-autoradiography revealed the absence of DAT and GMM in the *aftC* repressed *M. bovis* BCG strain, but the remaining lipids measured remained consistent across the strains (Figure 3.11B). PI, lower PIMs (PIM_2) and higher PIMs (PIM_6) were also analysed on a 2-D TLC in solvent system E (Table 6.12). TLC-autoradiography revealed inconsistency in PIMs with accumulation of PI, Ac_2PIM_2 and Ac_2PIM_6 in the *aftC* repressed BCG-sgRNA3 (Figure 3.11C).

Cell wall bound FAMEs and MAMEs were extracted and analysed on a 1-D TLC using petroleum ether/acetone (95:5) (Table 6.12). The α- and ketomycolates were visualised by TLC-autoradiography and revealed a pronounced increase in α– and ketomycolates in BCG-sgRNA3 (Figure 3.11D). Densitometry was performed on three technical repeats and plotted for statistical analysis (Figure 3.12). A statistically significant increase in α– and ketomycolates was observed in the BCG-sgRNA3 strain grown both in the presence and absence of ATc as compared to BCG-VC. BCG-sgRNA3 grown in the absence of ATc has a significantly higher level of mycolates than the same strain grown in the presence of ATc (Figure 3.12). Although, the exact reason behind this discrepancy is unknown it is consistent

with the earlier result (Figure 3.9B). The ratio of α– to ketomycolates also increased in BCG-sgRNA3 as compared to BCG-VC when both were grown in the absence of ATc. However, this effect was not carried to BCG-sgRNA3 grown in the presence of ATc and there is no statistically significant difference in the ratio of α– to keto mycolates between this strain and BCG-VC grown in the absence of Atc (Figure 3.12).

Earlier *aftC* knockout studies in *M. smegmatis* revealed a reduction in AG esterified mycolic acids and increase in TDM production upon *aftC* deletion (Birch et al., 2008). In contrast, we observed an increase in α– and ketomycolates. Moreover, the ratio of α– to keto-mycolate also increased in BCG-sgRNA3 implying an abundance of α– over ketomycolates in *aftC* repressed BCG-sgRNA3 (Figure 3.12). A partial or incomplete *aftC* knockdown induced by CRISPRi might be responsible for this inconsistency. This has been reported in previous publications (Roc*k et al*., 2017), where up to 80 % of the transcriptional repression has been reported using CRISPRi (Singh *et al.*, 2016). Although, gene expression as quantified by RT-PCR revealed a complete repression of *aftC* transcripts (Figure 3.7), we possibly only achieved 80 % transcriptional repression of *aftC* enabling only facile gene manipulation in BCG-sgRNA3 contrary to the specialised transduction employed in earlier studies which made a permanent chromosomal deletion of *aftC* in *M. smegmatis* (Birch et al., 2008).

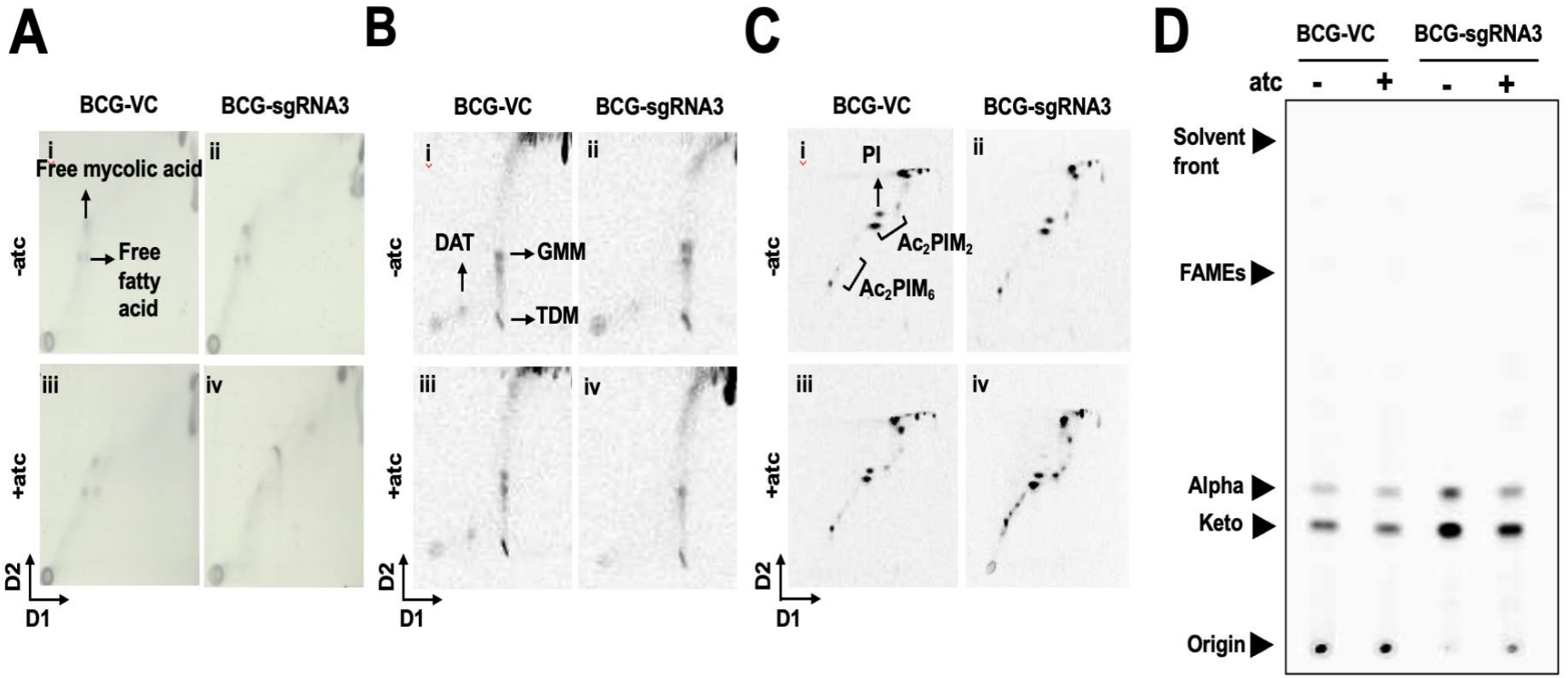

Figure 3.11: ***Cell wall lipid analysis of aftC knockdown M. bovis BCG planktonic cultures using autoradiography.*** *Cell wall associated lipids were analysed on 2-D TLC and visualised using autoradiography. (A) system C solvent system (B) system D solvent system (C) system E solvent system (D) Cell wall bound lipids (FAMES and MAMEs) were separated on a 1-D TLC in 60-80 Pet ether: acetone (95:5) solvent system and visualised using autoradiography.*

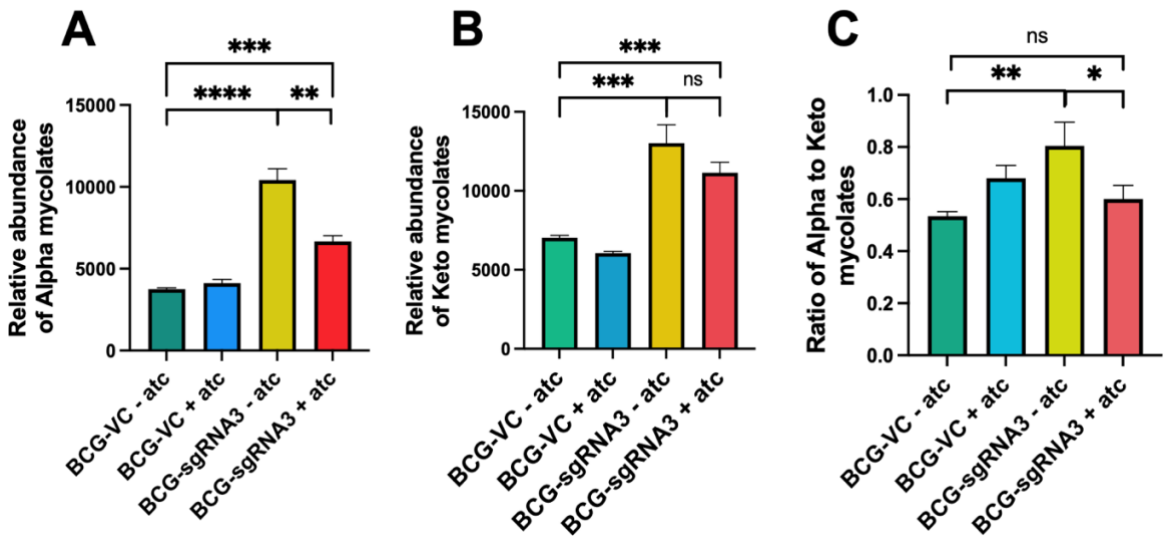

Figure 3.12: ***Quantification of planktonic cell envelope mycolates using densitometry****. (A) α-mycolates were increased in BCG-sgRNA3 grown both in the presence and absence of ATc. (B) Keto mycolates also increased. (C) Ratio of alpha to keto mycolates also increased upon aftC repression in M. bovis BCG*

3.2.2 Effect of *aftC* repression on *M. bovis* BCG biofilms

3.2.2.1 *aftC* repression affects biofilm formation in *M. bovis* BCG

It has been reported that mutants with compromised cell wall integrity fail to form mycobacterial biofilms (Recht and Kolter, 2001; Chen et al., 2006; Ojha *et al*., 2008, 2010; Pacheco et al., 2013; Sambandan *et al*., 2013; Wright et al., 2017; Yang *et al*., 2017). For example, MDAG mutants fail to form pellicles (Chen et al., 2006; Pacheco et al., 2013; Wright et al., 2017), similarly GPL mutants had delayed biofilm formation (Recht and Kolter, 2001; Yang *et al*., 2017). *M. smegmatis* and *M. tuberculosis* mutants with defective mycolic acid profiles could not initiate biofilm formation (Ojha *et al*., 2008, 2010; Sambandan *et al*., 2013). Earlier *aftC* deletion studies in *M. smegmatis* revealed aberrant mycolic acid profiles (Birch *et al.*, 2008). However, they did not assess the consequences of this on biofilm formation. Also, *glmM* knockdown and *upk* deletions in *M. smegmatis* affected its biofilm formation. These mutants with defects in PG synthesis failed to form biofilms possibly due to reduced covalently attached mycolic acids or overall change in the cell wall composition affecting cell wall integrity. Therefore, it will be interesting to study the effect of AftC depletion on biofilm formation as it is shown to effect mycobacterial cell wall integrity in planktonic cultures of *M. bovis* BCG (Figure 3.10 and Figure 3.11).

The earlier CRISPRi studies in mycobacteria only used planktonic cultures of different mycobacterial species (Choudhary *et al*., 2015; Singh *et al.*, 2016; Rock *et al.*, 2017). For the first time, we developed a protocol to generate *aftC* repressed *M. bovis* BCG in biofilm cultures.

Three biological replicates of BCG-VC, BCG-sgRNA1, BCG-sgRNA2 and BCG-sgRNA3 were set up in quadruplet to form biofilms in Sauton's minimal medium at 37 °C and 5% CO_2 (**6.2.5**). Mature biofilms were observed at the end of 5 weeks. The experiment was repeated twice, and images were recorded (Figure 3.13). Whilst BCG-VC formed mature biofilms in the liquid-air interface in five weeks, BCG-sgRNA3 failed to form mature biofilms (Figure 3.13). Moreover, BCG-VC forms mature biofilm, when grown in the presence of ATc, negating the possibility of ATc induced defective biofilm

formation. This also highlights that ectopic expression of dCas9 without sgRNA targeting *aftC,* has no effect on biofilm formation. Additionally, BCG-sgRNA1 similar to its planktonic cultures (Figure 3.5) has no change in biofilm formation upon ATc addition (Figure 3.13). Inefficient binding of sgRNA1 to *Mb2692 (aftC)* at ORF +114 position is the plausible reason for the lack of *aftC* repression seen in BCG-sgRNA1. For this reason, it was discarded in further experiments involving biofilms. Similarly, consistent with the planktonic cultures (Figure 3.5), BCG-sgRNA2 forms defective biofilms even in the absence of ATc induced transcriptional repression of *aftC* (*Mb2692*) (Figure 3.13). Again, due to inability to obtain the required biofilm biomass from BCG-sgRNA2, it was discarded from the subsequent biofilm analysis. BCG-sgRNA3 forms biofilms in the absence of ATc and forms defective biofilms upon ATc induced transcriptional repression of *aftC* (*Mb2692*) (Figure 3.13). Although, BCG-sgRNA3 forms a biofilm when grown in the absence of ATc, there is a difference in its texture when compared to biofilms formed by BCG-VC. They lack the organised ridges and troughs characteristic to mycobacterial biofilms and rather have a cluster of multiple microcolonies aggregated together (Figure 3.13). Despite the presence of the underlying cellular arrangement essential for the biofilm formation, they lost the smooth finishing of a mature mycobacterial biofilm rich in ridges and troughs. The reduction in biofilm formation seen in BCG-sgRNA3 grown in the absence of ATc can be attributed to partial knockdown of *aftC* in this strain due to leaky expression of sgRNA3 and dCas9 with defective bacilli, as confirmed by microscopy (Figure 3.9). However, this defect in biofilm formation was amplified when BCG-sgRNA3 was grown in the presence of ATc inducing CRISPRi mediated transcriptional repression of *Mb2692 (aftC;* Figure 3.13).

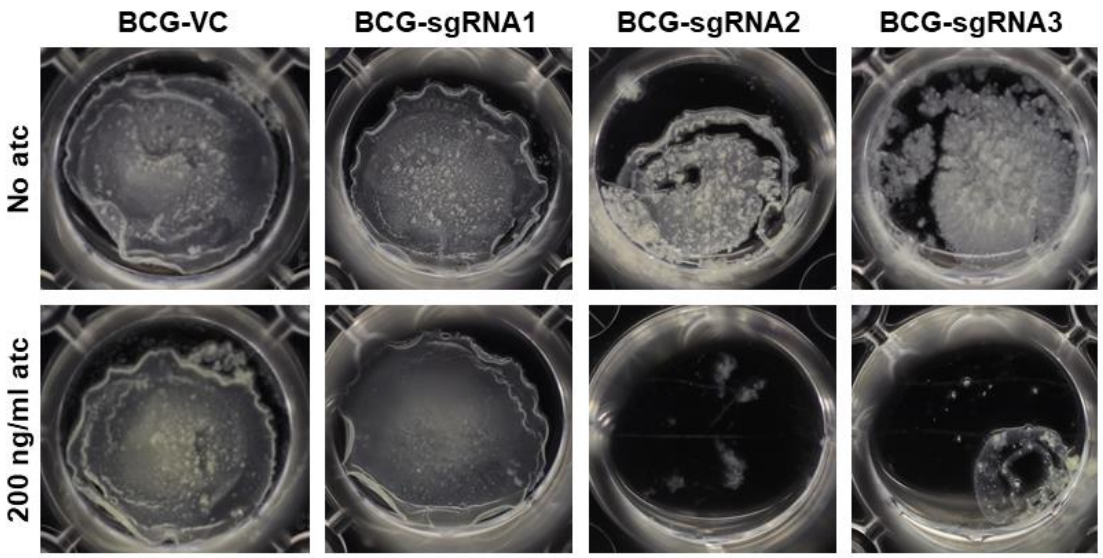

Figure 3.13: ***Defective biofilm formation seen in aftC knockdown M. bovis BCG.*** *BCG-VC has a stable biofilm formation irrespective of ATc addition. BCG-sgRNA1 also has no effect on biofilm formation upon ATc addition. BCG-sgRNA2 and 3 have a significant reduction in biofilm formation upon ATc addition.*

3.2.2.2 Crystal volet and Alcian blue staining of biofilms

To quantify the reduction in biofilm formation, crystal violet staining was used to measure biofilm formation of individual strains. Crystal violet assay is a colorimetric method which indirectly correlates the extent of biofilm formation to amount of dye retained by the biofilm matrix and cells as measured by optical density. Crystal violet binds to negatively charged particles in the cells and the ECM thereby estimating the total biofilm biomass (Amador *et al*., 2021; Ebert *et al*., 2021). Similarly, the carbohydrate content within the biofilm matrix was measured using alcian blue staining. Alcian blue is a polyvalent basic dye which stains acidic polysaccharides (Dong *et al*., 2012). Using this calorimetric method we quantified the total carbohydrates within the biofilm matrix of BCG-VC and BCG-sgRNA3 grown in the presence and absence of ATc.

To perform the crystal violet assay, we used quadruplets of a single biological replicate of both BCG-sgRNA3 and BCG-VC. Biofilms were stained with 0.5% w/v crystal violet for 10 minutes and subsequently de-stained by 95% v/v ethanol for 20 minutes at room temperature. The absorbance at 400 nm was used to quantify the retention of crystal violet (**6.2.5**). Statistical analysis was performed

between the individual groups using unpaired parametric t-test with Welch's correction in GraphPad Prism 9.0.1 on quadruplet sets of BCG-VC and BCG-sgRNA3 biofilms grown in the absence and presence of ATc. When compared to BCG-VC grown in the presence of ATc there is a 2-fold reduction in biofilm biomass of BCG-sgRNA3 grown in the absence of ATc and a 10-fold reduction in biofilm biomass in BCG-sgRNA3 grown in the presence of ATc (Figure 3.14A). This demonstrates that in *M. bovis* BCG, *aftC* plays a significant role in biofilm formation.

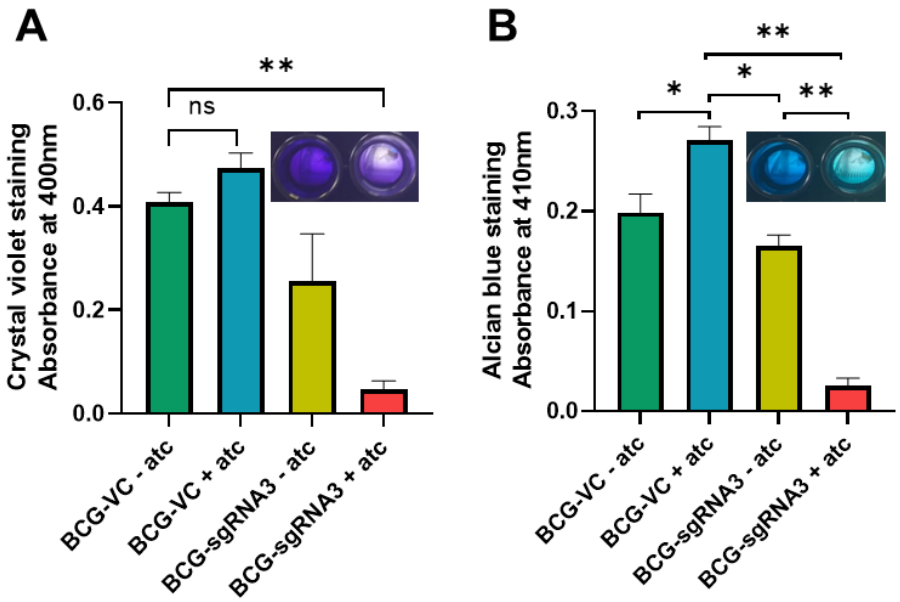

Figure 3.14: ***Quantification of defective biofilm formation seen in aftC repressed M. bovis BCG****. (A) Crystal violet assay – statistically significant 2-fold reduction in biofilm biomass of BCG-sgRNA3 grown in the absence of ATc and a 10-fold reduction in biofilm biomass in BCG-sgRNA3 grown in the presence of ATc when compared to BCG-VC was observed (B) Alcian blue staining –statistically significant 7-fold reduction in stain retention in BCG-sgRNA3 biofilms grown in the presence of ATc as compared to those grown in the absence of ATc was observed*

Alcian blue staining was performed similar to the crystal violet assay, quadruplets of a single biological replicate were stained with alcian blue stain and destained with 33% (v/v) acetic acid. Absorbance at 410 nm was measured to correlate stain retention to polysaccharide content within the biofilm matrix (**6.2.5**). Since *aftC* is involved in the assembly of mycobacterial lipoglycans, we performed alcian blue staining to measure the effect of *aftC* repression on the overall polysaccharide level within the biofilm matrix of *M. bovis* BCG. Alcian blue which stains acidic polysaccharides in both ECM and cells is a direct measure of polysaccharides within the biofilm matrix. Stain retention between BCG-VC and

BCG-sgRNA3 were comparable when both were grown in the absence of ATc. However, a 1.5-fold higher stain was retained in BCG-VC samples, when grown in the presence of ATc, compared to the same strain grown in the absence of ATc (Figure 3.14B). In BCG-VC, which lacks sgRNA targeting *aftC*, excess ATc accumulated in sub-lethal levels might have caused this increase in polysaccharide levels within its biofilm matrix. However, minimum inhibitory concentration (MIC) of ATc in *M. smegmatis* planktonic cultures is around 1 µ/ml (Ehrt et al., 2005) and 5-fold below its MIC in *M. bovis* BCG biofilms. Therefore, no possible ATc induced toxicity contributing to this effect. Also, similar ATc induced toxicity was not seen in planktonic cultures (Figure 3.5, Figure 3.7, Figure 3.9). Therefore, if there is an underlying mechanism for ATc induced effect on *M. bovis* BCG's biofilm formation, it is yet to be identified.

BCG-sgRNA3 biofilms grown in the presence of ATc showed a 7-fold reduction in acidic polysaccharide levels as compared to the same strain grown in the absence of ATc (Figure 3.14B). Although, there has been a slight increase in overall polysaccharide levels in BCG-VC biofilms, when grown in the presence of ATc, this effect hasn't been observed in BCG-sgRNA3. Alcian blue was retained 10-fold less in BCG-sgRNA3 biofilms grown in the presence of ATc as compared to BCG-VC biofilms grown in the presence of ATc (Figure 3.14B). This data suggests a role of *aftC* in mycobacterial glycolipid generation and assembly within the biofilm matrix of *M. bovis* BCG. Further experiments including electron microscopy using GFP expressing strains and a dye specifically binding to LAM would provide further evidence supporting our claims (Appendix 3). Also backing up this data with CFU measurements would have corroborated the role of *aftC* depletion in slowing biofilm formation.

To provide further evidence to our claims, we have used two biological replicates of BCG-sgRNA3. The two replicates were grown in triplicate with or without ATc addition over a period of 5 weeks in Sauton's minimal media at 37 °C and 5% CO_2 (**6.2.5**). Crystal violet and alcian blue staining were performed to measure the difference in biofilm formation and total polysaccharide levels between *aftC* repression induced and uninduced BCG-sgRNA3 across the two replicates (Figure 3.15). A significant growth defect was seen in both the replicates upon ATc addition (*aftC* repression). Biofilms formed in the absence of ATc did not match one another. While both had the underlying cellular arrangement

essential for the biofilm formation, one replicate lacks the organised ridges and troughs characteristic to mycobacterial biofilms and rather have an aggregate of multiple microcolonies, the other replicate has the smooth finishing of a mature mycobacterial biofilm rich in ridges and troughs (Figure 3.15A). However, both the replicates have a marked reduction in biofilm formation upon ATc addition which is a direct consequence of *aftC* repression and not ATc induced toxicity as we have seen a mature biofilm formation by BCG-VC when grown in the presence of ATc (Figure 3.13).

In both the replicates a statistically significant 5-fold reduction in biofilm biomass was measured using the crystal violet assay, having a difference in colorimetric measurement visible to the naked eye (Figure 3.15C-D). Alcian blue also has a similar difference in colorimetric measurement between BCG-sgRNA3 grown in the presence and absence of ATc, with the strains having a 6-fold and 4-fold reduction in stain retention upon *aftC* repression (Figure 3.15E-F). However, alcian blue has a broad specificity and stains any glycoconjugates including other sugars – PG, AG, polar forms of PIMs, LM, LAM and even glycoproteins (Angala *et al*., 2015; Dong *et al*., 2012). Due to this we cannot assume that the reduction in the alcian blue stain retention as seen in *aftC* repressed BCG-sgRNA3 is due to one particular sugar deficiency and can be an overall reduction in glycoconjugates.

To understand if the overall sugar reduction seen in *aftC* repressed BCG-sgRNA3 biofilms is due to inability to produce sugars or simply because of less biofilm and defective bacterial growth, we compared the alcian blue stain retention to crystal violet stain retention for each replicate grown in the presence and absence of ATc. The relative ratio of alcian blue to crystal violet was 3.5 and 1.3 for the two replicates when grown in the absence of ATc which was reduced to 1 when grown in the presence of ATc (Figure 3.15B). Due to inconsistency between the ratios of stain retention, we are unable to draw firm conclusions based on this assay if the reduction seen in acidic polysaccharide levels measured alcian blue staining is due to inability to produce sugars or reduced biofilm formation.

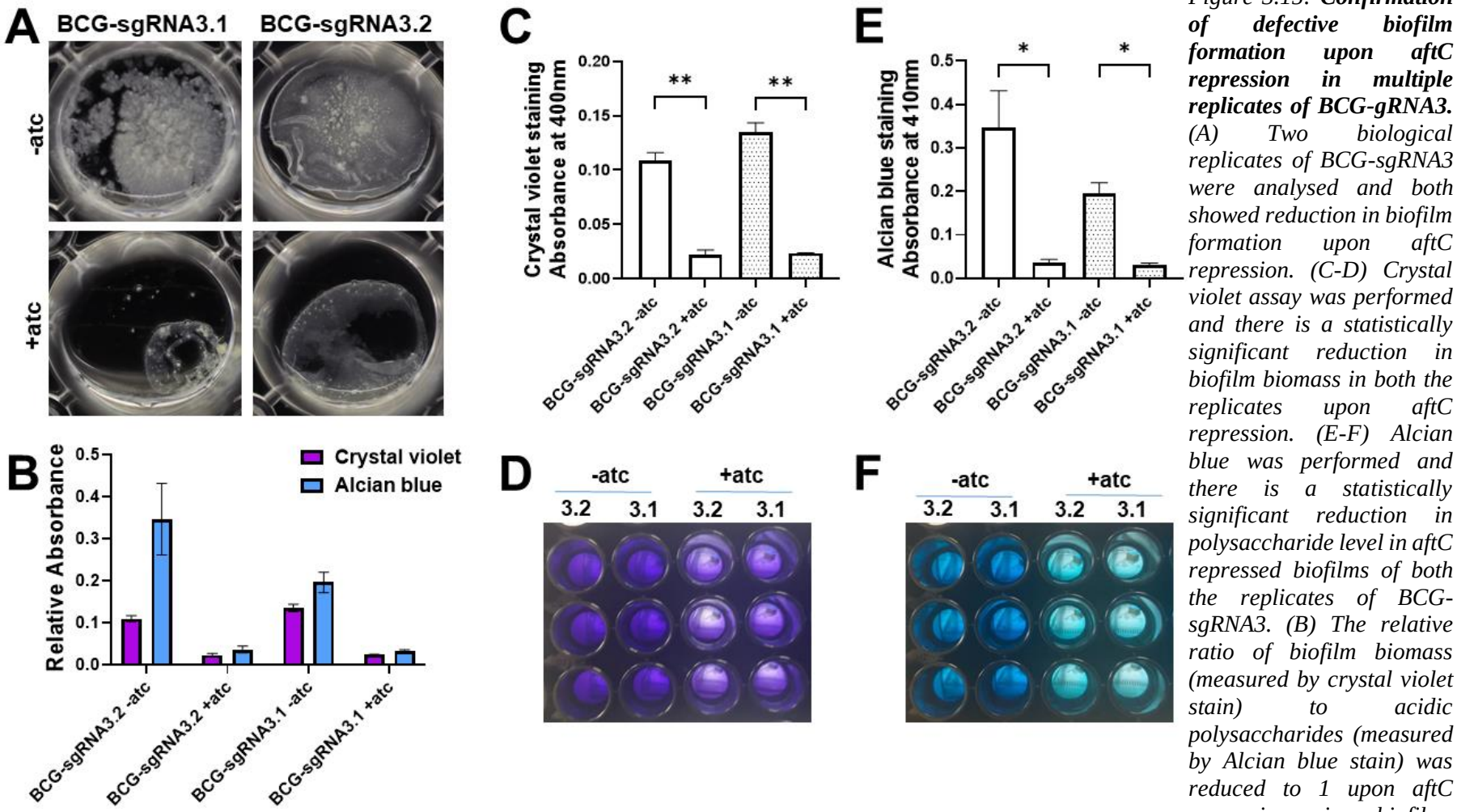

Figure 3.15: ***Confirmation of defective biofilm formation upon aftC repression in multiple replicates of BCG-gRNA3.*** *(A) Two biological replicates of BCG-sgRNA3 were analysed and both showed reduction in biofilm formation upon aftC repression. (C-D) Crystal violet assay was performed and there is a statistically significant reduction in biofilm biomass in both the replicates upon aftC repression. (E-F) Alcian blue was performed and there is a statistically significant reduction in polysaccharide level in aftC repressed biofilms of both the replicates of BCG-sgRNA3. (B) The relative ratio of biofilm biomass (measured by crystal violet stain) to acidic polysaccharides (measured by Alcian blue stain) was reduced to 1 upon aftC repression in biofilms formed by both the replicates*

In planktonic cultures of BCG-sgRNA3, the effect of ATc induced transcriptional repression of *aftC* is seen after 4 days of culture. Up until 4 days BCG-sgRNA3 grown in the absence of ATc and the same grown in the presence of ATc have similar OD_{600} values (Figure 3.5). After 4 days of growth, divergence between their OD_{600} was observed (Figure 3.5). To identify the point of divergence/difference between BCG-sgRNA3 biofilms grown in the presence and absence of ATc, time point analysis was performed. BCG-VC and BCG-sgRNA3 were inoculated from a starter culture into 3 plates in quadruplets and grown with and without ATc. Plates were incubated for 3-, 4-, and 5- weeks at the end of which biofilm biomass and total polysaccharide levels were measured using crystal violet and alcian blue staining.

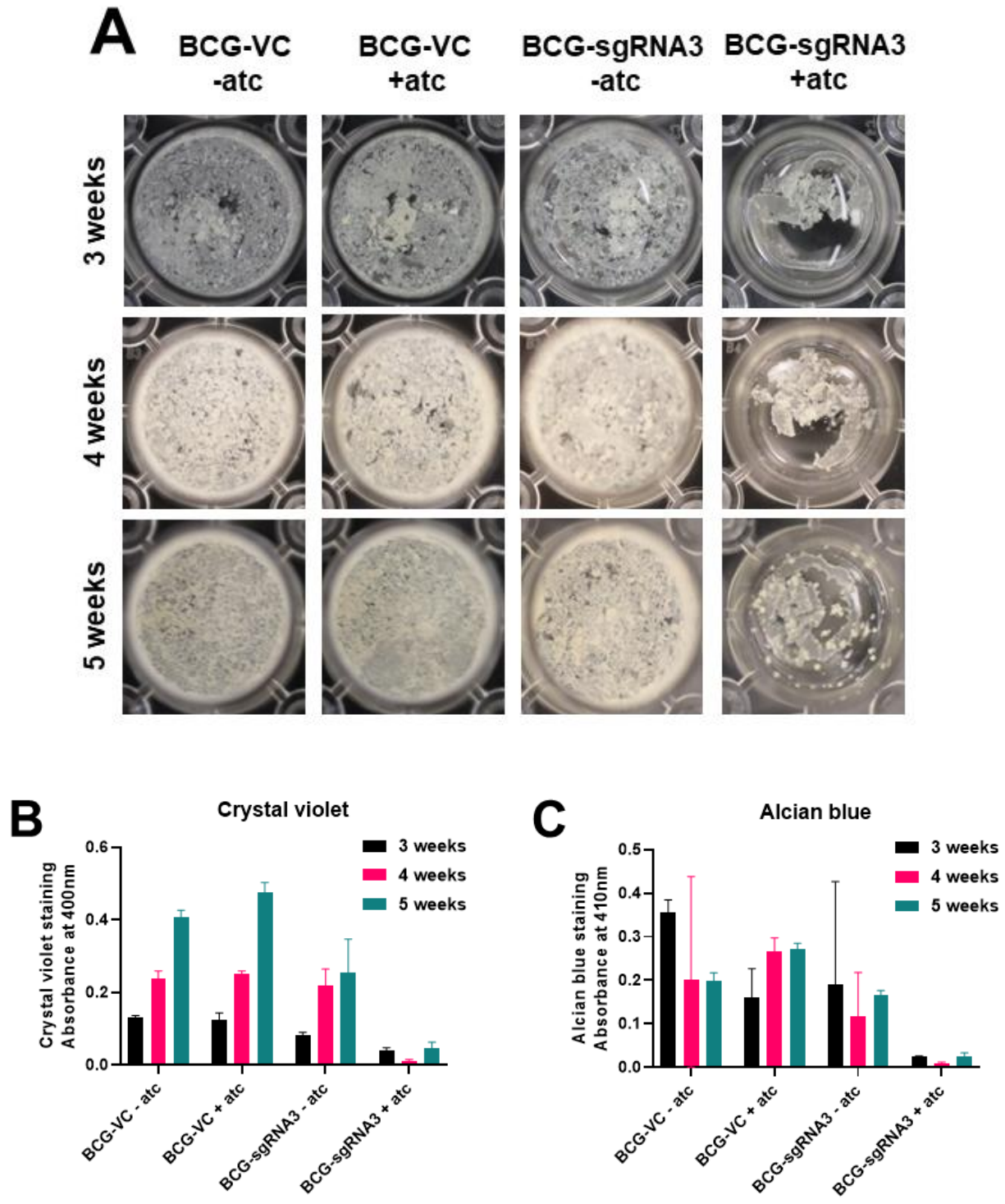

Figure 3.16: ***AftC repressed M. bovis BCG biofilm time point analysis.*** *(A) BCG-VC and BCG-sgRNA3 biofilms grown in the presence and absence of ATc over a period of 3-, 4- and 5- weeks of time were analysed for their biomass and polysaccharides within the biofilm matrix using crystal violet and alcian blue staining, respectively. (B) Crystal violet assay shows a steady increase in biofilm biomass for BCG-VC grown in the presence and absence of ATc. However, aftC repressed BCG-sgRNA3's growth is hampered from as early as 3 weeks of biofilm formation. (C) Alcian blue staining also reveals a significant reduction in acidic polysaccharide levels in the biofilm matrix from as early as 3 weeks into biofilm formation*

In *M. bovis* BCG, free-floating planktonic cells (formed within 24 hours), in the absence of detergent aggregate to form microcolonies which are visible to the naked eye in 7 days (1 week). These aggregates attach to the plasticware in about 10 days, eventually forming a thin sheet of surface pellicles covering the liquid air interphase in 14 days (2 weeks) (Alberto *et al.*, 2020). Following this, a thick extracellular matrix is developed, rich in DNA, polysaccharides and lipids especially mycolic acids which drive the biofilm towards maturation by the end of 5 weeks (Chakraborty and Kumar, 2019). Mature biofilms have a characteristic surface texture with ridges and troughs, along with sediments of reminiscent microcolonies (Ojha *et al.*, 2005). BCG-sgRNA3 forms aggregate of microcolonies which take up to 2 weeks to form but fail to mature into a biofilm. The surface texture including ridges and troughs begins in week 3, so this is where we expect to see the difference between BCG-VC and BCG-sgRNA3 and between BCG-sgRNA3 grown in the presence and absence of ATc. For this reason, we performed crystal violet and alcian blue staining at the end of 3-, 4-, and 5- weeks.

The difference between the textures of biofilms formed by BCG-VC and BCG-sgRNA3 is seen from as early as 3 weeks into biofilm formation. BCG-sgRNA3 grown in the presence of ATc has an aggregation of microcolonies but they fail to develop an extracellular matrix to form a mature biofilm, while the same strain when grown in the absence of ATc forms biofilms, but to a lesser extent when compared to BCG-VC (quantified by crystal violet stain in Figure 3.16B).

To understand the biochemical basis of the inability of BCG-sgRNA3 when grown in the presence of ATc, alcian blue staining was performed on the biofilms formed by BCG-sgRNA3 at the end of 3, 4, and 5 weeks (Figure 3.16C). BCG-VC grown in the presence and absence of ATc has a gradual increase in total glycoconjugate levels in the biofilm matrix. In BCG-sgRNA3 grown in the absence of ATc, this increase in glycoconjugate level is hampered at 4 weeks as they remain relatively constant. However, in BCG-sgRNA3 grown in the presence of ATc, transcriptional repression of *aftC* resulted in significant 5-fold reduction of overall glycoconjugate level within the biofilm matrix contributing to defective biofilm formation at the end of 5 weeks (Figure 3.16C).

This data indicates the role of *aftC* in biofilm formation of *M. bovis* BCG (Figure 3.13, Figure 3.14 and Figure 3.15). Transcriptional repression of *aftC* affects biofilm formation and this effect is seen as early as 3 weeks into biofilm formation (Figure 3.16). There is an overall reduction in glycoconjugate levels in the biofilm matrix of *aftC* repressed *M. bovis* BCG biofilms, however whether this reduction in glycoconjugate level is due to fewer biofilm or due to ineffective polysaccharide production and assembly in ECM remains unclear (Figure 3.14, Figure 3.15 and Figure 3.16).

3.2.2.3 *aftC* repression affects lipoglycans in M. bovis BCG biofilms

Polysaccharide extractions were performed similar to planktonic culture analysis to understand their level and composition within the biofilm matrix of BCG-VC and BCG-sgRNA3 biofilms grown in the presence and absence of ATc. For this, two biological replicates of each were grow in triplicate for 5 weeks in Sauton's medium at 37°C and 5% CO_2 for 5 weeks. Polysaccharides were extracted by ethanol reflux at 95°C for 3 hours twice followed by proteinase K treatment and dialysis. Carbohydrate mixtures containing α-glucan, LM, LAM and PIMs were obtained (**6.2.6**). Carbohydrate composition in the *aftC* repressed *M. bovis* BCG biofilms was analysed by silver staining and Western blotting. ATc addition has no effect on the lipoglycan composition of BCG-VC (Figure 3.17). However, BCG-sgRNA3 produced an intermediary sized LAM when grown in the presence of ATc (labelled as 'AftC-LAM'). This is like planktonic culture lipoglycan analysis (Figure 3.10) and consistent with the earlier knockout studies performed in *M. smegmatis* where depletion of AftC resulted in the depletion of 3,5-Ara*f* branching residues resulting in significant reduction in t-Ara*f*, 2-Ara*f* and 5-Ara*f*-linkages, thereby resulting in the generation of an intermediary sized AftC-LAM (Birch et al., 2008). The *aftC* knockout studies in *M. smegmatis* also observed that this intermediary sized LAM was restored upon AftC complementation (Birch et al., 2008, 2010). The silver staining and Western blotting analysis using the cs-35 antibody are consistent with these studies and show intermediary sized AftC-LAM production upon *aftC* depletion in *M. bovis* BCG (Figure 3.17). However, these studies are only indicative and linkage analysis and total sugar analysis by alditol acetate derivatisation would provide the confirmation

needed to corroborate these claims. Although, we performed these analysis, they remained inconclusive, the results of which are attached in appendices (1 and 2).

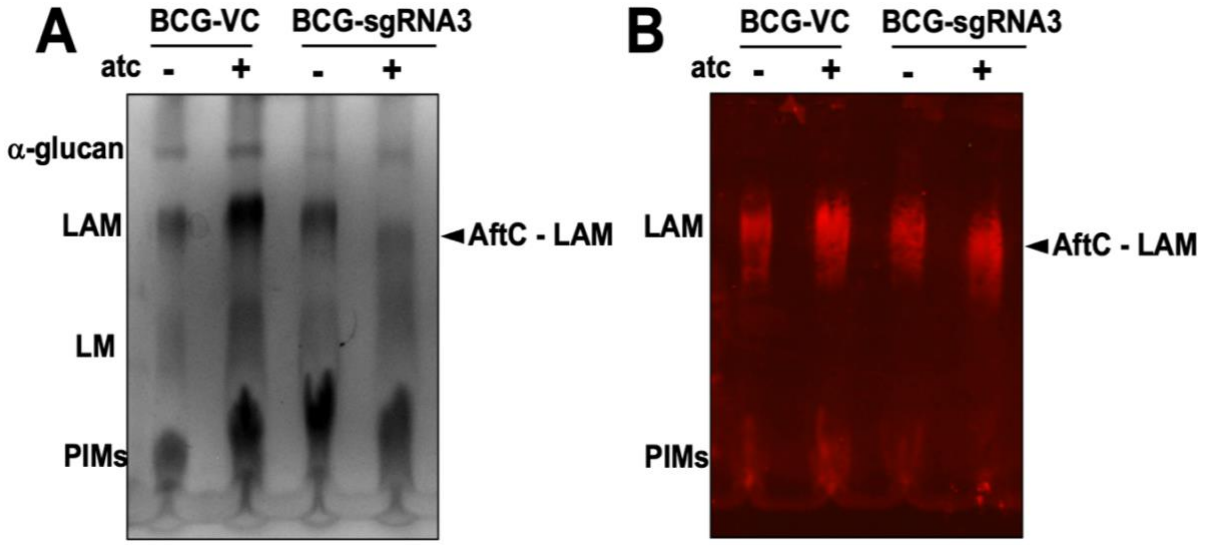

Figure 3.17: ***Carbohydrate analysis of aftC repressed M. bovis BCG biofilms using silver staining and Western blotting.*** *Carbohydrates from biofilm cultures were extracted, separated in 15% SDS-PAGE gels and analysed by (A) silver staining and (B) Western blotting using cs-35 antibody. aftC knockdown strain has a intermediary sized LAM molecule – labelled "AftC-LAM" when compared to control strains.*

3.2.2.4 *aftC* repression affects mycolic acids in *M. bovis* BCG biofilms

To verify the effect of *aftC* repression on cell envelope lipid composition in *M. bovis* BCG biofilms, cell wall associated lipids were extracted and analysed by TLC. For this, the same pellet used for carbohydrate extraction was used and treated with chloroform: methanol: water (10:10:3) at 50°C for 3 hours. The supernatant containing the cell wall associated lipids was purified from cellular debris by forming a biphase using 1.75 ml of chloroform and of 0.75 ml water. The lipids were further washed using a second extraction using 2 ml of chloroform: methanol: water (3:47:48) and spotted onto a silica plate for TLC analysis (**6.2.9**). The TLC was developed in chloroform: methanol: water (80:20:2) to visualise TMM, TDM, CL, PI and PIMs. These lipids were stained using MPA (left) and α-naphthol (right) to visualise the total lipids and sugar positive lipids, respectively (Figure 3.18A). There is an accumulation of TMM in *aftC* repressed BCG-sgRNA3 (Figure 3.18A) but no significant change in TDM, CL, PI and PIMs was observed.

Cell wall bound lipids were extracted from the same pellet of biofilm cultures using 5% tetra-butyl-ammonium hydroxide at 95 °C, followed by methylation at room temperature. Extracted cell wall bound lipids were washed three times with water and sonicated in the presence of diethyl ether and analysed by TLC using petroleum ether: acetone (95:5) (**6.2.9** and **6.2.11**). A reduction in both α- and keto mycolates was observed upon *aftC* repression in BCG-sgRNA3 (Figure 3.18B). To verify if mycolic acids were being retained in the cell wall associated lipid fraction, they were run in hexane: diethyl ether: glacial acetic acid (70:30:1) and stained using MPA to visualise DAG and mycolic acids in cell wall associated lipids. No conclusive evidence could be drawn from this TLC analysis suggesting the retention of mycolic acids in the cell wall associated fraction of *aftC* repressed BCG-sgRNA3 (Figure 3.18C).

The reduction in cell wall bound lipids was quantified using densitometry performed across three technical repeats from two biological replicates of BCG-VC and BCG-sgRNA3 grown in the presence and absence of ATc. There is a statistically significant reduction in both α- and ketomycolates upon *aftC* repression in BCG-sgRNA3 as compared to BCG-VC (Figure 3.19A-B). The relative ratio of α- to ketomycolic acids was measured by densitometry and it remained fairly consistent across BCG-VC and BCG-sgRNA3 grown in the presence and absence of ATc (Figure 3.19C). FAMES also reduced in *aftC* repressed BCG-sgRNA3 when grown in the presence of ATc as compared to the same grown in the absence of ATc, as well as BCG-VC control strain (Figure 3.19D). These results are consistent with the earlier *aftC* knockout studies in *M. smegmatis*, where reduction in mycolic acids and an increase in TDM production was observed in *M. smegmatis* planktonic cultures upon *aftC* depletion (Birch et al., 2008). In *aftC* repressed BCG-sgRNA3 biofilms no change in TDM levels was observed but, statistically significant increase in TMM and decrease in free fatty acids and free mycolic acids was observed when grown in presence of ATc (Figure 3.19).

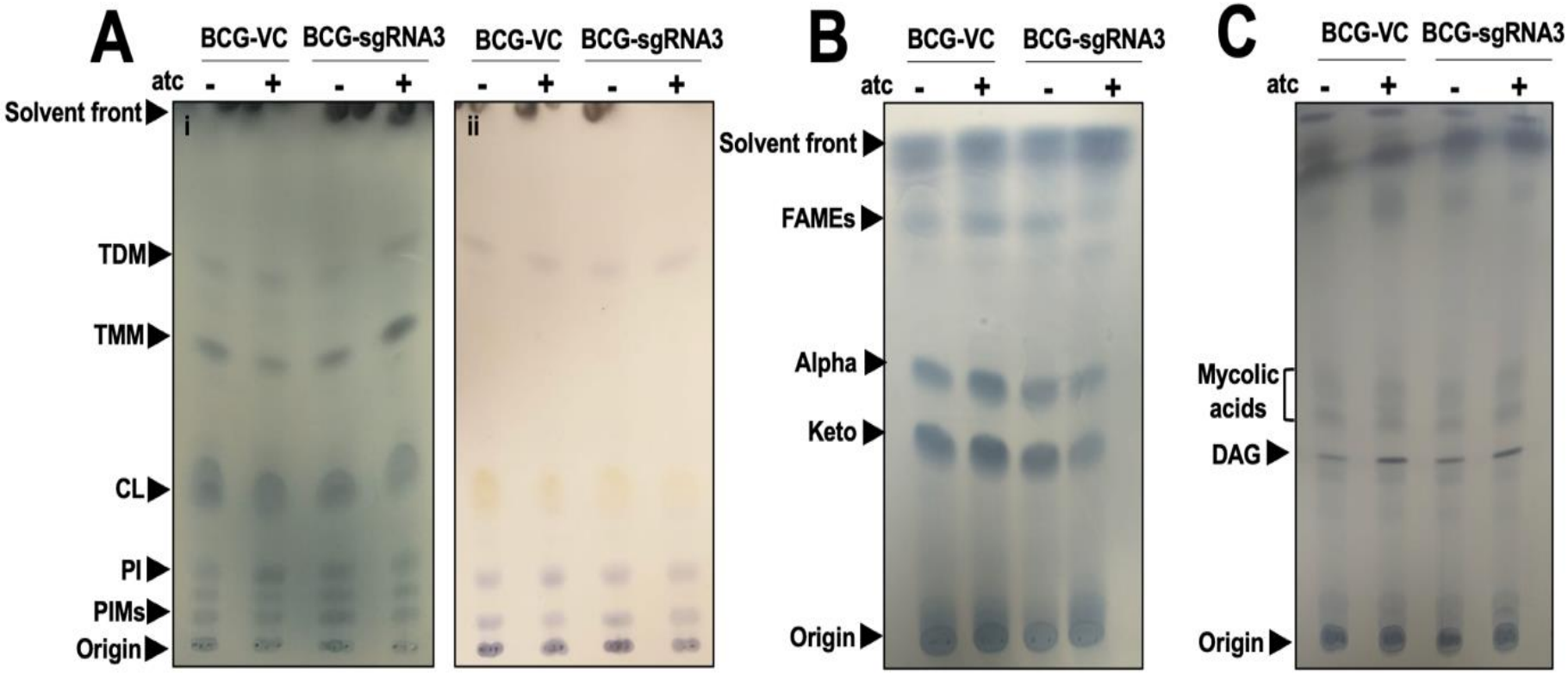

Figure 3.18: ***Lipid analysis of aftC repressed M. bovis BCG biofilms by 1-D TLC****. (A) Cell wall associated lipids were analysed in chloroform: methanol: water (80:20:2) solvent system and stained using MPA (left) and α-naphthol (right) to visualise the total lipids and sugar positive lipids, respectively. (B) Cell wall bound lipids were extracted and analysed using petroleum-ether: acetone (95:5) and subsequently stained using MPA. (C) Cell wall associated lipids were separated in hexane: diethyl ether: glacial acetic acid (70: 30: 1) solvent system and stained using MPA.*

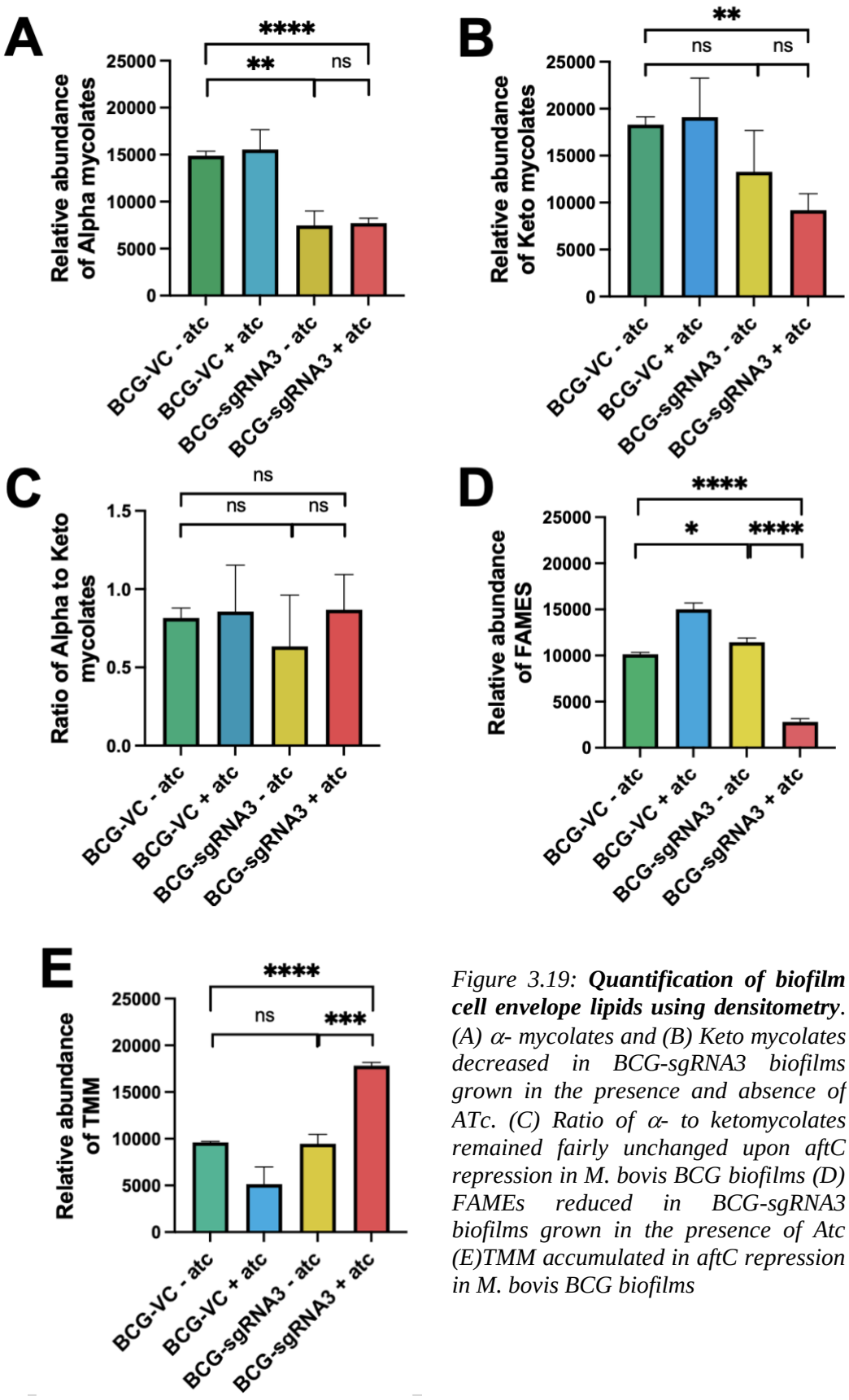

Figure 3.19: ***Quantification of biofilm cell envelope lipids using densitometry****. (A) α- mycolates and (B) Keto mycolates decreased in BCG-sgRNA3 biofilms grown in the presence and absence of ATc. (C) Ratio of α- to ketomycolates remained fairly unchanged upon aftC repression in M. bovis BCG biofilms (D) FAMEs reduced in BCG-sgRNA3 biofilms grown in the presence of Atc (E)TMM accumulated in aftC repression in M. bovis BCG biofilms*

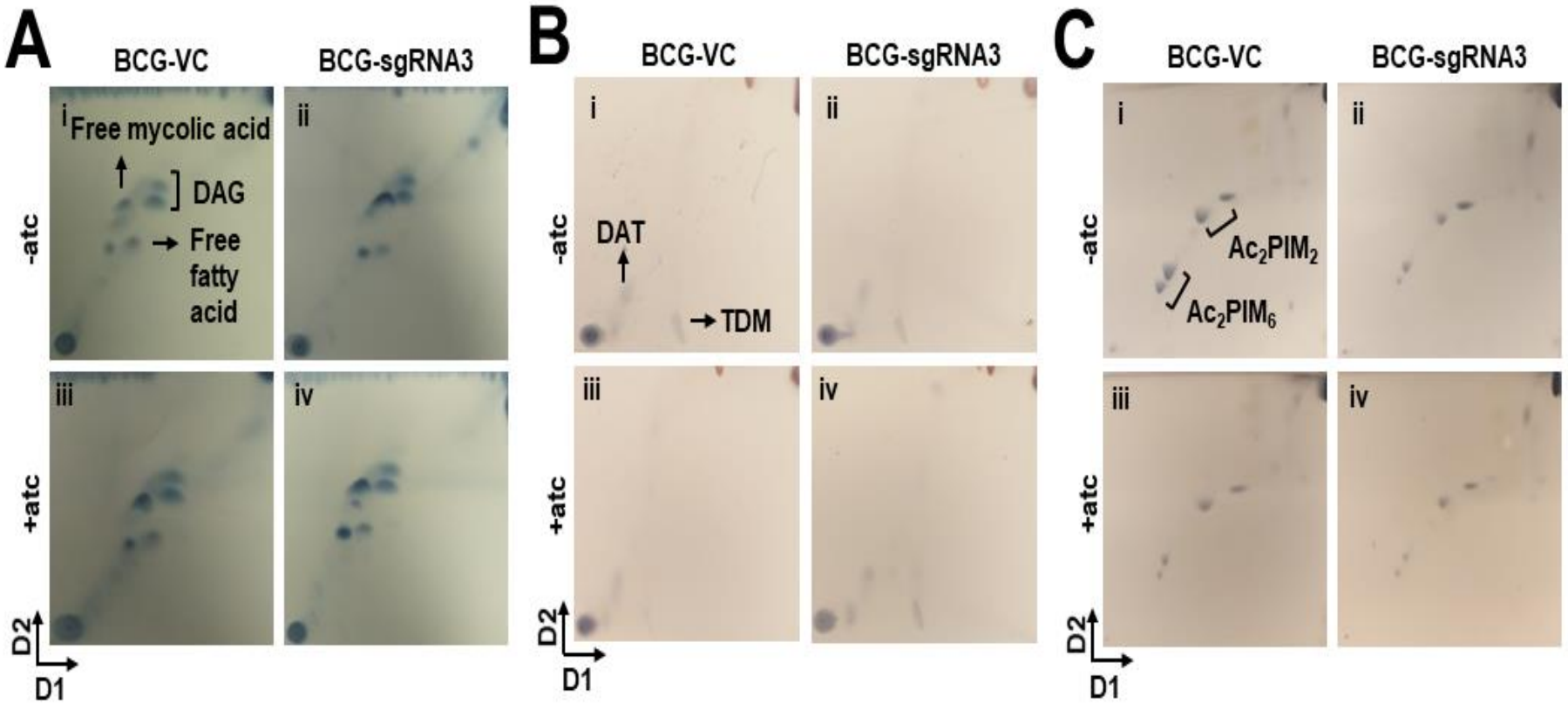

Figure 3.20: ***Lipid analysis of aftC repressed M. bovis BCG biofilms by 2-D TLC****. Cell wall associated lipids were analysed in (A) System C and stained using MPA, (B) System D and stained using α -naphthol, and (C) System E and stained using α -naphthol*

Further to this 2-D TLCs were run on the cell wall associated lipid fraction to measure the relative abundance of each lipid across BCG-VC and BCG-sgRNA3 grown in the presence and absence of ATc.

Firstly, free fatty acids, free mycolic acids and DAGs from cell wall associated fraction were analysed in solvent system C (Table 6.12), and accumulation of free mycolic acids in *aftC* repressed BCG-sgRNA3 was observed (Figure 3.20A). This is consistent with earlier studies in *M. tuberculosis, M. smegmatis, M. abscessus* and *M. chelonae* where accumulation of free mycolic acids has been observed in their pellicles (Ojha *et al.*, 2005, 2008, 2010; Sambandan *et al.*, 2013; Totani *et al.*, 2017; Vega-Dominguez *et al.*, 2020; Dokic *et al.*, 2021). In *M. tuberculosis* and *M. smegmatis* accumulation of short chain mycolic acids (C_{56}-C_{68}) is predominant (Ojha *et al.*, 2005) whereas in *M. abscessus* accumulation of long chain mycolic acids is predominant (Dokic *et al.*, 2021). This accumulation is mediated by serine esterase enzymatic hydrolysis of TDM resulting in an overall reduction in biofilm TDM levels as compared to planktonic *M. smegmatis* and *M. tuberculosis* (Ojha et al., 2010). In *aftC* repressed *M. bovis* BCG biofilms, we have seen a reduction in cell wall bound mycolates (Figure 3.19), and an increase in cell wall associated mycolate levels (Figure 3.20A). From this we can infer that although MAs are being synthesised, they are accumulated in the cell wall associated fraction and not being transferred to the cell envelope. This suggests that in BCG-sgRNA3 grown in the presence of ATc which has an intermediary sized LAM, there is a reduction in MAs in the cell envelope bound lipid fraction, and they are being accumulated in the cell wall associated lipid fraction.

DATs and TDMs were analysed using the 2-D TLC solvent system D (Table 6.12), and they remained unchanged in *aftC* repressed BCG-sgRNA3 biofilms (Figure 3.20B). *M. chelonae* biofilm analysis revealed differences in TDM accumulation levels depending on the biofilm maturation stage (Vega-Dominguez *et al.*, 2020). *M. chelonae* biofilm has higher levels of TDM in the earlier stages as compared to later stages when the biofilm is close to the dispersal stage (Vega-Dominguez *et al.*, 2020). Considering we processed matured BCG-VC and BCG-sgRNA3 biofilms which were grown for 5 weeks, we might have missed the differences in TDM levels contributing to the defective biofilm formation as seen in *aftC* repressed *M. bovis* BCG.

Ac_2PIM_2 and Ac_2PIM_6 were also analysed by 2-D TLC in solvent system E (Table 6.12), and they are similar in BCG-VC and BCG-sgRNA3 biofilms grown in the presence and absence of ATc (Figure 3.20C). Altered acylation of PIMs lead to defective biofilm formation (Li *et al*., 2020), however this is not the case in *aftC* repressed *M. bovis* BCG biofilms as they showed no discrepancies in PIMs.

Mycobacterial ECM is composed of lipids, carbohydrates, proteins and extracellular DNA. Of which free mycolic acids, especially ketomycolates are essential for mycobacterial pellicular biofilm formation (Ojha *et al*., 2008; Sambandan *et al*., 2013). Ojha *et al*. have shown the role of multiple mycolic acids including methoxy and ketomycolates in pellicle biofilm formation of *M. tuberculosis spp.* (Sambandan et al., 2013). Particularly they have highlighted the role of abundant extracellular free mycolic acids in formation of mature biofilm structures (Ojha *et al*., 2008, 2010). *AftC* repressed BCG-sgRNA3 has an altered mycolic acid profile with reduced α- to ketomycolic acids in the cell wall bound lipid fractions when compared to BCG-VC (Figure 3.18, Figure 3.19). The majority of mycolic acids are retained in the cell wall associated fractions preventing their attachment to the cell envelope upon *aftC* repression in BCG-sgRNA3 (Figure 3.20A). This can severely affect biofilm formation along with the intermediary sized LAM molecule observed in its cell envelope (Figure 3.17).

3.2.2.5 Planktonic and Biofilm cultures of *aftC* repressed *M. bovis* BCG show distinct MA profile

Numerous earlier studies have identified the difference in cell wall composition and relative abundance of individual components between planktonic and biofilm cultures of mycobacteria (Ojha *et al*., 2005, 2008, 2010; Vega-Dominguez *et al*., 2020; Dokic *et al*., 2021). Accumulation of free mycolic acids in biofilms is the hallmark of mycobacterial biofilm formation as this accumulation is not seen in planktonic cultures (Ojha *et al*., 2005, 2008, 2010; Vega-Dominguez *et al*., 2020; Dokic *et al*., 2021). In *aftC* repressed *M. bovis* BCG there is a defective biofilm formation and an aberrant mycolic acid profile (**section 3.2.2.4**). Planktonic and Biofilm cultures of BCG-VC and BCG-sgRNA3 were compared for their mycolic acid profile and there is a contrasting effect of *aftC* repression on mycolic acid abundance in the cell wall bound lipid fraction (Figure 3.21). In planktonic cultures, *aftC* repression

in BCG-sgRNA3 increased α- and ketomycolic acids as compared to BCG-VC. Whereas in biofilms, *aftC* repression reduced α- and ketomycolic acids in BCG-sgRNA3 when compared to BCG-VC.

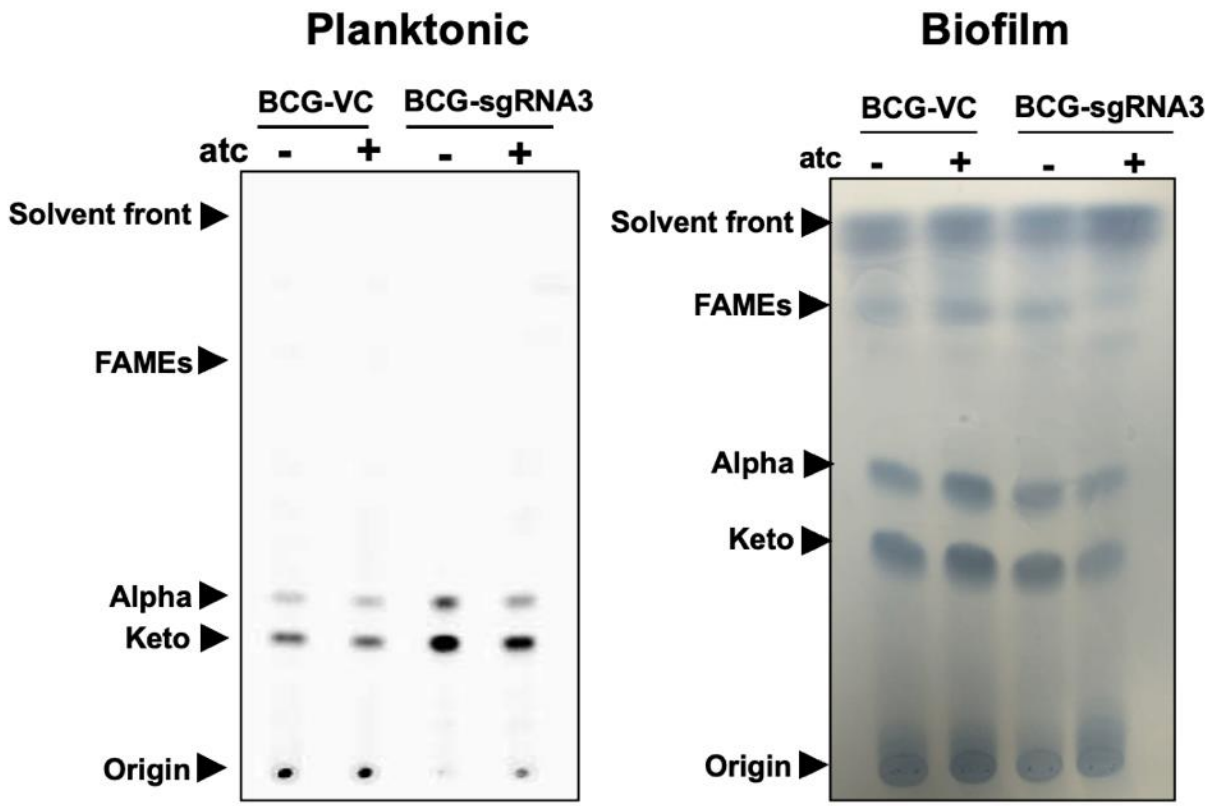

Figure 3.21: ***Cell wall bound lipids extracted from planktonic and biofilm cultures of BCG-VC and BCG-sgRNA3 grown in the presence and absence of ATc****: Planktonic cultures have an accumulation of a- and keto mycolates whereas biofilm cultures have a reduction of the same in BCG-sgRNA3 when compared to BCG-VC*

Densitometry performed on three technical repeats of TLCs separating cell wall bound fatty acids and mycolic acids in their methyl ester forms corroborated the same observation (Figure 3.22). There is a statistically significant increase in α- and ketomycolates of *aftC* repressed *M. bovis* BCG planktonic cultures but a significant reduction in the same mycolates when the strain was grown as a biofilm. It should be noted here that the main reason behind this staggering change is the increase in MA production in BCG-VC and not a decrease in mycolic acid production in BCG-sgRNA3 when both were grown as biofilms. BCG-VC when grown as biofilm produces approximately three times higher amounts of α- and ketomycolates than when they were grown as planktonic cultures (Figure 3.22). However, BCG-

sgRNA3 is unable to do the same and its relative mycolic acids have remained unchanged between planktonic and biofilm cultures (Figure 3.22). This is one of the main reasons contributing to its inability in biofilm formation. Increase in mycolic acid production is the hallmark of biofilm formation (Ojha *et al*., 2005), since *aftC* repressed *M. bovis* BCG is unable to do this, it is unable to form pellicular biofilms.

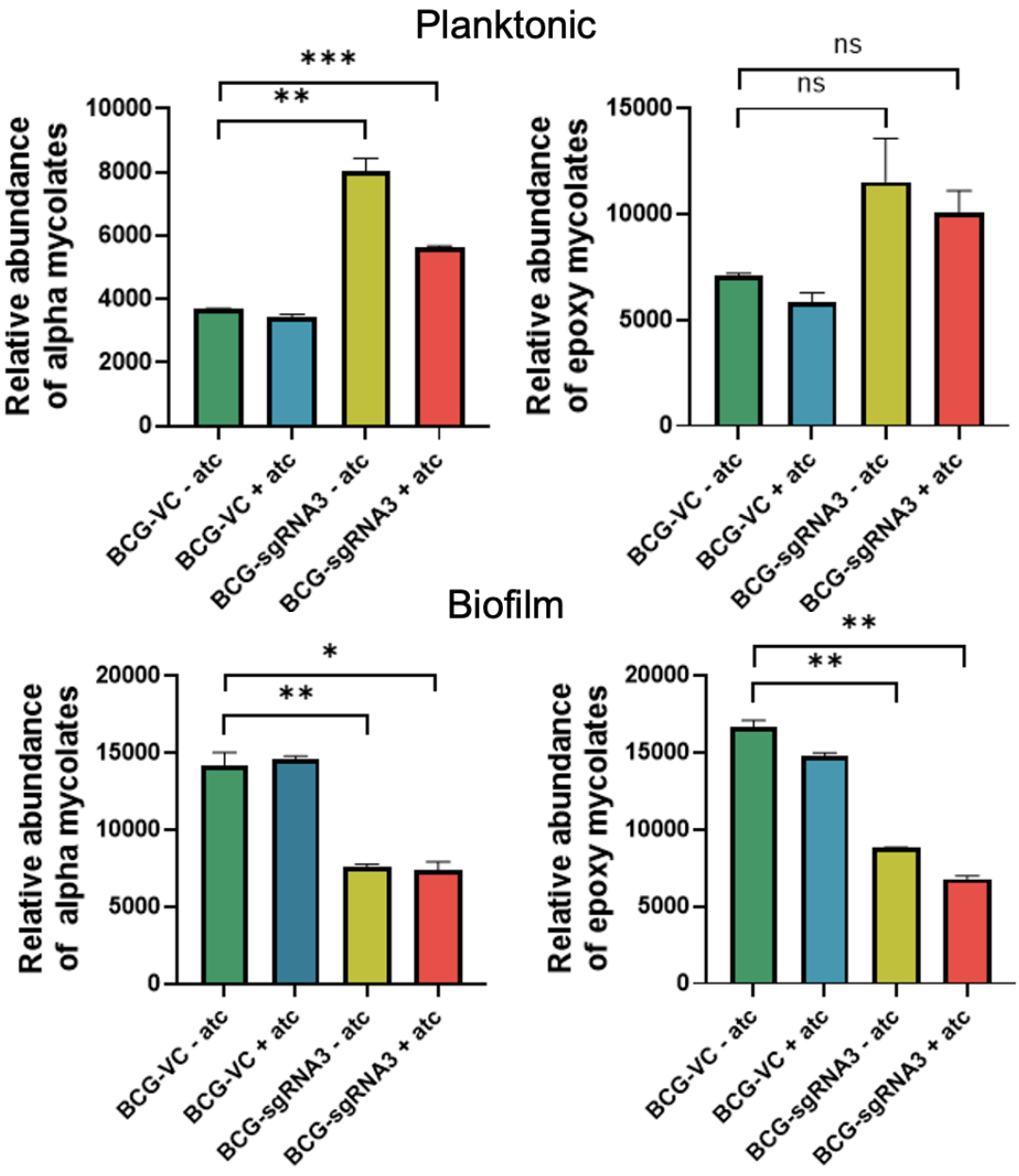

Figure 3.22: ***Comparison of planktonic and biofilm cell envelope mycolates:*** *Densitometry was performed on three technical repeats of FAMEs and MAMEs separated on TLC and compared for statistical significance of Graphpad prism 9.0.1. Statistical analysis was performed between individual groups using unpaired parametric t-test with Welch's correction ($p<0.05$ (*), $p<0.01$ (**), $p<0.001$ (***), $p<0.0001$ (****)).*

3.2.3 Effect of *aftC* repression in *M. bovis* BCG on macrophage cellular response

3.2.3.1 *aftC* repressed *M. bovis* BCG has reduced infectivity in THP1 cells

LAM is a crucial pathogen associated molecular pattern (PAMP) molecule and is essential for the initial interaction between mycobacteria and innate immune cells (Drickamer and Taylor, 2015; Schnaar, 2015). *AftC* repressed *M. bovis* BCG has a shorter 'AftC-LAM' (Figure 3.10). To study the effect of this truncated LAM on macrophage cellular responses of *M. bovis* BCG, we performed infection assays using the THP1 human monocytic cell line to evaluate macrophage uptake and intracellular survival of *aftC* repressed *M. bovis* BCG. THP1 cells were infected in quintuples at MOI 10 with BCG-sgRNA3 and BCG-VC grown in the presence and absence of ATc. Intracellular bacterial survival was measured 4 hours post-infection by plating serial dilutions of cell lysates and enumerating CFUs 4 weeks post-incubation at 37°C (**6.2.12**). Consistent with previous studies (Fukuda *et al*. 2013) BCG-sgRNA3 grown in the presence of ATc is more sensitive to macrophage killing. BCG-VC grown in the presence or absence of ATc is comparable to wild type *M. bovis* BCG in intracellular survival within macrophages (Figure 3.23). Similar to previous studies (Figure 3.9 and Figure 3.13), BCG-sgRNA3 grown in the absence of ATc showed reduced intracellular survival in THP1 cells (Figure 3.23). This effect is amplified in *aftC* repressed BCG-sgRNA3 grown in the presence of ATc (Figure 3.23). This data demonstrates the effect of *aftC* repression of intracellular survival of *M. bovis* BCG in THP1 cells.

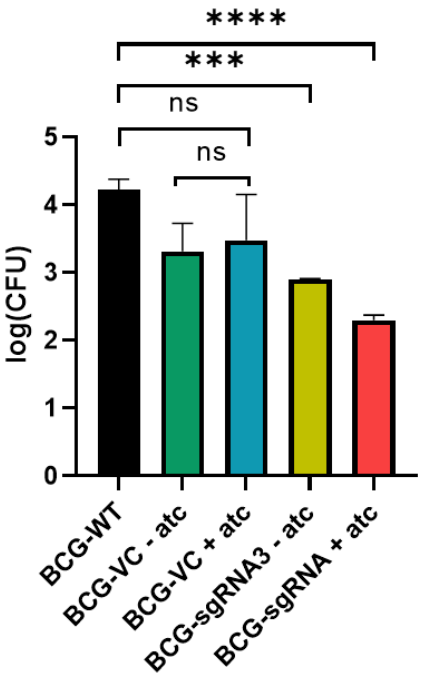

Figure 3.23: ***AftC repressed M. bovis BCG has reduced infectivity in THP1 cells.*** *The aftC knock down strain of BCG-sgRNA3 showed reduced survival in macrophages when compared to BCG-VC and BCG-WT*

3.2.3.2 *AftC* repression diminishes early cytokine stimulatory properties of *M. bovis* BCG

LAM in contrast to LM is a potent anti-inflammatory lipoglycan, owing to the presence of the bulky arabinan domain masking the "bioactive" mannan core (Vigna*l et al*., 2003; Quesniaux *et al*., 2004; Doz *et al.*, 2007; Nigou *et al.*, 2008). In *aftC* repressed *M. bovis* BCG which has a shorter 'AftC-LAM' this "bioactive" mannan core is potentially exposed (Birch *et al*., 2010). Earlier studies in *M. smegmatis* revealed increased pro-inflammatory activity of AftC-LAM obtained from an *aftC M. smegmatis* knockout strain (Birch *et al*., 2010). The study used purified AftC-LAM to stimulate THP1 and HEK293 cells expressing TLR2 to measure TNF-α and TLR2-dependent IL-8 production and observed higher TLR2 activation and increased pro-inflammatory activity as compared to wild type LAM (Birch *et al*., 2010). To verify if a similar effect can be seen in THP1 while using whole cell as opposed to purified lipoglycan, we infected differentiated THP1 cells with BCG-WT, BCG-VC and BCG-sgRNA3 grown in the presence and absence of ATc. Planktonic cultures were grown for 7 days in 7H9 media supplemented with OADC, Tween 80 and appropriate antibiotics with or without ATc (**6.2.2**). Infections were performed in sextuples at MOI 10 for 4 hours (**6.2.12**). Cytokines were measured from the culture

supernatants which were flash frozen and sent to Dr Stephen Taylor's lab in UKHSA, UK were Luminex ELISA multiplex assays were performed by Lauren Allen using Luminex 200. Cytokine measurements were interpolated from the standard curve using GraphPad Prism and plotted for comparison between BCG-WT and BCG-sgRNA3. In a 4-hour cytokine measurement, BCG-sgRNA3 grown in the absence of ATc is missing due to manual handling errors. For all the comparisons BCG-sgRNA3 grown in the presence of ATc was used against BCG-WT. All statistical analysis was performed on GraphPad Prism 8.

TNF-α and Macrophage inflammatory protein – 3A (MIP-3a) are the only two cytokines which showed statistically significant upregulation within 4 hours of infection with either BCG-WT or BCG-sgRNA3 grown in the presence of ATc. Other major cytokines including IFN-γ remained undetectable after 4 hours of infection (Figure 3.25).

A. TNF-a

TNF-α is a crucial pro-inflammatory cytokine essential for mycobacterial clearance. It is firstly produced by phagocytes, including macrophages resulting in immune activation (Wajant, Pfizenmaier and Scheurich, 2003). Upon 4 hours of infection, *aftC* repressed *M. bovis* BCG is unable to match the TNF-α level produced by wild type *M. bovis* BCG. Although it induces statistically significant levels of TNF-α as compared to uninfected cells, wild type *M. bovis* BCG produces three-fold higher levels of TNF-α in THP1 cells within 4 hours of infection (Figure 3.25A). When the infection progresses, TNF-α is also produced by $CD4^+$ and $CD8^+$ T helper cells to ensure optimal macrophage activation (Serbina and Flynn, 1999). As TNF-α sits at the cross roads of innate (produced in macrophages and dendritic cells) and adaptive immunity (T and B cell responses), it influences multiple cytokines and chemokines during mycobacterial infection resulting in the recruitment of chemokines essential for granuloma formation (Domingo-gonzalez *et al.*, 2016).

B. MIP-3a

Macrophage inflammatory protein – 3A (MIP3a) is one such chemokine recruited to the site of inflammation during mycobacterial infection. It belongs to the CC chemokine family and is also called CCL20 (Rivero-Lezcano *et al.*, 2010). CCL20 is the only ligand to CCR6, which is chemokine receptor produced on T cells, myeloid dendritic cells and B cells (Schutyser, Struyf and Damme, 2003). Therefore, CCL20 (MIP-3a) is a crucial chemoattractant for lymphocytes resulting in granuloma formation during mycobacterial infection (Schutyser, Struyf and Damme, 2003; Ito *et al.*, 2012). Mycobacterial stimulation of MIP-3a leads to recruitment of immature uninfected dendritic cells to the infection site as it participates in the first steps of the adaptive immune response (Rivero-Lezcano *et al*., 2010). However, when *M. tuberculosis* is not controlled, recruitment of immature dendritic cells to the site of infection, provides an additional niche for mycobacterial replication and eventual dissemination. Therefore, although MIP-3a is important in the early stages of infection, it is eventually downregulated by IFN-γ as it inhibits ROS production in the later stages of infection (Rivero-Lezcano *et al.*, 2010). MIP-3a is significant upregulated in THP1 cells upon infection with wild type *M. bovis* BCG. However, *aftC* repressed BCG-sgRNA3 fails to produce a similar effect in THP1 cells (Figure 3.25C). MIP-3a produced by *aftC* repressed BCG-sgRNA3 is in comparable levels to uninfected cells, whereas wild type *M. bovis* BCG induce two-fold increase in MIP-3a chemokine levels in THP1 cells (Figure 3.25C).

C. IFN-γ

In contrast to TNF-α which is primarily produced by macrophages, IFN-γ is initially produced by T-cells which then affects the migratory and functional capacity of phagocytes including macrophages, NK-cells and dendritic cells (Greenlund *et al.*, 1994; Kovarik *et al.*, 1998). These phagocytes once stimulated, produce IFN-γ themselves to maintain a continual expression of this crucial pro-inflammatory cytokine (Schroder *et al.*, 2004; Reed, Branigan and Bamezai, 2008). Our *in vitro* infection assays were designed to identify cytokine levels produced by THP1 cells independent of other immune cells. Since there is no prior stimulation, THP1 cells used in the assay failed to produce statistically significant levels of IFN-γ upon infection with *M. bovis* BCG or *aftC* repressed BCG-sgRNA3 when compared to uninfected cells (Figure 3.25B).

D. GM-CSF

Granulocyte-macrophage colony stimulating factor (GM-CSF) is another crucial cytokine in the absence of which mice where more susceptible to *M. tuberculosis* infection (Rothchil*d et al*., 2017). It promotes macrophage activation and inhibits intracellular mycobacterial growth (Rothchild *et al.*, 2017). As we differentiated THP1 monocytes into macrophages prior to infection, all the cells including uninfected cells produced comparable levels of GM-CSF. We failed to see statistical significance in GM-CSF levels between *M. bovis* BCG and *aftC* repressed BCG-sgRNA3 infected THP1 cells (Figure 3.25D).

E. IL-15

IL-15 is another cytokine involved in the crosstalk between innate immune cells and adaptive immune cells. It has been tested as an immune adjuvant to the BCG vaccine (Umemura *et al.*, 2003) to improve T cell mediated immunity by inducing long lasting memory cells (Bai *et al.*, 2020). However, *in vitro* THP1 cells showed no significant induction of IL-15 upon infection with *M. bovis* BCG. Due to this we are unable to draw any conclusions on early IL-15 induction of *aftC* repressed BCG-sgRNA3 (Figure 3.25E).

F. IL-12

IL-12 is a heterodimeric cytokine essentially produced by macrophages, dendritic cells and B cells that act as a link between innate and adaptive immune system (Domingo-Gonzalez et al., 2016). IL-12p70 is a heterodimer composed of p35 and p40 subunits that increases IFN-γ production and enhances pro-inflammatory activation of macrophages (Vignali and Kuchroo, 2014; Domingo-Gonzalez et al., 2016). It is extremely important in the context of *M. tuberculosis* infection as humans with IL-12p40 deficiency are pre-disposed to TB infection (Dorman and Holland, 2000; Picard *et al.*, 2002; Caragol *et al.*, 2003). Stable and prolonged production of IL-12 is necessary for continual IFN-γ production to limit bacterial growth in the long term (Feng *et al.*, 2005). IL-12 production is mediated by CD-40, mutations in which lead to impaired IL-12 production (Filipe-Santos *et al*., 2006). *In vitro* THP1 infections with and *aftC* repressed BCG-sgRNA3 showed no significant signs of early induction in IL-12p70 (Figure 3.25F) and CD40 (Figure 3.25G).

G. IL-6

IL-6 is induced in response to TNF-α and IFN-γ, and has pleiotropic influence on cell differentiation, proliferation and apoptosis (Van Snick, 1990). Its pluripotency is mediated by the regulation of inflammatory cytokine signalling conducted by suppressors of cytokine signalling proteins (SOCS) proteins which inhibit JAK/STAT signalling (Heinrich *et al.*, 1998, 2003). IL-6 has opposing effects during *M. tuberculosis* infection depending on the dose of infection. In large doses, IL-6 is crucial to potentiate IFN-γ responses (Appelberg *et al.*, 1994; Ladel *et al.*, 1997). On the contrary, in a low dose infection, IL-6 is dispensable in mice causing non-lethal *M. tuberculosis* infection (Saunders *et al.*, 2000). *In vitro* THP1 infection failed to produce IL-6 induction (Figure 3.25H). Again, like IFN-γ a cohort of multiple immune cells is required to understand the effect of *aftC* repressed *M. bovis* BCG on IL-6.

H. IL-4, IL-5 and IL-13

IL-4, IL-5, IL-13 are regulatory cytokines produced by T_H2 T cells to inhibit pro-inflammatory cytokines produced by T_H1 T cells (Mosmann *et al.*, 1986; Killar *et al.*, 2021). Their main function is to prevent the deleterious effects of excessive inflammation (McKenzie *et al.*, 1993; Minty *et al.*, 1993) produced during *M. tuberculosis* infection. However, they are constantly correlated with excessive bacterial burden and recurrent TB infection (Mihret *et al.*, 2013). IL-13 in particular is responsible for inhibiting IFN-γ induced autophagy mediated killing of *M. tuberculosis* (Harris *et al.*, 2007) and its overexpression is lethal in mice as they succumb to TB infection with increased necrotic granulomas within their lungs (Heitmann *et al.*, 2014). Although, much information isn't available on IL-5, it is reported to have similar effects as IL-5 deficient mice displayed effective BCG clearance (Erb *et al.*, 1998). We were unable to draw any conclusions regarding the early regulatory cytokine inducing ability of *aftC* repressed *M. bovis* BCG as measured by IL-13 (Figure 3.25I) and IL-5 (Figure 3.25K) levels.

I. IL-10

IL-10 is another crucial regulatory cytokine initially discovered as 'cytokine synthesis inhibitory factor' produced by T_H2 T cells (Vieir*a et al*., 1991; Redford, Murray and O'Garra, 2011). IL-10 production correlates with increased bacterial burden and severe TB (Eum *et al.*, 2008; Kumar *et al.*, 2015; Tebruegge *et al.*, 2015). In macrophages, IL-10 can block phagosome maturation and inhibit IL-12 production and IFN-γ mediated macrophage activation thereby creating a niche for mycobacterial replication (Oswald *et al.*, 1992; O'Leary et al., 2011). Like IL-13 and IL-5, we were unable to measure the early IL-10 stimulatory property of *aftC* repressed *M. bovis* BCG (Figure 3.25J).

J. IL-17

IL-17 is a family of six members – IL17A-F, primarily produced by T cells (Jin and Dong, 2013). These pro-inflammatory cytokines are crucial in protecting against invading aerosolised pathogens at mucosal sites, by promoting neutrophil accumulation (Umemura *et al.*, 2007). During infection, prostaglandin E2 (PGE_2) mediated induction of IL-23 is crucial for IL-10 downregulation allowing increased IL-12 and subsequent IFN-γ production to enable mycobacterial clearance (Gop*al et al*., 2012). This IL-17 production is also

K. IL-1β

IL-1β is another crucial cytokine produced primarily by macrophages and dendritic cells and is involved in mediating mycobacterial clearance (Chung *et al.*, 2009; Lalor *et al.*, 2011). It is also capable of inducing neutrophil recruitment *via* IL-17 production and mice lacking IL-1β are susceptible to chronic *M. tuberculosis* infection (Guler *et al.*, 2011; Mayer-Barber *et al.*, 2011; Bourigault *et al.*, 2013). In our *in vitro* experiments using *aftC* repressed *M. bovis* BCG infections, we failed to study IL-17A, IL-17E and IL-1β as the experiment could not measure the cytokine levels in uninfected cells compared with the levels produced by cells infected with different strains (Figure 3.25L-N).

This data demonstrates that *aftC* repressed *M. bovis* BCG has reduced immunogenic properties as compared to *M. bovis* BCG in THP1 cells upon 4 hours of infection. This claim is supported by the

reduced production of TNF-α (Figure 3.25A) and MIP-3a (Figure 3.25C) in cells infected with *aftC* repressed BCG-sgRNA3 as compared to cells infected with *M. bovis* BCG.

mediated by TGF-β and IL-6 (Figure 3.24)

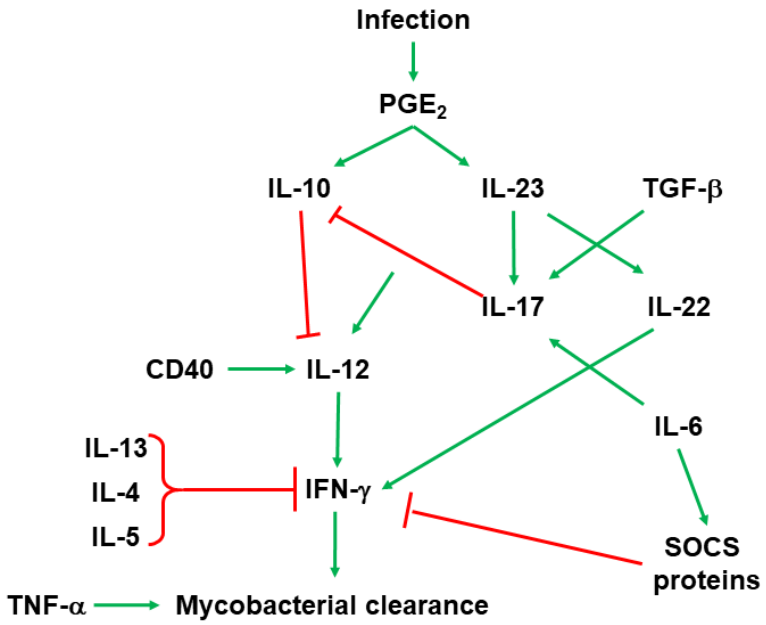

Figure 3.24: ***Role of different cytokines during mycobacterial infection.*** *Upon M. bovis BCG infection, phagocytes produce PGE_2 which induces both IL-10 and IL-23, with the latter being essential for IL-17 production. IL-17 then downregulates IL-10 production thereby promoting IL-12 (IL-12 induction is mediated by CD40) and eventually IFN-γ mediated mycobacterial clearance. IL-23 also is directly involved IFN- γ induction through IL-22. TGF-β and IL-6 can also mediate IL-17 induction, with the later regulating IFN-γ signalling through SOCS proteins. IL-13, IL-4 and IL-5 are regulatory cytokines inhibiting IFN-γ signalling. TNF-α is also crucial for mycobacterial clearance. (Red arrows represent inhibition and green arrows represent stimulation)*

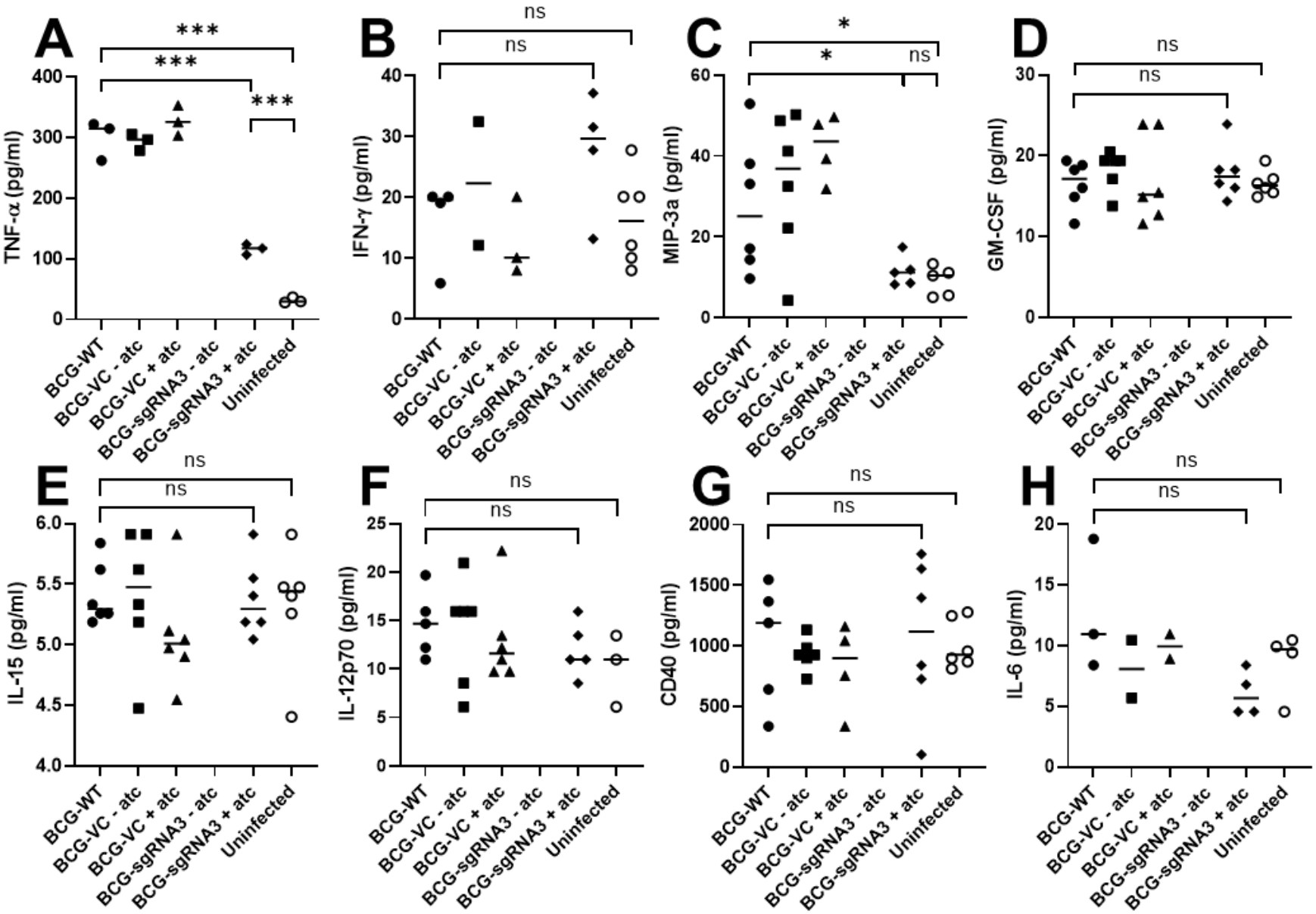
A
B
C
D
E
F
G
H
TNF-α (pg/ml)
IFN-γ (pg/ml)
MIP-3a (pg/ml)
GM-CSF (pg/ml)
IL-15 (pg/ml)
IL-12p70 (pg/ml)
CD40 (pg/ml)
IL-6 (pg/ml)
***
*
ns
BCG-WT
BCG-VC - atc
BCG-VC + atc
BCG-sgRNA3 - atc
BCG-sgRNA3 + atc
Uninfected

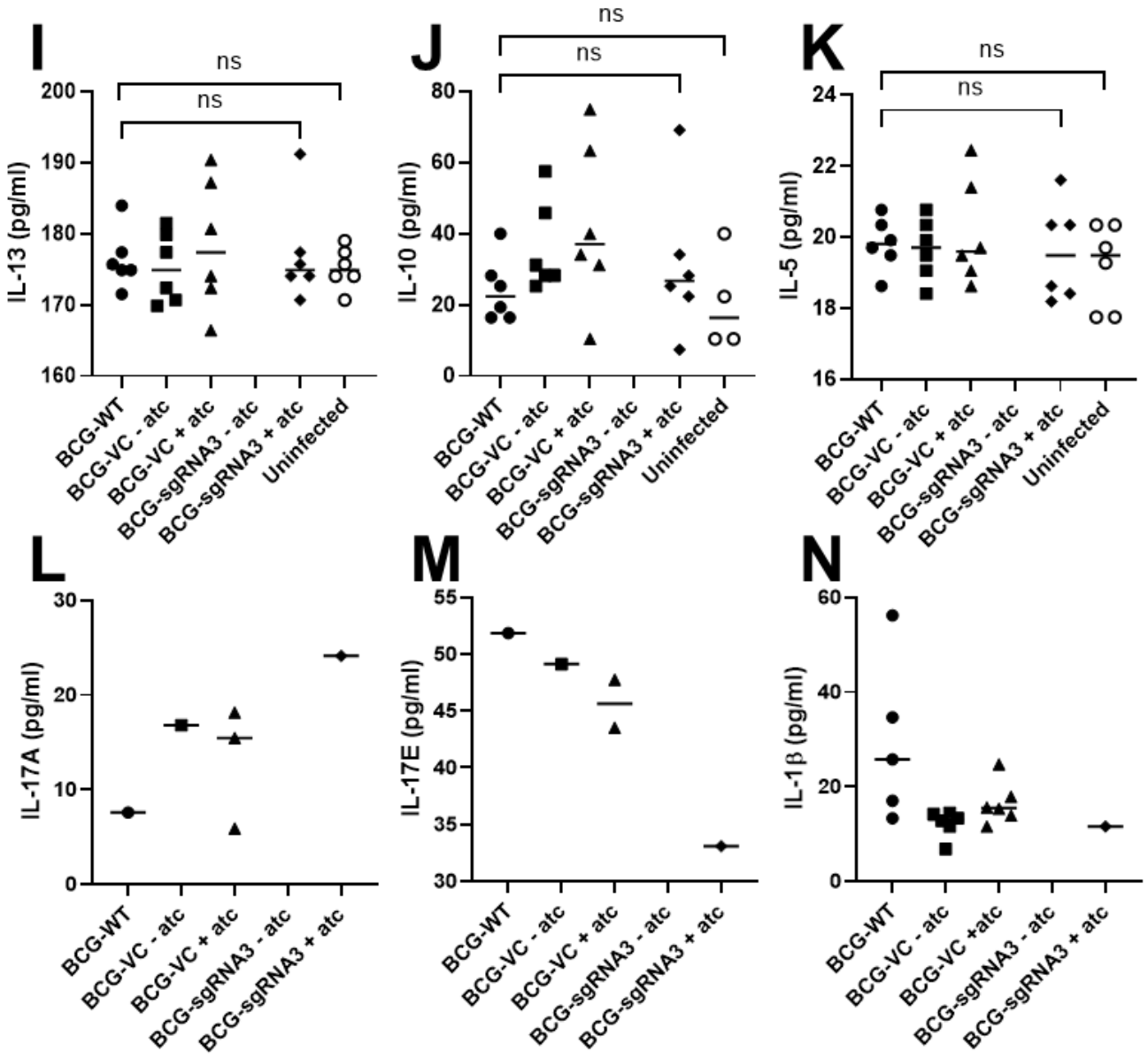

Figure 3.25: ***AftC repressed M. bovis BCG was analysed for early cytokine stimulation in THP1 cells.*** *THP1 cells were infected at multiplicity of infection (MOI) 10 for 4 hours with BCG-VC and BCG-sgRNA3 and supernatants were analysed for multiple cytokines. (A) TNF-α (B) IFN- γ (C) MIP-3a (D) GM-CSF (E) IL-15 (F) IL-12p70 (G) CD40 (H) IL-6 (I) IL-13 (J) IL-10 (K) IL-5 (L) IL-17A (M) IL-17E (N) IL-1β*

3.2.3.4 *AftC* enhances late cytokine stimulatory properties of *M. bovis* BCG

Early cytokine stimulatory assays revealed reduced TNF-α production by BCG-sgRNA3 + ATc as compared to BCG-WT, as well as diminished CCL20/MIP-3a levels which is crucial for granuloma formation. To verify if these levels are maintained throughout the infection and to measure the changes in other essential cytokines, we infected differentiated THP1cells with BCG-WT, BCG-VC and BCG-sgRNA3 grown in the presence and absence of ATc at MOI 10 for 24 hours (**6.2.12**). Cytokines were measured from the infection cell culture supernatants by Lauren Allen in Dr Stephen Taylor's lab at UKHSA, UK using Luminex 200. Cytokine measurements were interpolated from the standard curve using GraphPad Prism and plotted for comparison between BCG-WT and BCG-sgRNA3.

A. TNF-a

In contrast to early infection stage, *aftC* repressed *M. bovis* BCG produces higher levels of TNF-α as compared to *M. bovis* BCG. There is a statistically significant 3-fold higher TNF-α production in THP1s infected with *aftC* repressed *M. bovis* BCG for 24 hours as compared to those infected by *M. bovis* BCG for the same duration (Figure 3.26A).

B. IFN-γ

Like the early infection stage, IFN-γ was inconclusive upon 24 hours of infection with *aftC* repressed *M. bovis* BCG and *M. bovis* BCG. There is no statistically significant difference between the IFN-γ levels produced in uninfected cells and cells infected with either *aftC* repressed *M. bovis* BCG or *M. bovis* BCG. Macrophage stimulation by T cell induced IFN-γ is essential for them to produce IFN- γ themselves. A cohort of multiple immune cells is required to understand the effect of *aftC* repressed *M. bovis* on IFN-γ production in THP1 cell line (Figure 3.26B).

C. MIP-3a

MIP-3a levels produced by cells infected with wild type *M. bovis* BCG were reduced to a basal level at the end of 24 hours of infection. While *aftC* repressed *M. bovis* BCG failed to induce MIP-3a at early and late infection stages, *M. bovis* BCG induced MIP-3a is short lived and reverted to basal levels upon 24 hours of infection (Figure 3.26C).

D. GM-CSF

Similar to the early infection stage, we failed to see a change in GM-CSF levels in THP1 cells upon 24 hours of infection with either *M. bovis* BCG or *aftC* repressed BCG-sgRNA3. As all the monocytic THP1 cells were differentiated into macrophages prior to infection, they displayed similar levels of GM-CSF irrespective of infection (Figure 3.26D).

E. IL-1β

M. bovis BCG produced a 2-fold higher level of IL-1β as compared to *aftC* repressed *M. bovis* BCG in THP1 cells upon 24 hours of infection. Although, infected cells displayed higher levels of IL-1β as compared to uninfected cells, there was no statistical significance in between these cells upon 24 hours of infection (Figure 3.26E).

F. IL-12

IL-12, CD40 and IL-12p70 were measured in *M. bovis* BCG infected cells and *aftC* repressed *M. bovis* BCG infected cells and compared against the same in uninfected cells. There has been a statistically significant increase in IL-12p70 levels in cells infected with both *M. bovis* BCG and *aftC* repressed *M. bovis* BCG as compared to uninfected cells (Figure 3.26I). Also, they produced similar levels of IL-12p70 implying that *aftC* repression did not affect the IL-12p70 inducing ability of *M. bovis* BCG in THP1 cells upon 24 hours of infection. Similarly, IL-12 levels produced in THP1 cells infected with *M. bovis* BCG and *aftC* repressed *M. bovis* BCG were comparable upon 24 hours of infection (Figure 3.26F). However, there was no statistical significance when these were compared with uninfected cells. CD40 levels were also comparable in infected and uninfected cells, as a result change in CD40 induction was undetectable upon *aftC* repression in *M. bovis* BCG (Figure 3.26G).

G. IL-6

AftC repressed *M. bovis* BCG produced statistically significant 2-fold higher IL-6 levels in THP1 cells upon 24 hours of infection as compared to *M. bovis* BCG. Due to the wide variability seen in the IL-6 levels produced by uninfected cells, there is no statistical significance in IL-6 levels produced between infected cells and uninfected cells. However, *aftC* repressed *M. bovis* BCG produced higher IL-6 levels when compared to uninfected and *M. bovis* BCG infected cells (Figure 3.26H).

H. IL-17

IL-17A and IL-17E were measured within the IL-17 family. Both IL-17A and IL-17E were induced to a lower level in cells infected with *aftC* repressed *M. bovis* BCG as compared to those infected with *M. bovis* BCG. Cells infected with *aftC* repressed *M. bovis* BCG displayed lower IL-17A and IL-17E as compared to uninfected cells. This is surprising, as infection with any bacteria would induce the expression of IL-17 sub-family of cytokines (Umemura *et al.*, 2003; Chung *et al.*, 2009; Lalor *et al.*, 2011; Gopal *et al.*, 2012). However, upon 24 hours of infection with *aftC* repressed *M. bovis* BCG, THP1 cells produced lower levels of IL-17A and IL-17E as compared to uninfected cells, whereas *M. bovis* BCG produced statistically significant upregulation in these cytokine levels (Figure 3.26J-K).

I. IL-15

During early stages of infection IL-15 induction was undetectable in cells infected with both *M. bovis* and *aftC* repressed *M. bovis* BCG (Figure 3.26E). On the contrary, upon 24 hours of infection, both *M. bovis* and *aftC* repressed *M. bovis* BCG produce statistically significant upregulation of IL-15 as compared to uninfected cells. As there is no difference in the IL-15 levels induced by *M. bovis* and *aftC* repressed *M. bovis* BCG we can infer that there is no effect of *aftC* repression on IL-15 inducing ability of *M. bovis* BCG in THP1 cells (Figure 3.26L).

J. IL-10, IL-5 and IL-13

Regulatory cytokines IL-10, IL-5 and IL-13 were measured in THP1cells upon 24 hours of infection with *aftC* repressed *M. bovis* BCG and compared with the same produced by *M. bovis* BCG. *AftC* repressed *M. bovis* BCG induced 1.5-fold lower levels of IL-10 in THP1 cells as compared to *M. bovis*

BCG, thereby promoting enhanced mycobacterial clearance of the mutant strain as compared to the wild type strain (Figure 3.26M). *AftC* repressed *M. bovis* BCG produced significantly lower levels of IL-10 in comparison to uninfected cells implying a reduction in anti-inflammatory cytokine inducing ability of *M. bovis* BCG upon *aftC* repression (Figure 3.26M). This is also confirmed by the reduced IL-13 levels induced by *aftC* repressed *M. bovis* BCG as compared to *M. bovis* BCG. Although, there is no statistical significance between the IL-13 levels produced by THP1 cells upon 24 hours of infection with both *aftC* repressed *M. bovis* BCG and *M. bovis* BCG, there is a definite reduction in IL-13 levels upon *aftC* repression in *M. bovis* BCG as compared to uninfected cells (Figure 3.26O). However, IL-5 levels produced between *aftC* repressed *M. bovis* BCG and *M. bovis* BCG were comparable and there is no effect of *aftC* repression on long term IL-5 induction ability of *M. bovis* BCG (Figure 3.26N).

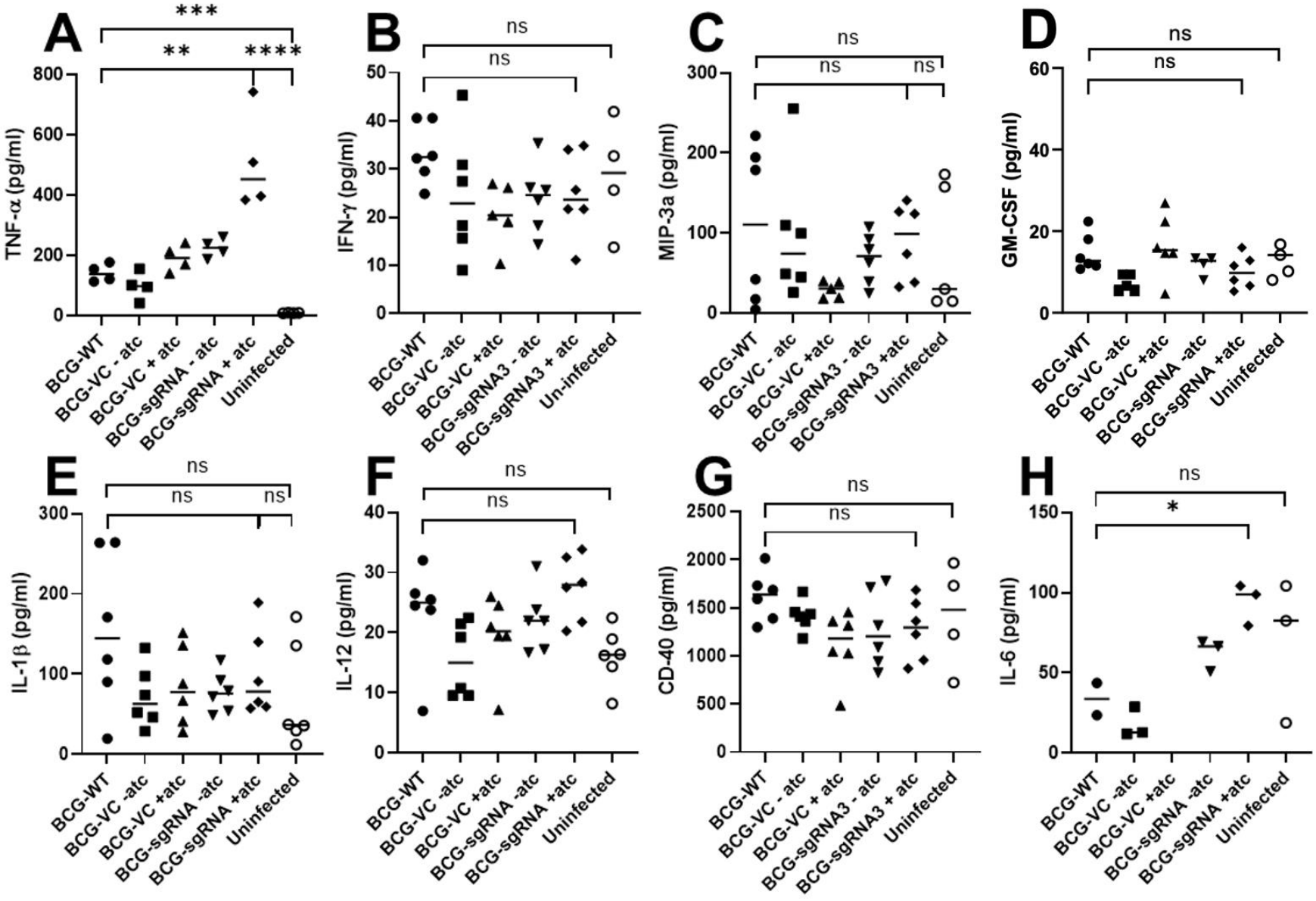
A
B
C
D
E
F
G
H
TNF-α (pg/ml)
IFN-γ (pg/ml)
MIP-3a (pg/ml)
GM-CSF (pg/ml)
IL-1β (pg/ml)
IL-12 (pg/ml)
CD-40 (pg/ml)
IL-6 (pg/ml)
***
**
****
ns
*
BCG-WT
BCG-VC - atc
BCG-VC + atc
BCG-sgRNA - atc
BCG-sgRNA + atc
Uninfected
BCG-VC -atc
BCG-VC +atc
BCG-sgRNA -atc
BCG-sgRNA +atc
BCG-sgRNA3 - atc
BCG-sgRNA3 + atc
Un-infected

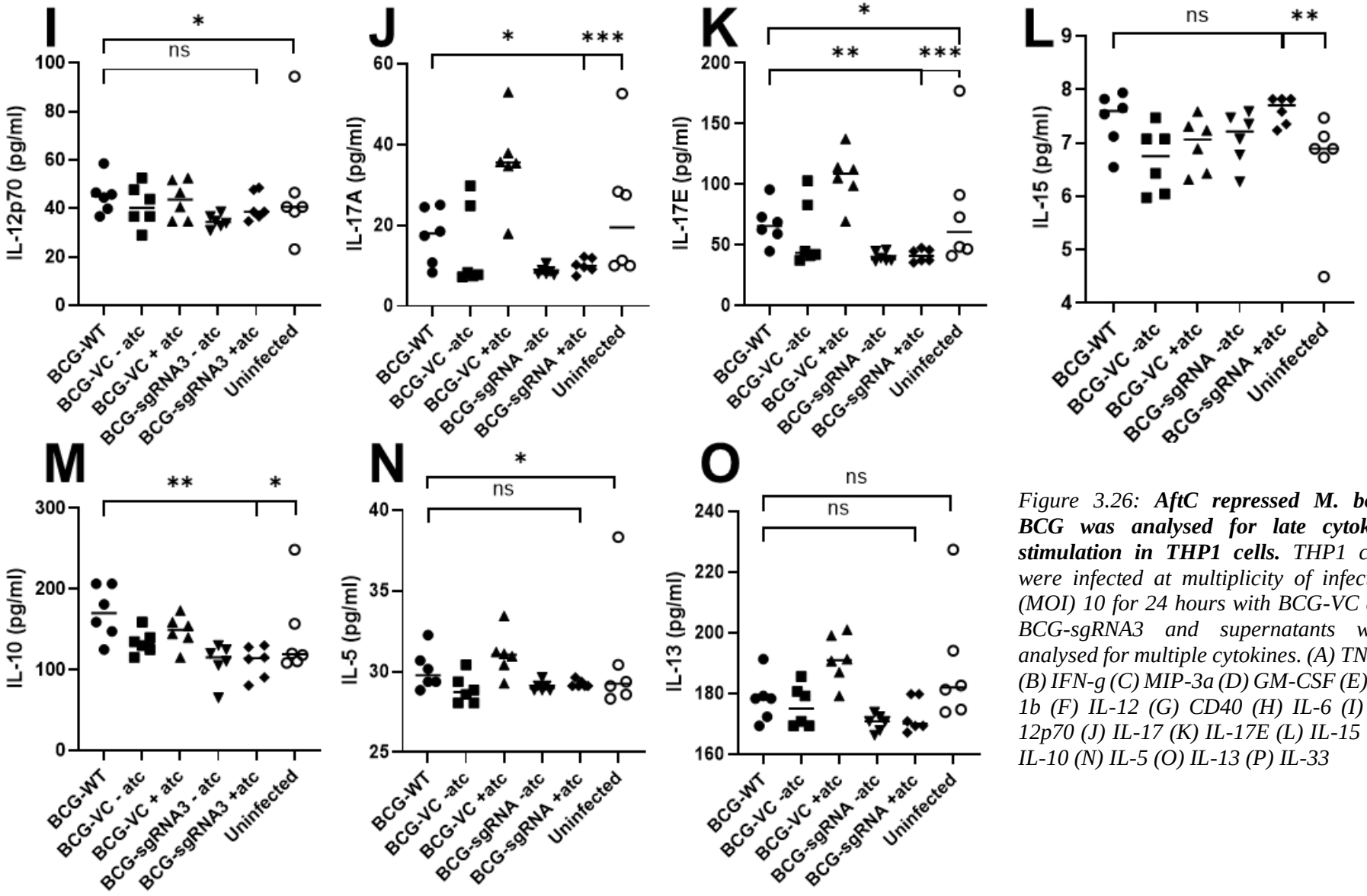

Figure 3.26: ***AftC repressed M. bovis BCG was analysed for late cytokine stimulation in THP1 cells.*** *THP1 cells were infected at multiplicity of infection (MOI) 10 for 24 hours with BCG-VC and BCG-sgRNA3 and supernatants were analysed for multiple cytokines. (A) TNF-a (B) IFN-g (C) MIP-3a (D) GM-CSF (E) IL-1b (F) IL-12 (G) CD40 (H) IL-6 (I) IL-12p70 (J) IL-17 (K) IL-17E (L) IL-15 (M) IL-10 (N) IL-5 (O) IL-13 (P) IL-33*

3.2.3.5 *AftC* repressed *M. bovis* BCG induces increased pro-inflammatory TNF-α and IL-6 cytokine production and reduced induction of anti-inflammatory IL-13 and IL-10 cytokines in THP1s as compared to wild type *M. bovis* BCG

Cytokine expression levels induced by *aftC* repressed *M. bovis* BCG and *M. bovis* BCG were compared in early (4 hours) and late (24 hours) infection stages. TNF-α expression induced by *M. bovis* BCG remained constant from early to late infection stages. However, TNF-α expression induced by *aftC* repressed *M. bovis* BCG increased gradually from early to late infection stages. In the early infection stage, *aftC* repressed *M. bovis* BCG induced lower expression of TNF-α as compared to *M. bovis* BCG (Figure 3.27A). This implies that *aftC* repression increases long term TNF-α expression ensuring macrophage activation and mycobacterial clearance in THP1 cells. Similarly, IL-6 expression level was compared from early to late infection stages upon infection with *aftC* repressed *M. bovis* BCG and *M. bovis* BCG. Although, it increased from early to late infection stage in both strains, *aftC* repressed *M. bovis* BCG produce higher levels of IL-6 as compared to *M. bovis* BCG in the late infection stage (Figure 3.27B).

Anti-inflammatory cytokines IL-13 and IL-10 were also compared from early to late infection stages in THP1 cells infected with *aftC* repressed *M. bovis* BCG and *M. bovis* BCG (Figure 3.27C-D). IL-13 induction increased from early to late stage upon infection with *M. bovis* BCG. On the contrary, IL-13 induction decreased from early to late stage upon infection with *aftC* repressed *M. bovis* BCG. Moreover, although at the early infection stage *aftC* repressed *M. bovis* BCG produced slightly higher levels of IL-13 as compared to *M. bovis* BCG, this was reversed at later stages on infection with *aftC* repressed *M. bovis* BCG producing significantly lower levels of IL-13 as compared to *M. bovis* BCG (Figure 3.27C). IL-10 on the other hand has a different trend. Its expression level increased from early to late stage upon infection with both *aftC* repressed *M. bovis* BCG and *M. bovis* BCG. However, at later stage of infection *aftC* repressed *M. bovis* BCG produced lower levels of IL-10 as compared to *M. bovis* BCG (Figure 3.27D).

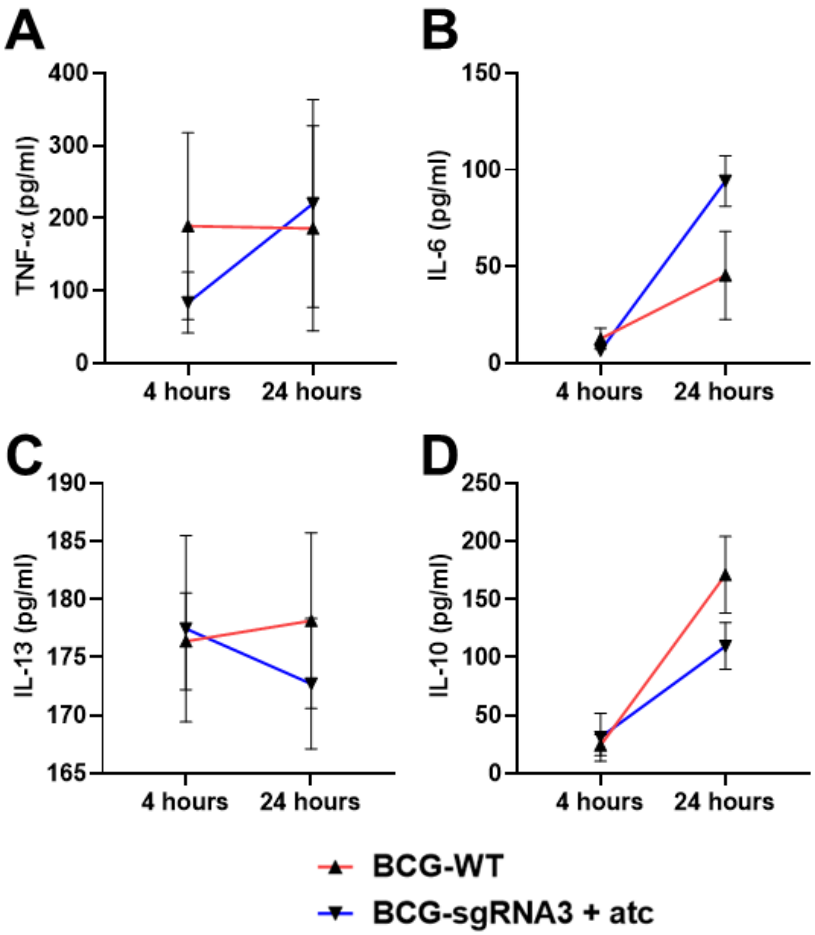

Figure 3.27: ***Comparison of early and late cytokine levels during M. bovis BCG infection and effect of aftC repression.*** *(A) TNF-α (B) IL-6 (C) IL-13 (D) IL-10*

This data demonstrates increased pro-inflammatory TNF-α and IL-6 producing ability and decreased anti-inflammatory IL-13 and IL-10 producing ability upon *aftC* repression in *M. bovis* BCG (Table 3.1).

3.2.3.6 *AftC* repression affects late-stage inflammatory cytokine production (IFN-γ, IL-1β, GM-CSF, IL-17A, MIP-3A, IL-17E, CD40) during *M. bovis* BCG infection in THP1 cells

IFN-γ

IFN-γ expression levels were compared from early to late infection stages in THP1 cells infected with *aftC* repressed *M. bovis* BCG and *M. bovis* BCG (Figure 3.28A). There is a gradual increase in its production from early to late stage upon infection with *M. bovis* BCG. However, there is a gradual decrease in its production in THP1 cells infected with *aftC* repressed *M. bovis* BCG from early to late

infection stage. Also, at the early infection stage *aftC* repressed *M. bovis* BCG produces higher levels of IFN-γ than *M. bovis* BCG, which is reversed at the late infection stage when *M. bovis* BCG surpasses *aftC* repressed *M. bovis* BCG in IFN-γ production (Figure 3.28A).

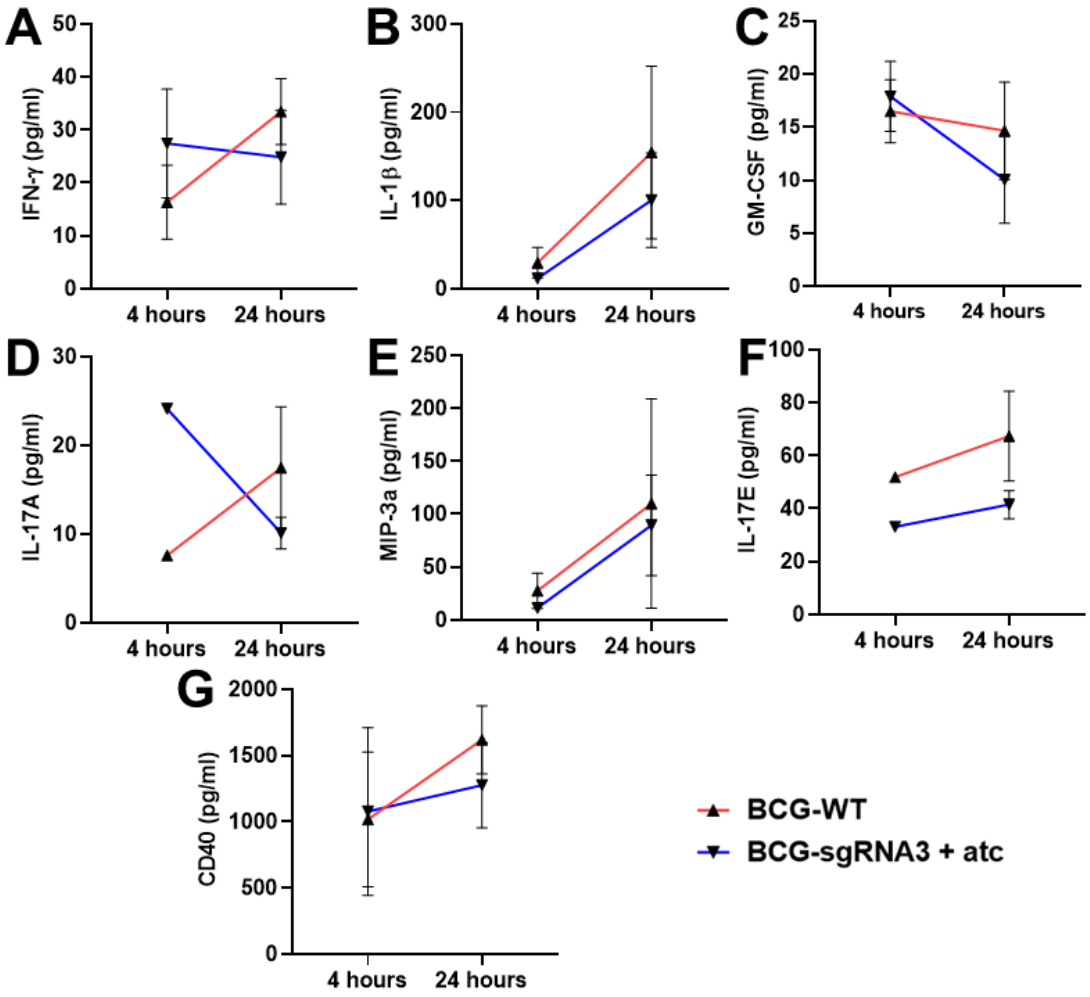

Figure 3.28: ***Comparison of early and late cytokine levels during M. bovis BCG infection and effect of aftC repression.*** *(A) IFN-γ (B) IL-1β (C) GM-CSF (D) IL-17A (E) MIP-3a (F) IL-17E (G) CD40*

IL-1β

IL-1β expression levels increased from early to late infection stage in THP1 cells infected with both *aftC* repressed *M. bovis* BCG and *M. bovis* BCG (Figure 3.28B). However, *M. bovis* BCG has a steeper increment rate surpassing *aftC* repressed *M. bovis* BCG in IL-1β production at both early and late stages of infection (Figure 3.28B).

GM-CSF

GM-CSF on the other hand has a different trend as it decreased from early to late infection stage in both *aftC* repressed *M. bovis* BCG and *M. bovis* BCG (Figure 3.28C). Although, *aftC* repressed *M. bovis* BCG produced higher GM-CSF levels at the early infection stage, it has a steeper decrease than *M. bovis* BCG and it produced lower GM-CSF levels at the late infection stage.

IL-17A

IL-17A has contrasting trends for *aftC* repressed *M. bovis* BCG and *M. bovis* BCG, as it increased from early to late infection stages for *M. bovis* BCG and decreased from early to late infection stages for *aftC* repressed *M. bovis* BCG (Figure 3.28D). Although, at the early infection stage *aftC* repressed *M. bovis* BCG produced 4-fold higher IL-17A levels as compared to wild type *M. bovis* BCG, it dropped to almost half of that produced by wild type *M. bovis* BCG at the later stages of infection (Figure 3.28D).

MIP-3a

MIP-3a has a similar trend as IL-1β as its expression level increased from early to late infection stage in THP1 cells infected with both *aftC* repressed *M. bovis* BCG and *M. bovis* BCG (Figure 3.28E). Although, both *aftC* repressed *M. bovis* BCG and *M. bovis* BCG has similar increases from early to late infection stages, *M. bovis* BCG was ahead of *aftC* repressed *M. bovis* BCG in MIP-3a production at both early and late infection stages (Figure 3.28E).

IL-17E

IL-17E also has a similar trend as its expression level also increased from early to late infection stage in THP1 cells infected with both *aftC* repressed *M. bovis* BCG and *M. bovis* BCG (Figure 3.28F). Although, both had a similar rate from the early to late infection stage, *M. bovis* BCG produced 1.5-fold higher IL-17E at both infection stages (Figure 3.28F).

CD40

CD40 expression levels also increased from early to late infection stages in both *aftC* repressed *M. bovis* BCG and *M. bovis* BCG (Figure 3.28G). At the early infection stage *aftC* repressed *M. bovis* BCG

produced slightly higher CD40 than *M. bovis* BCG. However, with the steep increase that *M. bovis* BCG has it surpassed *aftC* repressed *M. bovis* BCG at the later infection stage (Figure 3.28G).

This data reports the reduction in some inflammatory cytokines at later stages of infection with *aftC* repressed *M. bovis* BCG. These cytokines include IFN-γ, IL-1β, GM-CSF, IL-17A, MIP-3a, IL-17E, CD40 (Table 3.1).

3.2.3.7 *AftC* repression in *M. bovis* BCG does not affect IL-15, IL-12p70 and IL-5 cytokine production

IL-15, IL-12p70 and IL-5 are the three cytokines which remained unchanged upon *aftC* repression in *M. bovis* BCG (Figure 3.29). At the early infection stage both *aftC* repressed *M. bovis* BCG and *M. bovis* BCG produced similar levels of IL-5, IL-15 and IL-12p70 in THP1 cells. Similarly, at later stages of infection they produced comparable levels of IL-5, IL-15 and IL-12p70 in THP1s. Therefore, *aftC* repression has no effect on IL-5, IL-15 and IL-12p70 inducing ability of *M. bovis* BCG (Table 3.1).

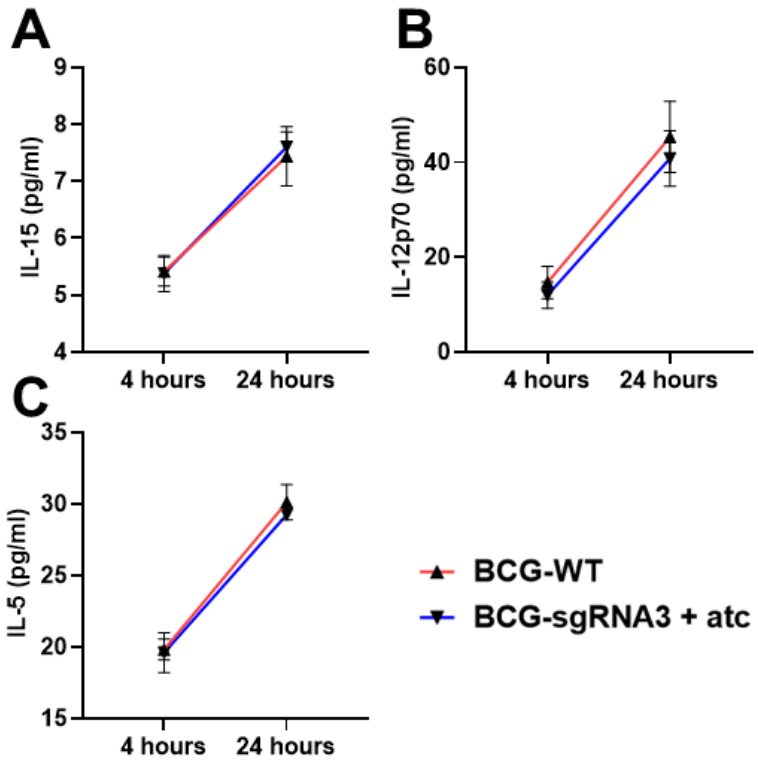

Figure 3.29: ***Comparison of early and late cytokine levels during M. bovis BCG infection and effect of aftC repression****. (A) IL-15 (B) IL-12p70 (C) IL-5*

Table 3.1: Summary of cytokine findings

Cytokine	Function	4 hours of infection			24 hours of infection			Trend from 4 hours to 24 hours	
		BCG-WT	BCG-sgRNA3	BCG-WT vs BCG-sgRNA3	BCG-WT	BCG-sgRNA3	BCG-WT vs BCG-sgRNA3	BCG-WT	BCG-sgRNA3
TNF-α	macrophage activation and granuloma formation	***	***	*** (BCG-WT > BCG-sgRNA3)	***	****	** (BCG-sgRNA3 > BCG-WT)	Remains same	Increases
MIP-3a	chemoattractant for lymphocytes resulting in granuloma formation	*	ns	* (BCG-WT > BCG-sgRNA3)	ns	ns	ns (BCG-WT > BCG-sgRNA3)	Increases	Increases
IFN-γ	Phagosome-lysosomal fusion and mycobacterial clearance	ns	ns	ns (BCG-sgRNA3 > BCG-WT)	ns	ns	ns (BCG-WT > BCG-sgRNA3)	Increases	Decreases
GM-CSF	macrophage activation and inhibits intracellular mycobacterial growth	ns	ns	ns (BCG-sgRNA3 > BCG-WT)	ns	ns	ns (BCG-sgRNA3 ~ BCG-WT)	Decreases	Decreases
IL-15	cross talk between innate immune cells and adaptive immune cells	ns	ns	ns	**	**	ns	Increases	Increases

				(BCG-sgRNA3 ~ BCG-WT)			(BCG-sgRNA3 ~ BCG-WT)		
IL-12	continual IFN-γ production to limit bacterial growth in the long term	No data			ns	ns	ns	Insufficient data	
IL-12p70	Subunit of IL-12 (heterodimer composed of p35 and p40)	ns	ns	ns (BCG-sgRNA3 ~ BCG-WT)	*	*	ns (BCG-sgRNA3 ~ BCG-WT)	Increases	Increases
CD40	Involved in IL-12 production	ns	ns	ns (BCG-sgRNA3 ~ BCG-WT)	ns	ns	ns (BCG-WT > BCG-sgRNA3)	Increases	Increases
IL-6	cell differentiation, proliferation and apoptosis	ns	ns	ns (BCG-sgRNA3 ~ BCG-WT)	ns		* (BCG-sgRNA3 > BCG-WT)	Increases	Increases
IL-1β	inducing neutrophil recruitment via IL-17 production	Insufficient data			ns	ns	ns (BCG-sgRNA3 > BCG-WT)	Increases	Increases
IL-17A		Insufficient data			ns	***	*	Increases	Decreases

	pro-inflammatory cytokines are crucial in protecting against invading aerosolized pathogens at mucosal sites, by promoting neutrophil accumulation						(BCG-WT > BCG-sgRNA3)		
IL-17E		Insufficient data			*	***	** (BCG-WT > BCG-sgRNA3)	Increases	Increases
IL-13	inhibiting IFN-g induced autophagy	ns	ns	ns (BCG-sgRNA3 ~ BCG-WT)	ns	ns	ns (BCG-WT > BCG-sgRNA3)	Increases	Decreases
IL-5	inhibits pro-inflammatory cytokines to prevent the deleterious effects of excessive inflammation	ns	ns	ns (BCG-sgRNA3 ~ BCG-WT)	*	*	ns (BCG-sgRNA3 ~ BCG-WT)	Increases	Increases
IL-10	cytokine synthesis inhibitory factor which blocks phagosome maturation and inhibits IL-12 production and IFN-g mediated macrophage activation	ns	ns	ns (BCG-sgRNA3 ~ BCG-WT)	**	*	** (BCG-WT > BCG-sgRNA3)	Increases	Increases (BCG-WT > BCG-sgRNA3)

3.3 Discussion

AftC is crucial for growth and virulence of *M. bovis* BCG. Our attempts at functional genomics of *aftC* in *M. bovis* BCG were foiled by the uncontrolled AftC expression in the *aftC* conditional deletion mutant. This prompted us to identify alternate gene manipulation strategies that would produce quick AftC depletion in *M. bovis* BCG.

CRISPR interference was recently optimised in mycobacteria for regulated gene silencing (Choudhary *et al.*, 2015; Singh *et al.*, 2016; Rock *et al.*, 2017) (Figure 3.1). This inducible transcriptional repression system is tuneable, providing close control over the degree of targeted gene repression, thereby enabling facile manipulation of essential genes as compared to the traditional recombination-based tools (Singh *et al.*, 2016). CRISPRi is also multiplexed which is particularly important in slow growing mycobacteria, such as *M. bovis* BCG and *M. tuberculosis*, reducing the long time consuming serial genetic manipulation as in case of conditionally expressed specialised transduction (Rock *et al.*, 2017). CRISPRi is also argued to bridge the gap between genomics and drug discovery with a potential to identify novel drug targets and mechanism of action of drugs (Rock *et al.*, 2017).

Considering these advantages, we generated a *M. bovis* BCG cell wall mutant strain by CRISPRi-mediated *aftC* transcriptional repression (Figure 3.2). In this work, we also describe an optimised system for CRISPRi mediated gene silencing in biofilm cultures of mycobacteria. We characterised the phenotypic and biochemical consequences of *aftC* repression in both planktonic and biofilm cultures of *M. bovis* BCG. Furthermore, we demonstrated the reduced infectivity and increased immuno-stimulatory properties of *aftC* repressed *M. bovis* BCG in THP1 cells.

Earlier *aftC* deletion in *M. smegmatis* and *C. glutamicum* revealed its role in α (1→3) branching of the arabinan domain within its cell envelope (Birch *et al.*, 2008). *AftC* is a crucial priming enzyme responsible for introducing the first 3,5-arabinofuranosyl branching residue within both AG (Birch *et al.*, 2008) and LAM (Birch *et al.*, 2010), which are then extended by other arabinofuranosyl transferases

to form long arabinan chains (Jankute *et al*., 2015b). The non-reducing terminal of the arabinan unit serves as an attachment site for mycolic acids (McNeil et al., 1991) and the *aftC* deletion strain with unbranched arabinan units within AG and LAM contained fewer cell wall bound mycolic acids (Birch *et al.*, 2008). This change in cell envelope makeup seen upon *aftC* deletion significantly affected acid-fastness, viability (Birch *et al.*, 2008), antibiotic sensitivity (rifampicin, chloramphenicol, and ethambutol) and the cytokine stimulatory profile of *aftC* depleted *M. smegmatis* (Birch *et al.*, 2010).

Here, transcriptional repression of *aftC* in *M. bovis* BCG resulted in pleiotropic variations.

3.3.1 Effect of *aftC* repression in planktonic culture of *M. bovis* BCG

CRISPR interference mediated AftC depletion in *M. bovis* BCG affected its planktonic growth (Figure 3.5). A similar observation was made in earlier *aftC* knockout studies in *M. smegmatis* where *aftC* knockout had poor growth in liquid medium, which was restored upon complementation with either *M. smegmatis – aftC* or *M. tuberculosis – aftC* (Birch *et al*., 2008). *M. smegmatis ΔaftC* also had altered colony morphology, where the rough crenulated appearance on solid media was replaced by a smooth glossy appearance (Birch *et al*., 2008). This could not be verified during transcriptional repression of *aftC* in *M. bovis* BCG as it was difficult to induce repression on solid media. *M. smegmatis ΔaftC* also had increased susceptibility to antibiotics, such as ethambutol, rifampicin, and chloramphenicol due to an altered cell wall (Birch *et al*., 2008). To observe and validate similar changes to cell wall assembly in *M. bovis* BCG upon *aftC* repression, confocal microscopy was used. Individual bacilli in *aftC* repressed *M. bovis* BCG looked morphologically different to the wild type strain. They predominantly had a reduced cell size with two major types of defects: 1) bacilli of normal length but discontinuous cell wall with fluffier appearance, and 2) bacilli of significantly smaller cell length (Figure 3.9). Similar altered phenotypes is well-established in genes involved in cell division. For example, *sepIVA* (involved in septum formation) deletion in *M. smegmatis* affects its septation pattern and cell length (Pickford *et al.*, 2020). Altered and elongated phenotypes were also reported in studies investigating genes involved in cell wall biosynthetic machinery (Gupta *et al.*, 2015; Grzegorzewicz *et al*., 2016). For example, SepF is essential in mycobacteria, which interacts with FtsZ and MurG, and thereby regulates cell division

and peptidoglycan biosynthesis (Gupta *et al.,* 2015). Mycobacteria with SepF knockdown had a distinct elongated phenotype (Gupta *et al.,* 2015). Altered phenotypes and similar septation with much smaller cell lengths was also observed in a *C. glutamicum* CpsA2 depletion mutant. CpsA2 is involved in the phosphotransferase reaction ligating AG to PG, in the absence of which extensive shedding of cell wall material is observed with dramatic changes in mycobacterial phenotype (Grzegorzewicz *et al*., 2016).

Biochemical characterisation of *aftC* repressed *M. bovis* BCG revealed generation of an intermediary sized LAM (termed 'AftC-LAM') in planktonic cultures of *M. bovis* BCG (Figure 3.10). This is consistent with earlier studies in *M. smegmatis* where *aftC* knockout resulted in truncation of AG and LAM with complete absence of 3, 5 – Ara*f* branching residues (Birch *et al.,* 2008; 2010). Through glycosyl composition and linkage analysis of extracted purified lipoglycans, using NMR spectroscopy and GC/MS they showed the absence of α(1→3) branching in AG and LAM in *aftC* knockout *M. smegmatis* (Birch *et al.,* 2008; 2010). An overall reduction in cell wall bound mycolates including α, α', and epoxy mycolates was also observed. This was coupled with increased accumulation of TDM due to reduced tethering of mycolic acids to AG was also observed in the *aftC* knockout *M. smegmatis* (Birch *et al.,* 2008). However, the lipid profile of *aftC* repressed *M. bovis* BCG is contrary to these studies, a statistically significant increase in α- and ketomycolates was observed with an overall increase in the α- to ketomycolate ratio (Figure 3.11). Leaky expression of sgRNA3 and dCas9 in BCG-sgRNA3 might be responsible for this inconsistency (Roc*k et al*.,, 2017). However, gene expression as quantified by RT-PCR (Figure 3.7) revealed complete repression of *aftC* negating this possibility. In any case, CRISPRi only enables facile gene manipulation with only 80% transcriptional repression (Singh *et al.*, 2016), contrary to specialised transduction employed in earlier studies which made a permanent chromosomal deletion of *aftC* in *M. smegmatis* (Birch et al., 2008). Also, similar inconsistencies were reported in earlier studies where CRISPRi was employed for gene manipulations in mycobacteria (Roc*k et al*., 2017).

3.3.2 Effect of *aftC* repression on *M. bovis* BCG biofilms

AftC repression affected biofilm formation of *M. bovis* BCG. Numerous earlier studies reported defective biofilm formation in mutants with compromised cell wall integrity (Recht and Kolter, 2001; Chen et al., 2006; Ojha *et al*., 2008, 2010; Pacheco et al., 2013; Sambandan *et al*., 2013; Wright et al., 2017; Yang *et al*., 2017). We observed the same in *aftC* repressed strain of *M. bovis* BCG which has defective biofilm formation upon ATc mediated CRISPRi induction and transcriptional repression. Even in the absence of ATc, BCG-sgRNA3 biofilm lacked organised ridges and troughs characteristic to mycobacterial biofilms and rather had a cluster of multiple microcolonies aggregated together (Figure 3.13). Despite the presence of the underlying cellular arrangement essential for the biofilm formation, they lost the smooth finishing of a mature mycobacterial biofilm rich in ridges and troughs. The defective biofilm formation is amplified upon ATc mediated transcriptional repression of *aftC* resulting in statistically significant reduction in biomass (Figure 3.14).

ECM provides this smooth finishing and the characteristic ridges and troughs seen in mycobacterial biofilms which protects the bacteria from antibiotic penetration and host defence systems (Tsuneda *et al.*, 2003; Chakraborty and Kumar, 2019). Polysaccharides form a major component of ECM in mycobacterial biofilms (Lemassu *et al*., 1996b; Lemassu and Daffé, 1994; Trivedi *et al*., 2016). To understand the implication of defective carbohydrate assembly in the *M. bovis* BCG cell wall core on polysaccharide levels in the biofilm matrix we used alcian blue staining. We observed an overall reduction in the acidic polysaccharide levels within the biofilm matrix (Figure 3.14), coupled with the presence of an intermediary sized LAM like molecule in planktonic cultures (Figure 3.17). Further biochemical analyses revealed a reduction in cell wall bound mycolate levels contradictory to planktonic cultures, where an increase in the same was observed. Earlier studies with a comparative lipid analysis between planktonic and biofilm cultures established accumulation of free mycolic acids as a hallmark of biofilm formation (Ojha *et al*., 2005, 2008, 2010; Sambandan *et al*., 2013). This was observed in multiple mycobacterial species including *M. tuberculosis, M. smegmatis, M. abscessus and M. chelonae* (Ojha *et al*., 2005, 2008, 2010; Sambandan *et al*., 2013; Vega-Dominguez *et al*., 2020; Dokic *et al*., 2021). We observed a reduction in both α- and ketomycolates along with FAMEs in *aftC* repressed *M.*

bovis BCG as compared to BCG-VC biofilms (Figure 3.19). Upon further analysis it was revealed that *aftC* repressed BCG-sgRNA3 was unable to produce excess MA and produced similar levels of MA in both its planktonic and biofilm cultures. On the contrary, BCG-VC produced excess MA in biofilm state as high as three times their planktonic counterpart (Figure 3.22). This is one of the main reasons contributing to its inability in biofilm formation. Similar defective biofilm formation was observed in a *groEL1* mutant in *M. smegmatis* which failed to form pellicular biofilms due to scarcity in short chain mycolic acids (C_{56}-C_{68}; Ojha *et al.,* 2005).

Enzymatic hydrolysis of TDM facilitates this accumulation of free mycolic acids in biofilms and therefore TDM is also crucial for mycobacterial biofilm formation (Ojha *et al.,* 2010). Due to this, reduction in TDM is observed in biofilms as compared with planktonic counterparts of the same strain (Ojha *et al.,* 2010). No such reduction of TDM levels were observed in *aftC* repressed *M. bovis* BCG (Figure 3.20). On the contrary, we observed an accumulation of TMM, the precursor of TDM in *aftC* repressed *M. bovis* BCG (Figure 3.19). Mycolic acids are transported outside of the bacterial cell wall as TMM for cell wall mycolylation (Varela *et al.,* 2012). Accumulation of TMM in *aftC* repressed *M. bovis* BCG biofilm cultures suggest its inability in cell wall mycolylation which is crucial for maintaining cell wall integrity and biofilm formation. We have also seen an accumulation of free mycolic acids in the cell wall associated fractions of *aftC* repressed *M. bovis* BCG biofilms, which may not be getting attached to the mycolic acid attachment sites present on the non-reducing terminal of AG (Figure 3.20). This is consistent with the earlier *aftC* knockout studies in *M. smegmatis* where reduction in AG esterified mycolic acids was reported upon *aftC* depletion (Birch et al., 2008). Our studies are in accordance with numerous earlier reports which show the effect of altered lipoglycan biosynthesis on mycolic acid composition (Takayama *et al.* 2005; Wang *et al*., 2006; Mishra *et al*., 2008; Birch *et al.,* 2008).

Thiol reductive stress induced biofilm showed the essentiality of cellulose in *M. tuberculosis* biofilm formation (Trivedi *et al*., 2016). These biofilms were disrupted by cellulase implying the significance of polysaccharides in mycobacterial biofilm formation (Trivedi *et al*., 2016; Wyk *et al*., 2017). *aftC*

repressed *M. bovis* BCG with altered LAM synthesis, an aberrant mycolic acid profile and scarcity in excess polysaccharides and mycolic acids is unable to form mycobacterial pellicles.

Bacterial populations have a strong propensity to grow in multicellular structures called biofilms. This switch includes genetic reprogramming from planktonic to a biofilm lifestyle and is induced by both environmental cues, such as nutrient limitations and genetic factors (Islam *et al.,* 2012). When within the phagosome of macrophages, mycobacteria are exposed to numerous stresses, including hypoxia, acidic pH, heat shock, nutrient deprivation etc. Some or most of these can contribute to redox metabolism imbalance that can trigger biofilm formation. Impaired respiration and reductive stress induces *M. smegmatis* biofilms as seen in the $NADH/NAD^+$ ratio which is three times that of its planktonic cultures and ATP levels which are halved from its planktonic cultures (Anand et *al.,* 2015). Biofilms also display altered carbon metabolism (Wolff *et al*., 2015), along with an increase in iron uptake (Ojha and Hatfull, 2007). Along these lines a recent study demonstrated that intracellular thiol reductive stress induces biofilm formation in *M. tuberculosis* (Trivedi *et al.* 2016). Curiously, stringent stress response marker cyclic nucleotide c-di-GMP is upregulated and is crucial for biofilm formation (Gupta *et al*., 2015; 2016). However, the exact cue which upregulates this second messenger during altered metabolic states promoting biofilm formation is yet to be explored. Once this switch from planktonic to pellicle growth occurs, bacteria achieve improved survival against antimicrobials and physicochemical stresses. These organised sessile communities, although containing drug sensitive bacteria display drug resistant phenotypes (Islam *et al.,* 2012).

The spontaneous shift of bacteria from a planktonic to biofilm lifestyle was first discovered *in vivo* in *Pseudomonas aeruginosa* from cystic fibrosis lung tissue (Lam *et al.,* 1980). This established the propensity of bacteria to form drug tolerant microcolonies encapsulated in ECM when exposed to environmental stresses. This was subsequently followed by the observation of *Staphylococcus aureus* biofilms on implant devices (Costerton *et al*., 1981). Several Gram-positive and Gram-negative bacteria are known to form biofilms on hospital equipment, catheters and plumbing for residential water supplies (Vega-Dominguez *et al*., 2020; Dokic *et al*., 2021). Nontuberculous mycobacteria (NTM) form biofilms in humans and animals (Qvist *et al*., 2013, 2015; Holland *et al*., 2017), which plays a key role in their

virulence (Faria *et al*., 2015), immune evasion and drug tolerance (Aung *et al*., 2016, 2017; Davidson *et al.,* 2011; Falkinham, 2009; Nessar *et al*.,2011; Orme and Ordway, 2014; Rhoades *et al*., 2019; Roux *et al.,*2016). Through biofilm formation NTMs cause skin and soft tissue infections, but they majorly cause pulmonary infections especially in immunocompromised patients (Dokic *et al*., 2021; Weathered *et al*., 2022). Increasing evidence suggests the role of *M. avium* and *M. abscessus* in cystic fibrosis (Chakraborty and Kumar, 2019). *M. avium* biofilm infection is associated with premature macrophage apoptosis (Rose and Bermudez, 2014) and invasion of airway epithelial cells (Yamazaki, 2006). *M. avium* biofilms also effects macrophage phagocytosis which was otherwise uninterrupted in planktonic cells (Dominici et al., 2008). This is particularly prevalent in mature biofilms (Rose and Bermudez, 2014) as their phenotypic precursors – microaggregates have been shown to increase phagocytosis (Keefe et al., 2021). Other than host pathogen interaction studies using NTMs there is a paucity in *M. tuberculosis* biofilm infection studies. With the growing evidence of *M. tuberculosis - in vivo* biofilm formation, there is a pressing need to study the innate and adaptive response to biofilm infections.

From biofilm infection studies using other prokaryotes, it is established that in neutrophils they induce chronic inflammation (Watters *et al.,* 2016), oxidate burst (Jensen *et al.,* 1990), and decreased phagocytosis (Bjarnsholt *et al.,* 2005). Similar observations were made in macrophages including excessive cytokine production and recalcitrance to phagocytosis (Mittal *et al*., 2006; Watters *et al.,* 2016). Interestingly, macrophages are also shown to enhance biofilm formation in *P. aeruginosa* and *C. albicans* (Chandra *et al.,* 2007; Watters *et al.,* 2016). Most of these studies have only considered Gram-positive and Gram-negative bacteria, and studies on mycobacterial biofilm infections are important in developing novel anti-tubercular therapies.

3.3.3 Effect of *aftC* repression on macrophage cellular response of *M. bovis* BCG

Infection studies in the THP1 cell line using *aftC* repressed *M. bovis* BCG revealed reduced bacterial uptake and intracellular survival of mutant strains as compared to *M. bovis* BCG (Figure 3.23). This is a direct consequence of 'AftC-LAM' present on the cell envelope of *aftC* repressed *M. bovis* BCG. LAM is a crucial immunomodulator and an important PAMP imperative for the initial interaction

between mycobacteria and innate immune cells. C-type lectins are an essential pattern recognition receptor expressed on the surface of macrophages, dendritic cells and neutrophils, which recognise LAM through their carbohydrate recognition domains (Drickamer and Taylor, 2015; Schnaar, 2015). Reduced bacterial uptake as seen in *aftC* repressed *M. bovis* BCG is contributed by the defective, shorter AftC-LAM which is unable to function as an efficient PAMP and activate pattern recognition receptors present on the surface of THP1 cells (Figure 3.10). Moreover, as it is intermediary sized with possibly reduced arabinan branching and mycolic acid attachment sites, AftC-LAM therefore has fewer mannose capping motifs (Birch *et al.*, 2008), which are also crucial for immunomodulation (Birch *et al.*, 2010). Mannose caps on LAM are essential for endocytic pathways within innate immune cells, especially for the mannose receptor and DC-SIGN, which bind to mannose caps on LAM resulting in efficient internalisation of mycobacteria (Maeda *et al.*, 2003; Kang *et al.*, 2005). *AftC* repressed *M. bovis* BCG with AftC-LAM and potentially fewer mannose caps displays reduced bacterial uptake and intracellular survival in THP1 cells.

Cytokine stimulatory activity of *aftC* repressed *M. bovis* BCG is consistent with the previous studies in *M. smegmatis* (Birch *et al.*, 2010). 'AftC-LAM' in *aftC* repressed *M. bovis* BCG suggestively has an exposed "bioactive" mannan core that was otherwise masked by the bulky arabinan domain in wild type LAM (Vignal *et al.*, 2003; Quesniaux *et al.*, 2004; Doz *et al.*, 2007; Nigou *et al.*, 2008). As a result of this, we have seen increased pro-inflammatory cytokine production, such as TNF-α and IL-6 and reduced anti-inflammatory IL-10 production in THP1 cells infected for 24 hours with *aftC* repressed *M. bovis* BCG as compared to BCG-WT (Figure 3.27). This is consistent with the earlier studies in *M. smegmatis* where purified LAM extracted from *aftC* knockout *M. smegmatis* showed increased production of pro-inflammatory cytokines TNF-α and IL-8 in THP1 cells as compared to *M. smegmatis* wild type LAM (Birch *et al.*, 2010).

Early and late cytokine stimulatory properties of *aftC* repressed *M. bovis* BCG revealed interesting trends in multiple pro- and anti-inflammatory cytokines involved in mycobacterial pathogenesis.

3.3.3.1 Increased inflammatory profile of *aftC* repressed *M. bovis* BCG

During early infection stage, TNF-α and MIP-3a were significantly upregulated in THP1 cells upon infection with *M. bovis* BCG (Figure 3.25). However, in the late infection stage *aftC* repressed *M. bovis* BCG induced statistically significant 3-fold higher TNF-α as compared to *M. bovis* BCG and MIP-3a was comparably induced by both bacterial strains (Figure 3.26). In the late infection stage, *aftC* repressed *M. bovis* BCG produced a 2-fold higher IL-6 in THP1 cells as compared to *M. bovis* BCG (Figure 3.26). Also, *aftC* repressed *M. bovis* BCG induced a 1.5-fold lower level of IL-10 in THP1 cells as compared to *M. bovis* BCG (Figure 3.25 and Figure 3.27), thereby promoting enhanced clearance of the mutant strain as compared to the wild type strain. Reduced IL-10 induction also signifies an increase in IL-12 mediated IFN-γ production (Figure 3.24) by *aftC* repressed *M. bovis* BCG. The reduction in anti-inflammatory cytokine induction ability of *M. bovis* BCG upon *aftC* repression is also confirmed by the reduced IL-13 levels induced by *aftC* repressed *M. bovis* BCG as compared to *M. bovis* BCG (Figure 3.27). Through this information we have demonstrated increased pro-inflammatory and reduced anti-inflammatory properties of *aftC* repressed *M. bovis* BCG.

3.3.3.2 Cytokines that require further study

Other inflammatory cytokines - IFN-γ, GM-CSF, IL-15, IL-12p70, CD40, IL-6, IL-1β and IL-17 were measured in the early infection stage but were inconclusive (Figure 3.28). Similarly, in late infection stage IFN-γ, IL-1β, GM-CSF, IL-12, CD40, and IL-12p70 have remained inconclusive, while IL-17 family of cytokines have been downregulated upon *aftC* repression in *M. bovis* BCG (Figure 3.26). However, considering our infection assay was designed to identify cytokines produced by THP1 cells independent of other cells of innate immunity, we failed to get a complete picture of cell mediated immunity induced by *aftC* repressed *M. bovis* BCG. This is particularly important because IFN-γ is initially produced by T-cells, leading to activation of macrophages and other phagocytes (Greenlund *et al.*, 1994; Kovarik *et al.*, 1998), which can then produce IFN-γ and other crucial cytokines themselves to enhance bacterial clearance (Schroder *et al.*, 2004; Reed, Branigan and Bamezai, 2008). Since there

was no prior stimulation of THP1 cells used in the assay, we failed to see the effect of *aftC* repressed *M. bovis* BCG on early expression level of some crucial cytokines (Figure 3.25 and Figure 3.26).

In conclusion cytokines measured in this study can be classified into three categories depending on the effect of *aftC* repression on cytokine stimulatory ability of *M. bovis* BCG in early and late infection stages: 1) Cytokines which prompt the increased immunogenicity of *aftC* repressed *M. bovis* BCG (TNF-α, IL-6, IL-10, IL-13 - Figure 3.27); 2); cytokines whose inflammatory profile is adversely affected by *aftC* repression (IFN-γ, IL-1β, GM-CSF, MIP-3a, IL-17A, IL-17E, CD40 - Figure 3.28); 3) cytokines which are unchanged by *aftC* repression (IL-5, IL-15, IL-12p70 - Figure 3.29). All the cytokines studied here need to be further analysed using a cohort of multiple immune cells (animal infection model), as some of them (example: IFN-γ) require immune cross talk between innate immune cells (macrophages, dendritic cells) and adaptive immune cells (T and B cells) to function efficiently. Also, animal infection models would provide a holistic overview of the effect of *aftC* repression on immunogenicity of *M. bovis* BCG.

In conclusion, *aftC* is an essential gene in *M. bovis* BCG (Sassetti *et al.*, 2003), depletion of which results in the generation of short, intermediary LAM within its cell envelope which effects lipid profile in both planktonic and biofilm cultures. Moreover, infection and cytokine studies in THP1 cells revealed reduced virulence and enhanced immunogenic properties of *aftC* repressed *M. bovis* BCG. Additionally, we confirmed CRISPRi to be a powerful technology for mycobacterial gene manipulation enabling facile manipulation of essential genes.

Summary:

In this chapter we have generated *aftC* transcriptionally repressed mutants in *M. bovis* BCG using CRISPR interference and major findings from it are:

- *aftC* repression affects planktonic and biofilm growth of *M. bovis* BCG
- *aftC* repression effected cell size and morphology of *M. bovis* BCG bacilli
- *aftC* repression results in generation of intermediary sized LAM in *M. bovis* BCG cell envelope
- In planktonic culture *aftC* repression results in an increase in cell wall bound mycolate levels in *M. bovis* BCG
- In biofilm cultures, *aftC* repression results in a decrease in cell wall bound mycolate levels in *M. bovis* BCG along with an accumulation of TMM
- There is contrasting effect on lipid profile in planktonic and biofilm cultures of *aftC* repressed *M. bovis* BCG due to its inability to synthesise excess mycolic acids in biofilms
- *aftC* repressed *M. bovis* BCG biofilms have reduced acidic polysaccharide levels in their biofilm matrix
- *aftC* repressed *M. bovis* BCG has increased pro-inflammatory TNF-α and IL-6 levels and reduced anti-inflammatory IL-10 and IL-13 levels as compared to *M. bovis* BCG
- Other inflammatory cytokines - IFN-γ, GM-CSF, IL-15, IL-12p70, CD40, IL-6, IL-1β and IL-17 were measured but were inconclusive as they require a cohort of multiple immune cells and cross talk between innate immune (macrophages, dendritic cells) and adaptive immune cells (T and B cells) to express and function efficiently

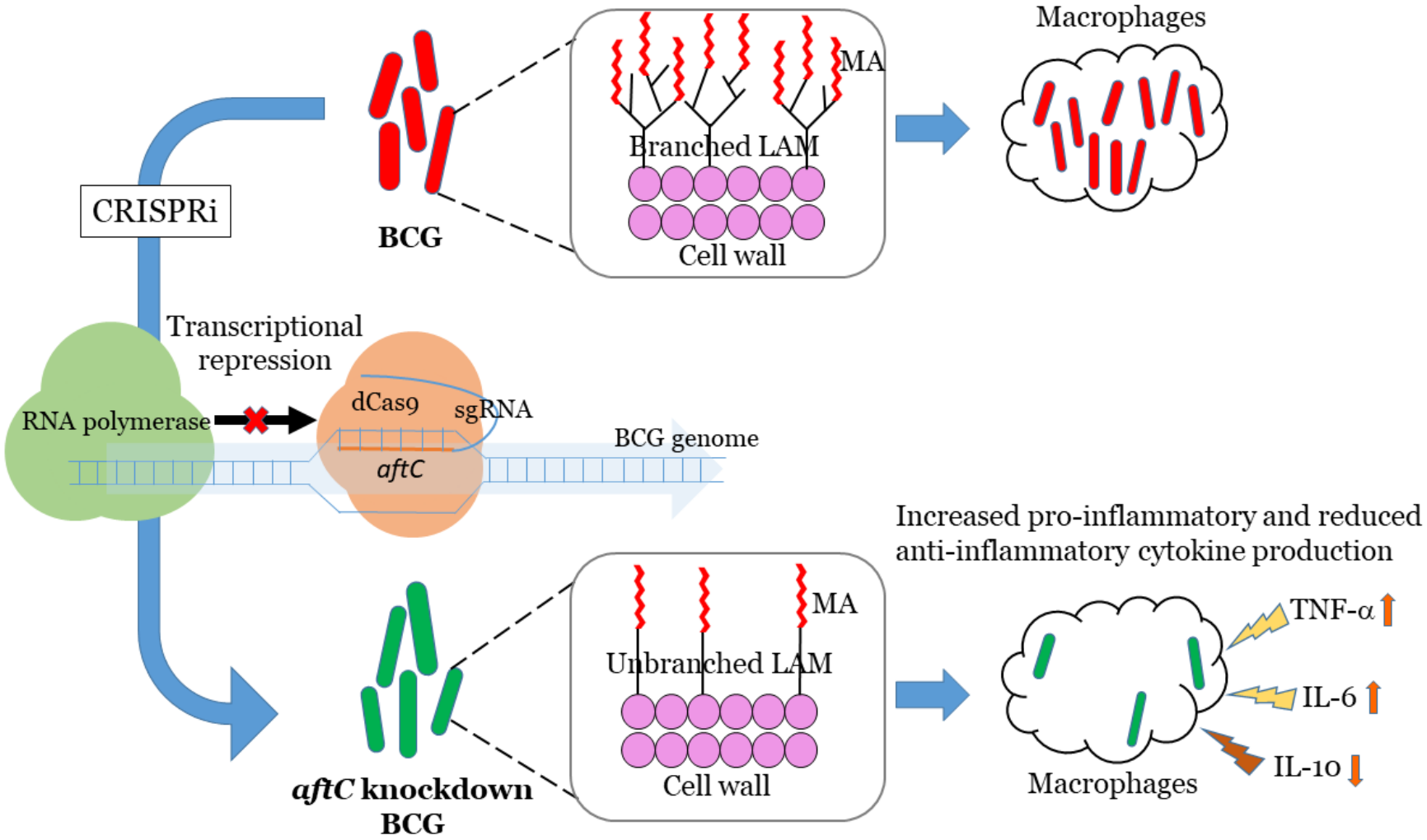

Figure 3.30: ***Effect of transcriptional repression of aftC on growth and pathogenesis of M. bovis BCG***

Chapter 4 : Role of SOCS1 in mycobacterial immune evasion strategies

4.1 Introduction

The Janus kinase (JAK)-signal transducer and activator of transcription (STAT) pathway is an evolutionarily conserved signalling pathway, whereby external factors including diverse cytokines, interferons, growth factors, hormones and related molecules control gene expression (Murray, 2007; O'Shea and Murray, 2008; O'Shea *et al*., 2015). It provides a direct communication from transmembrane receptors to the nucleus (Figure 4.1). It is composed of four JAKs and seven STATs whose differential combination induced by 40 different cytokine receptors (Murray, 2007) result in specific activation of different cell types involved in developmental and homeostatic processes, including haematopoiesis, immune cell development, stem cell maintenance, organismal growth, and mammary gland development (including but not limited to T/B cells, macrophages, cells of hematopoietic lineage and mammary epithelia; Harrison, 2012; Murray, 2007; Table 4.1).

Ligand – receptor engagement leads to activation of associated JAKs, resulting in its auto-phosphorylation as well as the phosphorylation of receptor cytoplasmic domain, thereby creating binding sites for the Src homology 2 (SH2) domain within STATs (Murray, 2007; O'Shea and Murray, 2008; O'Shea *et al.*, 2015). Recruited STATs are tyrosine or serine phosphorylated at key residues by JAKs leading to their dimerization and translocation into the nucleus affecting specific sequences in the genome to activate gene expression (Murray, 2007; O'Shea *et al.*, 2015).

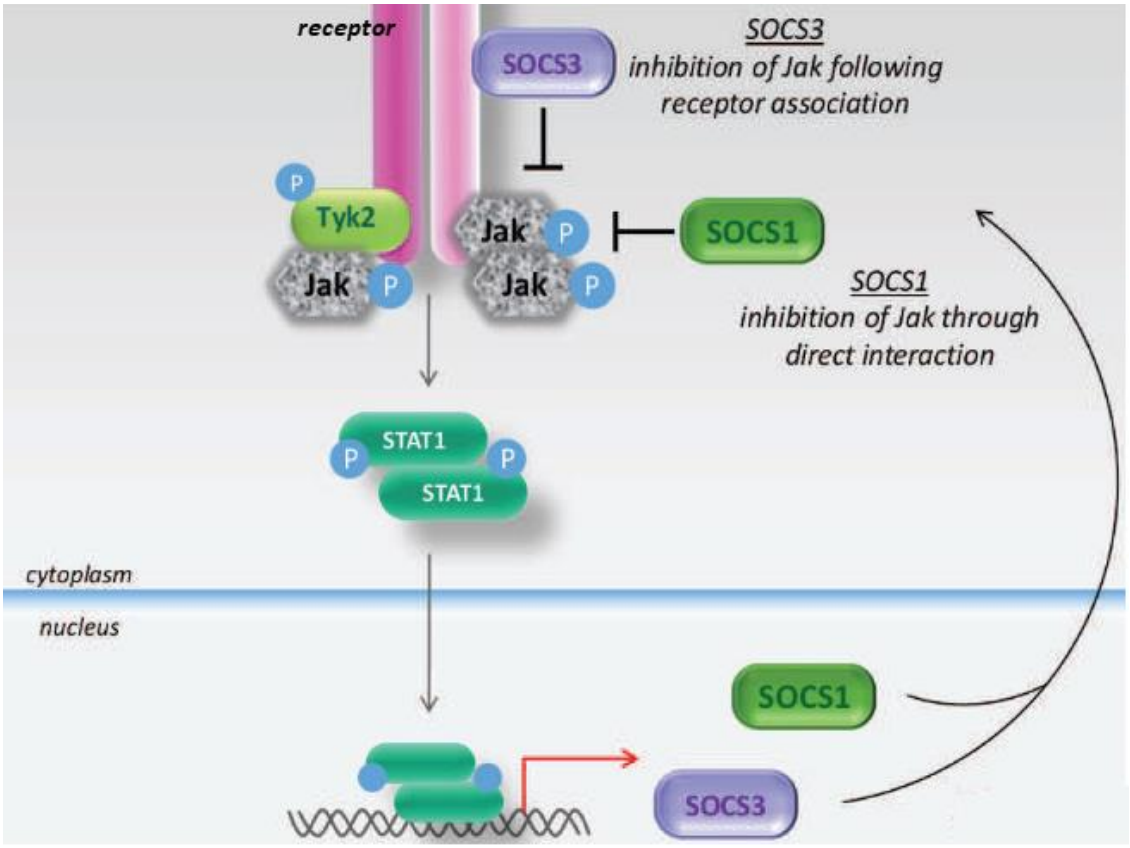

Figure 4.1: ***JAK/STAT signalling and role of SOCS1 in regulation of JAK/STAT signalling****. Image adapted from (Nicholas and Lesinski, 2011)*

Table 4.1: ***List of JAKs, STATs and associated ligands****. Adapted from* (O'Shea *et al*., 2015)

JAK/STAT	**Associated ligands**
JAK1	IFNα/β, IFNγ, IL-2, IL-4, IL-7, IL-9, IL-21, IL-6 family cytokines, IL-10 family cytokines
JAK2	IFNγ, IL-3, IL-5, GM-CSF, EPO, TPO, G-CSF, GH, leptin
JAK3	IL-2, IL-4, IL-7, IL-15, IL-21
TYK2	IFNα/β, IFNγ, IL-12, IL-23
STAT1	All IFNs
STAT2	Type I IFNs
STAT3	IL-6 and other gp130 cytokines
STAT4	IL-12, IL-23, type I interferons
STAT5a/STAT5b	IL-2, EPO, TPO, GM-CSF, GH, IL-7
STAT6	IL-4, IL-13

In the context of mycobacterial infection, IFN-γ is a crucial cytokine essential for host defence strategies and its function is carried out my JAK1/JAK2 and STAT1 molecules (Murray, 2007; O'Shea and Murray, 2008; O'Shea *et al.*, 2015). Loss of function of STAT1 is associated with recurrent mycobacterial infection and disseminated disease (O'Shea *et al.*, 2015).

4.1.1 Suppressor of cytokine signalling (SOCS) proteins

JAK/STAT signalling is regulated by a family of cytokine inducible intracellular proteins called Suppressor of cytokine signalling (SOCS) molecules and cytokine-inducible SRC homology 2 (SH2)-domain-containing proteins (CIS). They are generally induced by cytokines and act in a negative feedback loop to regulate the quality and quantity of STAT signals from cytokine receptors to inhibit excessive cytokine signalling and maintain tissue homeostasis (Hanada and Yoshimura, 2002; Kubo, Hanada and Yoshimura, 2003; Yoshimura, Naka and Kubo, 2007; Yoshimura *et al.*, 2012; Chikuma *et al.*, 2017). Knockout mice studies revealed their pleiotropic role in many other immunological processes including T cell differentiation (Chinen *et al.*, 2011a; Hiwatashi *et al.*, 2011; Takahashi *et al.*, 2011; Tamiya *et al.*, 2011), atherosclerosis (Taleb *et al.*, 2009), metabolism (Mori *et al.*, 2004; Torisu *et al.*, 2007) and cancer (Yoshida *et al.*, 2004; Ogata *et al.*, 2006; Yoshimura *et al.*, 2012).

There are 8 members in the CIS/SOCS family (CIS and SOCS1-SOCS7), each of which has a characteristic central SH2 domain and a 40 amino acid long SOCS box (after which they are named) in their carboxy terminal (Figure 4.2; Yoshimura *et al.*, 2012). Through SOCS box these proteins recruit elongin BC, cullin-5 and RING-box-2 (RBX2) resulting in the recruitment of of E2 ubiquitin transferase and subsequent unibuitination of associated proteins (Kamura *et al.*, 2004). They interact with phosphotyrosine containing molecules through their SH2 domain and function as E3 ligases in mediating the ubiquitination of associated singalling molecules (Kamura *et al.*, 2004; Yoshimura, Naka and Kubo, 2007; Yoshimura *et al.*, 2012).

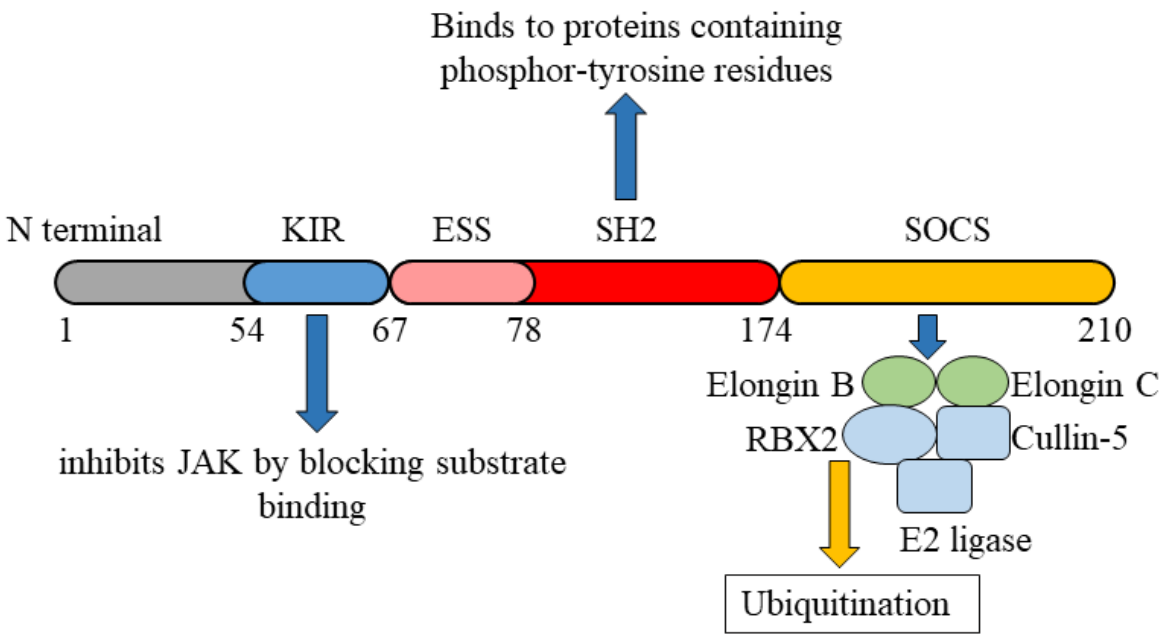

Figure 4.2: ***SOCS1 domain organisation and their functions.*** *SOCS1 has a central Src homology 2 (SH2) domain with which it binds to proteins containing phosphor-tyrosine residues. It also has a SOCS box (SOCS) after which it is named which recruits elongin BC and E2 ligase resulting in the ubiquitination of SOCS1 and any other proteins associated with it. These two regions are common to all the members of the SOCS family. SOCS1 and SOCS3 contain the third crucial region called Kinase inhibitory region (KIR) which acts as a pseudo-substrate blocking the substrate binding grove of JAK1*

Among SOCS proteins, SOCS1 and SOCS3 possess an additional 11 amino acid domain termed kinase inhibitory region (KIR) through which they can directly inhibit the tyrosine kinase activity of JAK and thereby inhibit JAK/STAT signalling other than ubiquitin mediated degradation of signalling molecules (Yoshimura, Naka and Kubo, 2007; Yoshimura *et al.*, 2012; Liau *et al.*, 2018). Liau *et al* provided the molecular basis of this inhibition where they have shown that SOCS1 inhibits the kinase activity of JAK1, JAK2 and TYK2 by blocking the substrate binding grove with KIR acting as a pseudo-substrate (Liau *et al.*, 2018). They also identified six continuous residues in KIR (His54 to Arg59) which are crucial for this interaction (Liau *et al.*, 2018). His54 that correspond to -1 of KIR motif (based on earlier definition) occupies the substrate binding site which is held in position by the hydrophobic interactions and hydrogen bonds formed by Phe55, Phe58 and Arg56, Arg59, respectively with residues in JAK1 (Figure 4.3; Liau *et al.*, 2018).

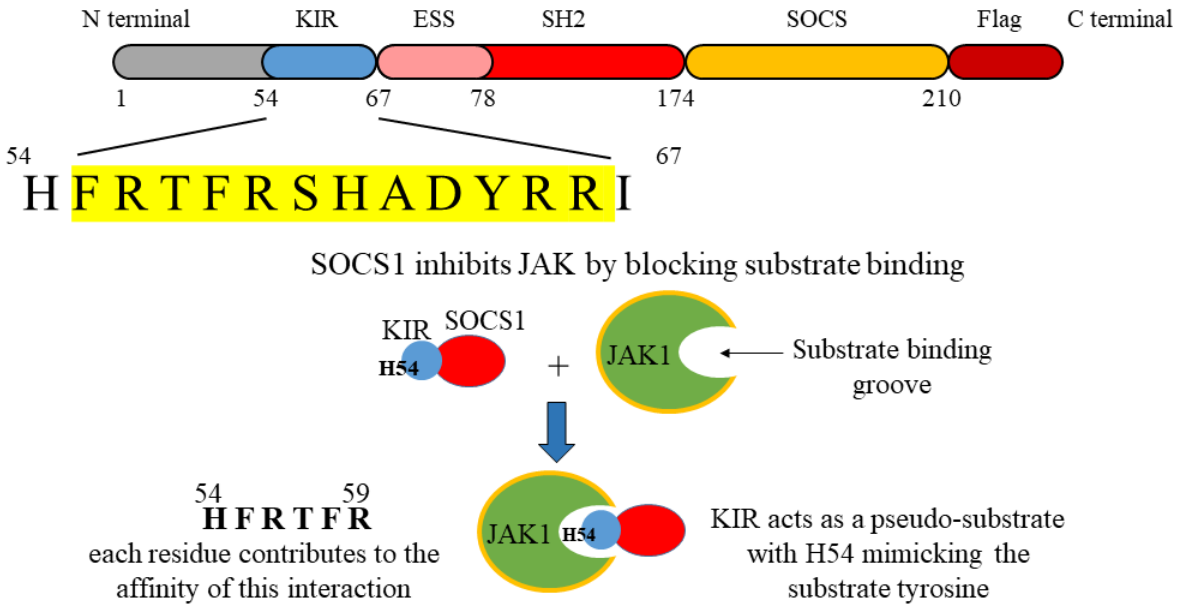

Figure 4.3: ***Role of KIR domain of SOCS1 in inhibition of JAK/STAT signalling.*** *Kinase inhibitory region of SOCS1 is an 11 amino acid long sequence (highlighted in yellow). His54 lying just outside the KIR of SOCS1 mimics the substrate tyrosine*

SOCS1 is extensively studied and the most potent member of SOCS family which is a primary regulator of number of cytokines including IFN-γ (Endo *et al.*, 1997; Carow *et al.*, 2011; Whyte *et al.*, 2011; Sukegawa *et al.*, 2014). SOCS1$^{-/-}$ is lethal to mice which die within 2-3 weeks of birth with excessive inflammation, liver necrosis and monocytin infiltration of several organs, including kidneys and the heart (Starr *et al.*, 1998). SOCS1$^{-/-}$IFN-g$^{-/-}$ double knockout mice although were rescued from neonatal death but still developed fatal inflammatory disease and polycystic kidneys (Alexander *et al.*, 1999; Metcalf *et al.*, 2002). This is because SOCS1 is crucial in attenuation of other STAT1 mediated cytokine signalling, including IFN-α/β (Fenner *et al.*, 2006), IL-12 (Eyles *et al.*, 2002) and IL-4 (Dickensheets *et al.*, 2007).

SOCS1 is induced during mycobacterial infection inhibiting IFN-γ responses, thereby promoting intracellular mycobacterial survial (Carow *et al.*, 2011; Masood *et al.*, 2013). This is carried out by reduction

in phosphorylation of STAT1, thereby preventing the transcription of IFN-γ responsive genes. $SOCS1^{-/-}$ improved mycobacterial clearence in IFN-γ dependent manner (Carow *et al.*, 2011).

Despite extensive study on the role of SOCS1 in inhibition of JAK/STAT signaling, there remain substantial gaps in understanding of the role of SOCS1 during mycobacterial infection. Considering the fatality of SOCS1 deletion in mice, the molecular basis of SOCS1 inhibition of IFN-γ signalling during mycobacterial infection hasn't been established. *In vitro* analysis performed on peripheral blood monomuclear cells improved mycobacterial clearence upon *SOCS1* knockdown using shRNA (Srivastava *et al.*, 2009). In accordance with this, we aim to understand the role of SOCS1, especially the KIR domain of SOCS1 in inhibition of JAK/STAT signalling and promoting intracellular mycobacterial survival. For this we plan to use the CRISPR/Cas9 technique to generate SOCS1 depleted macrophages, and complement them with KIR deleted SOCS1 to study the consequences of the mutation. We also aim to identify the crucial residues within KIR during mycobacterial infection for it to inhibit JAK/STAT signalling. Considering the ethical advantages and duration of the study, we used macrophage cell lines as a model of study including – THP1 and J774 cell lines. The THP1 human monocytic cell line produces the most similar cytokine profile to human monocyte-derived macrophages (Öhlinger *et al.*, 2020). Amongst, murine cell lines RAW264.7 and J774 are most commonly used tumor derived macrophage cell lines (Taciak *et al.*, 2018; Tran *et al.*, 2015). Of these, RAW264.7 cells permanently have M1 or classically activated polarisation state, which has a typical infection induced inflammatory profile (Taciak *et al.*, 2018). In contrast, J774 cells have a M0 type profile which can be differentiated into either infammatory M1 or alternatively activated M2 profiles (Tran *et al.*, 2015). Considering SOCS1 is associated with M2 polarisation of macrophages we used the J774 murine macrophage cell line.

The objectives of this chapter can be summed up to be:

1. Generation $SOCS1^{-/-}$ cell line using CRISPR/Cas9 technology to establish its role during mycobacterial infection

2. Identify the crucial residues in KIR domain of SOCS1 essential for the inhibition of JAK/STAT signalling during mycobacterial infection
3. Study the consequences of infection with *M. bovis* BCG cell wall mutants on SOCS1 and JAK/STAT signalling

4.2 Results

4.2.1 *M. bovis* BCG infection for 4 hours at MOI 0.5 is ideal to study SOCS1 and JAK/STAT signalling molecules in a THP1 cell line

SOCS1 expression levels were established along with JAK1 and STAT1 in THP1 monocytic cell lines upon infection with *M. bovis* BCG. For these two independent experiments were performed. One to determine the ideal infection time (Figure 4.4); and the other to determine the infection dosage (Figure 4.5). THP1 cells were differentiated into macrophages for 72 hours and infected for increasing amounts of time (0, 4, 8, 16, 24, 32, 48 hours) with *M. bovis* BCG at MOI 10. Cell lysates were collected at the end of each time point and analysed by Western blotting using SOCS1, STAT1, JAK1 and phosphorylated STAT1 primary antibodies. Actin and α-tubulin were used as loading controls (Figure 4.4). Infection assays were repeated twice, and cell lysates were collected and used in three independent Western blots as technical repeats for densitometry (**6.3.2** and **6.3.11**). Complete list of antibodies used in the assay are shown in Table 6.22.

Consistent with previously results (Carow *et al.*, 2011), SOCS1 expression levels increased and peaked at 8 hours into *M. bovis* BCG infection (Figure 4.4) and gradually dropped to the level of un-infected cells at 16 hours post-infection. A slight increase in SOCS1 level was observed at 32 hours which was restored to basal levels at 48 hours into infection. JAK1 levels remained relatively consistent throughout the infection time points with a slight dip seen at 8 hours post-infection, when SOCS1 expression was at its maximum (Figure 4.4). STAT1 levels gradually increased up to 8 hours of infection and remained relatively constant throughout (Figure 4.4). Phosphorylated STAT1 (PSTAT1) was used as a marker to check the functionality of JAK-STAT signalling during *M. bovis* BCG infection. P-STAT1 levels gradually increased up to 4 hours into *M. bovis* BCG infection but were promptly suppressed at 8 hours into infection when SOCS1 was at its peak expression level. Although P-STAT1 levels gradually rise from 16 hours to 32 hours of infection, it is never fully recovered, and its expression level does not go beyond the level seen in uninfected cells. This

confirms the inhibitory effect of SOCS1 on JAK-STAT signalling (Carow *et al.*, 2011). In JAK-STAT signalling, cytokine binding to cell surface receptor leads to JAK auto-phosphorylation and receptor phosphorylation. This is essential for subsequent binding, phosphorylation and activation of STATs, which eventually dimerises and translocates into nucleus to activate the transcription of downstream cytokine signalling proteins. During *M. bovis* BCG infection, as seen in Figure 4.4 P-STAT1 levels promptly dip after 8 hours of infection when SOCS1 expression level is at its peak thereby confirming the inhibitory effect of SOCS1 on JAK-STAT signalling in THP1 cells infected with *M. bovis* BCG.

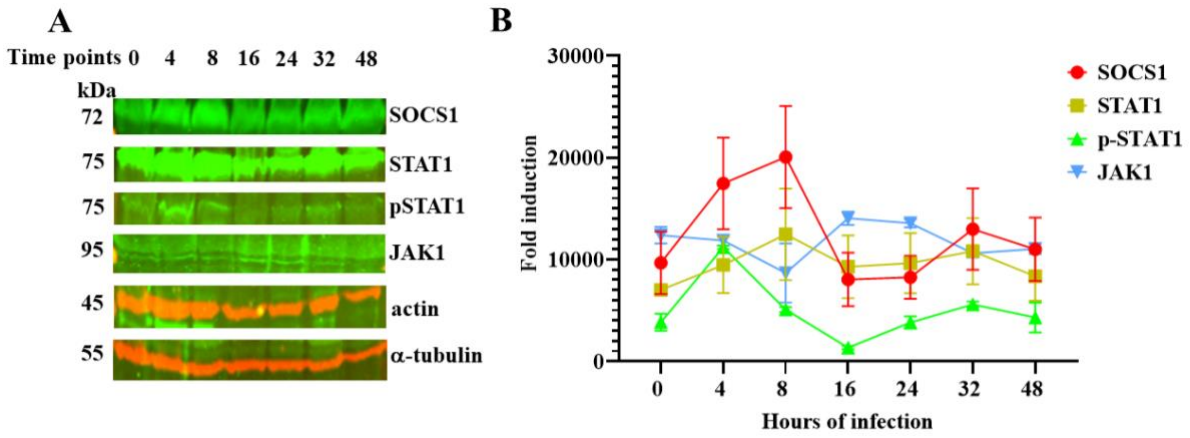

Figure 4.4: ***Establishing the expression levels of proteins involved in JAK-STAT signalling during M. bovis BCG infection in THP1 cell line.*** *THP1 monocytes were differentiated into macrophages for 72 hours and infected with M. bovis BCG at MOI 10 for the mentioned duration. Cell lysates were collected and used for Western blotting. A) Western blot B) Densitometry was performed on three independent western blots to plot the relative abundance of JAK-STAT signalling proteins upon M. bovis BCG infection. List of antibodies is mentioned in Table 6.22.*

Like time point infections, the effect of increasing the infection dosage on JAK-STAT signalling in THP1 cells line was analysed. For this, 72 hours differentiated THP1 cells were infected for 4 hours with increasing MOI (0, 0.5, 2, 5, 10, and 20) of *M. bovis* BCG and cell lysates were analysed by Western blotting using SOCS1, STAT1, JAK1 and P-STAT1 primary antibodies (Refer **6.3.2, 6.3.11** and Table 6.22). Actin and α-tubulin were used as loading controls (Figure 4.5). Infection assays were repeated twice and cell lysates collected and used for three independent Western blots as technical repeats for densitometry.

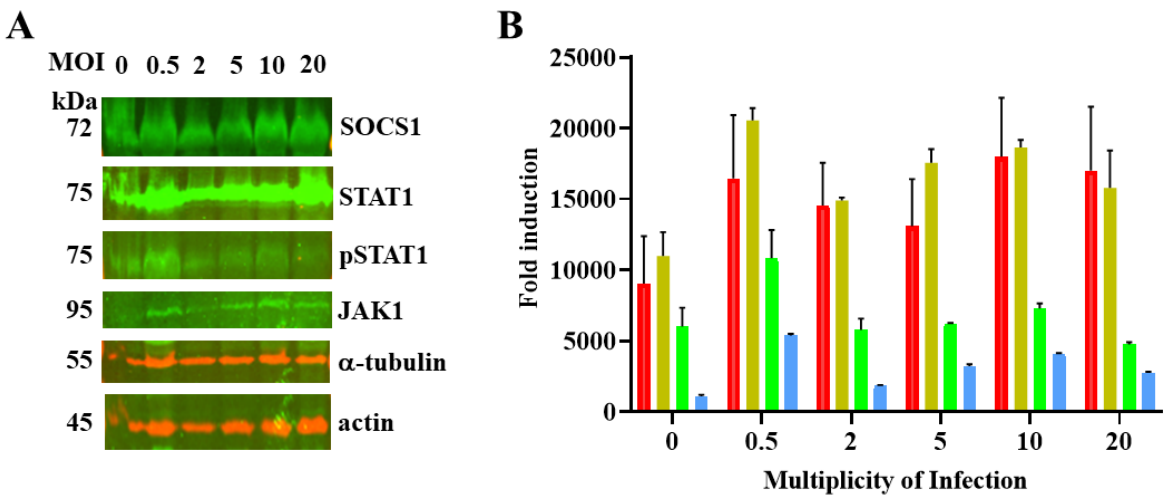

Figure 4.5: ***Identifying the ideal multiplicity of infection of M. bovis BCG to study JAK-STAT signalling in THP1 cell lines.*** *A) THP1 cells were infected with increasing MOI (0, 0.5, 2, 5, 10, 20) to identify the optimum MOI which produces the maximum effect of JAK-STAT signalling proteins B) Densitometry was performed on three independent western blots to plot the relative abundance of JAK-STAT signalling proteins upon M. bovis BCG infection (colour scheme similar to Figure 4.4)*

Consistent with the literature (Bettencourt *et al.*, 2017), MOI 10 produced a pronounced effect on the expression levels of SOCS1 and STAT1. However, we were curious about lower MOIs as *M. tuberculosis* establishes successful infection in humans at a low infection dose of 1-3 bacilli (Ramakrishnan, 2012; Cambier, Falkow and Ramakrishnan, 2014). For this purpose, we studied MOI 0.5, 2, 5 and compared them against the extreme MOIs - 0 and 20. MOI 0.5 induced 1.75-fold increased SOCS1 production as compared to MOI 0 and like MOI 10 and 20 confirming the efficiency of low infection dose of *M. bovis* BCG. JAK1 levels also peaked at the low infection dose of MOI 0.5 as compared to the high infection dose of 10 or 20. Similarly, STAT1 expression was also at its peak along with that of P-STAT1 at low infection dose of MOI 0.5. This is consistent with small aerosol droplets of *M. tuberculosis* (only 1-3 bacteria) being most efficient in initiating infection in lower lungs (Cambier, Falkow and Ramakrishnan, 2014).

We were then curious if this observation was carried to murine macrophage cells and if low infection doses were sufficient to study JAK/STAT signalling proteins in J774 cell line. We performed similar infection assays and infected J774 macrophages for 4 hours with increasing MOI (0, 0.5, 2, 5, 10, and 20) of *M. bovis*

BCG and cell lysates were analysed by Western blotting (Refer **6.3.2, 6.3.11** and Table 6.22). To maintain consistency actin and α-tubulin were used as a loading control and infection assays repeated twice and cell lysates collected were used for three independent Western blots as technical repeats for densitometry.

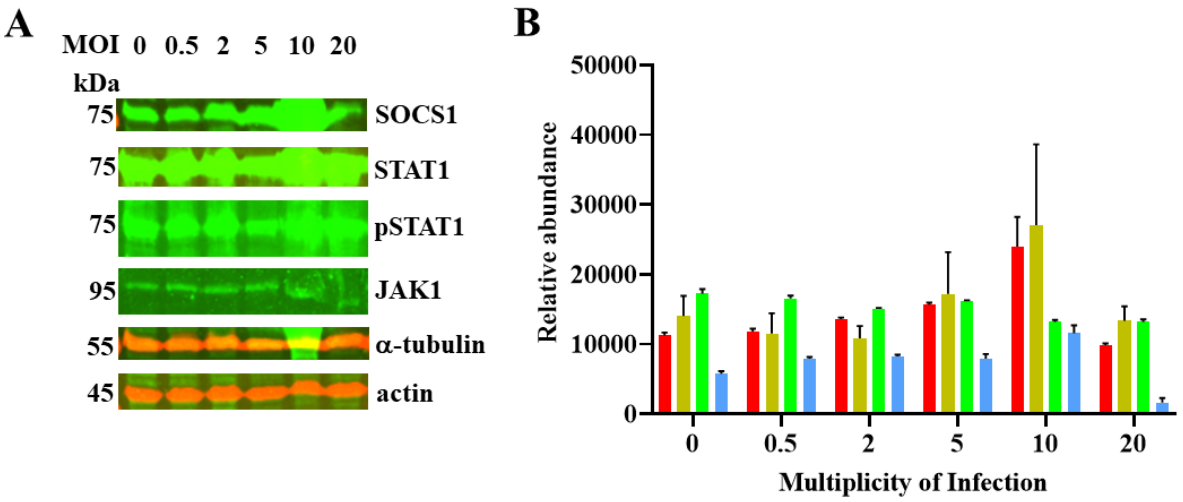

Figure 4.6: ***Identifying the ideal multiplicity of infection of M. bovis BCG to study JAK-STAT signalling in J774 cell line.*** *A) To compare the ideal MOI of THP1s with that of J774s, they were infected with increasing MOI (0, 0.5, 2, 5, 10, 20) to identify the optimum MOI which produces the maximum effect on JAK-STAT signalling proteins B) Densitometry was performed on three independent western blots to plot the relative abundance of JAK-STAT signalling proteins upon M. bovis BCG infection (colour scheme similar to Figure 4.4)*

Unlike THP1, J774 showed the most significant SOCS1 expression at MOI 10 in contrast to MOI 0.5. JAK1 and STAT1 were also significantly expressed at MOI 10 along with P-STAT1 levels. Although, this is contradicting the MOI infection assay in THP1 cells, it is consistent with the previously published literature (Bettencourt *et al.*, 2017), and highlights the consequence of using different host cell types in mycobacterial infection assays. Different host cell types respond differently to stimulus and in our infection assay we've seen that THP1 cell lines produce maximum SOCS1 expression when infected with *M. bovis* BCG at MOI 0.5 (Figure 4.5) and J774 cells produce maximum SOCS1 levels when infected with *M. bovis* BCG at MOI 10 (Figure 4.6).

HEK293T cells were used throughout the project to standardise different assay conditions. Therefore, we went on to perform time point and MOI infections in HEK293T cells using *M. bovis* BCG to check if they match with any of the macrophage cell lines used in this project. HEK293T cells were infected for 4 hours with increasing MOI (0, 0.5, 2, 5, 10, and 20) of *M. bovis* BCG and cell lysates were analysed by Western blotting (Figure 4.7). To maintain consistency actin and α-tubulin were used as a loading control and infection assays were repeated twice and cell lysates collected were used for three independent Western blots as technical repeats for densitometry (Refer **6.3.2, 6.3.11** and Table 6.22).

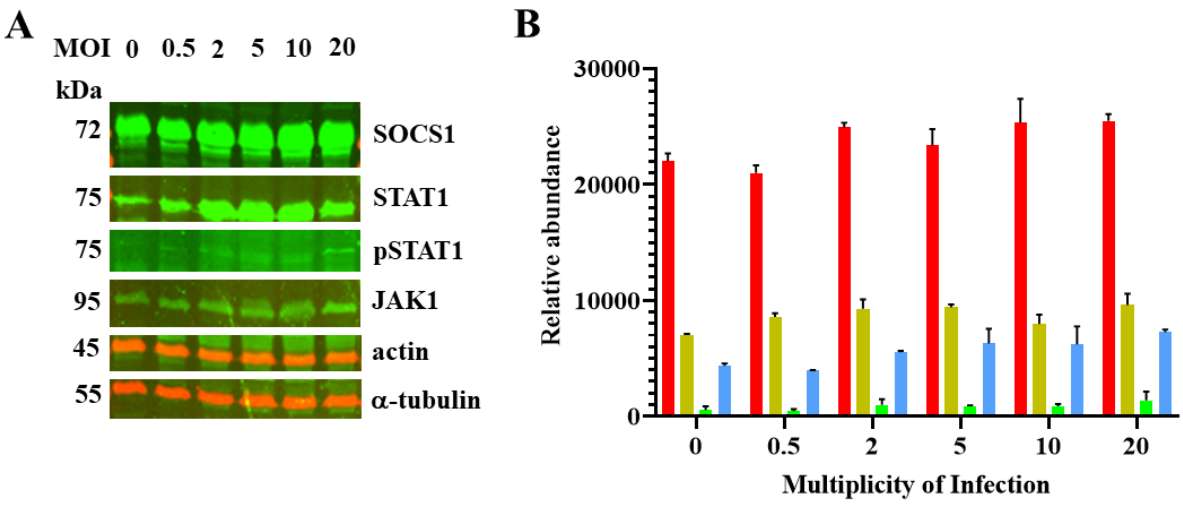

Figure 4.7: ***Identifying the ideal multiplicity of infection of M. bovis BCG to study JAK-STAT signalling in HEK293T cell line.*** *A) To compare the ideal MOI of THP1s and J774s with that of HEK293T, they were infected with increasing MOI (0, 0.5, 2, 5, 10, 20) to identify the optimum MOI which produces the maximum effect of JAK-STAT signalling proteins B) Densitometry was performed on three independent western blots to plot the relative abundance of JAK-STAT signalling proteins upon M. bovis BCG infection (colour scheme similar to Figure 4.4)*

HEK293T cells being human embryonic kidney cells don't produce JAK1, STAT1 and P-STAT1 similar to the levels seen in macrophage cell lines (Figure *4.7*). Irrespective of MOI, they constitutively express similar levels of SOCS1 in all experimental conditions and insignificant amounts of P-STAT1 (Figure *4.7*). This is expected as they are not leucocytes and hence don't respond to cytokine stimulation or infection on similar levels to that seen in macrophages.

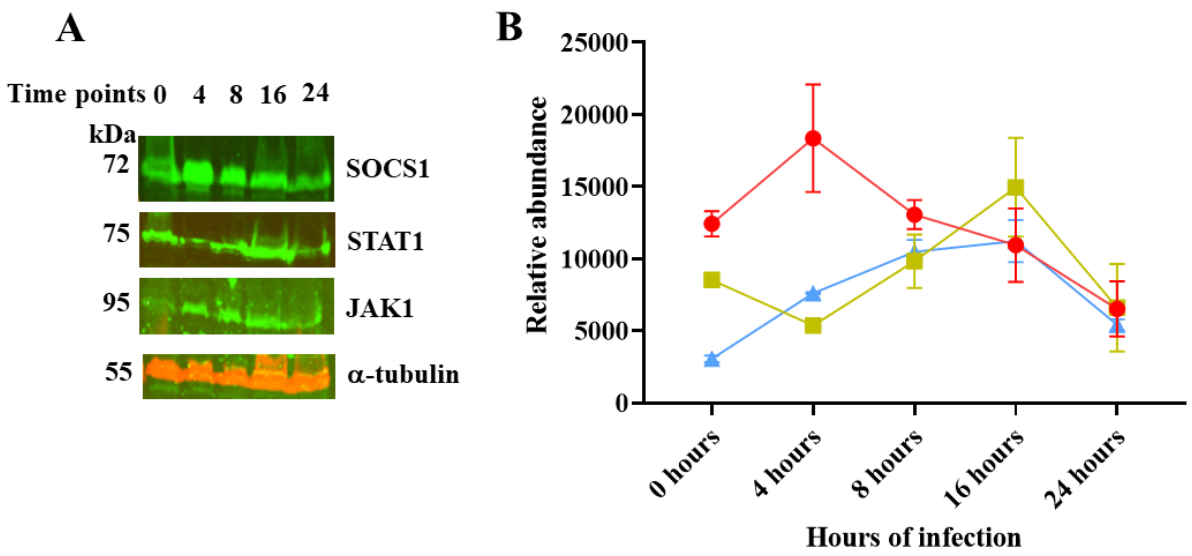

Figure 4.8: ***Establishing the ideal infection length in non-phagocytic HEK293T cell line.*** *A) HEK293T cells were infected with M. bovis BCG at MOI 10 for the aforementioned duration and cell lysates were used for western blot B) Densitometry was performed on three independent western blots to plot the relative abundance of JAK-STAT signalling proteins upon M. bovis BCG infection (colour scheme similar to Figure 4.7)*

To check if similar SOCS1 expression levels were produced irrespective of infection duration HEK293T cell were infected for increasing time points (0, 4, 8, 16, 24 hours) with *M. bovis* BCG at MOI 10. Cell lysates were used for Western blotting with actin and α-tubulin as loading controls (Refer **6.3.2, 6.3.11** and Table 6.22). To maintain consistency, the infection assay was repeated twice, and cell lysates collected were used for three independent Western blots as technical repeats for densitometry (Figure 4.8).

Unlike MOI infections, time point infections in HEK293T cells using *M. bovis* BCG showed a trend in SOCS1 expression level which increased at 4 hours of infection and reverted to levels similar to that seen in un-infected cells at 8 hours of infection. In contrast, at 16 and 24 hours of infection SOCS1 levels dip below the expression level seen in un-infected cells. Consistent with THP1 infections, STAT1 levels show a significant dip at 4 hours of infection when SOCS1 is at its maximum expression level, and peaks at 16 hours of infection when SOCS1 levels start dipping below the expression level seen in un-infected cells. JAK1 levels gradually rise and peak at 16 hours of infection and then revert back to levels similar that seen

in un-infected cells. This data confirms the inhibitory role of SOCS1 on JAK-STAT signalling in all cell lines irrespective of being leucocytes or not.

4.2.2 SOCS1 deletion in fatal to THP1 and J774 cell lines

SOCS1 is a negative regulator of IFN-γ signalling (Kinjyo *et al.*, 2002). It was initially identified as JAK binding protein (JAB) preventing JAK phosphorylation and function (Davey, Heath and Starr, 2006) and is now proven to contribute towards impaired mycobacterial control in macrophages (Carow *et al.*, 2011). $SOCS1^{-/-}$ mice had multiple abnormalities including growth retardation and reduced lymphocyte counts in thymus spleen and bone marrow and die within 2-3 weeks with liver necrosis and severe inflammation along with monocytic infiltration in pancreas, heart and lungs (Starr *et al.*, 1998; Alexander *et al.*, 1999; Marine *et al.*, 1999; Kinjyo *et al.*, 2002; Davey, Heath and Starr, 2006). $SOCS1^{-/-}$ mice are much more sensitive to bacterial infections (Kinjyo *et al.*, 2002) preventing a detailed analysis of the functional consequences of SOCS1 deletion on JAK-STAT signalling pathway and mycobacterial clearance. To address this issue, we aim to generate a $SOCS1^{-/-}$ macrophage cell line to study the consequences of SOCS1 deletion on cytokine signalling and mycobacterial clearance. CRISPR/Cas9 technology (Figure 4.9) was used to generate SOCS1 knockout cell line.

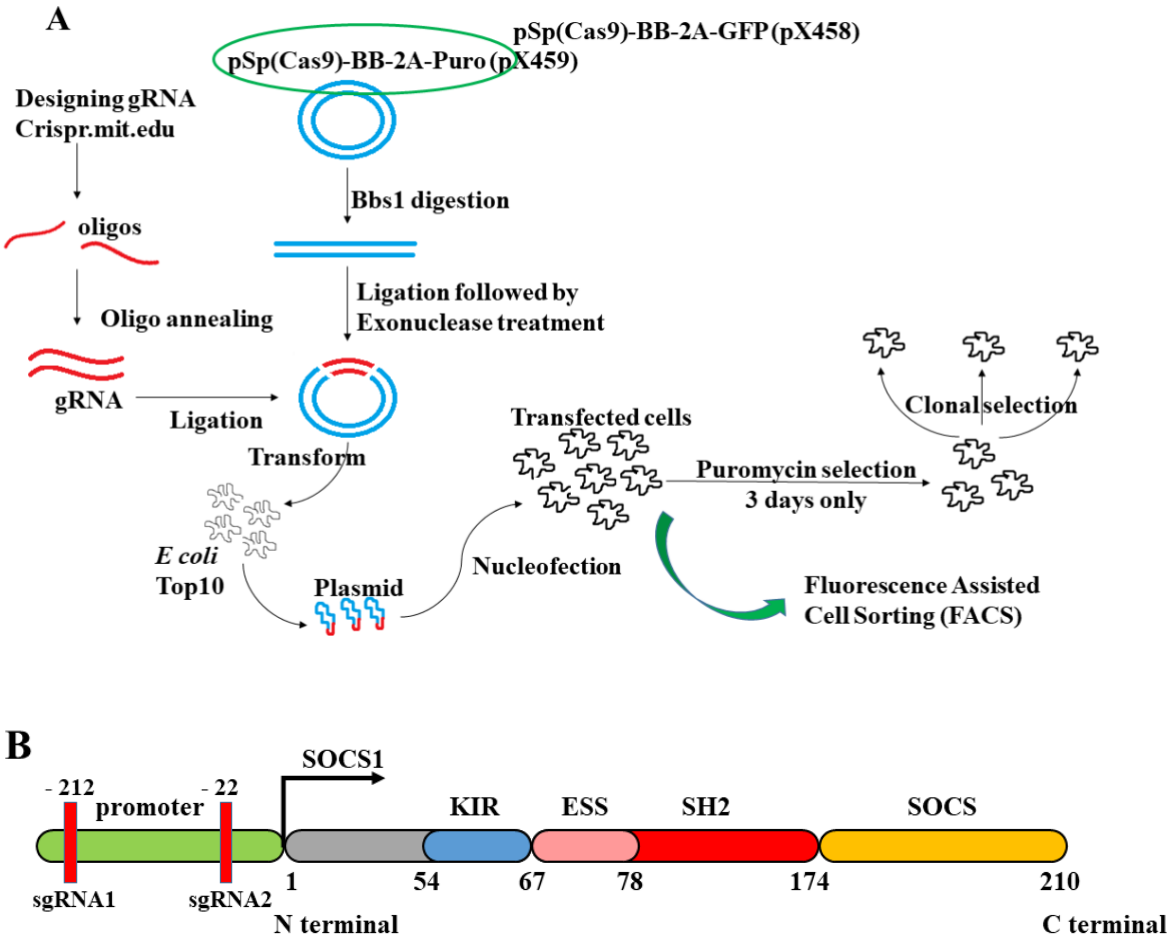

Figure 4.9: ***Utilisation of CRISPR/Cas9 to generate SOCS1$^{-/-}$ cell line.*** *(A) A schematic representation showing the methodology employed in deletion of SOCS1 from cell lines (B) Schematic showing the position of sgRNAs used in the study*

In this technique 25 nucleotide long single guide RNA (sgRNA) targeting both *homo sapien* and *mus musculus* SOCS1 were designed downstream of protospacer adjacent motif (PAM) (5'-NGG-3') which ensured Cas9 nuclease specificity (**6.3.3**). Minimisation of off target activity was ensured by maximum sequence similarity of sgRNA with the target sequence. sgRNA oligonucleotides were then annealed and cloned into pSp(Cas9)-BB-2A-Puro plasmid at bbs1 restriction site (Ran *et al.*, 2013). Sequence-verified endotoxin free CRISPR plasmid (pSpCas9(sgRNA)) was used for transfection into cell lines to generate

SOCS1 knockout cell line. Clonal isolation of cell lines was ensured by puromycin selection of transfection positive cells.

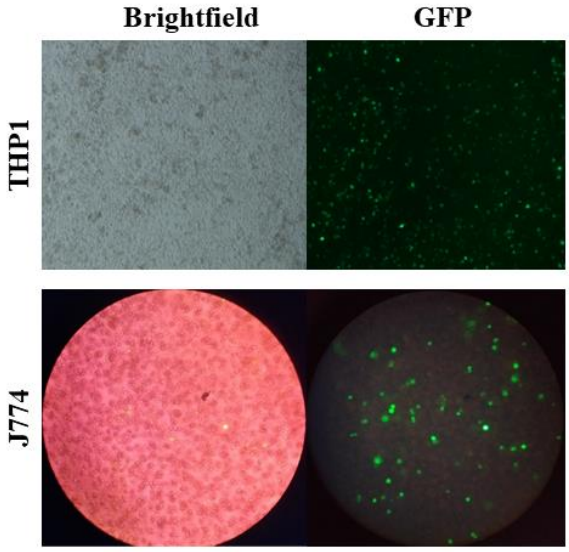

Figure 4.10: ***Standardising nucleofections in hard to transfect phagocytic cell lines (THP1-top and J774-bottom).*** *A) 4 million THP1 cells were nucleofected with 2 µg pMaxGFP and cells were visualised under a confocal microscope to confirm fluorescence B) 2 million J774 cells were nucleofected with 1 µg pMaxGFP and cells were visualised under a confocal microscope to confirm fluorescence*

THP1s and J774s are hard to transfect cell lines. To generate a SOCS1 knockout macrophage cell line, we first standardised the transfection method in hard to transfect macrophage cell lines (**6.3.5**). Nucleofection using 4D-Nucleofector system and program T-16 (Amaxa Nucleofector) or U008 (Lonza Nucleofector) worked best for both THP1 and J774 cell lines. For THP1 cells, 4 million cells were nucleofected with 2µg pMaxGFP and for J774s 2 million cells were nucleofected with 1µg pMaxGFP, positive clones were confirmed by confocal fluorescence microscopy (Figure 4.10).

Similarly, puromycin - antibiotic kill curve was performed on wild type cells to estimate the optimal working concentration of the drug which would kill 95% of the cells lacking the puromycin resistance gene (puromycin-N-acetyl-transferase (*pac*)) (Figure 4.11). Transfection positive clones harbouring *pac* gene would be resistant to puromycin treatment at this concentration (**6.3.6**). All three cell lines were incubated with increasing puromycin concentration and viable cells were counted at the end of 7 days using trypan

blue and the optimal working concentration was identified to be 0.9 µg/ml for THP1, 2 µg/ml for J774, and 3 µg/ml for HEK293T cells (Figure 4.13).

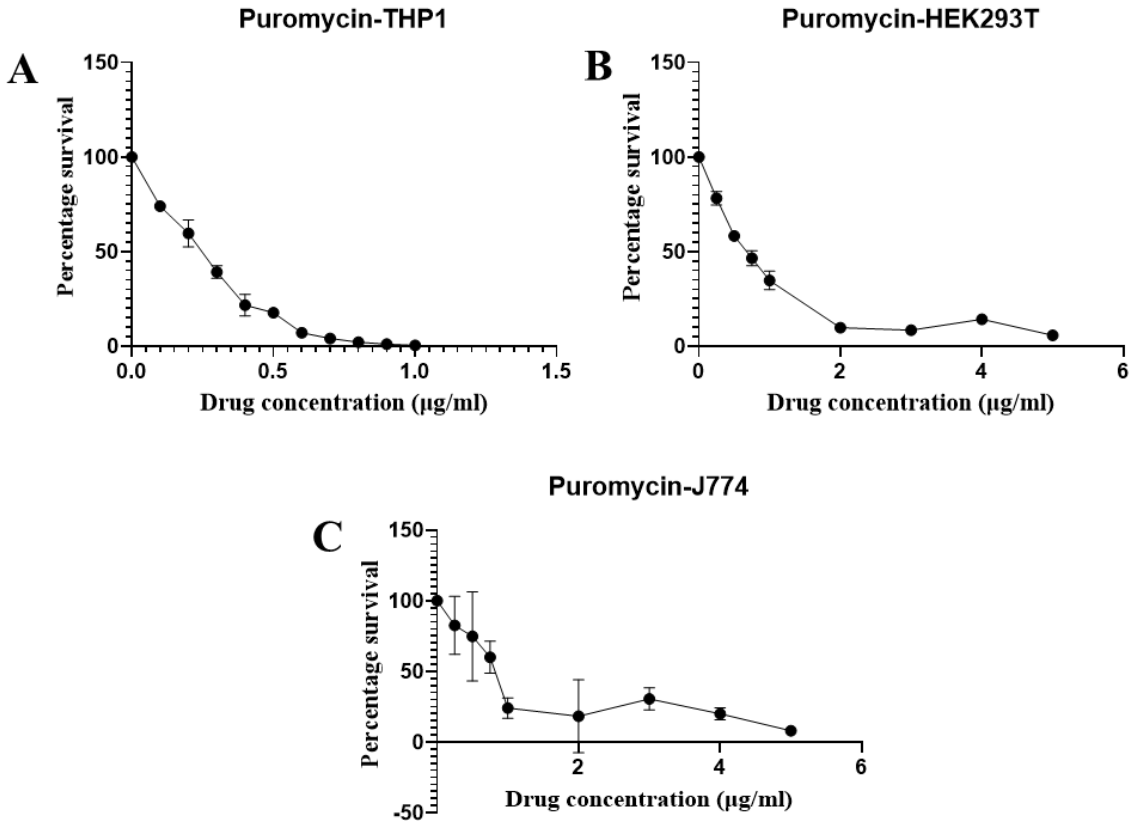

Figure 4.11: ***Puromycin kill curves to identify the optimum working concentration of the antibiotic in each cell line.*** *Cells- A) THP1s B) HEK293T C) J774s - were treated with increasing concentration of puromycin and optimum concentration was identified which had only 10% survival of wild type cells lacking puromycin resistance gene (puromycin-N-acetyl-transferase (pac))*

To generate a SOCS1 knockout THP1 cell line, cells were nucleofected with either pSp(Cas9)-BB-2A-Puro, pSp(Cas9)-BB-2A-Puro(HsgRNA1) or pSp(Cas9)-BB-2A-Puro(HsgRNA2) endotoxin free plasmids. Nucleofected cells were recovered for 72 hours following which transfection positive cells were isolated by puromycin selection at 0.9 µg/ml. Puromycin treatment was carried out for 72 hours. Viable cells were counted at the end of 72 hours and limiting dilution was performed at 1 cell/well in a 96 well plate to generate monoclonal knockout cell line (**6.3.7**). Cells were closely monitored to expand their numbers. However, SOCS1 deletion cells failed to survive and produce a monoclonal knockout cell line.

To confirm this result in the J774 murine macrophage cell line, J774s were nucleofected with pSp(Cas9)-BB-2A-GFP, pSp(Cas9)-BB-2A-GFP(MsgRNA1) or pSp(Cas9)-BB-2A-GFP(MsgRNA2) endotoxin free plasmids. Nucleofected cells were recovered in complete growth medium for 8 hours following which GFP positive cells were selected by FACS (refer **6.3.8;** Figure 4.12).

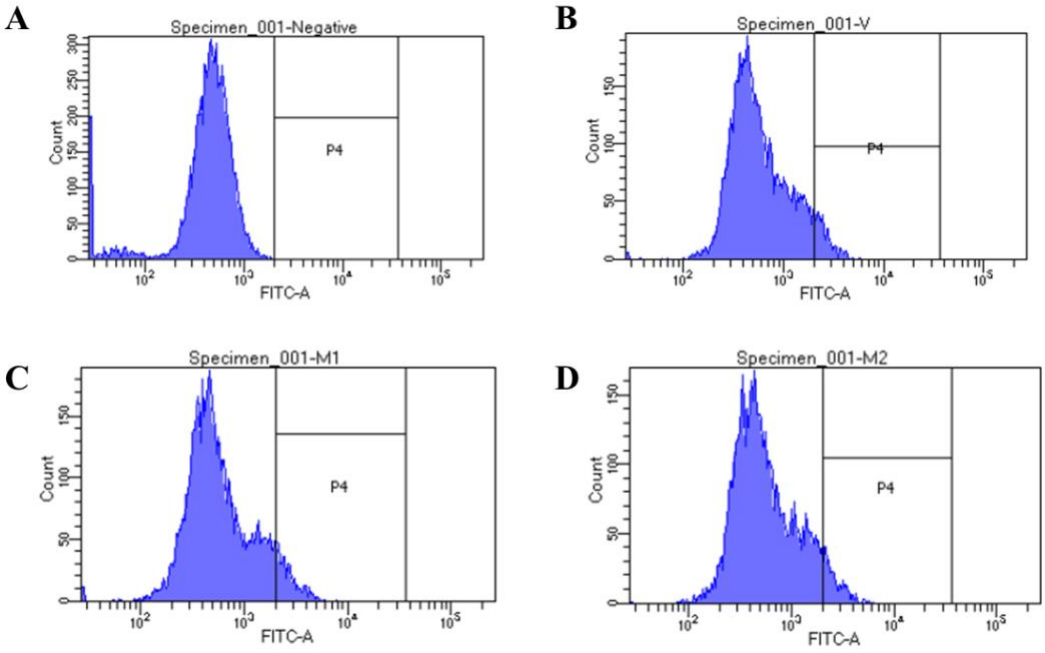

Figure 4.12: ***Fluorescence assisted cell sorting of GFP positive J774s.*** *J774s transfected with pSpCas9(BB)-2A-GFP(sgRNA) plasmid were collected using FACS A) channels were gated using wild type cells to ensure only GFP positive clones were collected B) pSpCas9(BB)-2A-GFP plasmid only transfected cells were collected and 1.2% cells were recovered C) pSpCas9(BB)-2A-GFP(sgRNA1) transfected cells were collected and 2.03% cells were recovered D) pSpCas9(BB)-2A-GFP(sgRNA2) transfected cells were collected and 1.83% cells were recovered*

2 million cells were used for transfection of each plasmid - pSp(Cas9)-BB-2A-GFP, pSp(Cas9)-BB-2A-GFP(MsgRNA1) or pSp(Cas9)-BB-2A-GFP(MsgRNA2). Of these 24,000 (1.2%) cells were recovered from pSp(Cas9)-BB-2A-GFP plasmid only transfected cells; 40,600 (2.03%) cells were recovered from pSp(Cas9)-BB-2A-GFP(MsgRNA1) transfected cells; 36,600 (1.83%) cells were recovered from pSp(Cas9)-BB-2A-GFP(MsgRNA2) transfected cell (Figure 4.12). Stable transfectants were recovered into complete growth medium and cultured at 37°C, 5% CO_2 to increase their numbers before further infection

assays were performed. However, like SOCS1 depletion in THP1 cells, SOCS1 knockout was fatal to J774 cells as they failed to survive beyond 24 hours upon SOCS1 depletion.

We were curious to see if SOCS1 depletion was fatal to any cell lines or if it was particular to leucocytes. So we transfected HEK293T cells with either pSp(Cas9)-BB-2A-Puro, pSp(Cas9)-BB-2A-Puro(HsgRNA1) or pSp(Cas9)-BB-2A-Puro(HsgRNA2) endotoxin free plasmids (**6.3.4**). Stable transfectants were infected with *M. bovis* BCG to enhance their SOCS1 expression (Figure 4.13).

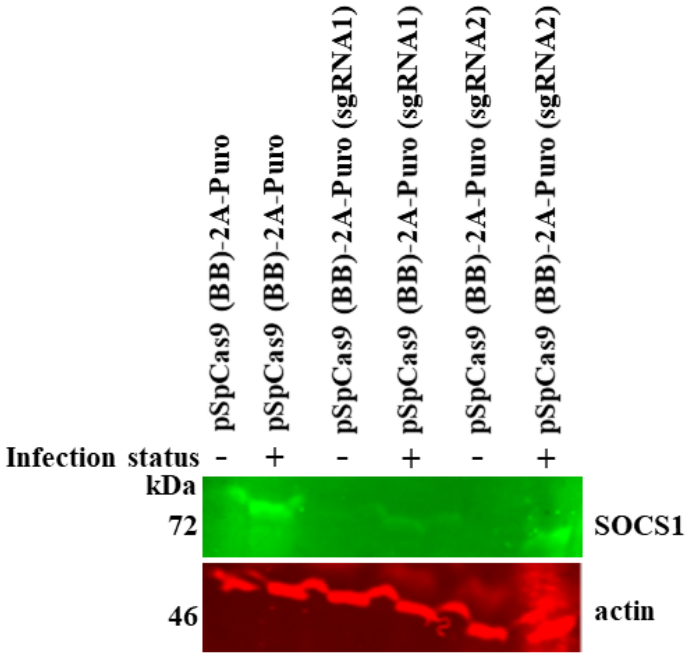

Figure 4.13: ***Generation and confirmation of SOCS1 knockout in HEK293T cells.*** *SOCS1 knockout HEK293T cells were infected with M. bovis BCG at MOI 10 and cell lysates were analysed by Western blotting using SOCS1 antibody standardised against actin loading control. A heterogeneous population of pSpCas9 (BB)-2A-Puro (sgRNA1) showed a clear SOCS1 knockout when infected with M. bovis BCG as compared to pSpCas9 (BB)-2A-Puro infected with M. bovis BCG*

First, in contrast to leucocytes, SOCS1 depletion was not fatal to HEK293T. Second, as expected SOCS1 levels were enhanced in HEK293T cells transfected with pSp(Cas9)-BB-2A-Puro (empty plasmid control) upon infection with *M. bovis* BCG (Figure 4.13). In cells transfected with pSp(Cas9)-BB-2A-

Puro(HsgRNA1) plasmid, SOCS1 was not expressed upon infection with *M. bovis* BCG confirming SOCS1 knockout (Figure 4.13). This SOCS1 knockout was not achieved in pSp(Cas9)-BB-2A-Puro(HsgRNA2) plasmid as SOCS1 was expressed in these cells upon infection with *M. bovis* BCG (Figure 4.13).

Considering HEK293T cells are not leucocytes, there was scepticism in drawing conclusions from SOCS1 knockout HEK293T cells. To clear this ambiguity SOCS1 expression levels were compared across the three cell lines (THP1, J774 and HEK293T) in both time dependent and dose dependent infection assays in which cells were infected with *M. bovis* BCG (Figure 4.14).

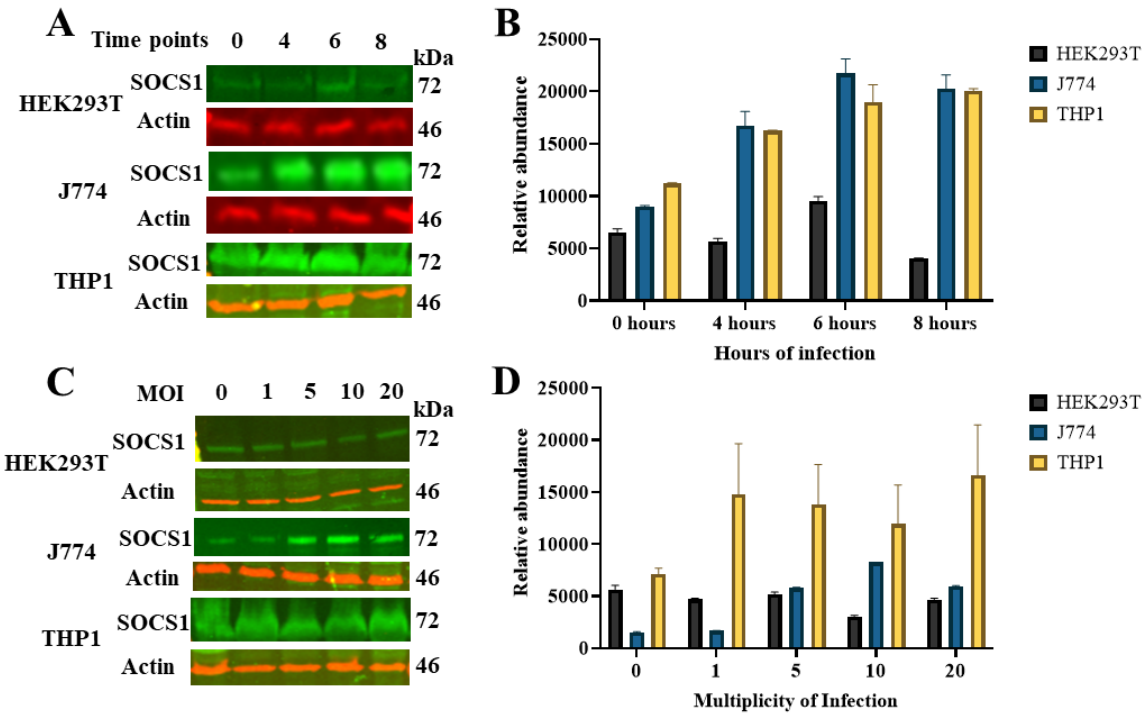

Figure 4.14: ***Comparing SOCS1 expression levels across the cell lines upon infection with M. bovis BCG, to validate the use of SOCS1$^{-/-}$ HEK293T cells.*** *All the three cell lines were tested for time point infections (at MOI 10) and dose dependent infections with increasing MOI of M. bovis BCG. In both the assays the expression level of phagocytic cell lines (J774 and THP1) is a minimum 3-fold higher than that produced in HEK293T*

Cells were infected with *M. bovis* BCG at MOI 10 for increasing hours of infection and SOCS1 levels were compared at 0, 4, 6, 8 hours of infection (Figure *4.14*A-B). At any time point considered SOCS1 levels produced in J774 and THP1 cell lines are at least double the amount seen in HEK293T cells with the difference being amplified to 4-fold at 8 hours of infection (Figure *4.14*A-B).

Similarly, when cells were infected with increasing MOI of *M. bovis* BCG, SOCS1 levels produced by THP1 cells were 3-fold higher when compared to HEK293T cells at MOI 1, 5, 10 and 20 (Figure 4.14C-D). SOCS1 levels seen in J774 cells were comparable to that produced to HEK293T cells at all other MOIs except MOI 10, where SOCS1 levels seen in J774 are double the amount seen in HEK293T cells (Figure 4.14C-D).

This data provides conclusive evidence to disregard the use of HEK293T- SOCS1$^{-/-}$ cells to study the effect of SOCS1 depletion on JAK-STAT signalling upon infection with *M. bovis* BCG.

4.2.3 SOCS1 binds to JAK1 and prevents the phosphorylation of STAT1 during *M. bovis* BCG infection

SOCS1 deletion is fatal to both THP1 and J774 cell lines preventing us from studying the functional consequences of SOCS1 deletion on JAK/STAT signalling during mycobacterial infection. To overcome this issue, we used the SOCS1 overexpression system. Commercially available *homo sapien* SOCS1 cloned into pcDNA3.1+/C-(K)-DYK plasmid was purchased and used to overexpress SOCS1 in the THP1 cell line. SOCS1 overexpressed cells were infected with *M. bovis* BCG for increasing amounts of time (0, 4, 8, 16, 24, 32, 48 hours) at MOI 0.5 (**6.3.9**). Immunoprecipitation using mouse anti-flag magnetic beads was performed on cell lysates to identify the interaction of SOCS1 with the JAK/STAT signalling proteins (**6.3.10**). Western blotting using Flag antibody confirmed the presence of Flag-tagged SOCS1 in all the samples (**6.3.11**).

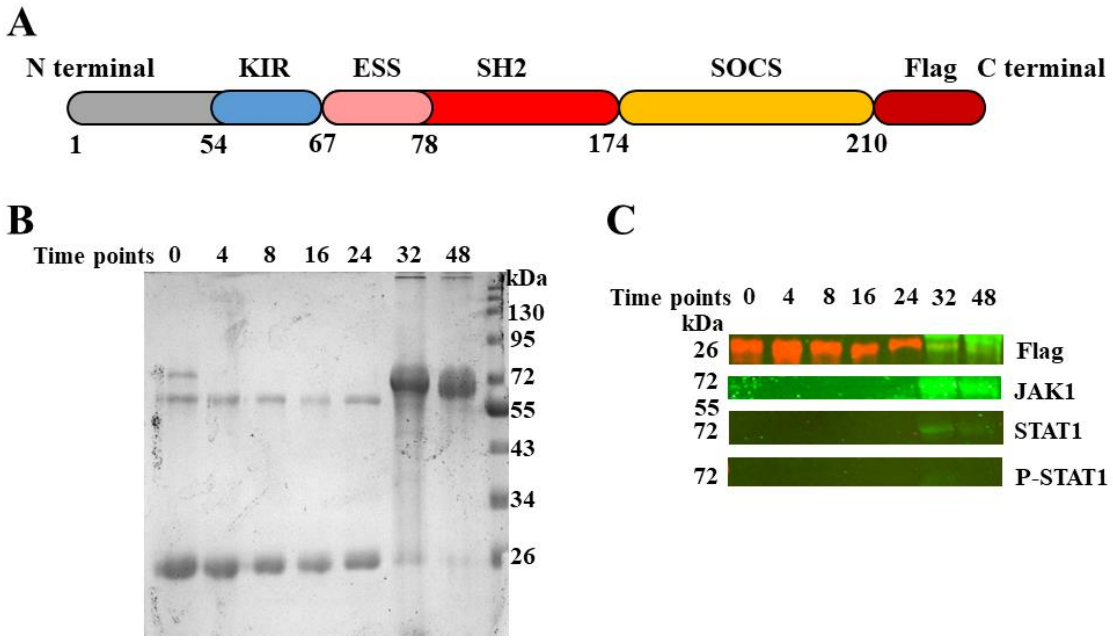

Figure 4.15: ***SOCS1 overexpression in THP1 cell line.*** *THP1 cells nucleofected with pcDNA3.1+/C-DYK tagged SOCS1 and were infected with M. bovis BCG at MOI 10 for increasing time points (0, 4, 8, 16, 24, 32 hours). Mouse anti-flag magnetic beads were used for immunoprecipitation on cell lysates. A) IP samples were run on an SDS-PAGE and stained with Instant blue to visualise the interaction of flag tagged SOCS1 with STAT1 upon 32 hours of infection with M. bovis BCG. B) Western blot was run on performed on with Flag and STAT1 primary antibody and their interaction was observed 32 hours into infection. C) Western blot was performed using multiple antibodies (Flag, JAK1, STAT1 and p-STAT1) to confirm SOCS1 interation with STAT1*

Immunoprecipitation and Western blot revealed SOCS1 interaction with STAT1 and JAK1 at 32 and 48 hours of infection (Figure 4.15). SOCS1 interacts with STAT1 at the substrate binding grove of JAK preventing the phosphorylation of STAT1 and thereby hindering JAK/STAT signalling during mycobacterial infection (Liau *et al.*, 2018). This is confirmed by the presence of STAT1 in the immunoprecipitation product at 32 hours of infection. The phosphorylation status of STAT1 at this time point was verified using phosphorylated (Tyr701) STAT1 antibody which confirmed the absence of phosphorylated STAT1 at 32 hours of infection. This data demonstrates the preventive role of SOCS1 in phosphorylation of STAT1 during mycobacterial infection (Figure 4.15).

4.2.4 KIR is crucial for the kinase inhibitory activity of SOCS1 during *M. bovis* BCG infection

Liau *et al*. established the molecular basis of JAK/STAT inhibition by SOCS1 (Liau *et al.,* 2018). SOCS1 can inhibit the kinase activity of JAK1directly through its KIR domain (Yoshimura *et al.,* 2012) which binds to the substrate binding grove of JAK1 and acts as a pseudo-substrate thereby inhibiting its tyrosine kinase activity (Liau *et al.,* 2018).

Six continuous residues in KIR (H54 to R59) corresponding to -1 to +5 (based on earlier definition) were identified to be crucial for its interaction with JAK1 (Liau *et al.,* 2018). Of these, H54 which lies just outside the KIR domain occupies the substrate binding site of JAK1, and it is held in position by the hydrophobic interactions and hydrogen bonds formed by the residues of the KIR domain with those in JAK1 (Liau *et al.,* 2018). F55 and F58 form hydrophic interactions with F, T and V from JAK1 and fix KIR domain at the substrate binding grove of JAK1 thereby enabling the formation of three hydrogen bonds between the side chains of R56, R59 and T57 with the activation loop of JAK1. All six residues contribute to the affinity of this interaction as revealed by mutagenesis which lead to complete loss of inhibitory activity (Liau *et al.,* 2018).

To confirm this interaction of the KIR domain with JAK1 and the role of these six residues during mycobacterial infection, we used alanine scanning method and replaced each of these residues with alanine in pcDNA3.1+/C-(K)-DYK plasmid containing SOCS1. We also used KIR deletion mutant and H54toR59 deletion mutant to study the effect of mutagenesis on the kinase inhibitory activity of SOCS1.

Site directed mutagenesis plasmids were nucleofected into THP1s and infected for 32 hours with *M. bovis* BCG at MOI 0.5 (**6.3.2** and **6.3.5**). Immunoprecipitation using mouse anti-flag magnetic beads was performed on cell lysates to identify the role of each residue in the interaction between SOCS1 and JAK1. KIR deletion mutant and H54toR59 deletion mutant were included to study the role of KIR in the kinase

inhibitory activity of SOCS1 during mycobacterial infection. Western blot using Flag antibody confirmed the presence of Flag tagged SOCS1 in all the samples (Figure 4.16).

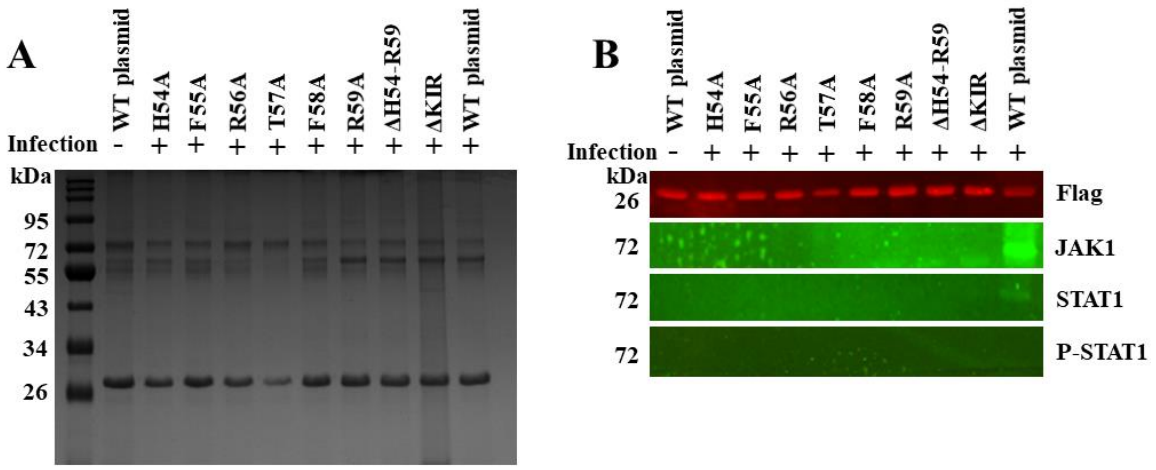

Figure 4.16: ***KIR SDM plasmids were transfected into THP1 cells to identify the crucial residue for its interaction with JAK/STAT signalling.*** *THP1 cells were nucleofected with pcDNA3.1+/C-DYK tagged SOCS1 with site directed mutagenesis at residues H54, F55, R56, T57, F58, R59. Cells were recovered for 72 hours and infected for 32 hours with M. bovis BCG at MOI 10. Immunoprecipitation was performed on cell lysates using mouse anti-flag magnetic beads. A) IP samples were run on an SDS-PAGE and stained with Instant blue to visualise the interaction of flag tagged SOCS1 with STAT1 upon 32 hours of infection with M. bovis BCG. B) Western blot was performed using multiple antibodies (Flag, JAK1, STAT1 and p-STAT1) to confirm SOCS1 interation with JAK-STAT1*

Immunoprecipitation and Western blotting using JAK1, STAT1 and p-STAT1 antibodies revealed the absence of these signalling proteins in the immunoprecipitation product of all the KIR site directed mutagenesis plasmid transfected cell lines (Figure 4.16). Wild type plasmid transfected THP1 cells have JAK1 and STAT1 in immunoprecipitation product upon 32 hours of infection with *M. bovis* BCG. In contrast, neither of H54A, F55A, R56A, T57A, F58A, R59A have either JAK1 or STAT1 upon immunoprecipitation with mouse antiflag beads. Similarly, the KIR deletion mutant and H54 to R59 deletion mutant also failed to bind to JAK1 during 32 hours of infection with *M. bovis* BCG. This is consistent with Liau *et al.* where they have seen a complete loss of kinase inhibitory activity upon KIR deletion or mutation of F58 (Liau *et al.*, 2018). While F55 mutation led to a 50-fold reduction in kinase inhibitory activity, mutation of other crucial residues including H54, R56, T57 and R59 has led to a 10-fold reduction in kinase

inhibitory activity of SOCS1 (Liau *et al.*, 2018). This data suggests that during mycobacteria infection the F55 and F58 of KIR domain in SOCS1 are crucial to insert H54 in the substrate binding grove of JAK1, which is then held in position by the hydrogen bonds formed by R56, T57 and R59 thereby affecting the tyrosine kinase activity of JAK1. This KIR mediated inhibtion of JAK1 tyrosine kinase activity results in the inhibition of JAK/STAT signalling which is essential for mycobacterial clearence.

4.2.5 *aftC* repressed *M. bovis* BCG also inhibits JAK/STAT signalling *via* SOCS1

aftC repressed *M. bovis* BCG has truncated LAM in its cell envelope resulting in increased production of pro-inflammatory cytokines and reduced production of anti-inflammatory cytokines (**3.2.3**). IL-10, which is a crucial anti-inflammatory cytokine promoting the intracellular survival of mycobacteria (Eum *et al.*, 2008; Kumar *et al.*, 2015; Tebruegge *et al.*, 2015) and it is downregulated upon infection with *aftC* repressed *M. bovis* BCG (**3.2.3**). IL-10 signalling is mediated by JAK1 which is regulated by SOCS1 (Table 4.1). We have shown that KIR mediated inhibition of JAK1-tyrosine kinase activity results in prevention of STAT1 phosphorylation leading to inhibition of JAK/STAT signalling. Therefore, SOCS1 also inhibits IL-10 mediated immune responses (Ding *et al.*, 2003). We hypothesised *aftC* repressed *M. bovis* BCG to have no effect on JAK/STAT signalling, as it is unable to produce the ligands (IL-10) to initiate ligand-receptor engagement essential for the activation of JAK/STAT signalling. To test this hypothesis, we infected SOCS1 (flag-tagged) overexpressed THP1 cells with BCG-VC and BCG-sgRNA3 grown in the presence and absence of ATc at MOI 0.5 for 32 hours. Immunoprecipitation was performed on cell lysates using mouse anti-flag magnetic beads to confirm the interaction of SOCS1 with JAK1. Western blot using Flag antibody confirmed the presence of Flag tagged SOCS1 in all the samples (Figure 4.17).

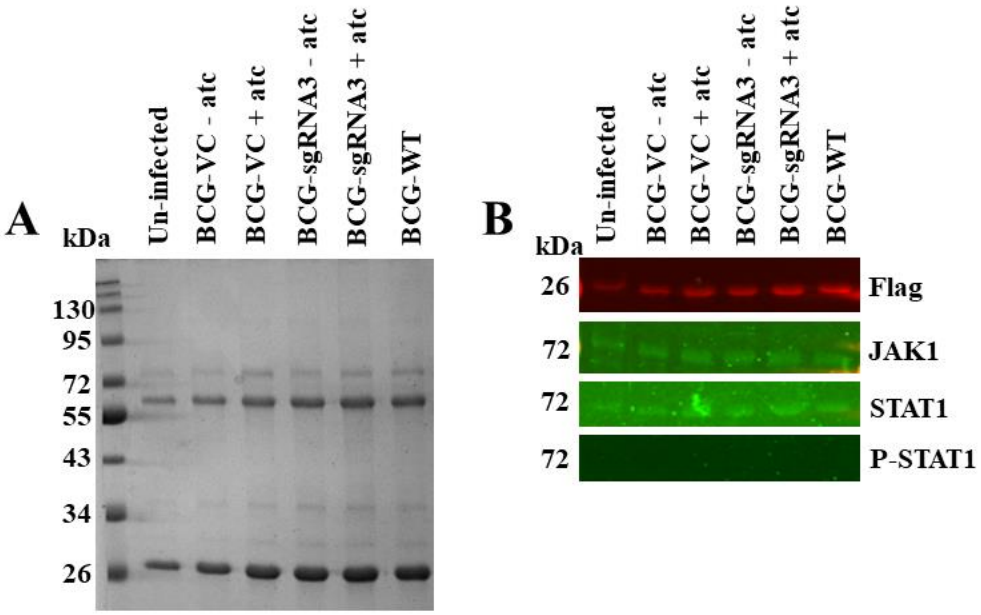

Figure 4.17: ***Effect of aftC repressed M. bovis BCG on the interaction of SOCS1 with JAK/STAT signalling proteins.*** *SOCS1 was overexpressed in THP1 cells and they were infected at MOI 10 with BCG-VC and BCG-sgRNA3 grown in the presence and absence of ATc. Immunoprecipitation was performed on cell lysates using mouse anti-flag magnetic beads. A) IP samples were run on an SDS-PAGE and stained with Instant blue to visualise the interaction of flag tagged SOCS1 with STAT1 upon 32 hours of infection with M. bovis BCG. B) Western blotting was performed using multiple antibodies (Flag, JAK1, STAT1 and p-STAT1) to confirm SOCS1 interation with JAK1 and STAT1 upon infection with aftC repressed BCG*

Immunoprecipitation and Western blotting revealed SOCS1 interaction with JAK1 and STAT1 upon infection with *aftC* repressed BCG. In contrast to our hypothesis, like wild type *M. bovis* BCG JAK1 is present in all the immunoprecipitation products including that obtained from BCG-sgRNA3 grown in the presence of ATc (*aftC* repressed BCG), as well as BCG-VC grown in the presence or absence of ATc (Figure 4.17). The immunoprecipitation product from *aftC* repressed BCG also revealed the presence of STAT1 in an un-phosphorylated form similar to wild type *M. bovis* BCG (Figure 4.17). This data confirms that the lipoglycan defect seen in *aftC* repressed BCG in the form of truncated 'AftC-LAM' does not affect the ability of *M. bovis* BCG in instigating SOCS1 mediated inhibition of JAK/STAT signalling.

4.3 Discussion

SOCS1 was first discovered as a JAK binding protein (JAB) and later designated as STAT-induced STAT inhibitor-1 (SSI-1) (Narazaki *et al.*, 1998). It is a critical inhibitor of IFN-γ signalling preventing the deleterious effects of excessive inflammation mediated by JAK/STAT signalling (Yoshimura *et al.*, 2012). SOCS1$^{-/-}$ mice have multiple abnormalities, including growth retardation and reduced lymphocyte counts in the thymus, spleen and bone marrow and die within 2-3 weeks with liver necrosis and severe inflammation along with monocytic infiltration in the pancreas, heart and lungs (Starr *et al.*, 1998; Alexander *et al.*, 1999; Marine *et al.*, 1999; Kinjyo *et al.*, 2002; Davey, Heath and Starr, 2006). Neonatal death seen in SOCS1$^{-/-}$ mice is because of uncontrolled IFN-γ signalling, as SOCS1$^{-/-}$ IFN-γ$^{-/-}$ double knockout mice do not die as neonates (Alexander *et al.*, 1999). However, these mice are much more sensitive to bacterial infections (Kinjyo *et al*., 2002).

SOCS1 is involved in suppression of inflammation in both immune and non-immune cells. While T cell specific conditional SOCS1$^{-/-}$ mice developed severe inflammatory disease (Tanaka *et al.*, 2008), SOCS1 deletion in hepatocytes induced hepatitis due to enhanced pro-apoptotic signals mediated by STAT1 in mice with SOCS1 deficient liver (Torisu *et al.*, 2008). SOCS1 also maintains intestinal immune homeostasis in prostaglandin E2 (PGE2)-mediated anti-inflammatory mechanism as mice lacking it developed colitis at 2–6 months of age (Chinen *et al.*, 2011b).

SOCS1 is highly upregulated during mycobacterial infection. At the early stages of infection, mycobacteria induced SOCS1 expression in macrophages hampers IL-12 mediated IFN-γ production in macrophages resulting in uncontrolled mycobacterial growth in phagocytes (Carow *et al.*, 2011). At later time points, despite SOCS1 expression in macrophages they respond to IFN-γ secretion by T and NK cells preventing SOCS1 mediated bacterial control (Carow *et al.*, 2011). However, at this later time points of infection,

SOCS1 produced in non-macrophage cells protect the host from infection induced harmful inflammation (Carow *et al.*, 2011).

Earlier SOCS1 deletion studies were all performed in mice which succumbed to excessive inflammation without giving detailed analysis of mycobacterial infection. SOCS1 knockdown studies using siRNA revealed enhanced IL-12 production and increased mycobacterial clearance in DCs and PBMC establishing the negative role of SOCS1 in DCs (Srivastava *et al.*, 2009). However, macrophages being the primary phagocytes might provide a wealth of knowledge upon SOCS1 deletion. For this purpose, as well as considering the ethical issues pertaining to animal studies, we proposed to use CRISPR/Cas9 methodology to generate SOCS1 deleted macrophage cell line to study the implication of this deletion on early stages of mycobacterial infection.

4.3.1 CRISPR/Cas9 to generate SOCS1$^{-/-}$ macrophage cells

CRISPR/Cas9 technology was first optimised to facilitate genome engineering in eukaryotic cells. The Zhang lab optimised this powerful tool to enable precise edits in mammalian cells. They described a highly efficient protocol that would facilitate Cas9 mediated genome editing to generate a modified clonal cell line within 2-3 weeks (Ra*n et al.*, 2013). Using this methodology, we attempted to generate a SOCS1$^{-/-}$ macrophage cell line. For this two sgRNAs both targeting the promoter region of *SOCS1* were cloned into a pSpCas9(BB)-2A-Puro (PX459) plasmid and transfected into THP1 cells and plated by serial dilution to isolate clonal cell lines with SOCS1 deletion. However, repeated unsuccessful attempts to generate SOCS1$^{-/-}$ THP1 prompted us to believe the lethality of SOCS1 deletion to the THP1 cell line. To confirm this in J774 murine macrophage cell line, we used FACS to isolate transfection positive cells (using pSpCas9(BB)-2A-GFP (PX458)). SOCS1 deletion was fatal to J774 cells like THP1 cells as we could isolate clonal cell lines transformed with empty plasmid in both the cell lines (Figure 4.12). As we could obtain SOCS1$^{-/-}$ HEK293T cell line using the same plasmids (Figure 4.13), this evidence demonstrates the lethality of SOCS1 deletion in macrophage cell lines. SOCS1 knockdown studies performed in DC and PBMC did not

report any lethality upon transcriptional repression of SOCS1 (Srivastav*a et al.*, 2009). However, considering they did not make a permanent chromosomal deletion, they might not have seen a similar effect in DCs. Considering the inability to perform *in vitro* experiments involving a $SOCS1^{-/-}$ macrophage cell line we switched to SOCS1 overexpression system using C-terminal flag tag to establish the interaction of SOCS1 with JAK1 during *M. bovis* BCG infection (Figure 4.15) (Carow *et al.*, 2011). Using the same model, we propose to study the role of KIR domain of SOCS1 during mycobacterial infection.

4.3.2 KIR domain of SOCS1

Yoshimura and colleagues studied SOCS proteins extensively and proposed their modes of action (Endo *et al.*, 1997; Kubo, Hanada and Yoshimura, 2003; Yoshimura *et al.*, 2012). They hypothesised the inhibitory activity of SOCS1 to be mediated by the SH2 domain which binds to phosphorylated tyrosine residues in the activation loop of JAK1 and JAK2 so that the KIR domain could directly inhibit the catalytic activity of the kinase (Yasukawa *et al.*, 1999). Liau *et al.* provided molecular basis to support this hypothesis (Liau *et al.*, 2018). They have also shown that KIR blocks the substrate binding groove of the kinase using a histidine residue present on the N-terminal of KIR (Liau *et al.*, 2018). While this histidine (H54) acts as a pseudo-substrate, it is held in this position by the hydrophobic and/or polar side chains formed by the first 5 residues (F55, R56, T57, F58 and R59) of KIR (Liau *et al.*, 2018). These 6 continuous residues in KIR are highly conserved in multiple orthologues of SOCS1 (human, *M. musculus, G. gallus, X. laevis, D. rerio*) and mutating any of these led to a significant decrease in its affinity to the substrate binding grove of JAK1 thereby reducing the kinase inhibitory activity of SOCS1 (Liau *et al.*, 2018). In this study, we have shown that during *M. bovis* BCG infection, each of these six residues are crucial for the interaction of SOCS1 with JAK1 and in preventing JAK/STAT signalling (Figure 4.16). Site directed mutagenesis by the alanine scanning method provided this loss of interaction when flag-tagged SOCS1 was used for immunoprecipitation and Western blotting (Figure 4.16). This data demonstrates that during mycobacteria infection F55 and F58 of the KIR domain in SOCS1 are crucial to insert H54 in the substrate binding grove

of JAK1, which is then held in a position by the hydrogen bonds formed by R56, T57 and R59 thereby affecting the tyrosine kinase activity of JAK1. This KIR mediated inhibtion of JAK1 tyrosine kinase activity results in the inhibition of JAK/STAT signalling which is essential for mycobacterial clearence.

4.3.3 Effect of *aftC* repressed BCG on JAK/STAT interaction

SOCS1 regulates multiple cytokine signalling including IFN-γ (Carow *et al.*, 2011) and IL-10 (Ding *et al.*, 2003). *AftC* repressed *M. bovis* BCG which has truncated 'AftC-LAM' in its cell envelope stimulates increased production of pro-inflammatory cytokines and reduced production of anti-inflammatory IL-10 production (Chapter 3). We hypothesised *aftC* repressed *M. bovis* BCG to have no effect on JAK/STAT signalling, as it is unable to produce the ligands (example: IL-10) to initiate ligand- receptor engagement essential for the activation of JAK/STAT signalling. However, in contrast to our hypothesis, *aftC* repressed BCG can also inhibit JAK/STAT signalling *via* SOCS1 (Figure 4.17). Similar to *M. bovis* BCG, *aftC* repressed BCG instigated KIR mediated SOCS1 interaction with JAK1 thereby preventing the phosphorylation of STAT1 and downstream cytokine signalling (Figure 4.17). This data confirms that lipoglycan defect seen in *aftC* repressed BCG in the form of truncated 'AftC-LAM' does affect the ability of *M. bovis* BCG in instigating SOCS1 mediated inhibition of JAK/STAT signalling (Figure 4.17).

Key findings

The major findings of the chapter are:

- SOCS1 deletion is lethal to J774 and THP1 macrophage cell lines but not for HEK293T cells
- SOCS1 binds to JAK1 and prevents the phosphorylation of STAT1 thereby inhibiting JAK/STAT signalling during *M. bovis* BCG infection
- During *M. bovis* BCG infection six continuous residues in KIR (H54 to R59) are crucial for the interaction of SOCS1 with JAK1 and in preventing JAK/STAT signalling
- Similar to *M. bovis* BCG, *aftC* repressed BCG can also inhibit JAK/STAT signalling via SOCS1

Chapter 5 : General Discussion

Before COVID19 pandemic, TB was ranked number one cause of global mortality (WHO, 2019). During the pandemic, many under-reported cases and a drop in TB diagnosis and treatment have worsened the implications on the End TB Strategy (WHO, 2021). Progress made so far in this WHO initiative is threatened by the emergence of MDR and XDR strains of *M. tuberculosis*. TB is the leading cause of death in immunocompromised people, including those infected with HIV/AIDS, especially in resource-limited countries (Pawlowski *et al.*, 2012). Genetic polymorphisms seen in Asians and Africans have been identified to have increased susceptibility to TB and HIV/AIDS (Pawlowski *et al.*, 2012; Domingo-Gonzalez et al., 2016). The only way to help this situation is by improving TB chemotherapy and development of a new vaccine candidate.

Current TB chemotherapy involves a cocktail of 4 drugs for a period of 6 months for drug sensitive strains and 5 drugs for 20 months for drug resistant strains, with only 56% treatment success rate in MDR strains (WHO, 2021). BCG is the widely used vaccine but with variable efficacy in adults. Novel drug discovery has been particularly slow in TB due the presence of waxy lipophilic cell envelope which serves as a permeability barrier for hydrophilic drugs making it resistant to many common antibiotics. However, the mycobacterial cell wall is also crucial for its survival and pathogenesis making it an attractive drug target. Amongst the front-line drugs, isoniazid targets mycolic acid biosynthesis (Banerjee *et al.*, 1994) and ethambutol targets arabinan synthesis in AG and LAM (Alderwick *et al.*, 2005). Several of the second line drugs also target cell wall biosynthesis, for example ethionamide targets mycolic acid biosynthesis (Banerjee *et al.*, 1994) and D-cycloserine targets PG biosynthesis (Bruning *et al*., 2011). Many more cell wall inhibitors are being explored for their anti-tubercular efficacy and are in the mycobacterial drug discovery pipeline (Lanne *et al.*, 2020).

A deeper understanding of cell wall assembly and the nature of genes involved this process will shed light on potential new drug targets. With this in mind, one project in this PhD thesis explores the role of arabinofuranosyltransferase C (a*ftC*) in *M. bovis* BCG cell wall biosynthesis and the implications of its deletion on the immunogenicity of the BCG vaccine strain. Biochemical and phenotypic characterisation of

the mutant strain revealed essentiality of the gene in planktonic and biofilm cultures and the role of *aftC* in maintaining structural integrity and cell wall architecture. Infection and cytokine analyses in macrophage cell lines revealed increased immunogenicity of the strain, however this needs further validation using animal models.

The other project explores host pathogen interactions of mycobacteria and the role of host factors in promoting intracellular mycobacterial survival. Mycobacteria is a complex pathogen which alters and modifies host responses to enable long term co-habitation within macrophages (Murray, 2007). JAK/STAT signalling is one such crucial pathway which is being corrupted by mycobacteria using suppressor of cytokine signalling (SOCS) molecules (Murray, 2007; O'Shea and Murray, 2008; O'Shea et al., 2015). Untimely induction of SOCS molecules by mycobacteria, inhibits JAK/STAT signalling resulting in sub-lethal levels of inflammatory cytokines preventing mycobacterial clearance (Carow *et al.*, 2011; Masood *et al.*, 2013). This pathway is studied in this project using SOCS1, and a particular domain - kinase inhibitory region (KIR). KIR is known to inhibit JAK/STAT signalling *via* binding to tyrosine residues in JAK1 preventing downstream signalling (Yoshimura, Naka and Kubo, 2007; Yoshimura *et al.*, 2012; Liau *et al.*, 2018). In this project the crucial residues within KIR have been identified during mycobacterial infection. SOCS1-KIR mimetics and antagonists represent an attractive small molecule for host directed therapies (HDT). In HDTs, small molecules are used with or without antibiotics to fine tune antimicrobial activity of immune cells and limit tissue damage (Kolloli and Subbian, 2017). As these molecules directly act on immune cell functions, there is limited possibility for drug resistance in HDTs. They also represent a promising treatment strategy to combat MDR and XDR strains of TB, as well as treatment of immunocompromised patients with existing comorbid conditions (Kolloli and Subbian, 2017).

Findings from each of these projects are summarised below with possible applications in adjuvant/vaccine development and HDTs.

5.1 Role of *aftC* in *M. bovis* BCG cell wall assembly

5.1.1 Conclusions

The mycobacterial cell wall core consisting of mycolyl-arabinogalactan-peptidoglycan layer is an extremely elaborate structure involving the work of numerous glycosyltransferases (Berg *et al*., 2007; Alderwick *et al*., 2015; Jankute *et al*., 2015). These glycosyltransferases involved in the assembly of crucial lipooligosaccharides present attractive targets for drug development. Mycobacteria predominantly contain GTs of the GT-C sub family particularly due to its lipophilic cell envelope (Berg *et al*., 2007). Numerous GTs of this group were discovered and many more are yet unidentified in AG and LAM biosynthesis (reviewed in Jankute *et al*., 2015). AftA is the priming enzyme responsible for the addition of the first $\alpha(1\rightarrow5)$ linked Ara*f* residue to $\beta(1\rightarrow6)$ linked Gal*f* in the galactan core of AG (Alderwick *et al*., 2006a). Similarly, AftB is responsible for $\beta(1\rightarrow2)$ Ara*f* residue (Seidel *et al*., 2007a). AftC is identified to function as a branching enzyme responsible for the addition of the first $\alpha(1\rightarrow3)$ linked Ara*f* residue to $\alpha(1\rightarrow5)$ linked Ara*f* core in AG and LAM thereby increasing their branching (Birch *et al*., 2008; 2010). There are at least ten other glycosyltransferases with unknown function, and they could be crucial drug targets.

Although, whole genome sequence of *M. tuberculosis* has been available for over two decades now, very few drug targets have been identified (Rock, 2019). Limited tools for functional genomics is one of the (many) reasons for the lack of TB drugs (Choudhary, Lunge and Agarwal, 2016; Chhotaray *et al.*, 2018; Rock, 2019). Identification of novel drug targets and the mechanism of action of drugs has been restricted by the lengthy time consuming serial gene manipulation strategies (Rock, 2019). Especially in case of essential genes which are attractive drug targets. The traditional approaches of conditional gene expression requires merodiploid strain construction which is limited by the inducible promoter systems available for use in *M. tuberculosis* (Singh *et al.*, 2016).

Earlier studies used allelic exchange based homologous recombination to generate an *aftC* knockout in *M. smegmatis* (Birch *et al.*, 2008). Similar attempts in *M. bovis* BCG were unsuccessful as *aftC* is an essential gene in *M. bovis* BCG unlike to *M. smegmatis* where is it non-essential (Chapter 2). Similar observations were made with the *emb* proteins, *embA* and *embB* knockout mutants were easily generated in *M. smegmatis* (Escuyer *et al*., 2001; Zhang *et al*., 2003) but similar attempts were unsuccessful in *M. tuberculosis* (Amin *et al*., 2008; Birch *et al.,* 2008). EmbCAB are non-essential in *M. smegmatis* as all three mutants are viable but possess an altered cell envelope (Amin *et al*., 2008; Birch *et al.,* 2008). Similar studies were not possible in *M. tuberculosis* due to the species in-tolerance to this gene manipulation (Amin *et al*., 2008).

We used CRISPRi to generate AftC depletion mutants in *M. bovis* BCG (Choudhary *et al.*, 2015; Singh *et al.*, 2016; Rock *et al.*, 2017). Using this technique, we have shown the essentiality of *aftC* in *M. bovis* BCG (Chapter 2). *aftC* repression affects the growth and cell size of *M. bovis* BCG in liquid culture. *aftC* repression generated a heterogeneous population of abnormal bacilli with discontinuous cell, fluffier appearance, significantly smaller length. Biochemical analysis of planktonic cultures revealed intermediary sized LAM, similar to earlier studies (Birch *et al.,* 2008). *aftC* deletion in *M. smegmatis* and *C. glutamicum* generated truncated and unbranched AG and LAM (Birch *et al.,* 2008, 2010). To confirm these changes to the cell wall core upon *aftC* repression in *M. bovis* BCG, glycosyl composition and linkage analysis could've been performed, but due to time constraints they could not be completed (Appendix 1 and 2).

The lipid profile of *aftC* repressed *M. bovis* BCG is contrary to earlier studies. It has an increase in α- and ketomycolates as opposed to the *aftC* knockout *M. smegmatis* which has an overall reduction in cell wall bound mycolates including α, α', and epoxymycolates. This was coupled with increased accumulation of TDM due to reduced tethering of mycolic acids to the AG *aftC* knockout of *M. smegmatis* (Birch *et al.,* 2008). No such observations were made in *aftC* repressed *M. bovis* BCG. Similar inconsistencies were reported in earlier CRISPRi studies (Roc*k et al*., 2017) as it only enables facile gene manipulation with only

80% transcriptional repression (Singh *et al.*, 2016), contrary to specialised transduction employed in earlier studies which made a permanent chromosomal deletion of *aftC* in *M. smegmatis* (Birch et al., 2008).

Biofilm analysis was also performed on *aftC* repressed *M. bovis* BCG. Similar to earlier studies, *aftC* repressed *M. bovis* BCG with compromised cell wall integrity failed to form pellicles in the liquid air interface (Recht and Kolter, 2001; Chen et al., 2006; Ojha *et al*., 2008, 2010; Pacheco et al., 2013; Sambandan *et al*., 2013; Wright et al., 2017; Yang *et al*., 2017).

All the biofilm analyses of *aftC* repressed *M. bovis* BCG were performed on pellicles grown at liquid – air interface. Although, pellicles are the widely used biofilm model, leukocyte lysate induced biofilm (Ackart *et al.* 2014a) and thiol reductive stress induced biofilm models (Trivedi *et al.,* 2016) were developed recently. Leukocyte lysate induced biofilm is an important model with a potential to mimic *in vivo* biofilm formation and has been used in the discovery of biofilm dispersing molecules which could improve the activity of first-line anti-TB drugs (Ackart *et al.* 2014b).

Environmental stress is a major inducer of biofilm formation. This could very well be true with the acidic, ROS filled environment within macrophages driving mycobacteria towards biofilm formation. Based on this, Kumar and others developed thiol reductive stress induced biofilm model where rapid biofilm formation is observed in response to reductive stress (Trivedi *et al.,* 2016). Using this model, they identified cellulose as an important component of the ECM (Trivedi *et al.,* 2016) which was then used as a biomarker to detect *in vivo* biofilm formation in *M. tuberculosis* infected mice, non-human primates and in lung tissue sections of TB patients (Chakraborty *et al*., 2021). Their observation that cellulose (with $\beta(1\rightarrow4)$ glycosidic linkages) as the primary polysaccharide in *M. smegmatis* and *M. tuberculosis* pellicles is contradictory to earlier understanding that α-glucan (with $\alpha(1\rightarrow4)$ glycosidic bonds) is the predominant polysaccharide in the ECM (Trivedi *et al.*, 2016). Their observation is supported by another group wherein overexpression of cellulase in *M. smegmatis* prevents it from biofilm formation (Wyk *et al*., 2017). However, neither of the studies performed any biochemical analyses, especially sugar linkage analysis would confirm the presence

of cellulose in mycobacterial ECM. Also, absence of genes encoding cellulose biosynthesis other than the presence of cellulase encoding genes raises doubts on the role of cellulose in mycobacterial biofilms (Trivedi *et al.*, 2016).

In this study of *aftC* repressed *M. bovis* BCG biofilms an overall reduction in the acidic polysaccharide level within biofilm matrix and presence of intermediary sized LAM similar planktonic cultures, was observed. Further sugar and linkage analysis would've delineated the composition and relative amounts of individual sugars within biofilm matrix. Alditol acetate derivatisation, TLC and GC analyses were attempted on carbohydrate mixture extracted from *aftC* repressed *M. bovis* BCG biofilms. However, these experiments could not be repeated to obtain meaningful conclusions from them (Appendix1 and 2). These analyses would improve our understanding of the effect of *aftC* repression on *M. bovis* BCG biofilm formation.

Along with polysaccharides, lipids are crucial in maintaining the ultrastructure of mycobacterial biofilms as they increase surface hydrophobicity facilitating cell-to-cell interaction in mycobacterial biofilms (Chakraborty and Kumar, 2019). Free mycolic acids, especially short chain mycolic acids (C_{56}-C_{68}) are abundant in biofilms along with GPL and MDAG (Recht and Kolter, 2001; Ojha *et al*., 2005; Pacheco et al., 2013; Yang *et al*., 2017; Wright et al., 2017). TDM is also crucial for biofilm formation as it facilitates accumulation of free mycolic acids *via* enzymatic hydrolysis (Ojha *et al*., 2010). Mycolic acid subtypes also effects biofilm formation as *M. tuberculosis* mutants defective of ketomycolic acids fail to form biofilms (Sambandan *et al*., 2013).

aftC repressed *M. bovis* BCG biofilms have a lipid profile contradictory to its planktonic counterpart. They have reduced cell wall bound mycolate levels contradictory to planktonic cultures, where an increase in the same was observed. Comparative planktonic and biofilm lipid analyses performed in other studies revealed accumulation of free mycolic acids as a hallmark of biofilm formation (Ojha *et al*., 2005, 2008, 2010; Sambandan *et al*., 2013; Vega-Dominguez *et al*., 2020; Dokic *et al*., 2021). Reduction in both α- and ketomycolates along with FAMEs in *aftC* repressed *M. bovis* BCG also contributes to defective biofilm

formation. The discrepancy between planktonic and biofilm lipid profiles is accounted for by the increase in biofilm mycolates in the control strain while the *aftC* repressed strain produced planktonic levels of mycolates even in biofilm growth conditions. Accumulation of TMM was also observed in *aftC* repressed *M. bovis* BCG, unlike TDM accumulation in the *M. smegmatis aftC* knockout (Birch *et al.*,2008). This accounts for the inability of cell wall mycolylation and accumulation of free mycolic acids in the cell wall associated fractions of *aftC* repressed *M. bovis* BCG biofilms.

eDNA is another crucial EPS in biofilm matrix which provides an attachment scaffold to microcolonies during various stages of biofilm formation (Tetz, Artemenko and Tetz, 2009; Cavaliere *et al*., 2014; Rose *et al*., 2015; Ibáñez de Aldecoa, Zafra and González-Pastor, 2017; Pakkulnan *et al*., 2019). Its role in maintaining strutctural integrity of biofilms was also observed in thiol-induced biofilms (Trivedi et al., 2016) and reduced drug tolerance of microcolonies was observed in leukocyte lysate induced biofilms upon DNase treatment (Ackart *et al.* 2014a). Proteins are also part of the mycobacterial ECM. Although there is limited information about them, their role in aggregation and adhesion has been shown in *M. tuberculosis* thiol reductive stress induced biofilms using proteinase K which dispersed the biofilm and prevented biofilm formation (Trivedi et al., 2016; Chakraborty and Kumar, 2019). Due to time limitations eDNA and proteins analysis were not performed on *aftC* repressed *M. bovis* BCG biofilms. To sum up, *aftC* repressed *M. bovis* BCG with altered LAM synthesis, aberrant mycolic acid profiles and a scarcity in excess polysaccharides and mycolic acids is unable to form mycobacterial pellicles.

During *M. tuberculosis* infection, mycobacteria within the granulomatous region can enter an extracellular region and persist with a biofilm like phenotype. Numerous reports suggest mycobacterial biofilm growth within the host due to the presence of antibiotic tolerant persisters and co-localisation of mycolic acids along the acellular rim of necrotising lesions (Lenaerts et al., 2007; Hoff et al., 2011; Basaraba and Ojha, 2017). A recent study also detected mycobacterial cells encapsulated in the cellulose matrix with a biofilm like phenotype in *M. tuberculosis* infected mice and rhesus macaques (Chakraborty *et al*., 2021). These reports

strongly suggest mycobacterial *in vivo* biofilm formation and emphasise the need to understand host pathogen interactions regarding biofilm like phenotypes.

There are very few reports of infection studies using biofilm like phenotypes. Most of our current understanding on the effect of biofilms on innate and adaptive immune responses is based on NTM infection studies. NTMs cause skin and soft tissue infections, but they majorly cause pulmonary infections especially in immunocompromised patients (Dokic *et al*., 2021; Weathered *et al*., 2022). Increasing evidence suggests the role of *M. avium* and *M. abscessus* in cystic fibrosis (Chakraborty and Kumar, 2019). *M. avium* biofilm infection is associated with premature macrophage apoptosis (Rose and Bermudez, 2014) and invasion of airway epithelial cells (Yamazaki, 2006). *M. avium* biofilms also effects macrophage phagocytosis which was otherwise uninterrupted in their planktonic cells (Dominici et al., 2008). This is particularly prevalent in mature biofilms (Rose and Bermudez, 2014) as their phenotypic precursors – microaggregates have been shown to increase phagocytosis (Keefe et al., 2021). Other than host pathogen interaction studies using NTMs there is a paucity in *M. tuberculosis* biofilm infection studies. With the growing evidence of *M. tuberculosis* - *in vivo* biofilm formation, there is a pressing need to study the innate and adaptive response to biofilm infections.

Due to time limitations only planktonic macrophage infections were performed using *aftC* repressed *M. bovis* BCG. AftC depleted *M. bovis* BCG has decreased infectivity and altered immunogenicity in THP1 cells. It induces higher inflammatory TNF-α and IL-6 and reduced anti-inflammatory IL-10 levels as compared to *M. bovis* BCG. This could be a consequence of intermediary sized LAM present on the cell envelope of *aftC* repressed *M. bovis* BCG. LAM is a crucial immunomodulator and an important PAMP imperative for the initial interaction between mycobacteria and innate immune cells (Birch *et al.*, 2010). C-type lectins are an essential pattern recognition receptor expressed on the surface of macrophages, dendritic cells and neutrophils, which recognise LAM through their carbohydrate recognition domains (Drickamer and Taylor, 2015; Schnaar, 2015). Reduced bacterial uptake as seen in *aftC* repressed *M. bovis* BCG is

contributed by the defective, shorter AftC-LAM which is unable to function as an efficient PAMP and activate pattern recognition receptors present on the surface of THP1 cells. Moreover, as it is intermediary sized with possibly reduced arabinan branching and mycolic acid attachment sites, AftC-LAM therefore has fewer mannose capping motifs (Birch *et al.*, 2008), which are also crucial for immunomodulation. Mannose caps on LAM are essential for endocytic pathways within innate immune cells, especially for the mannose receptor and DC-SIGN, which bind to mannose caps on LAM resulting in efficient internalisation of mycobacteria (Maeda *et al.*, 2003; Kang *et al.*, 2005). *aftC* repressed *M. bovis* BCG with AftC-LAM and potentially fewer mannose caps displays reduced bacterial uptake and intracellular survival in THP1 cells, along with increased TNF-α and IL-6 induction and reduced IL-10 levels. Induction of other crucial cytokines remains unclear as our infection assay was designed to identify cytokines produced by THP1 cells independent of other immune cells. Further studies involving animal models can shed light on the effect *aftC* repression in *M. bovis* BCG on innate and adaptive immunity and corroborate the increased immunogenicity of *aftC* repressed *M. bovis* BCG.

5.1.2 Application of LAM in active and passive protection against TB

LAM has a profound impact on innate immune response, due to which it is being tested for therapeutic purposes including antibody treatment and in the construction of vaccine candidates against TB (Correia-Neves *et al.*, 2019). It is the main carbohydrate antigen accounting for 15% of bacterial weight and is a major immunomodulator (Bhowruth *et al*., 2008; Birch *et al.*, 2014; Alderwick *et al.*, 2015). It is an important PAMP and is involved in the initial interaction of mycobacteria with PRR on phagocytes (Vergne, Gilleron and Nigou, 2015). As a result of this other than its impact on innate immune response, it effects T cells (LAM activates CD1b restricted T cells and induce IFN-γ) and humoral immune responses (LAM induces IL-10 in B cells through TLR2) (Correia-Neves *et al.*, 2019).

Anti-LAM antibodies are induced during both *M. tuberculosis* infection and after BCG vaccination (Correia-Neves *et al.*, 2019). In children with TB, inverse correlation was detected between disseminated

disease and anti-LAM antibodies suggesting their importance in limiting TB dissemination (Moreno *et al.*, 1992). Due to this, therapeutic application of several monoclonal antibodies against LAM are being tested in mice and other primates. Mice infected with *M. tuberculosis* exhibited lower bacterial loads, weight loss and prolonged survival following LAM antibody therapy (Hamasur *et al.*, 2004). Further, infected mice developed well organised pulmonary granulomas, with bacilli localised in the centre of granuloma (Teitelbaum *et al.*, 1998). Although, these studies suggested the role of antibodies in conferring protection by enhancing cellular immune response, they provide little information on the possible mechanism of protection (Teitelbaum *et al.*, 1998; Hamasur *et al.*, 2004). By understanding the innate immune response to LAM, the receptor signalling induced by it and crucial epitopes involved in this signalling, we can understand the mechanism of protection conferred by its antibodies (Figure 5.1). Our work on AftC depleted in *M. bovis* BCG, resulted in the generation of intermediary sized, potentially immunogenic LAM molecule. This molecule along with other derivatives of LAM can aid understanding this mechanism of protection and help in developing LAM based antibody therapy.

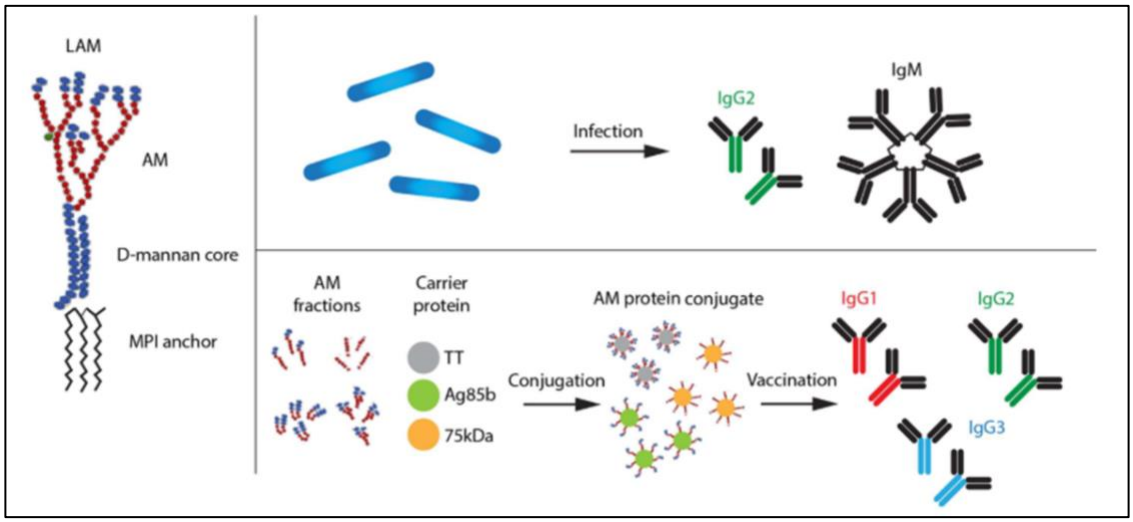

Figure 5.1: ***Application of LAM in antibody therapy and as a potential vaccine candidate in conjugation with Ag85*** *(Image extracted with permission from* (Correia-Neves *et al.*, 2019).

5.1.3 Applications in Vaccine development

BCG is the only available vaccine against TB which was first discovered more than 100 years ago (Davenne and McShane, 2016). It is now rendered ineffective in conferring protection against pulmonary TB in adults (Davenne and McShane, 2016). The possibility of using mycobacterial sub-cellular carbohydrate antigens as vaccine components is currently under study. Glycoconjugate vaccines have been licenced for *Haemophilus influenzae* type b (Hib), *Streptococcus pneumonia*, *Neisseria meningitidis* and *Salmonella typhi* (Correia-Neves *et al.*, 2019). Attempts are underway to develop similar vaccines for TB using LAM and its derivatives in conjugation with *M. tuberculosis* proteins antigen 85A (Ag85A) or ESAT-6 (Zhu *et al.*, 2018). Initial results in mice (Wang *et al.*, 2015) and rabbit models (Hamasur, Kallenius and Svenson, 1999) are encouraging with the induction of robust LAM specific antibodies that could confer partial protection against *M. tuberculosis* challenge. Various other subunit vaccines are under study such as MVA85A which delivered *M. tuberculosis* Ag85A using modified vaccinia virus Ankara (MVA) vector (Sable, Posey and Scriba, 2019). The major problem with this approach is vaccine efficacy and significant improvement over BCG (Tameris *et al*., 2013, Ndiaye *et al*., 2015). Use of multiple antigens can improve their efficacy and hence LAM and its derivatives are attractive candidates for subunit vaccine development.

Live *M. tuberculosis* deletion mutants are also under clinical study with defects in cell wall composition. MTBVAC is double deletion attenuated strain of *M. tuberculosis* with complete abolishment of PDIM biosynthesis and defects in ESX-1 system (Aguilo *et al.*,2017). It is currently in phase 2 clinical trials and shows promising results. Based on this cell wall mutants represent an attractive vaccine candidate with exposed/altered antigens on their cell envelope and potentially increased immunostimulatory properties (Aguilo *et al.*,2017; Sable, Posey and Scriba, 2019). Considering *aftC* repressed *M. bovis* BCG already has an RD1 deletion, it would be cleared within phagolysosomal compartments of macrophages and there might be a problem of it not being able to induce long lasting T cell mediated immunity. Recombinant BCG vaccines with cytosolic escape capability and increased immunogenicity can induce long lasting cellular

and humoral immune responses and can be safer in immunocompromised individuals (Groschel *et al.*, 2017).

5.2 Role of mycobacteria induced SOCS1 in immune evasion

5.2.1 Conclusions

SOCS1 was first discovered as a JAK binding protein (JAB) and later designated as STAT- induced STAT inhibitor-1 (SSI-1) (Narazaki *et al.*, 1998). It is a critical inhibitor of IFN-γ signalling preventing the deleterious effects of excessive inflammation mediated by JAK/STAT signalling (Yoshimura *et al.*, 2012). $SOCS1^{-/-}$ mice have multiple abnormalities, including growth retardation and reduced lymphocyte counts in the thymus, spleen and bone marrow and die within 2-3 weeks with liver necrosis and severe inflammation along with monocytic infiltration in the pancreas, heart and lungs (Starr *et al.*, 1998; Alexander *et al.*, 1999; Marine *et al.*, 1999; Kinjyo *et al.*, 2002; Davey, Heath and Starr, 2006). Neonatal death seen in $SOCS1^{-/-}$ mice is because of uncontrolled IFN-γ signalling, as $SOCS1^{-/-}$ IFN-$\gamma^{-/-}$ double knockout mice do not die as neonates (Alexander *et al.*, 1999). However, these mice are much more sensitive to bacterial infections (Kinjyo *et al.*, 2002).

During mycobacterial infection SOCS1 is highly upregulated. This mycobacteria induced SOCS1 is involved in IFN-γ suppression thereby promoting intracellular survival of mycobacteria (Carow *et al.*, 2011). This SOCS1 inhibition of STAT1 mediated responses during *M. tuberculosis* and *M. bovis* BCG infection were confirmed using $SOCS1^{-/-}$ mice, and it is shown to inhibit the phosphorylation and nuclear translocation of STAT1 disrupting JAK/STAT signalling (Carow *et al.*, 2011).

In this study, we attempted to generate a SOCS1 deficient macrophage cell line to study the inhibitory effect of SOCS1 on JAK/STAT signalling and establish the role of kinase inhibitory region of SOCS1 during *M.*

bovis BCG infection. For this, CRISPR/Cas9 was used to generate a SOCS1$^{-/-}$ macrophage cell line. We used two macrophage cell lines human monocytic cell line – THP1 and murine macrophage cell line – J774. However, this attempt was foiled by the intrinsic lethality of this deletion, and we switched to an SOCS1 overexpression system. In accordance with the earlier studies SOCS1 overexpression and immunoprecipitation revealed SOCS1 mediated inhibition of STAT1 phosphorylation during *M. bovis* BCG infection (Carow *et al.*, 2011). Now using the same system, the role of KIR during *M. bovis* BCG infection was explored using side directed mutagenesis. Point mutations were made in 6 consecutive conserved residues of KIR from histidine 54 to arginine 59 (His54, Phe55, Arg56, Thr57, Phe58, Arg59) along with a KIR deletion mutant to check SOCS1 mediated inhibition of STAT1 response in each. Consistent with the earlier *in vitro* analysis, all the 6 residues are crucial for SOCS1's interaction with STAT1 as they bind to the substrate binding grove of JAK1, preventing the phosphorylation of STAT1 (Liau *et al.*, 2018). This KIR mediated inhibition of JAK1 tyrosine kinase activity results in the inhibition of JAK/STAT signalling which is essential for mycobacterial clearence.

5.2.2 Applications in Host directed therapy

Host directed therapy is an emerging concept where the host immune response is modulated using small molecules including peptides to ensure better TB control (Kolloli and Subbian, 2017). This is a promising treatment strategy to combat MDR and XDR strains as well as co-infection with HIV/AIDS, while reducing the treatment duration (Kolloli and Subbian, 2017). Small molecules can be used for host directed therapies in conjugation with adjunct antibodies or antibiotics (Kolloli and Subbian, 2017). Currently there are multiple host-directed agents for TB that are under study. Some of them include (Kolloli and Subbian, 2017):

1) Targeting autophagy induction and vitamin D pathway to enhance intracellular bacterial killing,
2) Targeting granuloma structure to induce its disintegration that augments drug penetration and accessibility

3) Enhance cell mediated immune response (T cell response) resulting in increased phagosome maturation
4) Anti-*M. tuberculosis* antibody therapy using Anti-LAM monoclonal IgG3/IgA/IgM to ensure phagosome-lysosome fusion and phagocyte antigen presentation resulting in suppression of *M. tuberculosis* growth
5) SOCS1 mimetics and antagonists to regulate immune function (Figure 5.2)

SOCS1 mimetics and antagonists are recently developed small peptide molecules (about 20 amino acids) to control the expression level of JAKs similar to physiological regulation by SOCS1 (Ahmed, Larkin and Johnson, 2015). SOCS1 mimetics are based on the kinase inhibitory region of SOCS1 which bind to the activation loop or substrate binding groove of JAK1 or JAK2 to inhibit STAT1 mediated IFN-γ signalling (Yasukawa et al., 1999; Ahmed, Larkin and Johnson, 2015). This strategy controls excessive inflammation and tissue destruction preventing necrosis and uncontrolled *M. tuberculosis* dissemination (Ahmed, Larkin and Johnson, 2015). SOCS1 antagonists are conceptualised to enhance IFN-γ mediated immune response promoting mycobacterial clearance. For this identification of SOCS1-KIR binding site on JAK1 or JAK2 is crucial as antagonists are developed based on the activation loop and binding site on JAK1/JAK2 (Waiboci *et al.*, 2007). For JAK2, activation loop peptide which is 12 amino acids long are developed to increase IFN-γ and IL-6 biological activity by blocking SOCS1 function in cells (Waiboci *et al.*, 2007; Ahmed, Larkin and Johnson, 2015). Our research contributes to the development of SOCS1 mimetics and antagonists to advance host-directed TB therapy. The six residues within KIR region studied in this work are identified to be crucial for inhibition of JAK/STAT signalling during mycobacterial infection. This information can aid in development of SOCS-KIR antagonists from sequences similar to the activation loop of JAK1 and aid anti-tubercular therapies.

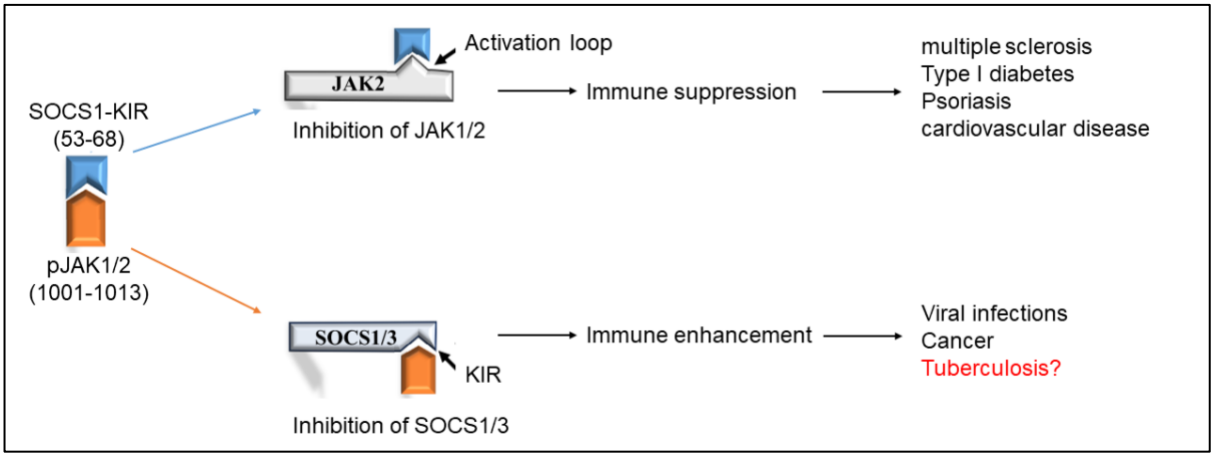

Figure 5.2: ***Application of SOCS1 mimetics and antagonists in host directed therapy****. Image adapted from* (Ahmed, Larkin and Johnson, 2015).

Chapter 6 : Materials and Methods

6.1 Homologous recombination mediated *aftC* (*Mb2692*) deletion in *M. bovis* BCG

6.1.1 Bacterial strains and growth conditions

E. coli Top10 was grown in Luria–Bertani broth (LB, Difco) at 37°C, 180 rpm, and supplemented with antibiotics where necessary (hygromycin 150 μg/ml; kanamycin 100 μg/ml). *M. smegmatis* mc^2 155 was grown in tryptic soy broth (TSB) or Middlebrook 7H9 supplemented with 0.05% (v/v) Tween-80 along with antibiotics where necessary (hygromycin 100 μg/ml; kanamycin 50 μg/ml). *M. bovis* BCG Pasteur was cultured statically in 7H9 broth at 37°C and supplemented 0.05% Tween-80, 10% oleic albumin dextrose catalase (OADC) growth supplement, and with antibiotics where necessary (hygromycin 100 μg/ml; kanamycin 50 μg/ml). All the strains used in this thesis are listed in Table 6.1

Table 6.1: Strains used in the generation of AftC knockout M. bovis BCG

Strain	Description	Source
E. coli MG1655	TOP10	Lab strain
E. coli K12	HB101	Lab strain
M. smegmatis mc^2 155	Parental wild type strain	Snapper et al., 2010
M. bovis BCG Pasteur	Parental wild type strain	
M. bovis BCG::pTIC6-Mb2692	Merodiploid strain containing pTIC6-Mb2692	This work
M. bovis BCGΔMb2692:: pTIC6-Mb2692	Conditional mutants in which genomic Mb2692 is replaced by *hyg* cassette by conditional expression of pTIC6-Mb2692	This work

6.1.2 DNA extraction

6.1.2.1 Genomic DNA extraction from mycobacterial cells

Bacterial cultures (10 ml) were centrifuged at 4000 x *g* for 15 minutes and the cell pellet re-suspended in 200 µl of Tris – EDTA buffer (pH 8.0). Lysozyme (50 µl, 10 mg/ml) was also added to the suspension and incubated at 37°C overnight. SDS (100 µl, 10% w/v) and 50 µl of proteinase K (20 mg/ml) were added and incubated at 55°C for 30 minutes. NaCl (200 µl, 5M) was added and further incubated at 65°C for 15 minutes. Chloroform (500 µl) was added and vortexed for 10 seconds. The suspension was then centrifuged at 11000 x *g* for 5 min and the upper aqueous phase transferred to a fresh tube. To precipitate the DNA, 0.7 volumes of isopropanol was added and centrifuged at 11000 x *g* for 10 minutes. The supernatant was carefully discarded, and the DNA pellet was washed with 500 µl of 70% ethanol at 11000 x *g* for 10 minutes. The pellet was air dried and resuspended in 45 µl EB (10 mM Tris-HCl, pH 8.5) buffer and 5 µl of RNaseA (10 mg/ml).

6.1.2.2 Plasmid DNA extraction

Plasmid extraction was carried out using QIAGEN QIAprep spin kits. Colonies from the transformant plates were used to inoculate 5 ml of LB broth supplemented with appropriate antibiotics and grown overnight at 37°C and shaking at 180 rpm. Bacterial cells were harvested by centrifugation and plasmids were extracted according to manufacturer's protocol. Plasmids were confirmed by restriction digestion and sequencing (Source BioScience). All plasmids and phages used in the study are listed in in Table 6.2

Table 6.2: List of phages and plasmids used in generation of AftC knockout M. bovis BCG

Plasmid	Derivative	Description	Reference
p0004s		Cosmid vector containing λ phage cis site and a HygR cassette (hyg); used in the cloning of allelic exchange constructs to be used for specialised transduction	Bardarov S et al., 2002
	p∆*Mb2692*	p0004s derivative designed for allelic exchange of *M. bovis* Mb2692	This work
pTIC6		Integrative, single copy plasmid for replication in *E coli*, with a KanR cassette and tetracycline inducible promoter	Glover et al., 2007
	pTIC6-*Mb2692*	Mb2692 cloned into pTIC6	This work
Phage	**Derivative**	**Description**	**Source**
phAE159		Temperature sensitive – conditionally replicating mycobacteriophage TM4 derived shuttle phasmid	Bardarov S et al., 2002
	ph∆*Mb2692*	phAE159 derivative containing p∆*Mb2692* in its *PacI* site	This work

6.1.3 Polymerase chain reaction

PCR was carried out using the Q5 High-Fidelity DNA polymerase (NEB) using the master mix listed in Table 6.3. Conditions used for the reaction are described in the Table 6.4. All primers used in this thesis are listed in Table 6.5.

Table 6.3: PCR master mix for amplification of genomic DNA using Q5 High-Fidelity DNA Polymerase

5X Q5 Reaction buffer	5 µl
10mM dNTPs	0.5 µl
10µM Forwards Primer	1.25 µl
10µM Reverse Primer	1.25 µl
Template DNA	X µl (100 ng)
Q5 High-Fidelity DNA Polymerase	0.25 µl
5X Q5 High GC Enhancer	5 µl
Water	X µl (to 25µl)
Total	**25 µl**

Table 6.4: Thermal cycler conditions for PCR using Q5 DNA Polymerase

Step	**Temperature**	**Time**	**Passes**
Initial denaturation	98°C	1 minute	1
Denaturation	98°C	10 seconds	35
Annealing	50-72°C	30 seconds	35
Extension	72°C	30 seconds/kb	35
Final Extension	72°C	2 minutes	1
Hold	4°C	∞	1

Table 6.5: Primers used in generation of aftC knockout M. bovis BCG

Primer	Sequence (5' - 3')
Mb2692_LL	TTTTTTTTCCATAAATTGGCGCCAGACTGATCCTCGACT
Mb2692_LR	TTTTTTTTCCATTTCTTGGTTGAAATCGTCGGTGATGTT
Mb2692_RL	TTTTTTTTCCATAGATTGGTGGATCGCTGGCTGCTGTTC
Mb2692_RR	TTTTTTTTCCATCTTTTGGCGTCGAGGCCCTAGAGCTGA
HL	AGGCAGGACCTGCCAAT
HR	CTTCACCGATCCGGAGGAAC
OL	CGGCCGATAATACGACTCA
OR	CTGACGCTCAGTCGAACGAA
Mb2692_Comp_F	GATCGATCAAGCTTGTGTACGGTGCGCTGGTGACGGCAGCT
Mb2692_Comp_R	GATCGATCGAATTCTCACCGCTGGCCCTCCCGCTCGGGCGT
pTIC6-F	CAGCACGGCATACATCATTT
pTIC6-R	TTGAGACACAACGTGGCTTT
Mb2692_KO_F	CACTTTGACCGCGACGAGAT
Mb2692_KO_R	CGCGGAGACACCGTTTTTCA

6.1.4 Restriction digestion

Plasmids and PCR products were digested using the master mix listed in Table 6.6 at 37°C for 2 hours.

Table 6.6: Restriction digestion master mix

DNA	1 µg
Restriction Enzyme (NEB)	1 µl
Cutsmart Buffer (NEB)	3 µl
Water	X µl
Total	**30 µl**

6.1.5 Agarose gel Electrophoresis

0.8 – 1% agarose gels were prepared using Molecular Biology Grade Agarose (Bioline) dissolved in 1X Tris-acetate EDTA (TAE) buffer (Life Science Products). The mixture was heated to dissolve agarose into the solution and cooled sufficiently before adding 0.1µl/ml Midori Green DNA stain (ThermoFisher). The mixture was then poured into a cast to set the gel along with a comb to create wells for loading. Once set, the gel was completely immersed in 1X TAE buffer in an electrophoresis tank. DNA samples were mixed with 1X loading dye (NEB) and ran alongside a 1 kb or 100 bp DNA ladder (NEB) at 100-140 V, 400 mA, until the dye front had migrated sufficiently for adequate DNA separation. DNA was visualised using an ultraviolet (UV) transilluminator.

6.1.6 DNA extraction from agarose gel

DNA was extracted from agarose gel using QIAgen Gel Extraction Kit (Qiagen) according to manufacturer's protocol.

6.1.7 Ligation

Digested and purified PCR products and plasmids were quantified using a Nanodrop Spectrophotometer (ThermoFisher) and ligated using the mastermix listed in Table 6.7 either at room temperature for 3-4 hours or overnight at 4°C.

Table 6.7: Ligation mastermix

Plasmid	50 ng
PCR product	37.5 ng
T4 DNA ligase (NEB)	1 µl
T4 DNA Ligase buffer (NEB)	2 µl
Water	X µl
Total	**20 µl**

6.1.8 Preparation of competent cells

6.1.8.1 *E. coli* chemically competent cells

LB broth (5 ml) was inoculated from a glycerol stock and grown overnight at 37°C, 180 rpm. This starter culture was used to inoculate 50 ml of LB broth supplemented with 20 mM $MgSO_4$. Once the OD_{600} measured between 0.5 - 1.0, cells were pelleted at 4000 x *g* for 15 minutes, resuspended in 20 ml of ice-cold transformation buffer 1 (15% glycerol, 30 mM CH_3CO_2K, 10 mM $CaCl_2$, 50 mM $MnCl_2$, 100 mM RbCl, pH 5.8; filter sterilised and stored at 4°C) and incubated on ice for 40 minutes. Cells were pelleted at 4000 x *g* for 15 minutes, resuspended in 2 ml of transformation buffer 2 (15% glycerol, 75 mM $CaCl_2$, 10 mM MOPS, 100 mM RbCl, pH 6.5; filter sterilised and stored at 4°C) and incubated on ice for 2 hours. Cells were aliquoted into 100 µl suspensions, snap frozen and stored at -80°C until further use.

6.1.8.2 Mycobacterial electrocompetent cells

A starter culture (5 ml) of the required mycobacterial strain grown from a glycerol stock was used to inoculate a 50 ml culture grown until an OD_{600} was 0.8 - 1.0. The cell suspension was incubated on ice for 1.5 hours and centrifuged at 4000 x *g* for 15 minutes. *M. bovis* BCG was centrifuged at room temperature and *M. smegmatis* was centrifuged at 4°C to enhance transformation efficiency. Pelleted cells were

successively washed with 50 ml, 25 ml, 12 ml, and 5 ml of 10% glycerol. Cells were finally resuspended in 1 ml of 10% glycerol, aliquoted into 200 µl suspensions, snap frozen and stored at -80°C until further use.

6.1.9 Transformation of bacterial cells

6.1.9.1 Transformation of chemically competent *E. coli* by heat shock method

Chemically competent *E.coli* (100 µl) was mixed with 5 µl of ligation product or purified plasmid DNA and incubated on ice for 30 minutes. Cells were transferred into a water bath at 42°C for 45 seconds and incubated on ice for 5 minutes. Transformed cells were recovered in 1 ml LB broth at 37°C, 180 rpm for 1 hour. Cells were pelleted and plated onto LB agar supplemented with appropriate antibiotics and grown at 37°C for overnight until the transformant colonies were visible.

6.1.9.2 Transformation of competent mycobacterial cells by electroporation

Electrocompetent mycobacterial cell suspension (200 µl) was mixed with 5 µl (100 ng/µl) of plasmid DNA in a 1 mm electroporation cuvette (Cell Projects). *M. smegmatis* electroporation cuvette was pre-chilled, and the mixture was incubated on ice for 5 minutes, for *M. bovis* BCG the mixture was incubated at room temperature without pre-chilling the cuvettes to enhance transformation efficiency. Electroporation was carried out at 1800 V and cells were allowed to stand for 15 minutes (on ice for *M. smegmatis* and at room temperature for *M. bovis* BCG). Cells were recovered in 1 ml of media (TSB broth for *M. smegmatis* and 7H9 broth for *M. bovis* BCG) at 37°C for one generation time (3-4 hours for *M. smegmatis* and 24 hours for *M. bovis* BCG) and subsequently plated on agar supplemented with appropriate antibiotics (TSB agar for *M. smegmatis* and Middlebrook 7H11 agar for *M. bovis* BCG). Plates were incubated at 37°C until the transformant colonies were visible.

6.1.10 Generation of mycobacterial gene knockout strain

6.1.10.1 Construction of allelic exchange substrate (AES)

A 1k up- and down-stream of region of interest (*Mb2692*) were PCR amplified (**6.1.3**) from wild type *M. bovis* BCG using primers - Mb2692_LL, Mb2692_LR, Mb2692_RL, Mb2692_RR listed in the Table 6.5 inserting a Van91I recognition site at their 5' ends. Digested PCR products (**6.1.4**) were cloned into the Van91I digested p0004s vector (**6.1.7**). Ligation products were transformed into chemically competent *E coli* TOP 10 cells and plated onto LB agar plates supplemented with 150 µg/ml hygromycin and incubated at 37°C, overnight (**6.1.9**). Colonies were screened for recombinant plasmid by Van91I restriction digestion and sequencing using the primers HL, HR, OL, OR (Table 6.5).

6.1.10.2 Phasmid construction

Sequence confirmed AES plasmid was linearised by PacI digestion alongside the temperature sensitive mycobacteriophage vector phAE159 DNA. Approximately, 2-4 µl of phage digest and 4-6 µl of AES digest were ligated together in a ligation reaction of 10 µl total volume. The ligation mixture of 5 µl was added directly to the MaxPlax packaging extract tube and incubated at room temperature for 90 minutes. The reaction was stopped by the addition of 200 µl mycobacteriophage (MP) buffer (50 mM Tris-HCl pH 7.6, 150 mM NaCl, 10 mM $MgCl_2$, 2 mM $CaCl_2$; filter sterilised and stored at room temperature), followed by further incubation at room temperature for 30 minutes. *E coli* HB101 cell suspension (100 µl) was added to the packaging reaction tube and incubated for 1 hour at 37°C. Cells were harvested at 11000 x *g* for 1 min and supernatant was discarded. The cell pellet was re-suspended in fresh LB broth and plated onto LB agar plates supplemented with 150 µg/ml of hygromycin, and incubated at 37°C, overnight. Hygromycin resistant colonies were screened for potential phasmid by PacI digestion and separated by agarose gel electrophoresis (**6.1.5**) to visualise two bands of approximate length 40 kb (phage genomic DNA) and 7 kb (corresponding to linearized AES).

E coli HB101 cells were prepared for the previously described transduction from a 50 ml LB broth supplemented with 10 mM $MgSO_4$ and 0.2% maltose, inoculated with 0.1 ml of overnight fresh starter culture. Cells were grown at 37°C, shaking at 200 rpm until OD_{600} reached 0.8 – 1.0, pelleted at 3000 *xg* for 10 minutes and re-suspended in 300 µl MP buffer.

6.1.10.3 Generation of knockout phage

Phasmid DNA (5-10 µl) was electroporated into 200 µl of electrocompetent *M smegmatis* mc^2155 cells. Cells were recovered in 1 ml TSB broth for 1 hour at 30°C. The following dilutions were setup

Dilution 1 – 300 µl of transformed *M smegmatis* mc^2155 cells were added to 200 µl actively growing *M smegmatis* mc^2155 culture.

Dilution 2 – 100 µl of transformed *M smegmatis* mc^2155 cells were added to 200-300 µl actively growing *M smegmatis* mc^2155 culture.

Dilutions 1 and 2 were added separately onto 4 ml of molten top agar at 50°C in a snap cap tube, mixed by inversion and poured onto a pre-warmed 7H9 basal agar plate. Plates were incubated at 30°C for 3 days until plaques were observed. The plaques formed were cored and soaked in 200 µl MP buffer for 90 minutes at room temperature to recover the phage.

6.1.10.4 Preparation of high titre phage lysate

The 7H9 basal agar plates were overlaid with 4 ml of top agar containing 400 µl of actively growing *M smegmatis* mc^2155 culture. 10-fold serial dilutions of the phage lysate were prepared in MP buffer to 10^{-6} and 10 µl was spotted onto the overlaid plate. Plates were incubated at 30°C for 3 days until plaques were observed. The plaque forming units (PFU) of the phage lysate was calculated using the zones that contained individual plaques. The 7H9 basal agar plate was overlaid with 400 µl of actively growing *M smegmatis* mc^2155 culture mixed with appropriate dilution of the phage lysate which would result in approximately

1000 plaques per overlaid plate. Plates were incubated at 30°C for 3 days until plaques were observed. The plates were soaked with 3-4 ml MP buffer at room temperature for 3-4 hours to recover high titre phage lysate, which was then filter sterilised using 0.22 µm filter to remove bacterial debris and stored at 4°C until further use. Ideal titre for transduction would produce a characteristic lacy pattern and have approximately 10^{10} PFU per ml.

6.1.10.5 Specialised transduction

7H9 broth (50 ml) supplemented with 0.2% glycerol, 10% OADC and 0.05% Tween 80 was inoculated with *M bovis* BCG for specialised transduction and grown to an OD_{600} of 0.8-1.0 at 37°C. Cells were pelleted at 4000 x *g* for 15 minutes and washed twice in 50 ml MP buffer before final resuspension in 5 ml MP buffer. A 2 ml of the cell suspension was mixed with 2 ml of high titre knockout phage lysate and incubated at 37°C (non-permissive temperature for phage replication) for 3-4 hours to allow phage infection and transduction of AES. A negative control of 2 ml of the cell suspension was mixed with 2 ml MP buffer. Following transduction, cells were pelleted and recovered overnight at 37°C in 3 ml 7H9 supplemented with 0.2% glycerol, 10% OADC and 0.05% tween80. The cell suspension was pelleted at 4000 x *g* for 15 minutes and plated onto 7H11 agar plates supplemented with 10% OADC and 100 µg/ml hygromycin and incubated at 37°C until transductant colonies were visible. Colonies were verified by confirmatory PCR and whole genome sequencing (performed by Microbes NG).

6.1.10.6 Merodiploid strain generation

Genomic DNA was extracted from wild type *M. bovis* BCG (**6.1.2**) was used as a template to PCR amplify *Mb2692* (**6.1.3**) using the primers Mb2692_Comp_F and Mb2692_Comp_R. HindIII and EcoRI restriction sites were inserted at their 5' ends (Table 6.5). Digested PCR product (**6.1.4**) was cloned into HindIII and EcoRI digested pTIC6 vector downstream of the tetracycline promoter to generate the single copy integrating construct pTIC6-*aftC* which was confirmed by colony PCR. The merodiploid strain was

generated by electroporating (**6.1.9**) wild type *M. bovis* BCG with pTIC6-Mb2692 and selecting for kanamycin resistant colonies upon incubation at 37°C on 7H11 agar plates supplemented with 10% OADC and 50 µg/ml kanamycin.

6.1.10.7 Conditionally expressed specialised transduction essentiality test (CESTET)

Specialised transduction was performed as described earlier (**6.1.10.5**) using the merodiploid strain generated containing the single copy integrating construct pTIC6-Mb2692. Transduced cells were plated onto 7H11 agar plates supplemented with 10% OADC, 100 µg/ml hygromycin, 50 µg/ml kanamycin and 0.1 µg/ml ATc and incubated at 37°C until transductant colonies were visible. Colonies were verified by confirmatory PCR and whole genome sequencing (**6.1.10.8**).

6.1.10.8 Confirmation of deletion strains

Confirmatory PCR

Genomic DNA was extracted from the knockout strain (**6.1.2**) and was used as a template for confirmatory PCR reaction. Two PCR reactions were carried out, one using the primers Mb2692_KO_F and HL, and the other PCR reaction using HR and Mb2692_KO_R (Table 6.5). PCR master mix and reaction conditions were as listed in Table 6.3 and Table 6.4.

Whole genome sequencing

Whole Genome sequencing was performed by Microbes NG (http://www.microbesng.uk), which is supported by the Postgraduate Research Scholarship Fund (Grant Number GAM2666).

6.1.10.9 Conditional depletion of *aftC*

M. bovis BCGΔMb2692:: pTIC6-Mb2692 was grown in 7H9 broth supplemented with 10% OADC, 100 µg/ml hygromycin, 50 µg/ml kanamycin and 0.1 µg/ml ATc to an OD_{600} of 0.3. Cells were washed twice with media to remove traces of ATc and resuspended in original volume of media. Culture was used as 20% inoculum in 7H9 broth without ATc to deplete intracellular AftC. The depleted sub-culture was used an inoculum for cultures with or without 0.1 µg/ml ATc.

6.2 CRISPR interference mediated transcriptional repression of *aftC (Mb2692)* in *M. bovis* BCG

6.2.1 Construction of CRISPR interference mediated transcriptionally repressed strains of *M. bovis* BCG

Catalytically inactive or deactive Cas9 (*dCas9*) and single guide RNA (sgRNA) were introduced into *M. bovis* BCG using two different TetR regulated plasmids pRH2502 and pRH2521 (Table 6.8). Designing and cloning sgRNA into pRH2521 was done as described in Singh *et al*. (2016).

Table 6.8: Plasmids used in CRISPR interference mediated transcriptional repression of aftC

Plasmid	Derivative	Description	Reference
pRH2502		Vector with a kanamycin resistance marker expressing an enzymatically inactive version of *Streptococcus pyogenes cas9* with mutations at codon 10 (Asp to Ala) and codon 820 (His to Ala) from a TetR-regulated uvtetO promoter	(Singh *et al.*, 2016)
pRH2521		Vector with a hygromycin resistance marker in which the sgRNA is expressed from a TetR-regulated smyc promoter (P_{myc1}tetO)	(Singh *et al.*, 2016)
	pRH2521-sgRNA1	pRH2521 containing sgRNA1 cloned under TetR-regulated smyc promoter (P_{myc1}tetO)	This work
	pRH2521-sgRNA2	pRH2521 containing sgRNA2 cloned under TetR-regulated smyc promoter (P_{myc1}tetO)	This work
	pRHS2521-sgRNA3	pRH2521 containing sgRNA3 cloned under TetR-regulated smyc promoter (P_{myc1}tetO)	This work

Three sets of oligonucleotides (labelled as sgRNA1, 2, 3) with least off target effects and a PAM sequence (5'-NGG-3') on the 3' end of the non-template strand were designed to target *Mb2692* at positions +113,

+143 and +336 of *M. bovis* BCG (Table 6.9). Oligonucleotides were inserted with overhangs complementary to the Bbs1 restriction site of pRH2521. Cloning was carried out according to the protocol from Zhang lab (Ran *et al.*, 2013). Refer to 6.3.3.2 for detailed method.

Plasmids were confirmed by sequencing using KS primer (Table 6.9).

Table 6.9: Oligonucleotides used in transcriptional repression of Mb2692

Primer	**Sequence (5' - 3')**
sgRNA1 – A	GGGATATAGATGTCCCATCCGCGC
sgRNA1 – B	AAACGCGCGGATGGGACATCTATA
sgRNA2 – A	GGGACGGGGGGATACAGGTAGTGC
sgRNA2 – B	AAACGCACTACCTGTATCCCCCCG
sgRNA3 – A	GGGAGGGTGCCACCGGGGGGATAC
sgRNA3 – B	AAACGTATCCCCCCGGTGGCACCC
KS primer	CCTCGAGGTCGACGGTATCG
Mb2692 – F	GCCGGTCTACCGCGCGGTGCTG
Mb2692 – R	GTGAACACCAGCGTGTTGGTCACGGTC
SigA – F	TACGACCAGCACCATCCCGAAAAGGAAG
SigA – R	TCTTCGTCGTCGCCCGAGTCGAGGTC

pRH2502 expressing dCas9 regulated by TetR uvtetO promoter with kanamycin selectable marker was electroporated into *M. bovis* BCG along with either one of the pRH2521-sgRNA clones harbouring hygromycin selectable marker at 2.5kV in 1 mm gap electroporation cuvettes (**6.1.9.2**). Electroporated cells were recovered overnight in 3 ml of 7H9- 10% OADC- 0.05% Tween 80 and plated onto 7H11 agar plates supplemented with 10% OADC, 25 µg/ml kanamycin and 50 µg/ml hygromycin and incubated at 37°C for 4 weeks.

6.2.2 Growth kinetics of transformant BCG strains

Mycobacterial strains expressing *dCas9* and sgRNA (Table 6.10) isolated from 7H11-OADC-antibiotic plates were grown both in the presence and absence of ATc in 7H9 - 10% OADC - 0.05% Tween 80 -

antibiotics (25 µg/ml kanamycin and 50 µg/ml hygromycin) medium. ATc was supplemented every 48 hours to maintain the expression of dCas9 and sgRNA and the cultures were grown for 8-10 days. Absorbance at 600nm was measured in every 24 hours in monitor the growth kinetics of individual strains upon transcriptional repression of *Mb2692.*

Table 6.10: Strains used in CRISPR interference mediated transcriptional repression of Mb2692

Strain	**Description**	**Source**
BCG-VC	*M. bovis* BCG transformed with pRH2502 and pRH2521	This work
BCG-sgRNA1	*M. bovis* BCG transformed with pRH2502 and pRH2521-sgRNA1	This work
BCG-sgRNA2	*M. bovis* BCG transformed with pRH2502 and pRH2521-sgRNA2	This work
BCG-sgRNA3	*M. bovis* BCG transformed with pRH2502 and pRH2521-sgRNA3	This work

6.2.3 RNA extraction and RT-PCR

M. bovis BCG strains were grown as described above in the presence or absence of ATc (**6.2.2**). A bacterial culture (10 ml) was centrifuged at 4000 x *g* for 10 min to collect the bacterial pellet. The cell pellet was resuspended in 600 µl of freshly prepared 5mg/ml lysozyme and supplemented with 10 µl of β-mercaptoethanol. The mycobacterial cell wall was digested using glass beads in a bead beater using the pre-programmed '*M. tuberculosis'* settings (2 cycles of 45s each at 6.5 m/s). 90 µl of 0.3 M sodium acetate (pH 5.2) was added to the cell lysate followed by the addition of 600 µl of acidic phenol. Samples were thoroughly mixed by inverting the tube (about 60 times) and incubated at 65°C for 5 min. The upper aqueous phase was separated by centrifuging at 17000 x *g* for 5 min and was transferred into a new RNase free tube where the phenol treatment was repeated. The resulting mixture of nucleic acids was cleaned with an equal

volume (600 µl) of chloroform: isoamyl alcohol (24:1) and transferred into a new tube. The nucleic acid mixture was incubated with 90 µl of 0.3 M sodium acetate (pH 5.2) and 900 µl of 100% ethanol overnight at -20 °C to precipitate RNA. The supernatant was decanted and the RNA extract was further cleaned using 500 µl of 70% ethanol, air dried, resuspended in DEPC treated RNase free water and quantified using a Nanodrop.

To remove contaminating DNA, rigorous DNase treatment was performed using the TURBO DNase Enzyme (ThermoFisher) according to manufacturer's instructions, and its complete removal was confirmed by PCR (Table 6.3). The concentration and purity of extracted RNA was analysed using Abs_{260}/Abs_{280} readings on a Nanodrop spectrophotometer. Total RNA obtained was used for cDNA synthesis. SuperScript™ III First-Strand Synthesis System (ThermoFisher) was used according to manufacturer's instructions for cDNA synthesis using 2 µg RNA and 2 pmol of gene specific reverse primer of AftC and the housekeeping gene, SigA. 2 µg RNA, 2 pmol primer, 1 µl dNTP mix was made up to 13 µl using deionised water and heated at 65°C for 5 min. Further to this mixture, 4 µl of 5X first-strand buffer, 1 µl of 0.1M DTT and 2 µl of Superscript™ III RT were added and incubated at 50°C for 1 hour. The reaction was terminated at the end of 1 hour by incubating at 70°C for 15 minutes. RNA complementary to the cDNA produced was removed by incubating with RNaseA at 37°C for 20 minutes. For semi-quantitative estimation of Mb2692 transcripts in the total RNA, PCR was performed using Mb2692 – F and Mb-2692 – R (Table 6.9) primer pair and standardised against the expression of housekeeping gene sigA (SigA –F and SigA – R; Table 6.9) in a thermal cycler (Fisher Scientific - Eppendorf Master cycler Nexus GX2e) using the conditions listed in Table 6.11.

Table 6.11: PCR conditions for semi quantitative estimation of Mb2692 transcripts

Step	Temperature	Time	Passes
Initial denaturation	98°C	3 minute	1
Denaturation	98°C	10 seconds	30
Annealing	70.0°C (*aftC)*	15 seconds	30
	69.1°C (*sigA)*		
Extension	72°C	30 seconds	30
Final Extension	72°C	3 minutes	1

6.2.4 Microscopy

M. bovis BCG strains in which *Mb2692* is repressed were grown to exponential log phase (OD_{600} of 0.4 – 0.6), washed thrice with 500 µl of 1X PBS containing 0.05% Tween 80 and resuspended in 100 µl of PBS with 0.5% Tween 80. A 1% agarose made in dH_2O (500 µl per slide) was used to coat microscopy slides and immobilise bacteria for visualisation. Coverslips were sealed using clear nail polish. Cell morphology was visualised using Leica DMRE Widefield Microscope equipped with a 63x/1.25 HC plan Apo objective (oil immersion). Photographs were collected by USB Colour CCD Photometrics MP6 (6 megapixel) camera with standard RBG filter. Cell length was measured using ImageJ – Fiji software. To enumerate the reduction of cell length, the length of 100 different bacilli from each strain were measured using ImageJ-Fiji software and the results were plotted using Graphpad Prism 9.0.1. To analyse the statistical significance between individual groups non-parametric t-test was performed between individual groups with Welch's correction (without the assumption that they have equal standard deviation).

6.2.5 Biofilm growth condition, crystal violet and alcian blue staining

M. bovis BCG biofilms were grown in Sauton's media supplemented with 50 µg/ml of kanamycin and 50 µg/ml of hygromycin in 12 well plates at 37°C and 5% CO_2 for 5 weeks with 1x PBS along the walls to minimise the effect of evaporation. ATc at 200 ng/ml was added carefully along the walls once every 48 hours to maintain CRISPRi induced AftC knock down. Each biofilm assay was performed using 4 biological replicates and 3 technical repeats were performed.

Once biofilms were matured, photographs were captured using a Canon EOS R f/2.8 camera. Biofilm biomass was quantified using crystal violet assay (Chen et al., 2020). Biofilms were dried and incubated with 500 µl of 0.5% (w/v) crystal violet (Sigma Aldrich) at room temperature for 10 minutes. Wells were washed thrice with 500 µl of water and biofilms were air dried. Biofilms were de-stained by 500 µl of 95% (v/v) ethanol and stain retention was quantified by absorbance at 400 nm in BMG PHERAstar FS microtiter plate reader.

Polysaccharide content within the biofilm matrix was quantified using alcian blue staining assay (Rose, Babrak and Bermudez, 2015). Dried biofilms were stained with 500 µl of 1% (w/v) alcian blue 8G in acetic acid pH 2.5 (Sigma Aldrich) for 20 minutes at room temperature, washed in 500 µl of water and air dried. The alcian blue from the biofilms was de-stained into 500 µl of 33% (v/v) acetic acid and stain retention was quantified using absorbance at 410 nm in BMG PHERAstar FS microtiter plate reader.

6.2.6 Extraction of Carbohydrates

Planktonic culture (10 ml) and pellicles were grown in 6 well plates of 3 ml of each were used for carbohydrate extraction (**6.2.2** and **6.2.5**). Bacteria was pelleted at 4000 x *g* for 10 minutes, washed twice in original volume of 1x PBS and transferred into a glass tube. Pellets were resuspended in 3 ml of 50% ethanol and heated at 90°C for 3 hours. The supernatant containing carbohydrates were collected by centrifugation at 3000 x *g* for 10 minutes, transferred into a fresh tube and dried at 50°C under N_2. The

ethanol reflux was repeated to ensure the extraction of the residual carbohydrates in the biomass. A 1 ml of 2 mg/ml proteinase K prepared in 10 mM Tris (PH 7.5), 20 mM $CaCl_2$, 50% glycerol was added to the dried extract incubated at 37°C for 48 hours to ensure complete digestion of proteins in the carbohydrate extract. This was followed by dialysis against endotoxin free water using Pur-a-lyser dialysis kit (MWCO 3.5kDa) for 48 hours. The dialysed material was collected into a fresh tube, dried and resuspended in deionised water with 1% azide to a final concentration of 100 mg/ml.

6.2.7 Silver staining of extracted carbohydrates

Mycobacterial carbohydrates extracted as above, were separated in a 15% SDS-PAGE gel by electrophoresis at 200V, 50mA for 75 minutes and stained by a series of solvents: 1) 50% v/v CH_3OH, 12% w/v TCA, 2% w/v $CuCl_2$ (120 min); 2) 10% v/v C_2H_5OH, 5% v/v CH_3COOH (10 minutes); 3) 0.7% w/v periodic acid, 40% v/v C_2H_5OH, 5% v/v CH_3COOH (10 minutes); 4) 10% v/v C_2H_5OH (10 minutes); 5) deionised water (20 minutes); 6) 0.1% w/v $AgNO_3$ (10 minutes); 7) 10% w/v K_2CO_3 (5 minutes); 8) 2% w/v K_2CO_3 (overnight). Stained gel was visualised by Bio-Rad Gel doc imaging systems.

6.2.8 Western blotting

Mycobacterial carbohydrates were separated in a 15% SDS-PAGE gel by electrophoresis at 200V, 50mA for 1 hour. Separated carbohydrates were transferred onto a nitrocellulose membrane in Tris/glycine transfer buffer (25mM, 192mM, and 10 % (v/v) methanol) at 25V, 300mA for 1.5 hours, and blocked for 1 hour in 5% skim milk in Tris-buffered saline –Tween buffer (20 mM Tris, 150 mM NaCl, and 0.1 % (w/v) Tween 20). The blot was probed with mouse mycobacterial anti-LAM primary antibody - CS-35 (1:1000) overnight at 4°C, followed by a couple of TBST washes and secondary antibody probing with anti-mouse Alexa Fluor™ 633 (Invitrogen) (1 :15000) at room temperature for 2 hours. Blot were visualised using LICOR/Odyssey Western blot imaging system.

6.2.9 Lipid extraction and analysis

Post carbohydrate extraction, the bacterial pellet was used for the extraction of cell wall associated lipids. Chloroform: methanol: water (10:10:3; 2 ml) was added to the pellet and heated at 50°C for 3 hours. The supernatant containing lipids were collected by centrifugation at 3000 x *g* for 10 minutes and transferred into a new tube. The 10:10:3 extraction was repeated to ensure the complete extraction of cell wall associated lipids. Lipids were separated from residual cell debris by mixing for 10 minutes with 1.75 ml chloroform and 0.75 ml water. In this mixture, lipids separate into chloroform and debris into water. To further clean them, lipids were washed three times with 2ml of chloroform: methanol: water (3:47:48) and the clean lipids were collected by centrifugation into a fresh pre-weighed tube and concentrated. They were made up to 100 mg/ml in chloroform: methanol (2:1), spotted onto a silica plate and analysed by thin layer chromatography (TLC, Table 6.12).

The bacterial cell pellet was further used for the extraction of cell wall bound lipids – FAMES and MAMES. The cell pellet was heated with 2 ml of 5% tetra-butyl-ammonium hydroxide at 95°C overnight. This was followed by methylation using 2 ml of water, 4 ml of dichloromethane, and 500 µl of iodomethane for 30 min at room temperature. A bi-phase was obtained through centrifugation and the lower organic phase containing the cell wall bound lipids were extracted into a fresh tube and washed three times with water. Lipids were then dried and sonicated in the presence of 4 ml of diethyl ether, the supernatant containing FAMES and MAMES was transferred into a new tube, dried and resuspended in 200 µl of chloroform: methanol (2:1).

6.2.10 [^{14}C] radiolabelling and quantification of radioactivity

M. bovis BCG cultures were radiolabelled with 1 µl of [^{14}C] acetic acid (1 µCi/µl PekinElmer) per 10 ml of bacterial culture and grown in the presence of the radioisotope for 7 days. Cultures were harvested and radioactive waste was discarded according to University's policy. The cell pellet was washed in 5 ml of 1X

PBS and transferred into glass tubes sealed with polytetrafluoroethane (Teflon®)-lined screw cap, where subsequent carbohydrate and lipid extractions were performed as described above.

Radioactive counts in extracted lipids and lipoglycans was quantified in scintillation vial using10 ml of scintillation liquid (Ecoscint A, National Diagnosis). A pre-set protocol for [^{14}C]-labelled samples in the TRI-CARB 2700TR Liquid Scintillation Analyzer was used to measure counts per minute (CPM) for each sample. Drops per minute (DPM) was calculated in each sample using the equation DPM = CPM/0.95 where 0.95 represents the decimal efficiency of the Analyzer for ^{14}C radioisotope. Equalised loading was ensured by loading 25,000 counts of each sample for silver staining (for carbohydrates) or TLC (for lipids) analysis.

6.2.11 Thin-layer chromatography (TLC)

Lipids were made up to 100 mg/ml in chloroform: methanol (2:1) and 80 – 100 µg was spotted onto a silica plate and analysed by thin layer chromatography (TLC, Table 6.12).

Table 6.12: Solvent systems for thin layer chromatography

2 Dimensional TLC		
System	**Direction 1**	**Runs**
A	Petroleum ether 60-80/ Ethyl acetate (98:2)	3
B	Petroleum ether 60-80/ Acetone (92:8)	3
C	Chloroform/ Methanol (96:4)	1
D	Chloroform/ Methanol/ Water (100:14:0.8)	1
E	Chloroform/ Methanol/ Water (60:30:6)	1
System	**Direction 2**	**Runs**
A	Petroleum ether 60-80/ Acetone (98:2)	1
B	Toluene/ Acetone (95:5)	1
C	Toluene/ Acetone (80:20)	1
D	Chloroform/ Acetone/ Methanol / Water (50:60:2.5:3)	1
E	Chloroform/ Acetic acid (glacial)/ Methanol / Water (40:25:3:6)	1
1 Dimensional TLC		
F	Petroleum ether/ Acetone (95:5)	1

Radioactive TLCs were visualised using autoradiography or phosphor imaging. In case of non-radioactive TLCs, dry TLC plate (with lipids separated on it) was dipped either in 5% ethanolic molybdophosphoric acid (MPA) or 1% ethanolic 1-naphthol and heated at 100°C using a heat gun to visualise lipids and carbohydrates respectively.

6.2.12 Infections and Cytokine analysis in THP1 cell line

THP1 cells were cultured in Gibco RPMI 1640 supplemented with 10% heat inactivated fetal bovine serum (HI-FBS) (Sigma-Aldrich) and 1% penicillin-streptomycin (P/S) (Sigma-Aldrich) (growth medium) at 37°C and 5% CO_2.

For measuring the infectivity of *M. bovis* BCG *aftC* knockdown strains, $1x10^4$ cells were plated in each well of a 96 well plate and cultured for 72 hours at 37°C and 5% CO_2 in RPMI 1640 supplemented with 20% HI-FBS, 10 ng/ml PMA and 50 µM 2-mercaptoethanol (called Infection medium) for differentiation of monocytes into macrophages. After 72 hours, they were infected at MOI 10 with BCG-VC and BCG-sgRNA3 strains grown in the presence or absence of ATc, along with respective controls including wild type *M. bovis* BCG and uninfected cells. Post 4 hours into infection, cells were washed 3 times with 1x PBS and incubated with 200 µl of 50 µg/ml gentamycin for 45 minutes to remove extracellular bacteria within the wells. This was followed by thorough washing with 1x PBS, and cell lysis with 1% (v/v) Triton X-100 in 1X PBS. Cell lysates were diluted and plated on 7H11 agar plate supplemented with 10% OADC and respective antibiotics (**6.2.2**). Plates were incubated for 4 weeks at 37°C until colonies appeared. Each infection assay had five biological replicates and the assay was repeated three times.

For the cytokine analysis $1x10^5$ THP1 cells were plated in each well of a 48 well plate, differentiated and infected as described above. At 24 hours post infection, supernatants were collected and stored at -80 °C. ELISA was performed by Lauren Allen in Dr Stephen Taylor's lab at Public Health England (Porton Down, Salisbury, UK). Data is analysed from five biological replicates of each strain of each time point.

6.3 Role of SOCS1 in mycobacterial immune evasion strategies

6.3.1 Maintenance of cell lines

Three cell lines were used in this study – HEK293T, THP1 and J774 cell lines. All cell lines were grown at 37°C, 5% CO_2. HEK293T and J774 were grown in cDMEM (complete DMEM) consisting of Gibco Dulbecco's Modified Eagle Media GlutaMAXTM-I (DMEM) (ThermoFisher Scientific) supplemented with 10% fetal bovine serum (FBS) (Sigma-Aldrich) and 1% penicillin/streptomycin (P/S) (Sigma-Aldrich). THP1 cells were grown in cRPMI (complete RPMI) consisting of Gibco RPMI 1640 supplemented with 10% heat inactivated fetal bovine serum (HI-FBS) (Sigma-Aldrich) and 1% penicillin/streptomycin (Sigma-Aldrich).

6.3.1.1 Defrosting

Cells frozen in liquid N_2 were gently defrosted by swirling the tube in a 37°C water bath to enable equal heat distribution to all the cells. Defrosted cells were transferred into a 15 ml flacon tube containing 9 ml of pre-warmed complete media and centrifuged at 300 x *g* for 10 minutes. The supernatant was discarded and cells were resuspended in respective complete media and grown in cell culture treated flasks (Thermo Scientific) at 37°C, 5% CO_2 (Table 6.13). Adherent J774 (doubling time ~20h) and HEK293T (doubling time ~17h) cells were grown up to 80% confluence and THP1 suspension cells (doubling time ~72h) were grown up to 1.0 x 10^6 cells/ml.

6.3.1.2 Passaging

For adherent cells, old media was replaced by an equal volume of fresh media and cells were dislodged from the flask using a cell scraper (VWR Collection). Cells were aliquoted according to desired split into fresh flasks and sub-cultured to a maximum to 18 passages. For suspension THP1 cell line, cells were

counted and fresh cRPMI was added to adjust the final cell count to 0.5 x 10^6 cells/ml, without discarding the old media. Cells were sub-cultured to a maximum of 8 passages.

6.3.1.3 Freezing

8.0 x 10^6 J774 and HEK cells were pelleted down and resuspended in 1 ml of freezing medium each (50% FBS, 40% DMEM, 10% DMSO) and frozen in 1.2 ml external thread Corning cryogenic vials. Similarly, 5.0 x 10^6 THP1 cells were pelleted down and resuspended in 1 ml freezing medium each (50% HI-FBS, 40% RPMI, 10% DMSO) and frozen in 1.2 ml external thread Corning cryogenic vials. Cells were initially frozen at -20°C for 2 hours, then -80°C for 24hours and finally moved to liquid N_2 for long term storage.

6.3.2 Infection studies

J774s and HEK293T cells were seeded in tissue culture treated dish at seeding density as stated in Table 6.13 in infection medium (IM) (DMEM supplemented with 10% FBS, no P/S) 24 hours prior to infection and incubated at 37°C with 5% CO_2. On the day of infection, cells were infected with wild type *M. bovis* BCG. Mycobacterial OD_{600} measurement of 1 is equivalent to 3.13 x 10^7 cfu/ml (Peñuelas-urquides *et al.*, 2013). Bacterial inoculum was calculated based on this equation and diluted in IM to infect at MOI 10. Infection was carried out for 4 hours at 37 °C, 5% CO_2 and cells were lysed using cell lysis buffer (Table 6.20).

For THP1 cells as they are from a human monocytic cell line, they need to be differentiated into macrophages for 72 hours using IM consisting of RPMI supplemented with 20% HI-FBS, 10 ng/ml PMA and 50 µM 2-mercaptoethanol. As they cannot multiple once monocytes are differentiated into macrophages, seeding density is adjusted accordingly (Table 6.13). On the day of infection, bacterial inoculum was calculated based on OD_{600} measurement as stated earlier (Peñuelas-urquides *et al.*, 2013), diluted in IM and cells were infected at MOI 10. Infection was carried out for 4 hours at 37 °C, 5% CO_2 and cells were lysed using cell lysis buffer (Table 6.20).

Table 6.13: Useful numbers for cell culture conditions

Dish	Seeding density	Cells at confluency	Growth medium
6-well	0.6×10^6	1.2×10^6	3.0 ml
12-well	0.25×10^6	0.5×10^6	2.0 ml
24 well	0.12×10^6	0.24×10^6	1.0 ml
48 well	0.06×10^6	0.12×10^6	0.4 ml
96-well	0.02×10^6	0.04×10^6	0.2 ml
T-25	0.7×10^6	2.8×10^6	4.0 ml
T-75	2.1×10^6	8.4×10^6	12.0 ml

6.3.3 Generation of SOCS1 knockout cell line using CRISPR/Cas9

6.3.3.1 Designing sgRNA

A 25 bp long sgRNA targeting *mus musculus* and *homo sapien* SOCS1 downstream of PAM sequence (5' – NGG – 3') were designed using http://crispr.mit.edu/ platform (Ran *et al.*, 2013). 2 sgRNAs with least off target effects and maximum target sequence match were identified for each of human and murine SOCS1 (Table 6.14).

Table 6.14: Oligonucleotides designed for CRISPR/Cas9 deletion of SOCS1

Oligonucleotides for *mus musculus* SOCS1	
Name	**Sequence 5'>3'**
MsgRNA1a	CACCGCGGGGCCTCGTACGCGCTGT
MsgRNA1b	AAACACAGCGCGTACGAGGCCCCGC
MsgRNA2a	CACCGCCTCGTACGCGCTGTCGGC
MsgRNA2b	AAACGCCGACAGCGCGTACGAGGC
Oligonucleotides for *homo sapien* SOCS1	
Name	**Sequence 5'>3'**
HsgRNA1a	CACC GCCTCGTACGCGCTCTCGGC
HsgRNA1b	AAACGCCGAGAGCGCGTACGAGGC
HsgRNA2a	CACC GCCTGCGATACCGGGTGGGG
HsgRNA2b	AAACCCCCACCCGGTATCGCAGGC

6.3.3.2 Cloning sgRNA into the pSpCas9(BB) vector

Preparation of the sgRNA oligos inserts: Oligonucleotides were phosphorylated and annealed using T4 Polynucleotide kinase (NEB) as described in Table 6.15. Reaction was performed in a thermocycler with the parameters: 37°C for 30 minutes; 95°C for 5 minutes; ramp down to 25°C at 5°C/minutes (Ran *et al.*, 2013).

Table 6.15: Mixture for preparation of the sgRNA oligos inserts

Component	**Amount (µl)**
sgRNA top (100µM)	1
sgRNA bottom (100µM)	1
T4 ligation buffer 10x	1
T4 PNK	1
ddH_2O	6
Total	10

Cloning the sgRNA oligos into pSpCas9(BB): Each phosphorylated and annealed sgRNA oligos were diluted 1:200 and used in the ligation reaction (Table 6.16) along with a no insert pSpCas9(BB)-only negative control (Ran *et al.*, 2013).

Table 6.16: Mixture for cloning the sgRNA oligos into pSpCas9(BB)

Component	**Amount (µl)**
pSpCas9(BB)	X (100ng)
Diluted oligo duplex	2
Tango buffer 10x	2
DTT (10mM)	1
ATP (10mM)	1
Fast digest BbsI	1
T7 Ligase	0.5
ddH_2O	to 20
Total	20

Ligation reaction was carried out for 1hour in a thermocycler using the conditions listed in Table 6.17.

Table 6.17: Conditions for cloning the sgRNA oligos into pSpCas9(BB)

Cycle number	Condition
1 - 6	37°C for 5 minutes, 21°C for 5 minutes

Ligation product was treated with PlasmidSafe Exonuclease (NEB) to digest any residual linearized DNA using the mixture described in the Table 6.18 (Ran *et al.*, 2013).

Table 6.18: Mixture for Exonuclease treatment

Component	Amount (µl)
Ligation product	11
PlasmidSafe buffer 10x	1.5
ATP (10mM)	1.5
PlasmidSafe Exonuclease	1
Total	15

Exonuclease treatment was performed by incubating the reaction mixture at 37°C for 30 minutes followed by 70°C for 30 minutes.

Transformation: Exonuclease treated plasmid was transformed into chemically competent *E. coli* TOP10 cells. An aliquot, 2 µl of the plasmid was added to 20 µl of chemically competent TOP10 cells and briefly incubated on ice for 10 minutes. This was followed by heat shock at 42°C for 30 seconds and immediate incubation on ice for 2 minutes. Cells were recovered into 100 µl LB broth and plated onto LB agar plate supplemented with 100 µg/ml ampicillin (Ran *et al.*, 2013). Plates were incubated at 37°C overnight to isolate individual colonies containing sgRNA cloned into pSpCas9(BB)-2A-GFP and pSpCas9(BB)-2A-Puro plasmids.

6.3.4 HEK293T transfections

Sequence-verified CRISPR plasmid (pSpCas9(sgRNA)) was extracted in a large volume using endotoxin free Maxiprep kit (Thermo Fisher) according to manufacturer's instructions. On the day before transfection HEK293T cells were plated in a dish according to Table 6.19. On the day of transfection, Optimem serum-free medium (Thermo Fisher) was mixed with DNA before the addition of PEI solution (1 mg/ml) as listed in Table 6.19. The mixture was vortexed at half speed and left at room temperature for 10 minutes to allow DNA/PEI complex to form which was then added to cells and mixed completely by gently tilting the plate in all directions. Cells were incubated for 72 hours at 37°C, 5% CO_2 before further analysis.

Table 6.19: Transfection conditions for HEK293T cells

Plate size	Cells (x 10^6)	Media volume (ml)	Opti-mem (ml)	DNA (µg)	PEI (µl)
6-well	0.5	2	0.1	1	4
6 cm	1	4	0.2	2	8
10 cm	3	10	1	9	36
15 cm	6	20	2	18	72

6.3.5 J774 and THP1 transfections

Electroporation, nucleofection and lipofection were performed to identify the most stable transfection method for J774 and THP1 cell lines. Of these, nucleofection worked best for both the cell lines. On the day of nucleofection, 2 x 10^6 cells were centrifuged at 300 x *g* for 10 minutes, washed with 1X PBS, and resuspended in 100 µl of Ingenio Electroporation Solution (Mirus). An aliquot of 1 µg ultrapure endotoxin free DNA was added along the walls of 2 mm gap electroporation cuvette; to this serum free cell suspension was added and allowed to stand at room temperature for 5 minutes for complete mixing of DNA with the cell suspension. Cuvettes were transferred into 4D-Nucleofector system and program T-16 (Amaxa Nucleofector) or U008 (Lonza Nucleofector) were applied to perform nucleofection. Cells were rested for 1 minute at room temperature and recovered by gentle addition of 500 µl of culture medium supplemented

with 20% of FBS and transferred into a 6 well plate containing 1.5 ml medium. Nucleofected cells were recovered for 72 hours at 37 °C, 5% CO_2 before further analysis.

6.3.6 Puromycin kill curve

Puromycin antibiotic was used to ensure effective positive selection of CRISPR clones expressing pSpCas9(BB)-2A-Puro(sgRNA) plasmid. To determine the optimal working concentration of puromycin, an antibiotic kill curve assay was performed on each of the cell lines. Cells were seeded in 24 well tissue culture plates according to Table 6.13 and cultured overnight at 37°C, 5% CO_2. Increasing amounts of puromycin- 0, 0.5, 1.0, 2.0, 3.0, 4.0, 5.0, 6.0, 7.0, 8.0, 9.0, and 10.0 µg/ml were added to duplicate wells of cells plated in complete growth media. Media containing selection antibiotic was replaced every 2-3 days for up to a week. Viable cells were counted at the end of 7 days using a haemocytometer and optimal working concentration was determined for each cell line.

6.3.7 Puromycin treatment and dilution for single cell colonies

Cells transfected with pSpCas9(BB)-2A-Puro(sgRNA) plasmid (harbouring puromycin-N-acetyl-transferase (*pac*) gene) were recovered in complete growth medium for 72 hours following which stable transfectants were obtained by transferring them into medium containing puromycin at a concentration determined from the above kill curve (THP1 - 0.9 µg/ml; J774 – 2 µg/ml; HEK293t – 3 µg/ml). 72 hours post clonal selection viable cells were counted using trypan blue 0.4% (Thermo Fisher) and diluted to 1 cell/200 µl in media containing puromycin and seeded in 96 well plate to obtain single cell colonies.

6.3.8 FACS for J774 (pSpCas9 (BB)-2A-GFP plasmid)

Cells transfected with pSpCas9(BB)-2A-GFP(sgRNA) plasmid were recovered in complete growth medium for 8 hours following which cells were transferred into PBS supplemented with 2.5 mM EDTA, 5% FBS and 0.1% sodium azide and stable transfectants were obtained by fluorescence assisted cell sorting (Flow

Cytometry core facility is based in the Institute of Biomedical Research (IBR) in the College of Medical and Dental Sciences). GFP positive cells were recovered into complete growth medium and cultured at 37°C, 5% CO_2.

6.3.9 SOCS1 Over expression using C-terminal flag-tagged pCDNA3. 1- SOCS1 (commercial) by nucleofection

Homo sapien SOCS1 cloned into pcDNA3.1+/C-(K)-DYK plasmid was purchased from GenScript (https://www.genscript.com/). THP1 cells were transfected as above (**6.3.5**) and recovered in complete growth medium for 72 hours. Stable transfectants expressing pcDNA3.1- SOCS1/C-(K)-DYK plasmid (harbouring G418 resistant *neo*^{R} resistance gene) were selected by transferring them into medium containing G418 sulphate at concentration determined from G418 sulphate kill curve (THP1 – 800 µg/ml). 72 hours post clonal selection viable cells were counted using trypan blue 0.4% (Thermo Fisher) and used for continuing experiments.

6.3.10 Cell lysis and Immunoprecipitation

Cells were washed twice with ice cold PBS (Thermo Fisher) and lysed using fresh cell lysis buffer (Table 6.20) for 30 minutes on an orbital shaker at 4°C. Cells were scraped from the plate using cell scraper and cell lysate solution was centrifuged at 14,000 rpm for 15 minutes at 4°C. 10% of the cleared cell lysate was saved as the whole cell lysate-control for immunoprecipitation. The remaining cell lysate was incubated with prewashed (three times in 500 µl of TBS) 30 µl of Anti-FLAG Magnetic Beads (Sigma Aldrich) overnight on rotating wheel at 4°C. Beads were washed three times with 1 ml lysis buffer and proteins were eluted in 30 µl 1X SDS loading buffer at 95 °C for 10 minutes.

Table 6.20: Buffer compositions

Buffer	Composition
Cell lysis buffer	1% Triton X-100, 50 mM Tris pH 7.4, 150 mM NaCl, 1 mM EDTA, 2 mM sodium orthovanadate, 10 mM NaF, protease inhibitor tablet
6X loading dye	1% SDS, 0.5% bromophenol blue, 50% Glycerol, 20 mM, 100 mM Tris pH 6.8, (add on the day 8% β-mercaptoethanol)
TBS	20mM Tris-HCl pH7.5, 150mM NaCl
TBS-T	TBS with 0.05% Tween-20

6.3.11 SDS- PAGE and Western blot

12% SDS-PAGE gels with 5% stack were casted using the components in Table 6.21 and Bio-Rad gel assembly system. Cell lysates were boiled with 6X loading dye (Table 6.20) at 95°C for 10 min. 12% SDS-PAGE gel was assembled in Bio-Rad gel tank and filled with 1X Tris-Glycine-SDS running buffer (Scientific laboratory supplies). Boiled cell lysates were loaded onto the gel along with Blue broad range protein standard (NEB) and gel was run at 200V, 50mA until the dye front reached the bottom of the gel (~60min).

Table 6.21: components of 12% SDS-PAGE gel

Ingredients	Resolving gel (ml)	Stacking gel (ml)
30% Acrylamide (Bio-Rad)	4.2	0.83
1.5M Tris-HCl pH 8.8	2.5	-
0.5M Tris-HCl pH6.8	-	1.25
Water	3.3	2.89
10% SDS	0.1	0.05
Temed (Sigma Aldrich)	0.03	0.015
20% APS (Thermo Fisher)	0.03	0.015

To visualise the separated protein bands, gel was incubated in Instant blue gel stain (Expedeon) for 20 minutes and destained for 1 hour in deionised water at room temperature on an orbital shaker. The stained gel was imaged using Bio-Rad Gel doc system.

To perform the Western blot, proteins separated on SDS-PAGE were transferred onto a nitrocellulose membrane preassembled in iBlot2 Transfer Stacks (Thermo Fisher) using iBlot2 Western Blot Transfer - Rapid Dry Blotting Device (Thermo Fisher). Membranes were blocked for 1 hour at room temperature with 5% skim milk (Sigma Aldrich) prepared in TBS-T and incubated overnight at 4°C in primary antibody (Table 6.22) diluted in TBS-T buffer. Membranes were washed three times in TBS-T buffer for a minimum of 10 minutes at room temperature to avoid non-specific antibody interactions and incubated with appropriate secondary antibody (Table 6.22) for 1 hour at room temperature. Membranes were washed twice in TBS-T and once in TBS to remove excessive secondary antibody and residual traces of tween before being visualised using the LICOR/Odyssey western blot imaging system.

Table 6.22: List of antibodies

Primary Antibody	**Supplier**	**Raised in**	**WB dilution (µl)**
SOCS1	Source Bioscience	Rabbit	1:3000
STAT1	Source Bioscience	Rabbit	1:3000
JAK1	Gene Tex	Rabbit	1:3000
α-tubulin	Sigma Aldrich	Mouse	1:3000
Actin	Santacruz biotech	Mouse	1:3000
Flag	Sigma Aldrich	Mouse	1:2000
Phosphorylated STAT1	Thermo Fisher	Rabbit	1:3000
SOCS3	Proteintech Europe	Rabbit	1:3000
Phosphorylated JAK2	Thermo Fisher	Rabbit	1:3000
Secondary antibody	**Supplier**	**Raised in**	**WB Dilution (µl)**
Mouse 690	Licor	Mouse	1:15000
Rabbit 800	Licor	Rabbit	1:15000

References

Adams D. O. (1974). The structure of mononuclear phagocytes differentiating in vivo. I. Sequential fine and histologic studies of the effect of Bacillus Calmette-Guerin (BCG). *The American journal of pathology*, *76*(1), 17–48.

Ahmed, C. M. I., Larkin, J. and Johnson, H. M. (2015) 'SOCS1 Mimetics and Antagonists: A Complementary Approach to Positive and Negative Regulation of Immune Function', *Frontiers in Immunology*, 6, 183. doi: 10.3389/fimmu.2015.00183.

Akira, S., Uematsu, S. and Takeuchi, O. (2006) 'Pathogen recognition and innate immunity', *Cell*, 124(4), 783–801. doi: 10.1016/j.cell.2006.02.015.

Alberto, M. *et al.* (2020) 'Transcriptional portrait of M . bovis BCG during biofilm production shows genes differentially expressed during intercellular aggregation and substrate attachment', *Scientific Reports*. 10(1), 12578. doi: 10.1038/s41598-020-69152-2.

Alderwick, L. J. *et al.* (2005) 'Deletion of Cg-emb in corynebacterianeae leads to a novel truncated cell wall arabinogalactan, whereas inactivation of Cg-ubiA results in an Arabinan-deficient mutant with a cell wall galactan core', *Journal of Biological Chemistry*. 280(37), pp. 32362–32371. doi: 10.1074/jbc.M506339200.

Alderwick, L. J. *et al.* (2006) 'Identification of a novel arabinofuranosyltransferase (AftA) involved in cell wall arabinan biosynthesis in Mycobacterium tuberculosis', *Journal of Biological Chemistry*, 281(23), pp. 15653–15661. doi: 10.1074/jbc.M600045200.

Alderwick, L. J. *et al.* (2011) 'The C-terminal domain of the arabinosyltransferase mycobacterium tuberculosis EmbC is a lectin-like carbohydrate binding module', *PLoS Pathogens*, 7(2). doi: 10.1371/journal.ppat.1001299.

Alderwick, L. J. *et al.* (2015) 'The Mycobacterial Cell Wall—Peptidoglycan and Arabinogalactan', *Cold Spring Harbor Perspectives in Medicine*, 5(8), p. a021113. doi: 10.1101/cshperspect.a021113.

Alexander, W. S. *et al.* (1999) 'SOCS1 is a critical inhibitor of interferon γ signaling and prevents the potentially fatal neonatal actions of this cytokine', *Cell*, 98(5), pp. 597–608. doi: 10.1016/S0092-8674(00)80047-1.

Amador, C. I. *et al.* (2021). 'High-throughput screening alternative to crystal violet biofilm assay combining fluorescence quantification and imaging'. *Journal of microbiological methods*, 190, 106343. https://doi.org/10.1016/j.mimet.2021.106343

Angala, S. K. *et al.* (2014). 'The cell envelope glycoconjugates of Mycobacterium tuberculosis'. *Critical reviews in biochemistry and molecular biology*, 49(5), 361–399. doi: 10.3109/10409238.2014.925420

Apostolou, I. *et al.* (1999) 'Murine natural killer cells contribute to the granulomatous reaction caused by mycobacterial cell walls', *Proc Natl Acad Sci*, 96, pp. 5141–5146.

Appelberg, R. *et al.* (1994) 'Role of interleukin-6 in the induction of protective T cells during mycobacterial infections in mice.', *Immunology*, 82(3), pp. 361–4.

Appelmelk, B. J. *et al.* (2008) 'The mannose cap of mycobacterial lipoarabinomannan does not dominate the Mycobacterium-host interaction', *Cellular Microbiology*, 10(4), pp. 930–944. doi: 10.1111/j.1462-5822.2007.01097.x.

Arias, L. *et al.* (2020) 'Cording Mycobacterium tuberculosis Bacilli Have a Key Role in the Progression towards Active Tuberculosis , Which is Stopped by Previous Immune Response', *Microorganisms*, *8*(2), 228. doi: 10.3390/microorganisms8020228

Bai, C. *et al.* (2020) 'Fusion cytokines IL-7-linker-IL-15 promote mycobacterium tuberculosis subunit vaccine to induce central memory like T cell-mediated immunity', *Vaccines*, 8(4), 715 doi: 10.3390/vaccines8040715.

Ballou, C. E., Vilkas, E., & Lederer, E. (1963). Structural studies on the myo-inositol phospholipids of Mycobacterium tuberculosis (var. bovis, strain BCG). *The Journal of biological chemistry*, *238*, 69–76.

Ballou, C. E., & Lee, Y. C. (1964). The Structure Of A Myoinositol Mannoside From Mycobacterium Tuberculosis Glycolipid. *Biochemistry*, *3*, 682–685. https://doi.org/10.1021/bi00893a014

Barberis, I. *et al.* (2017) 'The history of tuberculosis: From the first historical records to the isolation of Koch's bacillus', *Journal of Preventive Medicine and Hygiene*, 58(1), pp. E9–E12. doi: 10.15167/2421-4248/jpmh2017.58.1.728.

Bardarov, Stoyan, Bardarov, Stoyan, *et al.* (2002) 'Specialized transduction : an ef cient method for generating marked and unmarked targeted gene disruptions in', *Microbiology*, 148(2002), pp. 3007–3017. doi: 10.1099/00221287-148-10-3007.

Bardarov, S *et al.* (2002) 'Specialized transduction: An efficient method for generating marked and unmarked targeted gene disruptions in Mycobacterium tuberculosis, M. bovis BCG and M. smegmatis', *Microbiology*, 148(10), pp. 3007–3017. doi: 10.1099/00221287-148-10-3007.

Basaraba, R. J. and Ojha, A. K. (2017) 'Mycobacterial Biofilms : Revisiting Tuberculosis Bacilli in Extracellular Necrotizing Lesions', *Microbiology Spectrum*, 5(3), pp. 1–7. doi: 10.1128/microbiolspec.TBTB2-0024-2016.

Behar, S. *et al.* (2011) 'Apoptosis is an innate defense function of macrophages against Mycobacterium tuberculosis', *Mucosal Immunology*, 4(3), pp. 279–287. doi: 10.1038/mi.2011.3.

Behr, M. A. and Small, P. M. (1999) 'A historical and molecular phylogeny of BCG strains', *Vaccine*, 17(7–8), pp. 915–922. doi: 10.1016/S0264-410X(98)00277-1.

Besra, G. S. *et al.* (1995) 'A New Interpretation of the Structure of the Mycolyl—Arabinogalactan Complex of Mycobacterium Tuberculosis as Revealed Through Characterization of Oligoglycosylalditol Fragments by Fast-Atom Bombardment Mass Spectrometry and 1H Nuclear Magnetic Resonance ', *Biochemistry*, 34(13), pp. 4257–4266. doi: 10.1021/bi00013a015.

Bettencourt, P. *et al.* (2017) 'Mycobacterial infection of macrophages: the effect of the multiplicity of infection', *Antimicrobial research: Novel bioknowledge and educational programs*, (August), pp. 651–664.

Bezuidenhout, J. *et al.* (2009) 'Pleural tuberculosis in patients with early HIV infection is associated with increased TNF-alpha expression and necrosis in granulomas', *PLoS ONE*, 4(1), p. e4228. doi: 10.1371/journal.pone.0004228.

Bhamidi, S. *et al.* (2008) 'The identification and location of succinyl residues and the characterization of the interior arabinan region allow for a model of the complete primary structure of Mycobacterium tuberculosis mycolyl arabinogalactan', *Journal of Biological Chemistry*, 283(19), pp. 12992–13000. doi: 10.1074/jbc.M800222200.

Bhatt, A. *et al.* (2005) 'Conditional Depletion of KasA , a Key Enzyme of Mycolic Acid Biosynthesis , Leads to Mycobacterial Cell Lysis', 187(22), pp. 7596–7606. doi: 10.1128/JB.187.22.7596.

Bhowruth, V., Alderwick, Luke J, *et al.* (2008) 'Tuberculosis: a balanced diet of lipids and carbohydrates.', *Biochemical Society transactions*, 36(Pt 4), pp. 555–65. doi: 10.1042/BST0360555.

Bhowruth, V., Alderwick, Luke J., *et al.* (2008) 'Tuberculosis: A balanced diet of lipids and carbohydrates', *Biochemical Society Transactions*, 36(4), pp. 555–565. doi: 10.1042/BST0360555.

Bikard, D. *et al.* (2013) 'Programmable repression and activation of bacterial gene expression using an engineered CRISPR-Cas system', *Nucleic Acids Research*, 41(15), pp. 7429–7437. doi: 10.1093/nar/gkt520.

Birch, H. L. *et al.* (2008) 'Biosynthesis of mycobacterial arabinogalactan: Identification of a novel α(1→3) arabinofuranosyltransferase', *Molecular Microbiology*, 69(5), pp. 1191–1206. doi: 10.1111/j.1365-2958.2008.06354.x.

Birch, H. L. *et al.* (2010) 'A truncated lipoglycan from mycobacteria with altered immunological properties', *Proceedings of the National Academy of Sciences*, 107(6), pp. 2634–2639. doi: 10.1073/pnas.0915082107.

Birch, H. L. *et al.* (2014) 'Genetics of Mycobacterial Arabinogalactan and Lipoarabinomannan Assembly', *Microbiology Spectrum*, 2(4), pp. 1–21. doi: 10.1128/microbiolspec.MGM2-0013-2013.

Bohn, E. *et al.* (1998) 'IL-18 (IFN-gamma-inducing factor) regulates early cytokine production in, and promotes resolution of, bacterial infection in mice.', *Journal of immunology (Baltimore, Md. : 1950)*, 160(1), pp. 299–307. Available at: http://www.ncbi.nlm.nih.gov/pubmed/9551984.

BoseDasgupta, S. and Pieters, J. (2014) 'Striking the right balance determines TB or not TB', *Frontiers in Immunology*, 5(OCT), pp. 1–9. doi: 10.3389/fimmu.2014.00455.

Bouley, D. M. *et al.* (2001) 'Dynamic Nature of Host-Pathogen Interactions in Mycobacterium marinum Granulomas', 69(12), pp. 7820–7831. doi: 10.1128/IAI.69.12.7820.

Bourigault, M. L. *et al.* (2013) 'Relative contribution of il-1α, il-1β and tnf to the host response to mycobacterium tuberculosis and attenuated m. Bovis bcg', *Immunity, Inflammation and Disease*, 1(1), pp. 47–62. doi: 10.1002/iid3.9.

Brennan, P. J. and Nikaido, H. (1995) 'The envelope of mycobacteria', *Annual Review of Biochemistry*, 64, pp. 29–63. doi: 10.1146/annurev.bi.64.070195.000333.

Brown, A. K. *et al.* (2007) 'Dimerization of inositol monophosphatase Mycobacterium tuberculosis SuhB is not constitutive, but induced by binding of the activator Mg2+', 14, pp. 1–14. doi: 10.1186/1472-6807-7-55.

Bussi, C. and Gutierrez, M. G. (2019) 'Mycobacterium tuberculosis infection of host cells in space and time', *FEMS Microbiology Reviews*. Oxford University Press, 43(4), pp. 341–361. doi:

10.1093/femsre/fuz006.

Cambier, C. J., Falkow, S. and Ramakrishnan, L. (2014) 'Host evasion and exploitation schemes of Mycobacterium tuberculosis', *Cell*. Elsevier Inc., 159(7), pp. 1497–1509. doi: 10.1016/j.cell.2014.11.024.

Caragol, I. *et al.* (2003) 'Clinical tuberculosis in 2 of 3 siblings with interleukin-12 receptor β1 deficiency', *Clinical Infectious Diseases*, 37(2), pp. 302–306. doi: 10.1086/375587.

Carow, B. *et al.* (2011) 'Silencing suppressor of cytokine signaling-1 (SOCS1) in macrophages improves Mycobacterium tuberculosis control in an interferon-γ (IFN-γ)-dependent manner', *Journal of Biological Chemistry*, 286(30), pp. 26873–26887. doi: 10.1074/jbc.M111.238287.

Chakraborty, P. and Kumar, A. (2019) 'The extracellular matrix of mycobacterial biofilms : could we shorten the treatment of mycobacterial infections ?', 6(2), pp. 105–122. doi: 10.15698/mic2019.02.667.

Chatterjee, D., Hunter, S. W., *et al.* (1991) 'Lipoarabinomannan: multiglycosylated form of the mycobacterial mannosylphosphatidylinositols.', *The Journal of biological chemistry*, 267, pp. 6228–6233. doi: 10.1016/S0021-9258(18)42685-3.

Chatterjee, D., Bozic, C. M., *et al.* (1991) 'Structural Features of the Arabinan Component of the Lipoarabinomannan of Mycobacterium tuberculosis *', *The Journal of biological chemistry*, (10 ml), pp. 9652–9660. doi: 10.1016/S0021-9258(18)92870-X.

Chatterjee, D. *et al.* (1992) 'Lipoarabinomannan of Mycobacterium tuberculosis', *Journal of Biological Chemistry*. Â© 1992 ASBMB. Currently published by Elsevier Inc; originally published by American Society for Biochemistry and Molecular Biology., 267(9), pp. 6234–6239. doi: 10.1016/S0021-9258(18)42686-5.

Chatterjee, D. *et al.* (1993) 'Structural definition of the non-reducing termini of mannose-capped LAM from Mycobacterium tuberculosis through selective enzymatic degradation and fast atom bombardment-mass spectrometry', *Glycobiology*, 3(5), pp. 497–506. doi: 10.1093/glycob/3.5.497.

Chen, F. *et al.* (2013) Dynamic imaging of genomic loci in living human cells by an optimized CRISPR/Cas system. Cell 155:1479–1491. doi: 10.1016/j.cell.2013.12.001.

Chhotaray, C. *et al.* (2018) 'Advances in the development of molecular genetic tools for Mycobacterium tuberculosis', *Journal of Genetics and Genomics*. Elsevier Limited and Science Press, 45(6), pp. 281–297. doi: 10.1016/j.jgg.2018.06.003.

Chikuma, S. *et al.* (2017) 'Suppressors of cytokine signaling: Potential immune checkpoint molecules for cancer immunotherapy', *Cancer Science*. doi: 10.1111/cas.13194.

Chinen, T. *et al.* (2011a) 'Prostaglandin E2 and SOCS1 have a role in intestinal immune tolerance', *Nature Communications*. Nature Publishing Group, 2(1). doi: 10.1038/ncomms1181.

Chinen, T. *et al.* (2011b) 'Prostaglandin E2 and SOCS1 have a role in intestinal immune tolerance', *Nature Communications*. Nature Publishing Group, 2(2), pp. 111–190. doi: 10.1038/ncomms1181.

Choudhary, E. *et al.* (2015) 'Gene silencing by CRISPR interference in mycobacteria', *Nature Communications*. Nature Publishing Group, 6, pp. 1–11. doi: 10.1038/ncomms7267.

Choudhary, E., Lunge, A. and Agarwal, N. (2016) 'Strategies of genome editing in mycobacteria: Achievements and challenges', *Tuberculosis*. Elsevier Ltd, 98, pp. 132–138. doi: 10.1016/j.tube.2016.03.005.

Chung, Y. *et al.* (2009) 'Critical Regulation of early Th17 differentiation by IL-1 signaling', *Immunity*, 30(4), pp. 576–587. doi: 10.1016/j.immuni.2009.02.007.Critical.

Colditz, G. A. *et al.* (1995) 'Weight gain as a risk factor for clinical diabetes mellitus in women', *Annals of Internal Medicine*, 122(7), pp. 481–486. doi: 10.7326/0003-4819-122-7-199504010-00001.

Cole, B. K. E. *et al.* (1998) 'Interferon – inducible T Cell Alpha Chemoattractant (I-TAC): A Novel Non-ELR CXC Chemokine with Potent Activity on Activated T Cells through Selective High Affinity Binding to CXCR3', 187(12), pp. 2009–2021. doi: 10.1084/jem.187.12.2009.

Cole, S. T. (1994) 'Mycobacterium tuberculosis: drug-resistance mechanisms', *Trends in Microbiology*, 2(10), pp. 411–415. doi: 10.1016/0966-842X(94)90621-1.

Cooper, A. M. *et al.* (1993) 'Disseminated tuberculosis in interferon gamma gene-distrupted mice', *J.Exp.Med.*, 178(December), pp. 2243–2247. doi: 10.1084/jem.178.6.2243.

Copin, R. *et al.* (2014) 'Sequence diversity in the pe_pgrs genes of Mycobacterium tuberculosis is independent of human T cell recognition', *mBio*, 5(1), pp. 1–11. doi: 10.1128/mBio.00960-13.

Correia-Neves, M. *et al.* (2019) 'Lipoarabinomannan in Active and Passive Protection Against Tuberculosis', *Frontiers in Immunology*, 10(September). doi: 10.3389/fimmu.2019.01968.

Crevel, R. Van, Ottenhoff, T. H. M. and Meer, J. W. M. Van Der (2002) 'Innate Immunity to Mycobacterium tuberculosis', 15(2), pp. 294–309. doi: 10.1128/CMR.15.2.294.

Daffe, M., Brennan, P. J. and McNeil, M. (1990) 'Predominant structural features of the cell wall arabinogalactan of Mycobacterium tuberculosis as revealed through characterization of oligoglycosyl alditol fragments by gas chromatography/mass spectrometry and by 1H and 13C NMR analyses', *Journal of Biological Chemistry*, 265(12), pp. 6734–6743. doi: 10.1016/s0021-9258(19)39211-7.

Dahl, K. E. *et al.* (1996) 'Selective induction of transforming growth factor β in human monocytes by lipoarabinomannan of Mycobacterium tuberculosis', *Infection and Immunity*, 64(2), pp. 399–405. doi: 10.1128/iai.64.2.399-405.1996.

Dalton, D. K. *et al.* (1993) 'Multiple defects of immune cell function in mice with disrupted interferon-γ genes', *Science*, 259(5102), pp. 1739–1742. doi: 10.1126/science.8456300.

Dannenberg, A. M. (1968) 'Cellular Hypersensitivity and Cellular Immunity the Pathogenesis of Tuberculosis : Specificity , Systemic and Local Nature , and Associated', *Bacteriological Review*, 32(2), pp. 85–102.

Datta, M. D. *et al.* (2016) 'Mathematical Model of Oxygen Transport in Tuberculosis Granulomas', *Annals of Biomedical Engineering*, 44(4), pp. 863–872. doi: 10.1007/s10439-015-1415-3.

Davenne, T. and McShane, H. (2016) 'Why don't we have an effective tuberculosis vaccine yet?', *Expert Review of Vaccines*. Taylor & Francis, 15(8), pp. 1009–1013. doi: 10.1586/14760584.2016.1170599.

Davey, G. M., Heath, W. R. and Starr, R. (2006) 'SOCS1: A potent and multifaceted regulator of cytokines and cell-mediated inflammation', *Tissue Antigens*, 67(1), pp. 1–9. doi: 10.1111/j.1399-0039.2005.00532.x.

Davey, M. E. and Toole, G. A. O. (2000) 'Microbial Biofilms : from Ecology to Molecular Genetics', *Microbiology and Molecular Biology Reviews*, 64(4), pp. 847–867. doi: https://doi.org/10.1128/MMBR.64.4.847-867.2000.

Davis, J. M. and Ramakrishnan, L. (2009) 'The Role of the Granuloma in Expansion and Dissemination of Early Tuberculous Infection', *Cell*, 136(1), pp. 37–49. doi: 10.1016/j.cell.2008.11.014.

Desvignes, L., Wolf, A. J. and Ernst, J. D. (2012) 'Dynamic roles of type I and type II interferons in early infection with Mycobacterium tuberculosis', *Journal of immunology*, 188(12), pp. 6205–6215. doi: 10.4049/jimmunol.1200255.Dynamic.

Dhiman, R. *et al.* (2009) ' IL-22 Produced by Human NK Cells Inhibits Growth of Mycobacterium tuberculosis by Enhancing Phagolysosomal Fusion ', *The Journal of Immunology*, 183(10), pp. 6639–6645. doi: 10.4049/jimmunol.0902587.

Dhiman, R. *et al.* (2014) 'Interleukin 22 inhibits intracellular growth of mycobacterium tuberculosis by enhancing calgranulin a expression', *Journal of Infectious Diseases*, 209(4), pp. 578–587. doi: 10.1093/infdis/jit495.

Dickensheets, H. *et al.* (2007) 'Suppressor of cytokine signaling-1 is an IL-4-inducible gene in macrophages and feedback inhibits IL-4 signaling', *Genes and Immunity*, 8(1), pp. 21–27. doi: 10.1038/sj.gene.6364352.

Diedrich, C. R., Mattila, J. T. and Flynn, J. L. (2013) ' Monocyte-Derived IL-5 Reduces TNF Production by Mycobacterium tuberculosis –specific CD4 T Cells during SIV/ M. tuberculosis Coinfection ', *The Journal of Immunology*, 190(12), pp. 6320–6328. doi: 10.4049/jimmunol.1202043.

Dinarello, C. A. (1991) 'Interleukin-1 and interleukin-1 antagonism', *Blood*. American Society of Hematology, 77(8), pp. 1627–1652. doi: 10.1182/blood.v77.8.1627.1627.

Ding, Y. *et al.* (2003) 'Suppressor of Cytokine Signaling 1 Inhibits IL-10-Mediated Immune Responses'. *Journal of immunology (Baltimore, Md. : 1950)*, *170*(3), 1383–1391. doi: 10.4049/jimmunol.170.3.1383.

Domingo-Gonzalez, R. *et al.* (2016) 'Cytokines and Chemokines in Mycobacterium tuberculosis infection', *Microbiology Spectrum*, 8(5), pp. 444–454. doi: 10.1128/microbiolspec.TBTB2-0018-2016.

Dong, W., Matsuno, Y. K., & Kameyama, A. (2012). 'A procedure for Alcian blue staining of mucins on polyvinylidene difluoride membranes'. *Analytical chemistry*, 84(20), 8461–8466. doi: 10.1021/ac301678z

Dorman, S. E. and Holland, S. M. (2000) 'Interferon-γ and interleukin-12 pathway defects and human disease', *Cytokine and Growth Factor Reviews*, 11(4), pp. 321–333. doi: 10.1016/S1359-6101(00)00010-1.

Doz, E. *et al.* (2007) 'Acylation determines the toll-like receptor (TLR)-dependent positive versus TLR2-, mannose receptor-, and SIGNR1-independent negative regulation of pro-inflammatory cytokines by mycobacterial lipomannan', *Journal of Biological Chemistry*, 282(36), pp. 26014–26025. doi: 10.1074/jbc.M702690200.

Draper, P. *et al.* (1997) 'Galactosamine in walls of slow-growing mycobacteria', *Biochemical Journal*, 327(2), pp. 519–525. doi: 10.1042/bj3270519.

Drickamer, K. and Taylor, M. E. (2015) 'Recent insights into structures and functions of C-type lectins in the immune system', *Current Opinion in Structural Biology*. Elsevier Ltd, 34, pp. 26–34. doi: 10.1016/j.sbi.2015.06.003.

Ebert C, et al., (2021) 'Correlation of crystal violet biofilm test results of Staphylococcus aureus clinical isolates with Raman spectroscopic read-out' Journal of Raman Spectroscopy 52(12) pp 2660-2670 https://doi.org/10.1002/jrs.6237

Ehlers, S. and Schaible, U. E. (2013) 'The granuloma in tuberculosis : dynamics of a host – pathogen collusion', *Frontiers in immunology, 3*, 411. doi: 10.3389/fimmu.2012.00411.

Endo, T. A. *et al.* (1997) 'A new protein containing an SH2 domain that inhibits JAK kinases', *Nature*, 387(6636), pp. 921–924. doi: 10.1038/43213.

Erb, K. J. *et al.* (1998) 'IL-4, IL-5 and IL-10 are not required for the control of M. bovis-BCG infection in mice', *Immunology and Cell Biology*, 76(1), pp. 41–46. doi: 10.1046/j.1440-1711.1998.00719.x.

Esin, S. and Batoni, G. (2015) 'Natural killer cells: A coherent model for their functional role in Mycobacterium tuberculosis infection', *Journal of Innate Immunity*, 7(1), pp. 11–24. doi: 10.1159/000363321.

Eum, S. *et al.* (2010) 'Neutrophils Are the Predominant Infected Phagocytic Cells in the Airways of Patients'. *Chest, 137*(1), 122–128. doi: 10.1378/chest.09-0903.

Eum, S. Y. *et al.* (2008) 'Tumor necrosis factor-alpha and interleukin-10 in whole blood is associated with disease progression in pulmonary mulitdrug-resistant tuberculosis patients', *Respiration*, 76(3), pp. 331–337. doi: 10.1159/000113932.

Eyles, J. L. *et al.* (2002) 'Negative regulation of interleukin-12 signaling by suppressor of cytokine signaling-1', *Journal of Biological Chemistry*. Â© 2002 ASBMB. Currently published by Elsevier Inc; originally published by American Society for Biochemistry and Molecular Biology., 277(46), pp. 43735–43740. doi: 10.1074/jbc.M208586200.

Fabre, M. *et al.* (2004) 'High genetic diversity revealed by variable-number tandem repeat genotyping and analysis of hsp65 gene polymorphism in a large collection of "Mycobacterium canettii" strains indicates that the M. tuberculosis complex is a recently emerged clone of "M. can', *Journal of Clinical Microbiology*, 42(7), pp. 3248–3255. doi: 10.1128/JCM.42.7.3248-3255.2004.

Farber, J. M. (1997) 'Mig and IP-lO : CXC chemokines', *Journal of leukocyte biology*, 61(March), pp. 246–257. doi: 10.1002/jlb.61.3.246.

Feng, C. G. *et al.* (2005) 'Maintenance of Pulmonary Th1 Effector Function in Chronic Tuberculosis Requires Persistent IL-12 Production', *The Journal of Immunology*, 174(7), pp. 4185–4192. doi: 10.4049/jimmunol.174.7.4185.

Feng, C. G. *et al.* (2006) 'NK Cell-Derived IFN-γ Differentially Regulates Innate Resistance and Neutrophil Response in T Cell-Deficient Hosts Infected with Mycobacterium tuberculosis', *Journal of immunology 177*(10), 7086–7093. doi: 10.4049/jimmunol.177.10.7086.

Fennelly, K. P. and Jones-López, E. C. (2015) 'Quantity and quality of inhaled dose predicts immunopathology in tuberculosis', *Frontiers in Immunology*, 6(JUN), pp. 1–13. doi:

10.3389/fimmu.2015.00313.

Fenner, J. E. *et al.* (2006) 'Suppressor of cytokine signaling 1 regulates the immune response to infection by a unique inhibition of type I interferon activity', *Nature Immunology*, 7(1), pp. 33–39. doi: 10.1038/ni1287.

Filipe-Santos, O., Bustamante, J., Chapgier, A., *et al.* (2006) 'Inborn errors of IL-12/23- and IFN-γ-mediated immunity: molecular, cellular, and clinical features', *Seminars in Immunology*, 18(6), pp. 347–361. doi: 10.1016/j.smim.2006.07.010.

Filipe-Santos, O., Bustamante, J., Haverkamp, M. H., *et al.* (2006) 'X-linked susceptibility to mycobacteria is caused by mutations in NEMO impairing CD40-dependent IL-12 production', *Journal of Experimental Medicine*, 203(7), pp. 1745–1759. doi: 10.1084/jem.20060085.

Flynn, J. A. L. *et al.* (1993) 'An essential role for interferon γ in resistance to mycobacterium tuberculosis infection', *Journal of Experimental Medicine*, 178(6), pp. 2249–2254. doi: 10.1084/jem.178.6.2249.

Flynn, J. L. *et al.* (1995) 'Tumor Necrosis Factor-a Is Required in the Protective Immune Response Against Mycobacterium tuberculosis in Mice', *Immunity*, 2, pp. 561–572. doi: 10.1016/1074-7613(95)90001-2.

Fukuda, T. *et al.* (2013) 'Critical Roles for Lipomannan and Lipoarabinomannan in Cell Wall Integrity of Mycobacteria and Pathogenesis of Tuberculosis', *mBio*, *4*(1), e00472-12. , pp. 8–10. doi: 10.1128/mBio.00472-12.

Garneau, J. E. *et al.* (2010) 'The CRISPR/cas bacterial immune system cleaves bacteriophage and plasmid DNA', *Nature*, 468(7320), pp. 67–71. doi: 10.1038/nature09523.

Gasiunas, G. *et al.* (2012) 'Cas9-crRNA ribonucleoprotein complex mediates specific DNA cleavage for adaptive immunity in bacteria', *Proceedings of the National Academy of Sciences of the United States of America*, 109(39), pp. 2579–2586. doi: 10.1073/pnas.1208507109.

Gessner, A., Mohrs, K. and Mohrs, M. (2005) 'Mast Cells, Basophils, and Eosinophils Acquire Constitutive IL-4 and IL-13 Transcripts during Lineage Differentiation That Are Sufficient for Rapid Cytokine Production', *The Journal of Immunology*, 174(2), pp. 1063–1072. doi: 10.4049/jimmunol.174.2.1063.

Goldberg, M. F., Saini, N. K. and Porcelli, S. A. (2013) 'Evasion of Innate and Adaptive Immunity by Mycobacterium tuberculosis', *Microbiology Spectrum*, (May 2020), pp. 1–24. doi: 10.1128/microbiolspec.MGM2-0005-2013.f1.

Golden, M. P. and Vikram, H. R. (2005) 'Extrapulmonary tuberculosis: An overview', *American Family Physician*, 72(9), pp. 1761–1768. doi: 10.5772/intechopen.81322.

Gopal, R. *et al.* (2012) 'Interleukin-23 dependent IL-17 drives Th1 responses following Mycobacterium bovis BCG vaccination', *European journal of immunology*, *42*(2), pp. 364–373. doi: 10.1002/eji.201141569.

Green, A., DiFazio, R. and Flynn, J. L. (2013) 'IFN-γ from CD4 T cells is essential for host survival and enhances CD8 T cell function during Mycobacterium tuberculosis infection1', *Journal of immunology*, 190(1), pp. 270–277. doi: 10.4049/jimmunol.1200061.

Greenlund, A. C. *et al.* (1994) 'Ligand-induced IFN(γ) receptor tyrosine phosphorylation couples the

receptor to its signal transduction system (p91)', *EMBO Journal*, 13(7), pp. 1591–1600. doi: 10.1002/j.1460-2075.1994.tb06422.x.

Griffith, J. W., Sokol, C. L. and Luster, A. D. (2014) 'Chemokines and Chemokine Receptors : Positioning Cells for Host Defense and Immunity', *Annual review of Immunology*, 32, pp. 659–702. doi: 10.1146/annurev-immunol-032713-120145.

Grosset, J. (2003) 'Mycobacterium tuberculosis in the Extracellular Compartment : an Underestimated Adversary', *Antimicrobial agents and chemotherapy*, 47(3), pp. 833–836. doi: 10.1128/AAC.47.3.833.

Gueardel, Y. *et al.* (2002) 'Structural Study of Lipomannan and Lipoarabinomannan from Mycobacterium chelonae', *The Journal of biological chemistry*, 277(34), pp. 30635–30648. doi: 10.1074/jbc.M204398200.

Guirado, E., Schlesinger, L. S. and Kaplan, G. (2013) 'Macrophages in tuberculosis: Friend or foe', *Seminars in Immunopathology*. *35*(5), 563–583. doi: 10.1007/s00281-013-0388-2.

Guler, R. *et al.* (2011) 'Blocking IL-1α but not IL-1β increases susceptibility to chronic Mycobacterium tuberculosis infection in mice', *Vaccine*. 29(6), pp. 1339–1346. doi: 10.1016/j.vaccine.2010.10.045.

Guo, H. *et al.* (2014) 'HIV-1 infection induces interleukin-1β production via TLR8 protein-dependent and NLRP3 inflammasome mechanisms in human monocytes', *Journal of Biological Chemistry*, 289(31), pp. 21716–21726. doi: 10.1074/jbc.M114.566620.

Hamasur, B. *et al.* (2004) 'A mycobacterial lipoarabinomannan specific monoclonal antibody and its F(ab′)2 fragment prolong survival of mice infected with Mycobacterium tuberculosis', *Clinical and Experimental Immunology*, 138(1), pp. 30–38. doi: 10.1111/j.1365-2249.2004.02593.x.

Hamasur, B., Kallenius, G. and Svenson, S. B. (1999) 'Synthesis and immunologic characterisation of Mycobacterium tuberculosis lipoarabinomannan specific oligosaccharide-protein conjugates', *Vaccine*, *17*(22), 2853–2861. doi: 10.1016/s0264-410x(99)00124-3.

Hanada, T. and Yoshimura, A. (2002) 'Regulation of cytokine signaling and inflammation', *Cytokine & Growth Factor Reviews*, 13(4), pp. 413–421. doi: 10.1016/S1359-6101(02)00026-6.

Harriff, M. J. *et al.* (2014) 'Human lung epithelial cells contain Mycobacterium tuberculosis in a late endosomal vacuole and are efficiently recognized by CD8+ T Cells', *PLoS ONE*, 9(5), pp. 1–12. doi: 10.1371/journal.pone.0097515.

Harris, J. *et al.* (2007) 'T Helper 2 Cytokines Inhibit Autophagic Control of Intracellular Mycobacterium tuberculosis', *Immunity*, 27(3), pp. 505–517. doi: 10.1016/j.immuni.2007.07.022.

Harrison D. A. (2012). The Jak/STAT pathway. *Cold Spring Harbor perspectives in biology*, 4(3), a011205. doi: 10.1101/cshperspect.a011205

Heinrich, P. C. *et al.* (1998) 'Anti-interleukin-6 monoclonal antibody induces regression of human prostate cancer xenografts in nude mice', *Prostate*, 48(1), pp. 47–53. doi: 10.1002/pros.1080.

Heinrich, P. C. *et al.* (2003) 'Principles of interleukin (IL)-6-type cytokine signalling and its regulation', *Biochemical Journal*, 374(1), pp. 1–20. doi: 10.1042/BJ20030407.

Heitmann, L. *et al.* (2014) 'The IL-13/IL-4Rα axis is involved in tuberculosis-associated pathology',

Journal of Pathology, 234(3), pp. 338–350. doi: 10.1002/path.4399.

Helming, L. and Gordon, S. (2008) 'The molecular basis of macrophage fusion', *Immunobiology*, *212*(9-10), pp. 785–793. doi: 10.1016/j.imbio.2007.09.012.

Henderson, R. A., Watkins, S. C. and Flynn, J. L. (1997) 'Activation of human dendritic cells following infection with Mycobacterium tuberculosis.', *Journal of immunology*, 159, pp. 635–643.

Hirota, K. *et al.* (2011) 'Fate mapping of interleukin 17-producing T cells in inflammatory responses', *Nat Immunol*, 12(3), pp. 255–263. doi: 10.1038/ni.1993.Fate.

Hirsch, C. S. *et al.* (1994) 'Enhancement of intracellular growth of mycobacterium tuberculosis in human monocytes by transforming growth factor-βl', *Journal of Infectious Diseases*, 170(5), pp. 1229–1237. doi: 10.1093/infdis/170.5.1229.

Hirsch, C. S. *et al.* (1997) 'In vitro restoration of T cell responses in tuberculosis and augmentation of monocyte effector function against Mycobacterium tuberculosis by natural inhibitors of transforming growth factor β', *Proceedings of the National Academy of Sciences of the United States of America*, 94(8), pp. 3926–3931. doi: 10.1073/pnas.94.8.3926.

Hiwatashi, K. *et al.* (2011) 'Suppression of SOCS3 in macrophages prevents cancer metastasis by modifying macrophage phase and MCP2/CCL8 induction', *Cancer Letters*. Elsevier Ireland Ltd, 308(2), pp. 172–180. doi: 10.1016/j.canlet.2011.04.024.

Hoff, D. R. *et al.* (2011) 'Location of Intra- and Extracellular M . tuberculosis Populations in Lungs of Mice and Guinea Pigs during Disease Progression and after Drug Treatment', *PloS one*, *6*(3), e17550. doi: 10.1371/journal.pone.0017550.

Hossain, M. M. and Norazmi, M.-N. (2013) 'Pattern recognition receptors and cytokines in Mycobacterium tuberculosis infection--the double-edged sword?', *BioMed research international*, 2013, p. 179174. doi: 10.1155/2013/179174.

Howard, A. D. and Zwilling, B. S. (1999) 'Reactivation of tuberculosis is associated with a shift from type 1 to type 2 cytokines', *International Journal of Leprosy and Other Mycobacterial Diseases*, 67(4 SUPPL.), p. 523. doi: 10.1046/j.1365-2249.1999.00791.x

Hryhorowicz, M. *et al.* (2017) 'CRISPR/Cas9 Immune System as a Tool for Genome Engineering', *Archivum Immunologiae et Therapiae Experimentalis*, 65(3), pp. 233–240. doi: 10.1007/s00005-016-0427-5.

Ishino, Y. *et al.* (1987) 'Nucleotide sequence of the iap gene, responsible for alkaline phosphatase isoenzyme conversion in Escherichia coli, and identification of the gene product', *Journal of Bacteriology*, 169(12), pp. 5429–5433. doi: 10.1128/jb.169.12.5429-5433.1987.

Ito, T. *et al.* (2012) 'CCR6 as a mediator of immunity in the lung and gut. *Experimental cell research*', *317*(5), pp. 613–619. doi: 10.1016/j.yexcr.2010.12.018.

Jain, P. *et al.* (2014) 'Specialized transduction designed for precise high-throughput unmarked deletions in Mycobacterium tuberculosis', *mBio*, 5(3), pp. 1–9. doi: 10.1128/mBio.01245-14.

Jankute, M., Byng, C. V., *et al.* (2014) 'Elucidation of a protein-protein interaction network involved in

Corynebacterium glutamicum cell wall biosynthesis as determined by bacterial two-hybrid analysis', *Glycoconjugate Journal*, 31(6), pp. 475–483. doi: 10.1007/s10719-014-9549-3.

Jankute, M., Grover, S., *et al.* (2014) 'Genetics of Mycobacterial Arabinogalactan and Lipoarabinomannan Assembly', *Microbiology spectrum*, *2*(4), MGM2–2013. doi: 10.1128/microbiolspec.MGM2-0013-2013.

Jankute, M. *et al.* (2015a) 'Assembly of the Mycobacterial Cell Wall', *Annual Review of Microbiology*, 69(1), pp. 405–423. doi: 10.1146/annurev-micro-091014-104121.

Jankute, M. *et al.* (2015b) 'Assembly of the Mycobacterial Cell Wall', *Annual Review of Microbiology*, 69(1), pp. 405–423. doi: 10.1146/annurev-micro-091014-104121.

Jankute, M. *et al.* (2017) 'Disruption of mycobacterial aftB results in complete loss of terminal β(1 → 2) arabinofuranose residues of Lipoarabinomannan', *ACS Chemical Biology*, 12(1), pp. 183–190. doi: 10.1021/acschembio.6b00898.

Jin, W. and Dong, C. (2013) 'IL-17 cytokines in immunity and inflammation', *Emerging Microbes and Infections*, 2(000), p. 0. doi: 10.1038/emi.2013.58.

Jinek, M. *et al.* (2012) 'A programmable dual-RNA-guided DNA endonuclease in adaptive bacterial immunity', *Science*, 337(6096), pp. 816–821. doi: 10.1126/science.1225829.

John J. O'Shea, Daniella M. Schwartz, Alejandro V. Villarino, Massimo Gadina, Iain B. McInnes, and A. L. (2017) 'The JAK-STAT Pathway: Impact on Human Disease and Therapeutic Intervention', *Physiology & behavior*, 176(12), pp. 139–148. doi: 10.1146/annurev-med-051113-024537.The.

Jones, B. W. *et al.* (2001) 'Different Toll-like receptor agonists induce distinct macrophage responses Abstract : We previously reported that gram-neg- ative bacterial lipopolysaccharide (LPS) activates'. *Journal of leukocyte biology*, *69*(6), 1036–1044. doi: 10.1189/jlb.69.6.1036.

Kalupahana, R. S. *et al.* (2005) 'Activation of murine dendritic cells and macrophages induced by Salmonella enterica serovar Typhimurium', *Immunology*, 115(4), pp. 462–472. doi: 10.1111/j.1365-2567.2005.02180.x.

Kamura, T. *et al.* (2004) 'VHL-box and SOCS-box domains determine binding specificity for Cul2-Rbx1 and Cul5-Rbx2 modules of ubiquitin ligases', *Genes and Development*, 18(24), pp. 3055–3065. doi: 10.1101/gad.1252404.

Kang, P. B. *et al.* (2005) 'The human macrophage mannose receptor directs Mycobacterium tuberculosis lipoarabinomannan-mediated phagosome biogenesis', *Journal of Experimental Medicine*, 202(7), pp. 987–999. doi: 10.1084/jem.20051239.

Karygianni, L. *et al.* (2020) 'Biofilm Matrixome : Extracellular Components in Structured Microbial Communities', *Trends in Microbiology*. The Author(s), 28(8), pp. 668–681. doi: 10.1016/j.tim.2020.03.016.

Kaufmann, S. H. E. (2013) 'Tuberculosis vaccines: Time to think about the next generation', *Seminars in Immunology*. Elsevier Ltd, 25(2), pp. 172–181. doi: 10.1016/j.smim.2013.04.006.

Kaur, D. *et al.* (2008) 'Lipoarabinomannan of Mycobacterium : Mannose capping by a multifunctional terminal mannosyltransferase', *Proceedings of the National Academy of Sciences*, 105(46), pp. 17973–17977. doi: 10.1073/pnas.0807761105.

Kawai, T. and Akira, S. (2006) 'TLR signaling', *Cell Death and Differentiation*, 13(5), pp. 816–825. doi: 10.1038/sj.cdd.4401850.

Khader, S. A. *et al.* (2011) 'IL-23 is required for long-term control of Mycobacterium tuberculosis and B cell follicle formation in the infected lung', *Journal of Immunology*, 187(10), pp. 5402–5407. doi: 10.4049/jimmunol.1101377.

Khan, N. *et al.* (2016) 'Alteration in the gut microbiota provokes susceptibility to tuberculosis', *Frontiers in Immunology*, 7(NOV), pp. 1–10. doi: 10.3389/fimmu.2016.00529.

Khoo, K. H. *et al.* (1995) 'Structural definition of acylated phosphatidylinositol mannosides from Mycobacterium tuberculosis: Definition of a common anchor for lipomannan and lipoarabinomannan', *Glycobiology*, 5(1), pp. 117–127. doi: 10.1093/glycob/5.1.117.

Killar, L. *et al.* (1987) 'Cloned , Ia-restricted T cells that do not produce interleukin 4 (IL 4)/ B cell stimulatory factor 1 (BSF-1) fail to help antigen-specific B Why The JI ? Submit online . • No Triage ! Every submission reviewed by practicing scientists • Fast Publicati', 138, pp. 1674–1679. Available at: http://www.ncbi.nlm.nih.gov/pubmed/2419430.

Killar, L. *et al.* (2021) 'Cloned , Ia-restricted T cells that do not produce interleukin 4 (IL 4)/ B cell stimulatory factor 1 (BSF-1) fail to help antigen-specific B cells', *Journal of immunology (Baltimore, Md. : 1950)*, *138*(6), 1674–1679.

Kindler, V. and Grau, G. E. (1989) 'The Inducing Role of Tumor Necrosis Factor in the Development of Bactericidal Granulomas during BCG Infection', 56, pp. 731–740.

Kinjyo, I. *et al.* (2002) 'SOCS1/JAB is a negative regulator of LPS-induced macrophage activation', *Immunity*, 17(5), pp. 583–591. doi: 10.1016/S1074-7613(02)00446-6.

Kleinnijenhuis, J. *et al.* (2011) 'Innate Immune Recognition of Mycobacterium tuberculosis', *Clinical and Developmental Immunology*, 2011, pp. 1–12. doi: 10.1155/2011/405310.

Kolloli, A. and Subbian, S. (2017) 'Host-Directed Therapeutic Strategies for Tuberculosis', *Frontiers in medicine*, *4*, 171.. doi: 10.3389/fmed.2017.00171.

Koo, H., Falsetta, M. L. and Klien, M. M. (2013) 'The Exopolysaccharide Matrix : A Virulence Determinant of Cariogenic Biofilm', *Journal of Dental Research*, 92(12), pp. 1065–1073. doi: 10.1177/0022034513504218.

Kovarik, P. *et al.* (1998) 'Stat1 combines signals derived from IFN-γ and LPS receptors during macrophage activation', *EMBO Journal*, 17(13), pp. 3660–3668. doi: 10.1093/emboj/17.13.3660.

Kubo, M., Hanada, T. and Yoshimura, A. (2003) 'Suppressors of cytokine signaling and immunity', *Nature Immunology*, 4(12), pp. 1169–1176. doi: 10.1038/ni1012.

Kumar, N. P. *et al.* (2015) 'Il-27 and tgfb mediated expansion of th1 and adaptive regulatory t cells expressing il-10 correlates with bacterial burden and disease severity in pulmonary tuberculosis', *Immunity, Inflammation and Disease*, 3(3), pp. 289–299. doi: 10.1002/iid3.68.

Ladel, C. H. *et al.* (1997) 'Lethal tuberculosis in interleukin-6-deficient mutant mice', *Infection and Immunity*, 65(11), pp. 4843–4849. doi: 10.1128/iai.65.11.4843-4849.1997.

Lagranderie, M. *et al.* (2000) 'Immunogenicity and protective capacity of Mycobacterium bovis BCG after oral or intragastric administration in mice', *Vaccine*, 18(13), pp. 1186–1195. doi: 10.1016/S0264-410X(99)00386-2.

Lalor, S. J. *et al.* (2011) 'Caspase-1–Processed Cytokines IL-1β and IL-18 Promote IL-17 Production by γδ and CD4 T Cells That Mediate Autoimmunity', *The Journal of Immunology*, 186(10), pp. 5738–5748. doi: 10.4049/jimmunol.1003597.

Lanoix, J., Lenaerts, A. J. and Nuermberger, E. L. (2015) 'Heterogeneous disease progression and treatment response in a C3HeB / FeJ mouse model of tuberculosis', *Disease Models & Mechanisms*, 8(6), pp. 603–610. doi: 10.1242/dmm.019513.

Lavollay, M. *et al.* (2008) 'The peptidoglycan of stationary-phase Mycobacterium tuberculosis predominantly contains cross-links generated by L,D-transpeptidation', *Journal of Bacteriology*, 190(12), pp. 4360–4366. doi: 10.1128/JB.00239-08.

Lee, A. *et al.* (2006) 'Sequencing of oligoarabinosyl units released from mycobacterial arabinogalactan by endogenous arabinanase: Identification of distinctive and novel structural motifs', *Biochemistry*, 45(51), pp. 15817–15828. doi: 10.1021/bi060688d.

Lee, S. W. *et al.* (2017) 'Suppressors of cytokine signaling in tuberculosis', *PLoS ONE*, 12(4), pp. 1–13. doi: 10.1371/journal.pone.0176377.

Lenaerts, A., Barry, C. E. and Dartois, V. (2015) 'Heterogeneity in tuberculosis pathology , microenvironments and therapeutic responses', *Immunological Reviews*, 264(1), pp. 288–307. doi: 10.1111/imr.12252.

Lenaerts, A. J. *et al.* (2007) 'Location of Persisting Mycobacteria in a Guinea Pig Model of Tuberculosis Revealed by R207910 □', *Antimicrobial agents and chemotherapy*, 51(9), pp. 3338–3345. doi: 10.1128/AAC.00276-07.

Letterio, J. J. and Roberts, A. B. (1998) 'Regulation of immune responses by neutrophils', *Annals of the New York Academy of Sciences*, 16, pp. 137–61. doi: 10.1111/nyas.12445.

Liau, N. P. D. *et al.* (2018) 'The molecular basis of JAK/STAT inhibition by SOCS1', *Nature Communications*. Springer US, 9(1), pp. 1–14. doi: 10.1038/s41467-018-04013-1.

Lin, P. L. *et al.* (2007) 'Tumor Necrosis Factor and Tuberculosis', *Journal of Investigative Dermatology*. Elsevier Masson SAS, 12(1), pp. 22–25. doi: 10.1038/sj.jidsymp.5650027.

Liu, J. *et al.* (1996) 'Mycolic acid structure determines the fluidity of the mycobacterial cell wall', *Journal of Biological Chemistry*. Â© 1996 ASBMB. Currently published by Elsevier Inc; originally published by American Society for Biochemistry and Molecular Biology., 271(47), pp. 29545–29551. doi: 10.1074/jbc.271.47.29545.

Lockhart, E., Green, A. M. and Flynn, J. L. (2006) ' IL-17 Production Is Dominated by γδ T Cells rather than CD4 T Cells during Mycobacterium tuberculosis Infection ', *The Journal of Immunology*, 177(7), pp. 4662–4669. doi: 10.4049/jimmunol.177.7.4662.

Lopez, D., Vlamakis, H. and Kolter, R. (2010) 'Biofilms', *Cold Spring Harb Perspect Biol*, 2, p. a000398. doi: 10.1101/cshperspect.a000398.

Lucey, D. R., Clerici, M. and Shearer, G. M. (1996) 'Type 1, and Type 2 cytokine dysregulation in human infectious, neoplastic, and inflammatory diseases', *Clinical Microbiology Reviews*, 9(4), pp. 532–562. doi: 10.1128/cmr.9.4.532.

Luke J. Alderwick, James Harrison, Georgina S. Lloyd, and H. L. B. and Institute (2015) 'The Mycobacterial Cell Wall—Peptidoglycan and Arabinogalactan', *Cold Spring Harb Perspect Med*, 5, pp. 1–15. doi: 10.1101/cshperspect.a021113.

Ma, X. and Trinchieri, G. (2001) 'Regulation of interleukin-12 production in antigen-presenting cells', *Advances in Immunology*, 79, pp. 55–92. doi: 10.1016/S0065-2776(01)79002-5.

Maeda, N. *et al.* (2003) 'The cell surface receptor DC-SIGN discriminates between Mycobacterium species through selective recognition of the mannose caps on lipoarabinomannan', *Journal of Biological Chemistry*, 278(8), pp. 5513–5516. doi: 10.1074/jbc.C200586200.

Maglione, P. J., Xu, J. and Chan, J. (2007) 'B Cells Moderate Inflammatory Progression and Enhance Bacterial Containment upon Pulmonary Challenge with Mycobacterium tuberculosis', *Journal of immunology*, 178, pp. 7222–7234. doi: 10.4049/jimmunol.178.11.7222.

Mahapatra, S. *et al.* (2005) 'N glycolylation of the nucleotide precursors of peptidoglycan biosynthesis of Mycobacterium spp. is altered by drug treatment', *Journal of Bacteriology*, 187(7), pp. 2341–2347. doi: 10.1128/JB.187.7.2341-2347.2005.

Marine, J. *et al.* (1999) 'SOCS1 Deficiency Causes a Lymphocyte-Dependent Perinatal Lethality', *Cell*, *98*(5), pp. 609–616. doi: 10.1016/s0092-8674(00)80048-3.

Marrakchi, H., Laneelle, M.-A. and Daffe, M. (2014) 'Review Mycolic Acids : Structures , Biosynthesis , and Beyond', *Chemistry & biology*, *21*(1), 67–85. https://doi.org/10.1016/j.chembiol.2013.11.011. doi: 10.1016/j.chembiol.2013.11.011.

Marshall, J. D. *et al.* (1999) 'Regulation of human IL-18 mRNA expression', *Clinical Immunology*, 90(1), pp. 15–21. doi: 10.1006/clim.1998.4633.

Masood, K. I. *et al.* (2013) 'Expression of M. tuberculosis-induced suppressor of cytokine signaling (SOCS) 1, SOCS3, FoxP3 and secretion of IL-6 associates with differing clinical severity of tuberculosis', *BMC Infectious Diseases*, 13(1), pp. 1–9. doi: 10.1186/1471-2334-13-13.

Massague, J. (1990) 'The transforming growth factor-β family', *Annual Review cell biology*, 6, pp. 597–641.

Mayer-Barber, K. *et al.* (2011) 'Innate and adaptive interferons suppress IL-1α and IL-1β production by distinct pulmonary myeloid subsets during Mycobacterium tuberculosis infection', *Bone*, 35(6), pp. 1023–1034. doi: 10.1016/j.immuni.2011.12.002.

Mazzarella, G. *et al.* (2003) 'T lymphocyte phenotypic profile in lung segments affected by cavitary and non-cavitary tuberculosis', *Clinical and Experimental Immunology*, 132(2), pp. 283–288. doi: 10.1046/j.1365-2249.2003.02121.x.

McAleer, J. P. and Kolls, J. K. (2014) 'Directing traffic: IL-17 and IL-22 coordinate pulmonary immune defense', *Immunology Rev*, 260(1), pp. 129–144. doi: 10.1111/imr.12183.Directing.

McKenzie, A. N. J. *et al.* (1993) 'Interleukin 13, a T-cell-derived cytokine that regulates human monocyte and B-cell function', *Proceedings of the National Academy of Sciences of the United States of America*, 90(8), pp. 3735–3739. doi: 10.1073/pnas.90.8.3735.

McNeil, M. *et al.* (1987) 'Demonstration that the galactosyl and arabinosyl residues in the cell-wall arabinogalactan of Mycobacterium leprae and Myobacterium tuberculosis are furanoid', *Carbohydrate Research*, 166(2), pp. 299–308. doi: 10.1016/0008-6215(87)80065-4.

McNeil, M., Daffe, M. and Brennan, P. J. (1990) 'Evidence for the nature of the link between the arabinogalactan and peptidoglycan of mycobacterial cell walls', *Journal of Biological Chemistry*, 265(30), pp. 18200–18206. doi: 10.1016/s0021-9258(17)44738-7.

McNeil, M., Daffe, M. and Brennan, P. J. (1991) 'Location of the mycolyl ester substituents in the cell walls of mycobacteria', *Journal of Biological Chemistry*, 266(20), pp. 13217–13223. doi: 10.1016/s0021-9258(18)98826-5.

Mcneil, M. R. *et al.* (1994) 'Enzymatic evidence for the presence of a critical terminal hexa-arabinoside in the cell walls of Mycobacterium tuberculosis', *Glycobiology*, 4(2), pp. 165–173.

Means, T. K. *et al.* (1999) 'Human Toll-Like Receptors Mediate Cellular Activation by Mycobacterium tuberculosis', *Journal of Immunology Research*, (163), pp. 3920–3927.

Medzhitov, R. and Janeway, C. A. (1998) 'An ancient system of host defense', *Current Opinion in Immunology*, 10(1), pp. 12–15. doi: 10.1016/S0952-7915(98)80024-1.

Metcalf, D. *et al.* (2002) 'Polycystic kidneys and chronic inflammatory lesions are the delayed consequences of loss of the suppressor of cytokine signaling-1 (SOCS-1)', *Proceedings of the National Academy of Sciences of the United States of America*, 99(2), pp. 943–948. doi: 10.1073/pnas.022628499.

Mihret, A. *et al.* (2013) 'Plasma cytokines and chemokines differentiate between active disease and non-active tuberculosis infection', *Journal of Infection*. Elsevier Ltd, 66(4), pp. 357–365. doi: 10.1016/j.jinf.2012.11.005.

Mikusova, K. *et al.* (2005) 'Decaprenylphosphoryl Arabinofuranose , the Donor of the D -Arabinofuranosyl Residues of Mycobacterial Arabinan , Is Formed via a Two-Step Epimerization of Decaprenylphosphoryl Ribose', *Journal of Bacteriology*, 187(23), pp. 8020–8025. doi: 10.1128/JB.187.23.8020.

Minty, A. *et al.* (1993) 'Interleukin-13 is a new human lymphokine regulating inflammatory and immune responses', *Nature*, 362(6417), pp. 248–250. doi: 10.1038/362248a0.

Miranda, M. S. *et al.* (2012) 'The Tuberculous Granuloma : An Unsuccessful Host Defence Mechanism Providing a Safety Shelter for the Bacteria ?', *Clinical & developmental immunology*, *2012*, 139127. doi: 10.1155/2012/139127.

Mishra, A. K. *et al.* (2011) 'Lipoarabinomannan and related glycoconjugates: Structure, biogenesis and role in Mycobacterium tuberculosis physiology and host-pathogen interaction', *FEMS Microbiology Reviews*, 35(6), pp. 1126–1157. doi: 10.1111/j.1574-6976.2011.00276.x.

Mogues, T. *et al.* (2001) 'The relative importance of T cell subsets in immunity and immunopathology of airborne Mycobacterium tuberculosis infection in mice', *Journal of Experimental Medicine*, 193(3), pp. 271–280. doi: 10.1084/jem.193.3.271.

Moreno, C. *et al.* (1992) 'Does antibody to mycobacterial antigens, including lipoarabinomannan, limit dissemination in childhood tuberculosis?', *Transactions of the Royal Society of Tropical Medicine and Hygiene*, 86(6), pp. 686–692. doi: 10.1016/0035-9203(92)90192-F.

Mori, H. *et al.* (2004) 'Socs3 deficiency in the brain elevates leptin sensitivity and confers resistance to diet-induced obesity', *Nature Medicine*, 10(7), pp. 739–743. doi: 10.1038/nm1071.

Mosmann, T. R. *et al.* (1986) 'Two types of murine helper T cell clone. I. Definition according to profiles of lymphokine activities and secreted proteins.', *Journal of immunology (Baltimore, Md. : 1950)*, 136(7), pp. 2348–57. Available at: http://www.ncbi.nlm.nih.gov/pubmed/2419430.

Murray, P. J. (2007) 'The JAK-STAT Signaling Pathway: Input and Output Integration', *The Journal of Immunology*, 178(5), pp. 2623–2629. doi: 10.4049/jimmunol.178.5.2623.

Nagabhushanam, V. *et al.* (2003) 'Innate inhibition of adaptive immunity: Mycobacterium tuberculosis-induced IL-6 inhibits macrophage responses to IFN-gamma', *J Immunol*, 171(9), pp. 4750–4757. doi: 10.4049/jimmunol.171.9.4750.

Narazaki, M. *et al.* (1998) 'Three distinct domains of SSI-1/SOCS-1/JAB protein are required for its suppression of interleukin 6 signaling', *Immunology*, 95, pp. 13130–13134. Available at: https://www.ncbi.nlm.nih.gov/pmc/articles/PMC23734/pdf/pq013130.pdf (Accessed: 8 January 2018).

Nicholas, C. and Lesinski, G. B. (2011) 'The Jak-STAT Signal Transduction Pathway in Melanoma'. doi: 10.5772/18876.

Nigou, J. *et al.* (2002) 'Mycobacterial lipoarabinomannans: Modulators of dendritic cell function and the apoptotic response', *Microbes and Infection*, 4(9), pp. 945–953. doi: 10.1016/S1286-4579(02)01621-0.

Nigou, J. *et al.* (2004) 'Structural analysis of mycobacterial lipoglycans', *Applied Biochemistry and Biotechnology - Part A Enzyme Engineering and Biotechnology*, 118(1–3), pp. 253–267. doi: 10.1385/ABAB:118:1-3:253.

Nigou, J. *et al.* (2008) 'Mannan Chain Length Controls Lipoglycans Signaling via and Binding to TLR2', *The Journal of Immunology*, 180(10), pp. 6696–6702. doi: 10.4049/jimmunol.180.10.6696.

Nigou, J., Gilleron, M. and Puzo, G. (2003) 'Lipoarabinomannans : from structure to biosynthesis', *Biochimie*, *85*(1-2), pp. 153–166. doi: 10.1016/s0300-9084(03)00048-8.

North, R. J. and Jung, Y. (2004) 'Immunity to Tuberculosis', *Annual review of Immunology*, 22, pp. 599–623. doi: 10.1146/annurev.immunol.22.012703.104635.

Nunes-Alves, C. *et al.* (2014) 'In search of a new paradigm for protective immunity to TB', *Nature Reviews Microbiology*. Nature Publishing Group, 12(4), pp. 289–299. doi: 10.1038/nrmicro3230.

Öhlinger, K., Absenger-Novak, M., Meindl, C., Ober, J., & Fröhlich, E. (2020). Different Sensitivity of Macrophages to Phospholipidosis Induction by Amphiphilic Cationic Drugs. International journal of molecular sciences, 21(21), 8391. doi: 10.3390/ijms21218391

O'Leary, S., O'Sullivan, M. P. and Keane, J. (2011) 'IL-10 blocks phagosome maturation in Mycobacterium tuberculosis-infected human macrophages', *American Journal of Respiratory Cell and Molecular Biology*, 45(1), pp. 172–180. doi: 10.1165/rcmb.2010-0319OC.

O'Shea, J. J. and Murray, P. J. (2008) 'Cytokine Signaling Modules in Inflammatory Responses', *Immunity*, 28(4), pp. 477–487. doi: 10.1016/j.immuni.2008.03.002.

O'Shea, J. J. and Paul, W. E. (2002) 'Regulation of TH 1 differentiation – controlling the controllers', *Nature Immunology*, 3(6), pp. 506–508. doi: 10.1126/science.1070884.

Ogata, Hisanobu *et al.* (2006) 'Deletion of the SOCS3 Gene in Liver Parenchymal Cells Promotes Hepatitis-Induced Hepatocarcinogenesis', *Gastroenterology*, 131(1), pp. 179–193. doi: 10.1053/j.gastro.2006.04.025.

Ogata, H. *et al.* (2006) 'Loss of SOCS3 in the liver promotes fibrosis by enhancing STAT3-mediated TGF-β1 production', *Oncogene*, 25(17), pp. 2520–2530. doi: 10.1038/sj.onc.1209281.

Ojha, A. *et al.* (2005) 'GroEL1 : A Dedicated Chaperone Involved in Mycolic Acid Biosynthesis during Biofilm Formation in Mycobacteria', *Cell*, *123*(5), pp. 861–873. doi: 10.1016/j.cell.2005.09.012.

Ojha, A. K. *et al.* (2008) 'Growth of Mycobacterium tuberculosis biofilms containing free mycolic acids and harbouring drug-tolerant bacteria', *Molecular microbiology*, *69*(1), pp. 164–174. doi: 10.1111/j.1365-2958.2008.06274.x.

Orme, I. M. (2014) 'A new unifying theory of the pathogenesis of tuberculosis', *Tuberculosis*. Elsevier Ltd, 94(1), pp. 8–14. doi: 10.1016/j.tube.2013.07.004.

Orme, I. M. and Cooper, A. M. (1999) 'Cytokine/chemokine cascades in immunity to tuberculosis', *Viewpoint Immunology today*, 5699(7), pp. 307–312.

Oswald, I. P. *et al.* (1992) 'Interleukin 10 inhibits macrophage microbicidal activity by blocking the endogenous production of tumor necrosis factor α required as a costimulatory factor for interferon γ-induced activation', *Proceedings of the National Academy of Sciences of the United States of America*, 89(18), pp. 8676–8680. doi: 10.1073/pnas.89.18.8676.

Othieno, C. *et al.* (1999) 'Interaction of Mycobacterium tuberculosis-induced transforming growth factor β1 and interleukin-10', *Infection and Immunity*, 67(11), pp. 5730–5735. doi: 10.1128/iai.67.11.5730-5735.1999.

Pang, J. M. *et al.* (2012) 'The Polyketide Pks1 Contributes to Biofilm Formation in Mycobacterium tuberculosis', *Journal of Bacteriology*, 194(3), pp. 715–721. doi: 10.1128/JB.06304-11.

Pawlowski, A. *et al.* (2012) 'Tuberculosis and HIV Co-Infection', *PLoS pathogens*, *8*(2), e1002464. doi: 10.1371/journal.ppat.1002464.

Peddireddy, V., Doddam, S. N. and Ahmed, N. (2017) 'Mycobacterial dormancy systems and host responses in tuberculosis', *Frontiers in Immunology*, 8(FEB), pp. 1–19. doi: 10.3389/fimmu.2017.00084.

Peng, W. *et al.* (2012) 'The galactosamine residue in mycobacterial arabinogalactan is α-linked', *Journal of Organic Chemistry*, 77(21), pp. 9826–9832. doi: 10.1021/jo301393s.

Peñuelas-urquides, K. *et al.* (2013) 'Measuring of Mycobacterium tuberculosis growth . A correlation of the optical measurements with colony forming units', *Brazilian journal of microbiology : [publication of the Brazilian Society for Microbiology]*, *44*(1), pp. 287–289. doi: 10.1590/S1517-83822013000100042.

Perez, E. E. *et al.* (2012) 'Editing Using Zinc-Finger Nucleases', *Nat Biotechnol*, 26(7), pp. 808–816. doi:

10.1038/nbt1410.

Peyron, P. *et al.* (2008) 'Foamy Macrophages from Tuberculous Patients ' Granulomas Constitute a Nutrient-Rich Reservoir for M . tuberculosis Persistence', *PLoS pathogens*, *4*(11), e1000204. pp. 1–14. doi: 10.1371/journal.ppat.1000204.

Picard, C. *et al.* (2002) 'Inherited interleukin-12 deficiency: IL12B genotype and clinical phenotype of 13 patients from six kindreds', *American Journal of Human Genetics*, 70(2), pp. 336–348. doi: 10.1086/338625.

Pieters, J. (2008) 'Mycobacterium tuberculosis and the Macrophage: Maintaining a Balance', *Cell Host and Microbe*, 3(6), pp. 399–407. doi: 10.1016/j.chom.2008.05.006.

Plummer, E. C. (1928) 'Pulmonary tuberculosis diagnosis and treatment', *British Medical Journal*, 1(3507), pp. 523–524. doi: 10.1136/bmj.1.3507.523-b.

Prideaux, B. *et al.* (2015) 'Mass spectrometry imaging of levofloxacin distribution in TB-infected pulmonary lesions by MALDI-MSI and continuous liquid microjunction surface sampling', *International Journal of Mass Spectrometry*. Elsevier B.V., 377, pp. 699–708. doi: 10.1016/j.ijms.2014.08.024.

Qi, L. S. *et al.* (2013) 'Repurposing CRISPR as an RNA-γuided platform for sequence-specific control of gene expression', *Cell*, 152(5), pp. 1173–1183. doi: 10.1016/j.cell.2013.02.022.

Quesniaux, V. J. *et al.* (2004) 'Toll-Like Receptor 2 (TLR2)-Dependent-Positive and TLR2-Independent-Negative Regulation of Proinflammatory Cytokines by Mycobacterial Lipomannans', *The Journal of Immunology*, 172(7), pp. 4425–4434. doi: 10.4049/jimmunol.172.7.4425.

R. Brosch, S. V. Gordon, M. Marmiesse, P. Brodin, C. Buchrieser, K. Eiglmeier, T. Garnier, C. Gutierrez, G. Hewinson, K. Kremer, L. M. Parsons, A. S. Pym, S. Samper, D. van Soolingen, and S. T. C. (2002) 'A new evolutionary scenario for the Mycobacterium tuberculosis complex: Commentary', *Proceedings of the National Academy of Sciences*, 99(6), pp. 3684–3689. doi: 10.1073/pnas.052548299.

Ramakrishnan, L. (2012) 'Revisiting the role of the granuloma in tuberculosis', *Nature Reviews Immunology*. Nature Publishing Group, 12(5), pp. 352–366. doi: 10.1038/nri3211.

Ran, F. A. *et al.* (2013) 'Genome engineering using the CRISPR-Cas9 system', *Nature Protocols*, 8(11), pp. 2281–2308. doi: 10.1038/nprot.2013.143.

Rana, A. K. *et al.* (2012) 'Ppm1-Encoded Polyprenyl Monophosphomannose Synthase Activity Is Essential for Lipoglycan Synthesis and Survival in Mycobacteria', *PloS one*, *7*(10), e48211. pp. 1–8. doi: 10.1371/journal.pone.0048211.

Raymond, J. B. *et al.* (2005) 'Identification of the namH gene, encoding the hydroxylase responsible for the N-glycolylation of the mycobacterial peptidoglycan', *Journal of Biological Chemistry*. Â© 2005 ASBMB. Currently published by Elsevier Inc; originally published by American Society for Biochemistry and Molecular Biology., 280(1), pp. 326–333. doi: 10.1074/jbc.M411006200.

Redford, P. S., Murray, P. J. and O'Garra, A. (2011) 'The role of IL-10 in immune regulation during M. tuberculosis infection', *Mucosal Immunology*, 4(3), pp. 261–270. doi: 10.1038/mi.2011.7.

Reed, J. M., Branigan, P. J. and Bamezai, A. (2008) 'Interferon gamma enhances clonal expansion and

survival of CD4+ T cells', *Journal of Interferon and Cytokine Research*, 28(10), pp. 611–622. doi: 10.1089/jir.2007.0145.

Richards, J. P. and Ojha, A. K. (2014) 'Mycobacterial Biofilms', *Microbiology spectrum*, *2*(5), 10.1128/microbiolspec.MGM2-0004-2013., pp. 1–11. doi: 10.1128/microbiolspec.MGM2-0004-2013.

Rivero-Lezcano, O. . *et al.* (2010) 'CCL 20 is overexpressed in Mycobacterium tuberculosis -infected monocytes and inhibits the production of reactive oxygen species (ROS)', *Clinical and experimental immunology*, *162*(2), pp. 289–297. doi: 10.1111/j.1365-2249.2010.04168.x.

Rock, J. (2019) 'Tuberculosis drug discovery in the CRISPR era', *PLoS Pathogens*, 15(9), pp. 1–10. doi: 10.1371/journal.ppat.1007975.

Rock, J. M. *et al.* (2017) 'Programmable transcriptional repression in mycobacteria using an orthogonal CRISPR interference platform', *Nature Microbiology*. Nature Publishing Group, 2(February), pp. 1–9. doi: 10.1038/nmicrobiol.2016.274.

Rodrigues, L. C., Diwan, V. K. and Wheeler, J. G. (1993) 'Protective effect of bcg against tuberculous meningitis and miliary tuberculosis: A meta-analysis', *International Journal of Epidemiology*, 22(6), pp. 1154–1158. doi: 10.1093/ije/22.6.1154.

Rothchild, A. C. *et al.* (2017) 'Role of Granulocyte-Macrophage Colony- Stimulating Factor Production by T Cells during Mycobacterium tuberculosis Infection'. *mBio*, *8*(5), e01514-17. doi: 10.1128/mBio.01514-17.

Russell, D. G. (2001) 'Mycobacterium tuberculosis: Here today, and here tomorrow', *Nature Reviews Molecular Cell Biology*, 2(8), pp. 569–577. doi: 10.1038/35085034.

Sambandan, D. *et al.* (2013) 'Keto-Mycolic acid-dependent pellicle formation confers tolerance to drug-sensitive Mycobacterium tuberculosis', *mBio*, 4(3), pp. 1–10. doi: 10.1128/mBio.00222-13.

Sanceau, J. *et al.* (1989) 'IFN-γ Is an Essential Cosignal for Triggering IFN-β2/BSF-2/IL-6 Gene Expression in Human Monocytic Cell Lines', *Annals of the New York Academy of Sciences*, 557(1), pp. 130–143. doi: 10.1111/j.1749-6632.1989.tb24006.x.

Saraav, I., Singh, S. and Sharma, S. (2014) 'Outcome of Mycobacterium tuberculosis and Toll-like receptor interaction: Immune response or immune evasion?', *Immunology and Cell Biology*, 92(9), pp. 741–746. doi: 10.1038/icb.2014.52.

Sassetti, C. M., Boyd, D. H. and Rubin, E. J. (2003) 'Genes required for mycobacterial growth defined by high density mutagenesis', *Molecular Microbiology*, 48(1), pp. 77–84. doi: 10.1046/j.1365-2958.2003.03425.x.

Saunders, B. M. *et al.* (2000) 'Interleukin-6 induces early gamma interferon production in the infected lung but is not required for generation of specific immunity to Mycobacterium tuberculosis infection', *Infection and Immunity*, 68(6), pp. 3322–3326. doi: 10.1128/IAI.68.6.3322-3326.2000.

Schäfer, G. *et al.* (2009) 'Non-opsonic recognition of mycobacterium tuberculosis by phagocytes', *Journal of Innate Immunity*, 1(3), pp. 231–243. doi: 10.1159/000173703.

Schleifer, K. H. and Kandler, O. (1972) 'Peptidoglycan types of bacterial cell walls and their taxonomic

implications.', *Bacteriological reviews*, 36(4), pp. 407–477. doi: 10.1128/mmbr.36.4.407-477.1972.

Schnaar, R. L. (2015) 'Glycans and glycan binding proteins in immune regulation: A concise introduction to glycobiology for the allergist', *The Journal of allergy and clinical immunology*, *135*(3), pp. 609–615. doi: 10.1016/j.jaci.2014.10.057.Glycans.

Schneider, Bianca, E. *et al.* (2010) 'A role for IL-18 in protective immunity against Mycobacterium tuberculosis', *European journal of immunology*, *40*(2), pp. 396–405. doi: 10.1002/eji.200939583.A.

Schroder, K. *et al.* (2004) 'Interferon-γ: an overview of signals, mechanisms and functions', *Journal of Leukocyte Biology*, 75(2), pp. 163–189. doi: 10.1002/eji.200939583.

Schutyser, E., Struyf, S. and Damme, J. Van (2003) 'The CC chemokine CCL20 and its receptor CCR6', 14, Cytokine & Growth Factor Reviews 14 pp. 409–426. doi: 10.1016/S1359-6101(03)00049-2.

Seidel, M. *et al.* (2007) 'Identification of a novel arabinofuranosyltransferase AftB involved in a terminal step of cell wall arabinan biosynthesis in Corynebacterianeae, such as Corynebacterium glutamicum and Mycobacterium tuberculosis', *Journal of Biological Chemistry*, 282(20), pp. 14729–14740. doi: 10.1074/jbc.M700271200.

Serbina, N. V., Lazarevic, V. and Flynn, J. L. (2001) ' CD4 + T Cells Are Required for the Development of Cytotoxic CD8 + T Cells During Mycobacterium tuberculosis Infection ', *The Journal of Immunology*, 167(12), pp. 6991–7000. doi: 10.4049/jimmunol.167.12.6991.

Serbina, N. V and Flynn, J. O. A. L. (1999) 'Early Emergence of CD8 ♂ T Cells Primed for Production of Type 1 Cytokines in the Lungs of Mycobacterium tuberculosis -Infected Mice', 67(8), pp. 3980–3988.

Severn, W. B. *et al.* (1998) 'Chemical and spectroscopic characterisation of the phosphatidylinositol manno-oligosaccharides from mycobacterium bovis AN5 and WAg201 and mycobacterium smegnzatis mc2 155', *Carbohydrate Research*, 308(3–4), pp. 397–408. doi: 10.1016/S0008-6215(98)00108-6.

Shammari, B. Al *et al.* (2015) 'The Extracellular Matrix Regulates Granuloma Necrosis in Tuberculosis', *Journal of Infectious Diseases*, 212(3), pp. 463–473. doi: 10.1093/infdis/jiv076.

Shi, L. *et al.* (2006) 'The Carboxy Terminus of EmbC from Mycobacterium smegmatis Mediates Chain Length Extension of the Arabinan in Lipoarabinomannan * □', *Journal of Biological Chemistry*. Â© 2006 ASBMB. Currently published by Elsevier Inc; originally published by American Society for Biochemistry and Molecular Biology., 281(28), pp. 19512–19526. doi: 10.1074/jbc.M513846200.

Singh, A. K. *et al.* (2016) 'Investigating essential gene function in *Mycobacterium tuberculosis* using an efficient CRISPR interference system', *Nucleic Acids Research*, 44(18), pp. e143–e143. doi: 10.1093/nar/gkw625.

Skovierov, H. *et al.* (2009) 'AftD , a novel essential arabinofuranosyltransferase from mycobacteria' *Glycobiology*, *19*(11), pp. 1235–1247. doi: 10.1093/glycob/cwp116.

Sneath, P. (2007) 'The species concept', *Microbiology Today*, 34(1), p. 45. doi: 10.1017/cbo9781139060196.016.

Van Snick, J. (1990) 'Interleukin-6: an overview', *Annual review of immunology*, *8*, pp 253–278. doi: 10.1146/annurev.iy.08.040190.001345.

Sreevatsan, S. *et al.* (1997) 'Restricted structural gene polymorphism in the Mycobacterium tuberculosis complex indicates evolutionarily recent global dissemination', *Proceedings of the National Academy of Sciences of the United States of America*, 94(18), pp. 9869–9874. doi: 10.1073/pnas.94.18.9869.

Srivastava, V. *et al.* (2009) 'Toll-like receptor 2 and DC-SIGNR1 differentially regulate suppressors of cytokine signaling 1 in dendritic cells during Mycobacterium tuberculosis infection', *Journal of Biological Chemistry*, 284(38), pp. 25532–25541. doi: 10.1074/jbc.M109.006221.

Starr, R. *et al.* (1998) 'Liver degeneration and lymphoid deficiencies in mice lacking suppressor of cytokine signaling-1', *Proceedings of the National Academy of Sciences of the United States of America*, 95(24), pp. 14395–14399. doi: 10.1073/pnas.95.24.14395.

Stoodley, P. *et al.* (2002) 'Biofilms as Complex Differentiated Communities', *Annual Review of Microbiology*, 56, pp. 187–209. doi: 10.1146/annurev.micro.56.012302.160705.

Sugawara, I. *et al.* (2000) 'IL-4 is required for defense against mycobacterial infection', *Microbiology and Immunology*, 44(12), pp. 971–979. doi: 10.1111/j.1348-0421.2000.tb02592.x.

Sukegawa, S. *et al.* (2014) 'Suppressor of cytokine signaling 1 counteracts rhesus macaque TRIM5α-induced inhibition of human immunodeficiency virus type-1 production', *PLoS ONE*, 9(10). doi: 10.1371/journal.pone.0109640.

Takahashi, R. *et al.* (2011) 'SOCS1 is essential for regulatory T cell functions by preventing loss of Foxp3 expression as well as IFN-γ and IL-17A production', *Journal of Experimental Medicine*, 208(10), pp. 2055–2067. doi: 10.1084/jem.20110428.

Takayama, K., Wang, L. and David, H. L. (1972) 'Effect of isoniazid on the in vivo mycolic acid synthesis, cell growth, and viability of Mycobacterium tuberculosis.', *Antimicrobial agents and chemotherapy*, 2(1), pp. 29–35. doi: 10.1128/AAC.2.1.29.

Takeda, K. and Akira, S. (2005) 'Toll-like receptors in innate immunity', *International Immunology*, 17(1), pp. 1–14. doi: 10.1093/intimm/dxh186.

Taleb, S. *et al.* (2009) 'Loss of SOCS3 expression in T cells reveals a regulatory role for interleukin-17 in atherosclerosis', *Journal of Experimental Medicine*, 206(10), pp. 2067–2077. doi: 10.1084/jem.20090545.

Tamiya, T. *et al.* (2011) 'Suppressors of cytokine signaling (SOCS) proteins and JAK/STAT pathways: Regulation of T-cell inflammation by SOCS1 and SOCS3', *Arteriosclerosis, Thrombosis, and Vascular Biology*, 31(5), pp. 980–985. doi: 10.1161/ATVBAHA.110.207464.

Tanaka, K. *et al.* (2008) 'Loss of Suppressor of Cytokine Signaling 1 in Helper T Cells Leads to Defective Th17 Differentiation by Enhancing Antagonistic Effects of IFN- γ on STAT3 and Smads'. *Journal of immunology (Baltimore, Md. : 1950)*, *180*(6), 3746–3756. doi: 10.4049/jimmunol.180.6.3746.

Tebruegge, M. *et al.* (2015) 'Mycobacteria-specific cytokine responses detect tuberculosis infection and distinguish latent from active tuberculosis', *American Journal of Respiratory and Critical Care Medicine*, 192(4), pp. 485–499. doi: 10.1164/rccm.201501-0059OC.

Teitelbaum, R. *et al.* (1998) 'A mAb recognizing a surface antigen of Mycobacterium tuberculosis enhances host survival', *Proceedings of the National Academy of Sciences of the United States of America*, 95(26), pp. 15688–15693. doi: 10.1073/pnas.95.26.15688.

Thoma-uszynski, S. *et al.* (2001) 'Induction of Direct Antimicrobial Activity Through Mammalian Toll-Like Receptors', *Science*, 291(February), pp. 1544–1548. doi: 10.1126/science.291.5508.1544.

Toossi, Z. *et al.* (1995) 'Enhanced production of TGF-β by blood monocytes from patients with active tuberculosis and presence of TGF-β in tuberculous granulomatous lung lesions', *Journal of immunology (Baltimore, Md. : 1950)*, 154(1), pp. 465–46573.

Torisu, T. *et al.* (2007) 'The dual function of hepatic SOCS3 in insulin resistance in vivo', *Genes to Cells*, 12(2), pp. 143–154. doi: 10.1111/j.1365-2443.2007.01044.x.

Torisu, T. *et al.* (2008) 'Suppressor of Cytokine Signaling 1 Protects Mice against Concanavalin A–Induced Hepatitis by Inhibiting Apoptosis', *Hepatology (Baltimore, Md.)*, *47*(5), pp. 1644–1654. doi: 10.1002/hep.22214.

Trunz, B. B., Fine, P. and Dye, C. (2006) 'Effect of BCG vaccination on childhood tuberculous meningitis and miliary tuberculosis worldwide: a meta-analysis and assessment of cost-effectiveness', *Lancet*, 367(9517), pp. 1173–1180. doi: 10.1016/S0140-6736(06)68507-3.

Tsai, M. C. *et al.* (2006) 'Characterization of the tuberculous granuloma in murine and human lungs : cellular composition and relative tissue oxygen tension', *Cellular microbiology*, *8*(2), pp. 218–232. doi: 10.1111/j.1462-5822.2005.00612.x.

Tsenova, L. *et al.* (1999) 'Tumor necrosis factor ⎵ is a determinant of pathogenesis and disease progression in mycobacterial infection in the central', 96(May), pp. 5657–5662.

Umemura, M. *et al.* (2003) 'Interleukin-15 as an immune adjuvant to increase the efficacy of Mycobacterium bovis bacillus Calmette-Guérin vaccination', *Infection and Immunity*, 71(10), pp. 6045–6048. doi: 10.1128/IAI.71.10.6045-6048.2003.

Umemura, M. *et al.* (2007) ' IL-17-Mediated Regulation of Innate and Acquired Immune Response against Pulmonary Mycobacterium bovis Bacille Calmette-Guérin Infection ', *The Journal of Immunology*, 178(6), pp. 3786–3796. doi: 10.4049/jimmunol.178.6.3786.

Venkataswamy, M. M. *et al.* (2012) 'In vitro culture medium influences the vaccine efficacy of Mycobacterium bovis BCG', *Vaccine*, 30(6), pp. 1038–1049. doi: 10.1016/j.vaccine.2011.12.044.

Vergne, I., Gilleron, M. and Nigou, J. (2015) 'Manipulation of the endocytic pathway and phagocyte functions by Mycobacterium tuberculosis lipoarabinomannan', *Frontiers in cellular and infection microbiology*, *4*, 187. pp. 1–9. doi: 10.3389/fcimb.2014.00187.

Via, L. E. *et al.* (2008) 'Tuberculous Granulomas Are Hypoxic in Guinea Pigs , Rabbits , and Nonhuman Primates □', *Infection and Immunity*, 76(6), pp. 2333–2340. doi: 10.1128/IAI.01515-07.

Via, L. E. *et al.* (2012) 'Infection Dynamics and Response to Chemotherapy in a Rabbit Model of Tuberculosis using [18 F] 2-Fluoro-Deoxy- D -Glucose Positron Emission Tomography and Computed Tomography', *Antimicrobial Agents and Chemotherapy*, 56(8), pp. 4391–4402. doi: 10.1128/AAC.00531-12.

Vieira, P. *et al.* (1991) 'Isolation and expression of human cytokine synthesis inhibitory factor cDNA clones: Homology to Epstein-Barr virus open reading frame BCRFI', *Proceedings of the National Academy of Sciences of the United States of America*, 88(4), pp. 1172–1176. doi: 10.1073/pnas.88.4.1172.

Vignal, C. *et al.* (2003) ' Lipomannans, But Not Lipoarabinomannans, Purified from Mycobacterium chelonae and Mycobacterium kansasii Induce TNF-α and IL-8 Secretion by a CD14-Toll-Like Receptor 2-Dependent Mechanism ', *The Journal of Immunology*, 171(4), pp. 2014–2023. doi: 10.4049/jimmunol.171.4.2014.

Vignali, D. A. . and Kuchroo, V. . (2014) 'IL-12 Family Cytokines: Immunological Playmakers', *Nature immunology*, *13*(8), pp. 722–728. doi: 10.1038/ni.2366.IL-12.

Vilchèze, C. and Kremer, L. (2017) 'Acid-Fast Positive and Acid-Fast Negative Mycobacterium tuberculosis : The Koch Paradox'. *Microbiology spectrum*, *5*(2), doi: 10.1128/microbiolspec.TBTB2-0003-2015.

Vincent, A. T. *et al.* (2018) 'The mycobacterial cell envelope: A relict from the past or the result of recent evolution?', *Frontiers in Microbiology*, 9(OCT), pp. 1–9. doi: 10.3389/fmicb.2018.02341.

Visintin, A. *et al.* (2001) 'Regulation of Toll-Like Receptors in Human Monocytes and Dendritic Cells', *The Journal of Immunology*, 166(1), pp. 249–255. doi: 10.4049/jimmunol.166.1.249.

Waiboci, L. W. *et al.* (2007) 'Both the Suppressor of Cytokine Signaling 1 (SOCS-1) Kinase Inhibitory Region and SOCS-1 Mimetic Bind to JAK2 Autophosphorylation Site: Implications for the Development of a SOCS-1 Antagonist', *The Journal of Immunology*, 178(8), pp. 5058–5068. doi: 10.4049/jimmunol.178.8.5058.

Wajant, H., Pfizenmaier, K. and Scheurich, P. (2003) 'Tumor necrosis factor signaling', *Cell Death and Differentiation*, 10(1), pp. 45–65. doi: 10.1038/sj.cdd.4401189.

Wan, N. *et al.* (2018) 'Bacterial Metabolism During Biofilm Growth Investigated by 13 C Tracing', *Frontiers in microbiology*, *9*, 2657, pp. 1–9. doi: 10.3389/fmicb.2018.02657.

Wang, L. *et al.* (2015) 'Synthetic and Immunological Studies of Mycobacterial Lipoarabinomannan Oligosaccharides and Their Protein Conjugates', *Journal of Organic Chemistry*, 80(20), pp. 10060–10075. doi: 10.1021/acs.joc.5b01686.

Watanabe, M. *et al.* (2001) 'Separation and characterization of individual mycolic acids in representative mycobacteria', *Microbiology*, 147(7), pp. 1825–1837. doi: 10.1099/00221287-147-7-1825.

Watanabe, M. *et al.* (2002) 'Location of functional groups in mycobacterial meromycolate chains; the recognition of new structural principles in mycolic acids', *Microbiology*, 148(6), pp. 1881–1902. doi: 10.1099/00221287-148-6-1881.

Weaver, C. T. *et al.* (2007) 'IL-17 family cytokines and the expanding diversity of effector T cell lineages', *Annual Review of Immunology*, 25, pp. 821–852. doi: 10.1146/annurev.immunol.25.022106.141557.

WHO (2020) *Global Tuberculosis Report*.

WHO (2021) *Global Tuberculosis report*.

Whyte, C. S. *et al.* (2011) 'Suppressor of cytokine signaling (SOCS)1 is a key determinant of differential macrophage activation and function', *Journal of Leukocyte Biology*, 90(5), pp. 845–854. doi: 10.1189/jlb.1110644.

Winder, F. G. and Collins, P. B. (1970) 'Inhibition by Isoniazid of Synthesis of Mycolic Acids in', *Journal of General Microbiology*, 63, pp. 41–48.

Wirth, T. *et al.* (2008) 'Origin, spread and demography of the Mycobacterium tuberculosis complex', *PLoS Pathogens*, 4(9). doi: 10.1371/journal.ppat.1000160.

Wong, K. and Jacobs, W. R. (2016) 'Postprimary Tuberculosis and Macrophage Necrosis : Is There a Big Connection?', *mBio*, 7(1), pp. e01589-15. doi: 10.1128/mBio.01589-15.Copyright.

Yasukawa, H, Sakamoto H, Masuhara M, Sasaki A, Wakioka T, Ohtsuka S, Imaizumi T, Matsuda T, N. I. J. and Y. A. (1999) 'The JAK-binding protein JAB inhibits Janus tyrosine kinase activity through binding in the activation loop', *The EMBO Journal*, 18(5), pp. 1309–1320. doi: 10.1093/emboj/18.5.1309.

Ying, S. *et al.* (1997) 'Expression of IL-4 and IL-5 mRNA and protein product by CD4+ and CD8+ T cells, eosinophils, and mast cells in bronchial biopsies obtained from atopic and nonatopic (intrinsic) asthmatics', *Journal of immunology*, 158, pp. 3539–3544.

Yoshida, T. *et al.* (2004) 'SOCS1 is a suppressor of liver fibrosis and hepatitis-induced carcinogenesis', *Journal of Experimental Medicine*, 199(12), pp. 1701–1707. doi: 10.1084/jem.20031675.

Yoshimura, A. *et al.* (2012) 'SOCS, inflammation, and autoimmunity', *Frontiers in Immunology*, 3(MAR), pp. 1–9. doi: 10.3389/fimmu.2012.00020.

Yoshimura, A., Naka, T. and Kubo, M. (2007) 'SOCS proteins, cytokine signalling and immune regulation', *Nature Reviews Immunology*, 7(6), pp. 454–465. doi: 10.1038/nri2093.

Zhang, S. Y. *et al.* (2008) 'Inborn errors of interferon (IFN)-mediated immunity in humans: Insights into the respective roles of IFN-α/β, IFN-γ, and IFN-λ in host defense', *Immunological Reviews*, 226(1), pp. 29–40. doi: 10.1111/j.1600-065X.2008.00698.x.

Zhu, B. *et al.* (2018) 'Tuberculosis vaccines: Opportunities and challenges', *Respirology*, 23(4), pp. 359–368. doi: 10.1111/resp.13245.

Zink, A. *et al.* (2001) 'Molecular analysis of skeletal tuberculosis in an ancient Egyptian population', *Journal of medical microbiology*, *50*(4), pp. 355–366. doi: 10.1099/0022-1317-50-4-355.

Appendices

Appendix 1

Alditol acetate derivatized carbohydrates extracted from *aftC* repressed *M. bovis* BCG biofilms

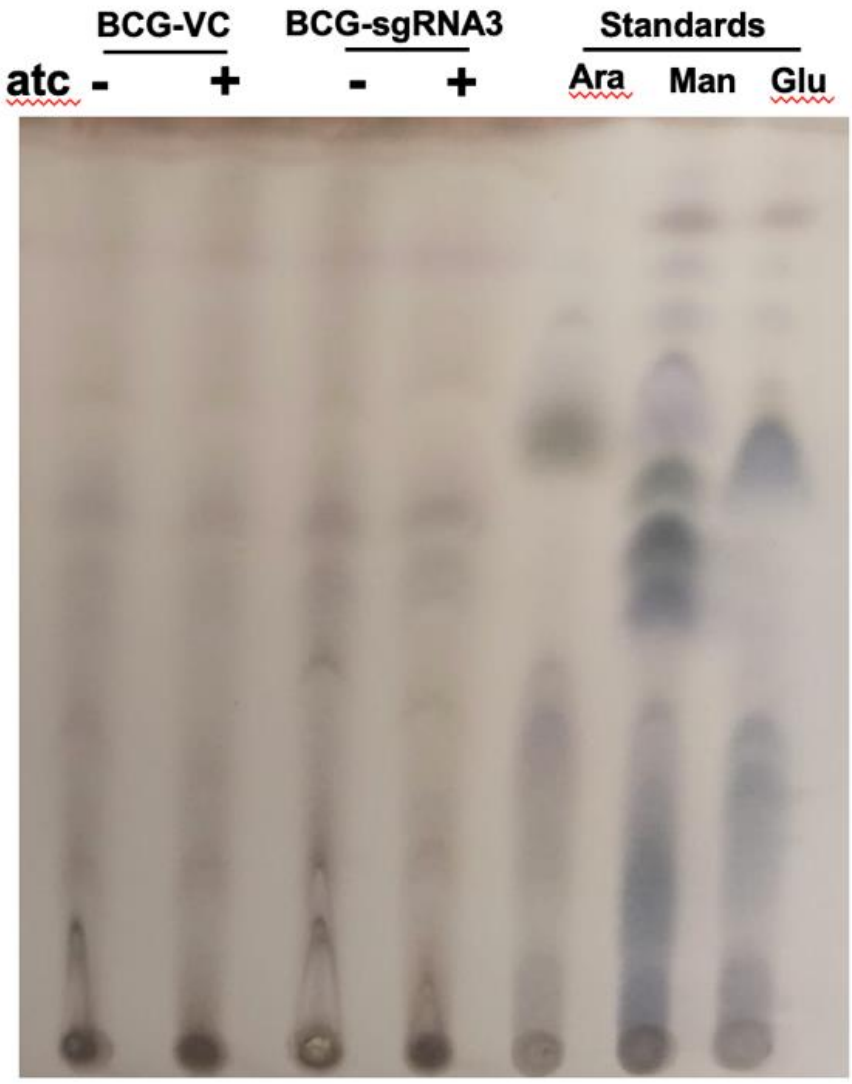

Appendix 2

Chromatograms of alditol acetate derivatized carbohydrates extracted from planktonic and biofilms of *aftC* repressed *M. bovis* BCG

Standards (Rhamnose, Fructose, Ribose, Arabinose, Mannose, Galactose, Glucose, Inositol)

5 Alditol Mix 1

Sample Name:	**Alditol Mix 1**	*Injection Volume:*	**1.0**
Vial Number:	**2**	*Channel:*	**FID**
Sample Type:	**unknown**	*Wavelength:*	**n.a.**
Control Program:	**Alditol Acetate I 500spl**	*Bandwidth:*	**n.a.**
Quantif. Method:	**Alditol Acetate**	*Dilution Factor:*	**1.0000**
Recording Time:	**15/2/2021 14:26**	*Sample Weight:*	**1.0000**
Run Time (min):	**20.00**	*Sample Amount:*	**1.0000**

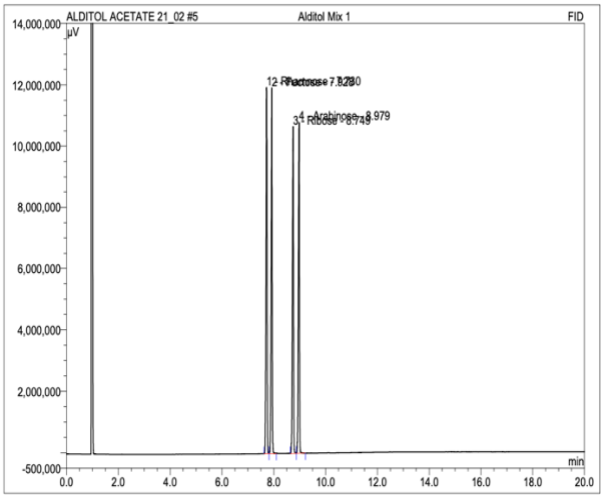

No.	Ret.Time min	Peak Name	Height µV	Area µV*min	Rel.Area %	Amount
1	7.73	Rhamnose	11945368.00	553260.8	26.07	n.a.
2	7.93	Fuctose	11926477.00	548788.8	25.86	n.a.
3	8.75	Ribose	10659075.00	511700.7	24.11	n.a.
4	8.98	Arabinose	10790673.00	508568.3	23.96	n.a.
Total:			45321593.00	2122318.56	100.00	0.000

7 Alditol Mix 2

Sample Name:	**Alditol Mix 2**	*Injection Volume:*	**1.0**
Vial Number:	**3**	*Channel:*	**FID**
Sample Type:	**unknown**	*Wavelength:*	**n.a.**
Control Program:	**Alditol Acetate I 500spl**	*Bandwidth:*	**n.a.**
Quantif. Method:	**Alditol Acetate**	*Dilution Factor:*	**1.0000**
Recording Time:	**15/2/2021 15:13**	*Sample Weight:*	**1.0000**
Run Time (min):	**20.00**	*Sample Amount:*	**1.0000**

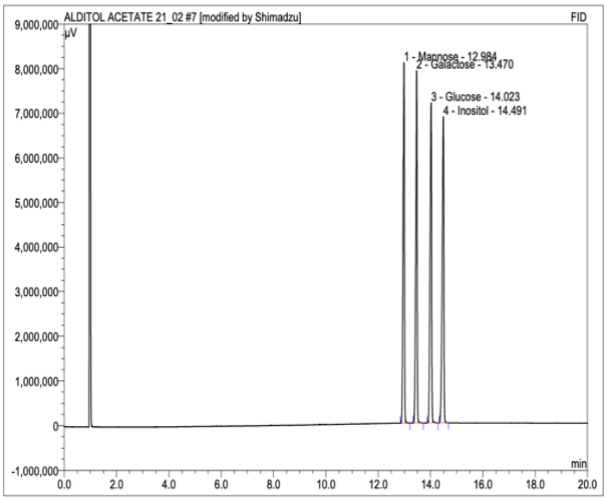

No.	Ret.Time min	Peak Name	Height µV	Area µV*min	Rel.Area %	Amount
1	12.98	Mannose	8078662.00	494141.0	24.91	n.a.
2	13.47	Galactose	7893662.00	499606.1	25.18	n.a.
3	14.02	Glucose	7171236.00	484432.5	24.42	n.a.
4	14.49	Inositol	6862725.00	505806.7	25.49	n.a.
Total:			30006285.00	1983986.40	100.00	0.000

Biofilm BCG-VC – atc (left); + atc (right)

Sample Name:	**24**	*Injection Volume:*	**2.0**
Vial Number:	**30**	*Channel:*	**FID**
Sample Type:	**unknown**	*Wavelength:*	**n.a.**
Control Program:	**Alditol Acetate I**	*Bandwidth:*	**n.a.**
Quantif. Method:	**Alditol Acetate**	*Dilution Factor:*	**1.0000**
Recording Time:	**15/12/2020 3:05**	*Sample Weight:*	**1.0000**
Run Time (min):	**20.00**	*Sample Amount:*	**1.0000**

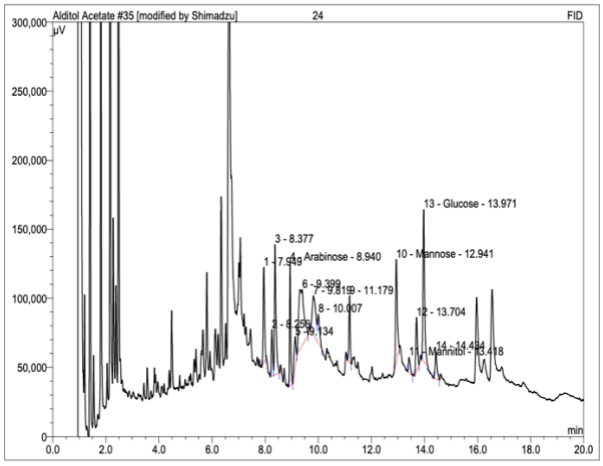

No.	Ret.Time min	Peak Name	Height µV	Area µV*min	Rel.Area %	Amount
1	7.95	n.a.	68928.00	4017.9	7.25	n.a.
2	8.26	n.a.	33555.00	1987.5	3.58	n.a.
3	8.38	n.a.	94046.00	6276.8	11.32	n.a.
4	8.94	Arabinose	89036.00	4579.1	8.26	n.a.
5	9.13	n.a.	22038.00	1771.5	3.19	n.a.
6	9.40	n.a.	40088.00	9537.5	17.20	n.a.
7	9.82	n.a.	27825.00	4321.7	7.79	n.a.
8	10.01	n.a.	20968.00	1897.9	3.42	n.a.
9	11.18	n.a.	48025.00	2505.9	4.52	n.a.
10	12.94	Mannose	73973.00	5540.4	9.99	n.a.
11	13.42	Mannitol	11193.00	940.1	1.70	n.a.
12	13.70	n.a.	38511.00	2651.7	4.78	n.a.
13	13.97	Glucose	109934.00	7795.6	14.06	n.a.
14	14.43	n.a.	19740.00	1626.0	2.93	n.a.
Total:			697860.00	55449.34	100.00	0.000

Sample Name:	**25**	*Injection Volume:*	**2.0**
Vial Number:	**31**	*Channel:*	**FID**
Sample Type:	**unknown**	*Wavelength:*	**n.a.**
Control Program:	**Alditol Acetate I**	*Bandwidth:*	**n.a.**
Quantif. Method:	**Alditol Acetate**	*Dilution Factor:*	**1.0000**
Recording Time:	**15/12/2020 3:28**	*Sample Weight:*	**1.0000**
Run Time (min):	**20.00**	*Sample Amount:*	**1.0000**

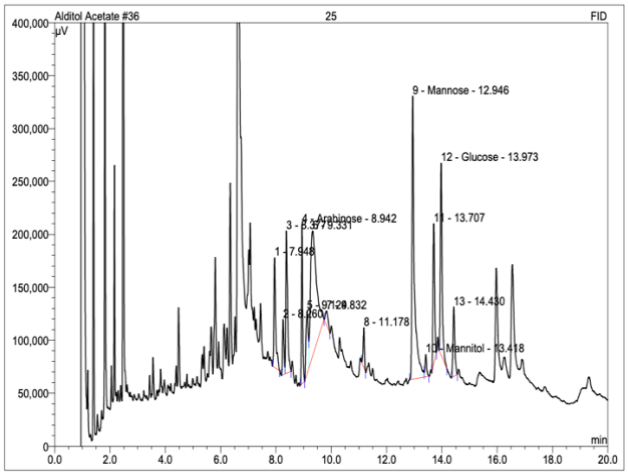

No.	Ret.Time min	Peak Name	Height µV	Area µV*min	Rel.Area %	Amount
1	7.95	n.a.	103366.00	7693.8	6.19	n.a.
2	8.26	n.a.	52039.00	3175.8	2.56	n.a.
3	8.38	n.a.	134367.00	9899.7	7.97	n.a.
4	8.94	Arabinose	150490.00	7793.3	6.27	n.a.
5	9.12	n.a.	58968.00	5497.8	4.42	n.a.
6	9.33	n.a.	117434.00	30017.4	24.16	n.a.
7	9.83	n.a.	13717.00	1570.7	1.26	n.a.
8	11.18	n.a.	37378.00	2027.7	1.63	n.a.
9	12.95	Mannose	267402.00	27649.4	22.25	n.a.
10	13.42	Mannitol	20865.00	1484.4	1.19	n.a.
11	13.71	n.a.	132376.00	8877.5	7.14	n.a.
12	13.97	Glucose	181613.00	13478.2	10.85	n.a.
13	14.43	n.a.	65352.00	5086.3	4.09	n.a.
Total:			1335367.00	124252.06	100.00	0.000

Biofilm BCG-sgRNA1 – atc (left); + atc (right)

Sample Name:	**26**	*Injection Volume:*	**2.0**
Vial Number:	**32**	*Channel:*	**FID**
Sample Type:	**unknown**	*Wavelength:*	**n.a.**
Control Program:	**Alditol Acetate I**	*Bandwidth:*	**n.a.**
Quantif. Method:	**Alditol Acetate**	*Dilution Factor:*	**1.0000**
Recording Time:	**15/12/2020 4:16**	*Sample Weight:*	**1.0000**
Run Time (min):	**20.00**	*Sample Amount:*	**1.0000**

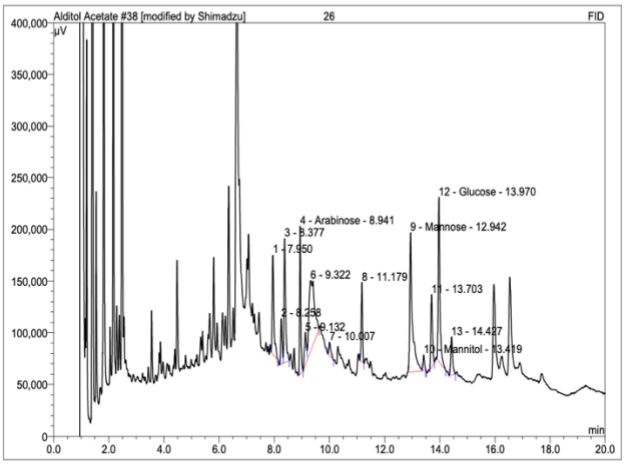

No.	Ret.Time min	Peak Name	Height µV	Area µV*min	Rel.Area %	Amount
1	7.95	n.a.	95755.00	6794.4	8.05	n.a.
2	8.26	n.a.	43763.00	2602.4	3.08	n.a.
3	8.38	n.a.	119902.00	8191.6	9.70	n.a.
4	8.94	Arabinose	142632.00	7357.0	8.71	n.a.
5	9.13	n.a.	31611.00	2616.0	3.10	n.a.
6	9.32	n.a.	68216.00	15722.1	18.62	n.a.
7	10.01	n.a.	12945.00	1072.1	1.27	n.a.
8	11.18	n.a.	76715.00	3992.4	4.73	n.a.
9	12.94	Mannose	134590.00	15363.0	18.20	n.a.
10	13.42	Mannitol	14859.00	943.4	1.12	n.a.
11	13.70	n.a.	70161.00	4800.9	5.69	n.a.
12	13.97	Glucose	158779.00	12071.9	14.30	n.a.
13	14.43	n.a.	36784.00	2900.7	3.44	n.a.
Total:			1006712.00	84427.84	100.00	0.000

Sample Name:	**27**	*Injection Volume:*	**2.0**
Vial Number:	**33**	*Channel:*	**FID**
Sample Type:	**unknown**	*Wavelength:*	**n.a.**
Control Program:	**Alditol Acetate I**	*Bandwidth:*	**n.a.**
Quantif. Method:	**Alditol Acetate**	*Dilution Factor:*	**1.0000**
Recording Time:	**15/12/2020 4:40**	*Sample Weight:*	**1.0000**
Run Time (min):	**20.00**	*Sample Amount:*	**1.0000**

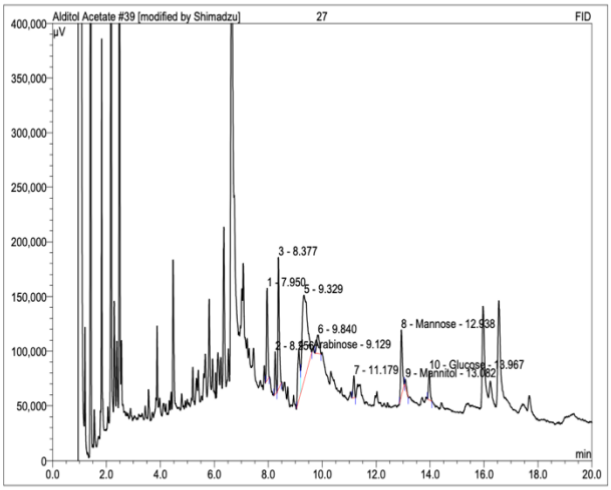

No.	Ret.Time min	Peak Name	Height µV	Area µV*min	Rel.Area %	Amount
1	7.95	n.a.	84189.00	4633.4	10.03	n.a.
2	8.26	n.a.	38537.00	1953.5	4.23	n.a.
3	8.38	n.a.	120291.00	7000.5	15.15	n.a.
4	9.13	Arabinose	45857.00	4385.6	9.49	n.a.
5	9.33	n.a.	77714.00	18243.6	39.48	n.a.
6	9.84	n.a.	16997.00	2031.0	4.39	n.a.
7	11.18	n.a.	19874.00	1189.0	2.57	n.a.
8	12.94	Mannose	60443.00	4558.1	9.86	n.a.
9	13.08	Mannitol	7057.00	406.0	0.88	n.a.
10	13.97	Glucose	26505.00	1812.0	3.92	n.a.
Total:			497464.00	46212.80	100.00	0.000

Biofilm BCG-sgRNA2 – atc (left); + atc (right)

Sample Name:	**28**	*Injection Volume:*	**2.0**
Vial Number:	**34**	*Channel:*	**FID**
Sample Type:	**unknown**	*Wavelength:*	**n.a.**
Control Program:	**Alditol Acetate I**	*Bandwidth:*	**n.a.**
Quantif. Method:	**Alditol Acetate**	*Dilution Factor:*	**1.0000**
Recording Time:	**15/12/2020 5:04**	*Sample Weight:*	**1.0000**
Run Time (min):	**20.00**	*Sample Amount:*	**1.0000**

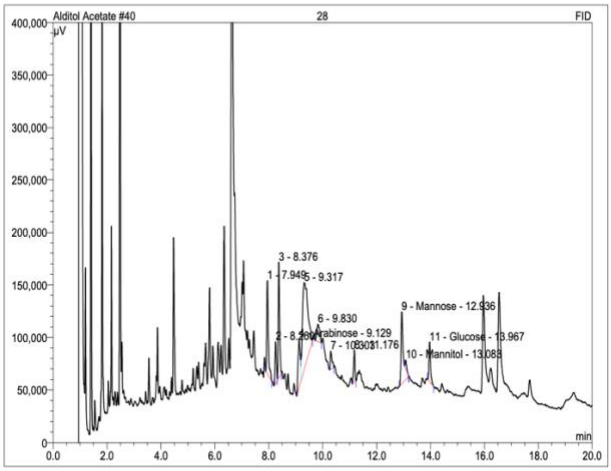

No.	Ret.Time min	Peak Name	Height µV	Area µV*min	Rel.Area %	Amount
1	7.95	n.a.	88626.00	5790.6	10.96	n.a.
2	8.26	n.a.	39205.00	2196.5	4.16	n.a.
3	8.38	n.a.	109939.00	6279.1	11.88	n.a.
4	9.13	Arabinose	45892.00	4263.5	8.07	n.a.
5	9.32	n.a.	82599.00	19201.5	36.33	n.a.
6	9.83	n.a.	16475.00	1976.5	3.74	n.a.
7	10.30	n.a.	16962.00	1281.5	2.42	n.a.
8	11.18	n.a.	30267.00	1731.2	3.28	n.a.
9	12.94	Mannose	68529.00	6956.7	13.16	n.a.
10	13.08	Mannitol	8436.00	518.3	0.98	n.a.
11	13.97	Glucose	37544.00	2655.2	5.02	n.a.
Total:			544474.00	52850.56	100.00	0.000

Sample Name:	**29**	*Injection Volume:*	**2.0**
Vial Number:	**35**	*Channel:*	**FID**
Sample Type:	**unknown**	*Wavelength:*	**n.a.**
Control Program:	**Alditol Acetate I**	*Bandwidth:*	**n.a.**
Quantif. Method:	**Alditol Acetate**	*Dilution Factor:*	**1.0000**
Recording Time:	**15/12/2020 5:28**	*Sample Weight:*	**1.0000**
Run Time (min):	**20.00**	*Sample Amount:*	**1.0000**

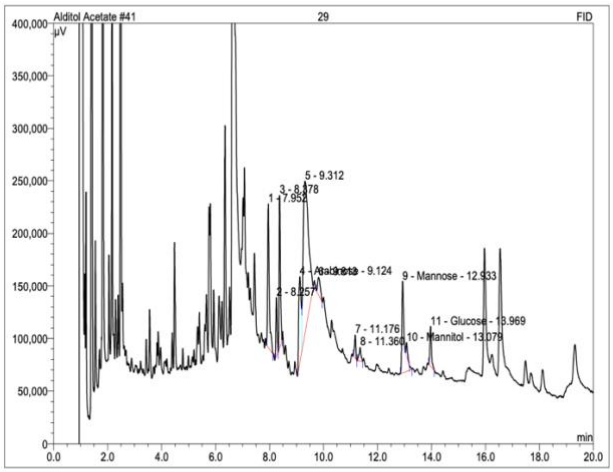

No.	Ret.Time min	Peak Name	Height µV	Area µV*min	Rel.Area %	Amount
1	7.95	n.a.	136387.00	9487.0	11.97	n.a.
2	8.26	n.a.	55749.00	3017.9	3.81	n.a.
3	8.38	n.a.	144354.00	7884.0	9.94	n.a.
4	9.12	Arabinose	82010.00	8410.7	10.61	n.a.
5	9.31	n.a.	145617.00	33224.5	41.91	n.a.
6	9.81	n.a.	16686.00	2006.1	2.53	n.a.
7	11.18	n.a.	22133.00	1251.6	1.58	n.a.
8	11.36	n.a.	12943.00	1095.0	1.38	n.a.
9	12.93	Mannose	87029.00	9363.7	11.81	n.a.
10	13.08	Mannitol	13042.00	831.3	1.05	n.a.
11	13.97	Glucose	37909.00	2712.0	3.42	n.a.
Total:			753859.00	79283.92	100.00	0.000

Biofilm BCG-sgRNA3 – atc (left); + atc (right)

Sample Name:	**30**	*Injection Volume:*	**2.0**
Vial Number:	**36**	*Channel:*	**FID**
Sample Type:	**unknown**	*Wavelength:*	**n.a.**
Control Program:	**Alditol Acetate I**	*Bandwidth:*	**n.a.**
Quantif. Method:	**Alditol Acetate**	*Dilution Factor:*	**1.0000**
Recording Time:	**15/12/2020 5:52**	*Sample Weight:*	**1.0000**
Run Time (min):	**20.00**	*Sample Amount:*	**1.0000**

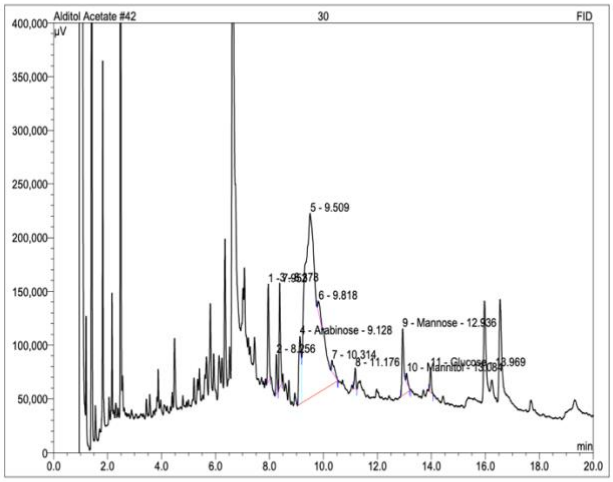

No.	Ret.Time min	Peak Name	Height µV	Area µV*min	Rel.Area %	Amount
1	7.95	n.a.	90715.00	5136.8	4.02	n.a.
2	8.26	n.a.	36431.00	1894.4	1.48	n.a.
3	8.38	n.a.	97027.00	5334.2	4.18	n.a.
4	9.13	Arabinose	62691.00	6267.2	4.91	n.a.
5	9.51	n.a.	171380.00	97049.6	75.98	n.a.
6	9.82	n.a.	10305.00	1203.5	0.94	n.a.
7	10.31	n.a.	10660.00	1366.2	1.07	n.a.
8	11.18	n.a.	18922.00	1113.8	0.87	n.a.
9	12.94	Mannose	61787.00	6337.1	4.96	n.a.
10	13.08	Mannitol	8585.00	550.0	0.43	n.a.
11	13.97	Glucose	22694.00	1471.5	1.15	n.a.
Total:			591197.00	127724.37	100.00	0.000

Sample Name:	**31**	*Injection Volume:*	**2.0**
Vial Number:	**37**	*Channel:*	**FID**
Sample Type:	**unknown**	*Wavelength:*	**n.a.**
Control Program:	**Alditol Acetate I**	*Bandwidth:*	**n.a.**
Quantif. Method:	**Alditol Acetate**	*Dilution Factor:*	**1.0000**
Recording Time:	**15/12/2020 6:16**	*Sample Weight:*	**1.0000**
Run Time (min):	**20.00**	*Sample Amount:*	**1.0000**

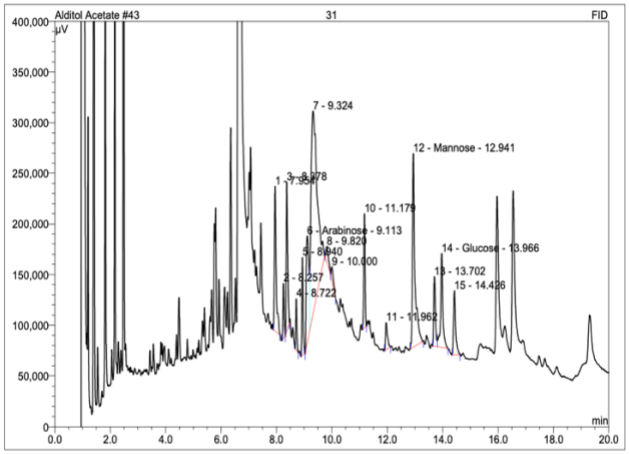

No.	Ret.Time min	Peak Name	Height µV	Area µV*min	Rel.Area %	Amount
1	7.95	n.a.	142789.00	10133.9	7.12	n.a.
2	8.26	n.a.	53923.00	2671.4	1.88	n.a.
3	8.38	n.a.	146613.00	8634.8	6.07	n.a.
4	8.72	n.a.	50637.00	2370.0	1.67	n.a.
5	8.94	n.a.	96283.00	5028.9	3.54	n.a.
6	9.11	Arabinose	105787.00	11308.0	7.95	n.a.
7	9.32	n.a.	200231.00	52160.5	36.67	n.a.
8	9.82	n.a.	15288.00	1647.7	1.16	n.a.
9	10.00	n.a.	13006.00	1178.9	0.83	n.a.
10	11.18	n.a.	112376.00	5842.5	4.11	n.a.
11	11.96	n.a.	26500.00	2156.5	1.52	n.a.
12	12.94	Mannose	191216.00	20057.5	14.10	n.a.
13	13.70	n.a.	68585.00	4928.0	3.46	n.a.
14	13.97	Glucose	92657.00	8614.0	6.06	n.a.
15	14.43	n.a.	62911.00	5517.8	3.88	n.a.

Planktonic BCG-VC – atc (left); + atc (right)

Sample Name:	**1**	*Injection Volume:*	**2.0**
Vial Number:	**7**	*Channel:*	**FID**
Sample Type:	**unknown**	*Wavelength:*	**n.a.**
Control Program:	**Alditol Acetate I**	*Bandwidth:*	**n.a.**
Quantif. Method:	**Alditol Acetate**	*Dilution Factor:*	**1.0000**
Recording Time:	**14/12/2020 17:08**	*Sample Weight:*	**1.0000**
Run Time (min):	**20.00**	*Sample Amount:*	**1.0000**

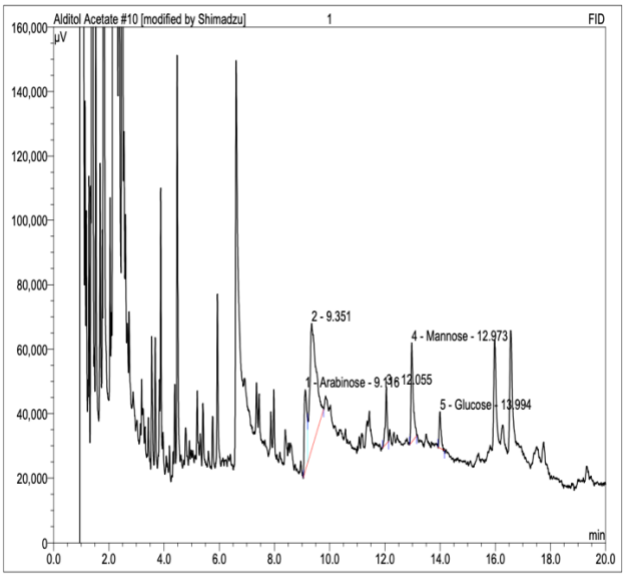

No.	Ret.Time min	Peak Name	Height µV	Area µV*min	Rel.Area %	Amount
1	9.12	Arabinose	25257.00	2808.0	15.53	n.a.
2	9.35	n.a.	38970.00	10206.4	56.47	n.a.
3	12.05	n.a.	17590.00	1320.1	7.30	n.a.
4	12.97	Mannose	30704.00	2839.0	15.71	n.a.
5	13.99	Glucose	11223.00	902.1	4.99	n.a.
Total:			123744.00	18075.59	100.00	0.000

Sample Name:	**2**	*Injection Volume:*	**2.0**
Vial Number:	**8**	*Channel:*	**FID**
Sample Type:	**unknown**	*Wavelength:*	**n.a.**
Control Program:	**Alditol Acetate I**	*Bandwidth:*	**n.a.**
Quantif. Method:	**Alditol Acetate**	*Dilution Factor:*	**1.0000**
Recording Time:	**14/12/2020 17:32**	*Sample Weight:*	**1.0000**
Run Time (min):	**20.00**	*Sample Amount:*	**1.0000**

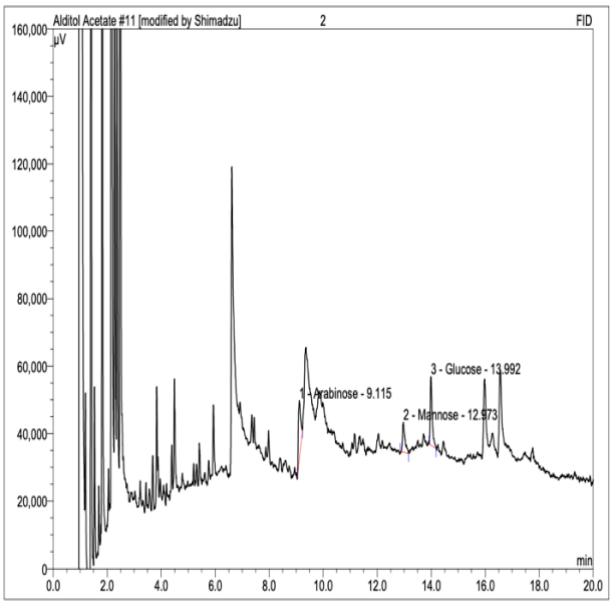

No.	Ret.Time min	Peak Name	Height µV	Area µV*min	Rel.Area %	Amount
1	9.11	Arabinose	17497.00	1602.4	37.99	n.a.
2	12.97	Mannose	8787.00	916.9	21.74	n.a.
3	13.99	Glucose	20156.00	1698.8	40.27	n.a.
Total:			46440.00	4218.06	100.00	0.000

Planktonic BCG-sgRNA1 - atc (left); + atc (right)

Sample Name:	**3**	*Injection Volume:*	**2.0**
Vial Number:	**9**	*Channel:*	**FID**
Sample Type:	**unknown**	*Wavelength:*	**n.a.**
Control Program:	**Alditol Acetate I**	*Bandwidth:*	**n.a.**
Quantif. Method:	**Alditol Acetate**	*Dilution Factor:*	**1.0000**
Recording Time:	**14/12/2020 17:55**	*Sample Weight:*	**1.0000**
Run Time (min):	**20.00**	*Sample Amount:*	**1.0000**

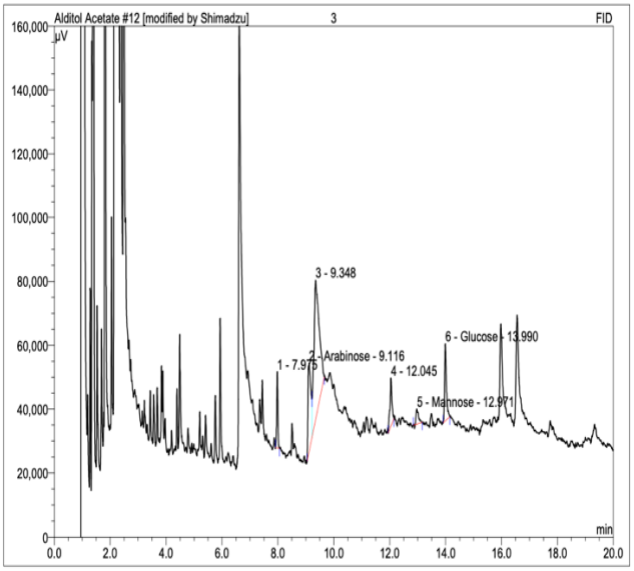

No.	Ret.Time min	Peak Name	Height µV	Area µV*min	Rel.Area %	Amount
1	7.97	n.a.	23728.00	1127.3	6.43	n.a.
2	9.12	Arabinose	27740.00	3172.6	18.11	n.a.
3	9.35	n.a.	43648.00	9655.8	55.11	n.a.
4	12.04	n.a.	15012.00	1233.9	7.04	n.a.
5	12.97	Mannose	4688.00	444.5	2.54	n.a.
6	13.99	Glucose	24060.00	1886.2	10.77	n.a.
Total:			138876.00	17520.25	100.00	0.000

Sample Name:	**4**	*Injection Volume:*	**2.0**
Vial Number:	**10**	*Channel:*	**FID**
Sample Type:	**unknown**	*Wavelength:*	**n.a.**
Control Program:	**Alditol Acetate I**	*Bandwidth:*	**n.a.**
Quantif. Method:	**Alditol Acetate**	*Dilution Factor:*	**1.0000**
Recording Time:	**14/12/2020 18:19**	*Sample Weight:*	**1.0000**
Run Time (min):	**20.00**	*Sample Amount:*	**1.0000**

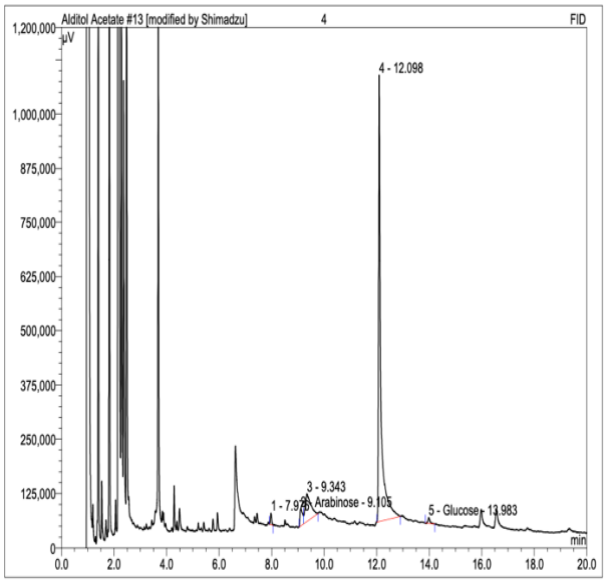

No.	Ret.Time min	Peak Name	Height µV	Area µV*min	Rel.Area %	Amount
1	7.98	n.a.	26174.00	1334.7	1.08	n.a.
2	9.11	Arabinose	38372.00	4406.4	3.56	n.a.
3	9.34	n.a.	63361.00	15149.5	12.25	n.a.
4	12.10	n.a.	1029363.00	101624.8	82.17	n.a.
5	13.98	Glucose	13272.00	1157.6	0.94	n.a.
Total:			1170542.00	123672.95	100.00	0.000

Planktonic BCG-sgRNA2 – atc (left); + atc (right)

Sample Name:	**5**	*Injection Volume:*	**2.0**
Vial Number:	**11**	*Channel:*	**FID**
Sample Type:	**unknown**	*Wavelength:*	**n.a.**
Control Program:	**Alditol Acetate I**	*Bandwidth:*	**n.a.**
Quantif. Method:	**Alditol Acetate**	*Dilution Factor:*	**1.0000**
Recording Time:	**14/12/2020 18:43**	*Sample Weight:*	**1.0000**
Run Time (min):	**20.00**	*Sample Amount:*	**1.0000**

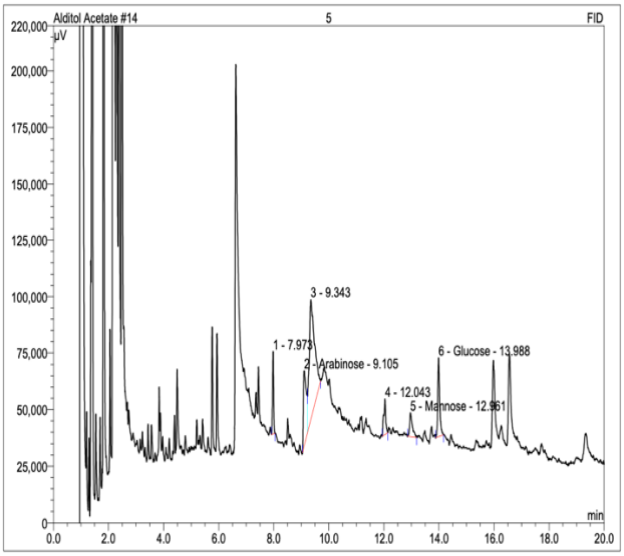

No.	Ret.Time min	Peak Name	Height µV	Area µV*min	Rel.Area %	Amount
1	7.97	n.a.	36396.00	1732.1	7.49	n.a.
2	9.11	Arabinose	33160.00	3943.3	17.06	n.a.
3	9.34	n.a.	53090.00	12063.4	52.18	n.a.
4	12.04	n.a.	15588.00	1333.4	5.77	n.a.
5	12.96	Mannose	10559.00	1229.0	5.32	n.a.
6	13.99	Glucose	34759.00	2818.6	12.19	n.a.
Total:			183552.00	23119.86	100.00	0.000

Sample Name:	**6**	*Injection Volume:*	**2.0**
Vial Number:	**12**	*Channel:*	**FID**
Sample Type:	**unknown**	*Wavelength:*	**n.a.**
Control Program:	**Alditol Acetate I**	*Bandwidth:*	**n.a.**
Quantif. Method:	**Alditol Acetate**	*Dilution Factor:*	**1.0000**
Recording Time:	**14/12/2020 19:31**	*Sample Weight:*	**1.0000**
Run Time (min):	**20.00**	*Sample Amount:*	**1.0000**

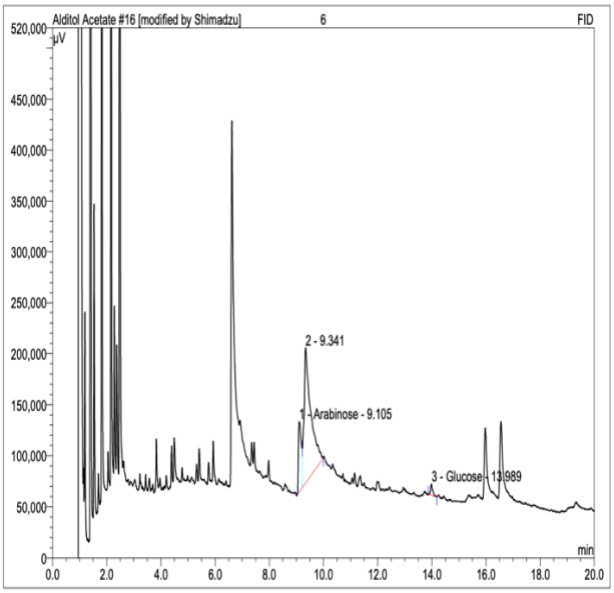

No.	Ret.Time min	Peak Name	Height µV	Area µV*min	Rel.Area %	Amount
1	9.10	Arabinose	68612.00	8448.8	17.56	n.a.
2	9.34	n.a.	132430.00	38689.0	80.42	n.a.
3	13.99	Glucose	10741.00	969.6	2.02	n.a.
Total:			211783.00	48107.44	100.00	0.000

Planktonic BCG-sgRNA3 – atc (left); + atc (right)

Sample Name:	**7**	*Injection Volume:*	**2.0**
Vial Number:	**13**	*Channel:*	**FID**
Sample Type:	**unknown**	*Wavelength:*	**n.a.**
Control Program:	**Alditol Acetate I**	*Bandwidth:*	**n.a.**
Quantif. Method:	**Alditol Acetate**	*Dilution Factor:*	**1.0000**
Recording Time:	**14/12/2020 19:54**	*Sample Weight:*	**1.0000**
Run Time (min):	**20.00**	*Sample Amount:*	**1.0000**

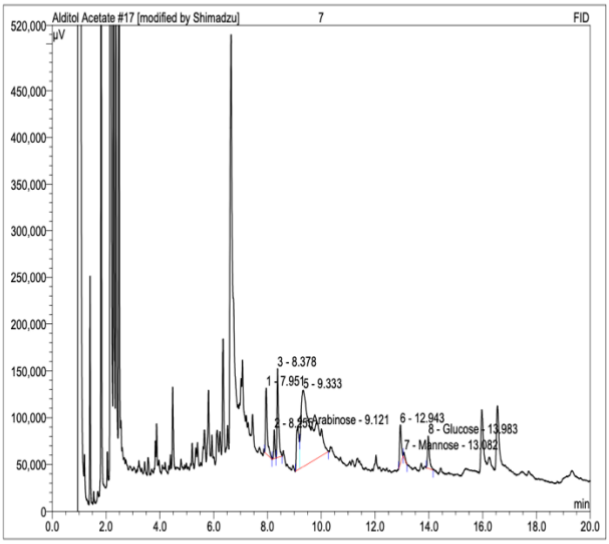

No.	Ret.Time min	Peak Name	Height µV	Area µV*min	Rel.Area %	Amount
1	7.95	n.a.	69993.00	5166.7	8.10	n.a.
2	8.26	n.a.	30372.00	1522.4	2.39	n.a.
3	8.38	n.a.	94826.00	6258.6	9.81	n.a.
4	9.12	Arabinose	46582.00	5203.9	8.15	n.a.
5	9.33	n.a.	81367.00	39292.9	61.57	n.a.
6	12.94	n.a.	41735.00	3193.7	5.00	n.a.
7	13.08	Mannose	5916.00	330.1	0.52	n.a.
8	13.98	Glucose	34530.00	2854.0	4.47	n.a.
Total:			405321.00	63822.44	100.00	0.000

Sample Name:	**8**	*Injection Volume:*	**2.0**
Vial Number:	**14**	*Channel:*	**FID**
Sample Type:	**unknown**	*Wavelength:*	**n.a.**
Control Program:	**Alditol Acetate I**	*Bandwidth:*	**n.a.**
Quantif. Method:	**Alditol Acetate**	*Dilution Factor:*	**1.0000**
Recording Time:	**14/12/2020 20:18**	*Sample Weight:*	**1.0000**
Run Time (min):	**20.00**	*Sample Amount:*	**1.0000**

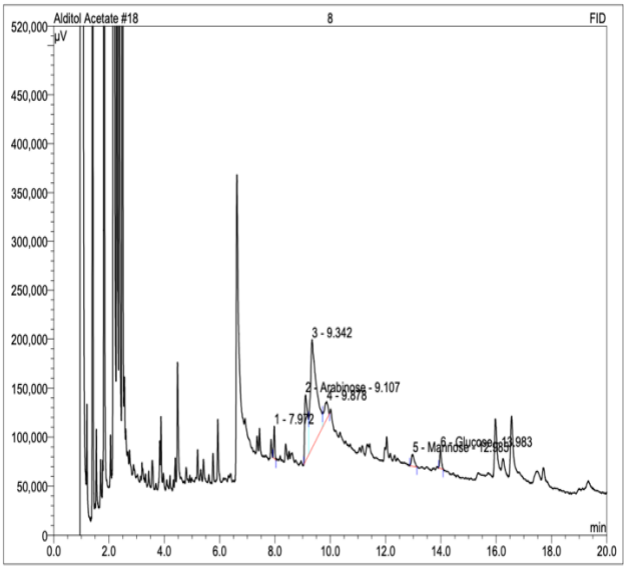

No.	Ret.Time min	Peak Name	Height µV	Area µV*min	Rel.Area %	Amount
1	7.97	n.a.	32727.00	1534.4	3.52	n.a.
2	9.11	Arabinose	67255.00	8074.0	18.54	n.a.
3	9.34	n.a.	110716.00	27848.3	63.96	n.a.
4	9.88	n.a.	17126.00	3293.1	7.56	n.a.
5	12.98	Mannose	11852.00	1405.0	3.23	n.a.
6	13.98	Glucose	19218.00	1383.1	3.18	n.a.
Total:			258894.00	43537.88	100.00	0.000

Appendix 3

Confocal electron microscopy on aftC repressed BCG-sgRNA3 and BCG-VC: BCG-VC and BCG-sgRNA3 biofilms grown in the presence and absence of atc were stained by ConcanavalinA which binds to polysaccharides within biofilm matrix and we have a seen that upon *aftC* repression, lipoglycans accumulate along the edges of biofilms in BCG-sgRNA3

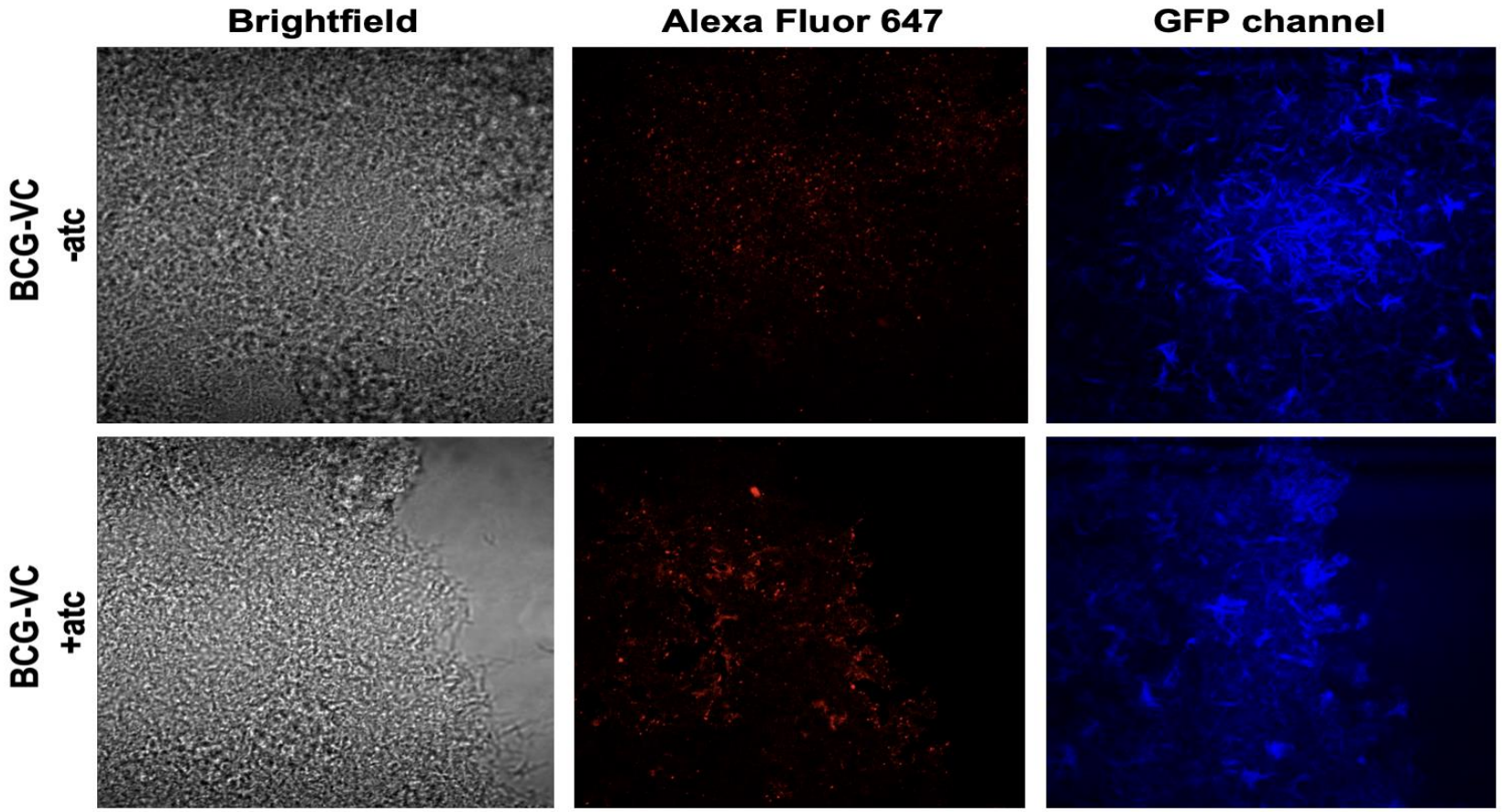

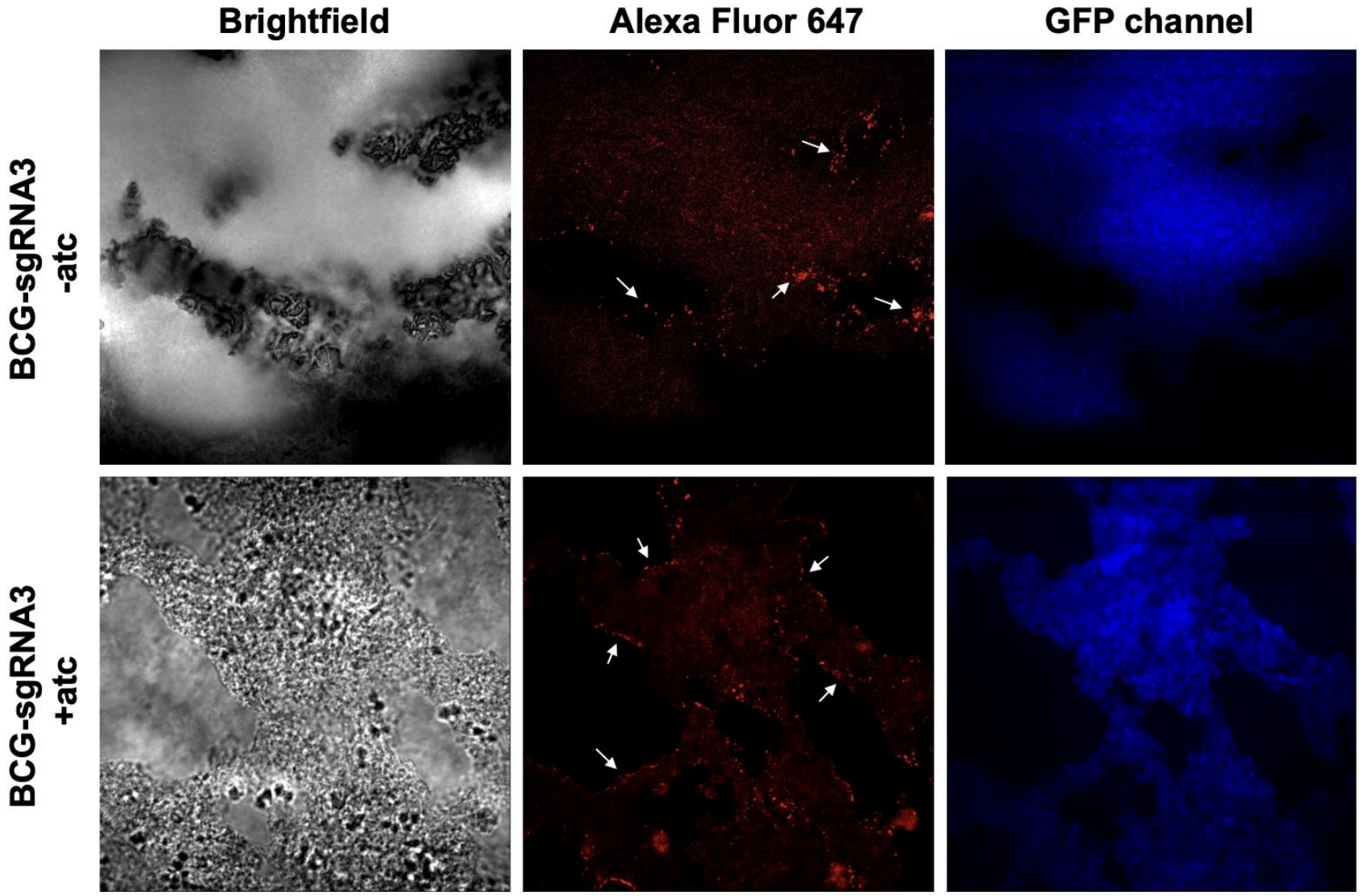
Brightfield
Alexa Fluor 647
GFP channel
BCG-sgRNA3
-atc
BCG-sgRNA3
+atc